UNIVERSITAT DE BARCELONA

Modelling the dynamics of cellular membranes

Andreu Fernández i Gallén

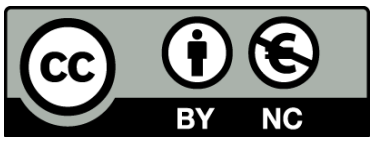

Modelling the dynamics of cellular membranes

Andreu Fernández i Gallén

Doctoral Thesis

UNIVERSITAT DE BARCELONA

Física de la Matèria Condensada

2022

Modelling the dynamics of cellular membranes

Programa de doctorat en Física

Autor: Andreu Fernández i Gallén

Directora: Aurora Hernandez Machado

Tutor: Giancarlo Franzese

Lo aprendido en esta tesis es que lo más importante tiene que ser el investigador y no la investigación, que no se tiene que sacrificar para crear. A toda persona que tenga pasión por algo: asegúrate que la estás disfrutando.

Some humans would do anything to see if it was possible to do it. If you put a large switch in some cave somewhere, with a sign on it saying 'End-of-the-World Switch. PLEASE DO NOT TOUCH', the paint wouldn't even have time to dry.

Terry Pratchett

Acknowledgements

First of all I want to acknowledge the most important person right now, the one who is actually reading this thesis right now.

Dar las gracias a Aurora por enseñarme todo lo que me ha enseñado y también por aprender muchas cosas conmigo. Gracias a los colaboradores que han conseguido que la suma de todos sea más que lo que habríamos sacado solos, ha sido muy interesante hablar con vosotros y construir cosas juntos desde Madrid con Mario y desde México con Rafael y Roberto.

Moltes gràcies a la meva família per la paciència que ha tingut amb mi. Gràcies als amics que m'ho han fet passar més fàcilment, en especial a l'Arnau, l'Álvaro i en Xavi i també gràcies per l'ajuda i el suport a la Clara H. i a la companyia de Clara G.! Berta no només em vas aguantar, sinó que em vas donar la plantilla de LaTeX que he fet servir i això no té preu. La gent del despatx i de la facultat heu fet possible aquesta tesi, ha sigut molt divertit i això també s'ha d'agraïr: Adrià, Helena, Josep M., Josep F., Irina, Carol, Mattia, Antonio, Eric, Gaspard i molta altra gent per qui no hi ha lloc que no em cabrien tots al full!

Contents

General Introduction

Thesis scope

Membranes are present in all cells, in some viruses, and are involved in all kinds of biological functions. The goal of this thesis is to expand our knowledge of this element, in hope that this –on top of all the other knowledge of biology and physics– can help someday improve people's life.

With this aim, we studied how cells react when an external stimulus is applied or big changes happen to them. This is due the fact that, while we know a lot of relaxed cells, we do not as much of cells when they do things or things are done to them. This is the drive behind the two different research paths written in this thesis: membranes inside a fluid flow, and membranes during topological transitions and fluctuations.

Stream function membrane phase field model

For the first research path –on membranes inside a flow– while this is not a new topic we wanted to start by making it more approachable. That has been achieved by introducing a new methodology to couple membranes and flows by using the stream function and the vorticity to solve the Navier Stokes equation. This approach creates a model derived straight from the hydrodynamic equations and grounded on the physics of the system rather than other more complex approaches. This methodology also ensures the incompressibility condition regardless of the accuracy of the numerical solver.

With this model we studied the effects of confinement for membranes inside a Poiseuille flow. We mainly focused on replicating red blood cell shapes as it is a very researched case and there is plenty of experimental data on them. First starting with cells inside channels slightly bigger than their diameter, which is known to give a set of shapes named parachutes and slippers. We use this knowledge to prove the validity of our model, and with that we study different flows.

For very wide channels, the low confinement Poiseuille flows have shown a different meta-stable shape which we named anti-parachute. We can use the vorticity and the stream function to analyse the stability and the convergence to an stationary state of the membrane. Moreover, tumbling can be produced by introducing a different viscosity

for the cell fluid, higher than the surrounding fluid. In very narrow super-confined channels we have a Poiseuille flow where the cell is much bigger than the channel. This confinement gives very different shapes which are more sensitive to the reduced volume of the cell. The results on this super-confinement show some agreement with the experimental data available.

However, the model is capable of studying other flows rather than Poiseuille. Couette flow has been studied, where one can see a lift perpendicular to the flow that depends on the reduced volume of the cell as well as the viscosity contrast. This lift is different from the more well known Segré-Silberberg effect of inertia-induced lateral migration, as these simulations do not include the inertial term for the flow.

The most important thing has been leaving behind a methodology ready for expansion to time-dependent flows, inertial flows, or to generalise to 3 dimensions. The final aim was not only showing the model but sharing the code where we implement it numerically through the world wide web.

Helfrich models and topological transitions

For the second research path –on topological transitions– we have implemented the Gaussian curvature energy term to the membrane model, to allow study of fission and fusion. To this end we do the computation in the complex space, as the denominator of the Gaussian energy term diverges easily.

With this methodology we study fission of tubes with the use of the spontaneous curvature, which deforms a membrane tube into a pearled tube. This pearled tube formed by an array of spheres connected through membrane tethers undergoes fission if the Gaussian rigidity is negative and high enough. A phase diagram of what happens depending on the values of Gaussian and bending rigidity is obtained. This diagram shows three distinct regimes: one in which the membrane develops holes, one in which the tube undergoes fission of vesicles, and one in which the membrane tube do not undergo topological transitions. We can see this explained as a competition between the curvature energy and the Gaussian curvature energy.

Then we expand to study geometries less helpful for fission, such as a flat planar membrane. To be able to induce fission in a flat membrane there is a new additional quality to take into account. It will not matter how big is the spontaneous curvature of the Gaussian rigidity, as a perfectly flat membrane is a meta-stable shape. This is due the fact that to start the fission process we need an area with enough curvature so that the spontaneous curvature can kick-off the membrane budding process. If budding does not happen we will not have fission and the vesicle formation process. To solve this, we added a white noise to mimic temperature. This noise makes each point of the membrane position to fluctuate.

The temperature, if high enough, will deform the membrane and promote the formation of vesicles. There is a phase transition between a flat membrane that is not undergoing fission and one that does. This phase transition can be induced by changing temperature, the spontaneous curvature of the membrane, or the ratio between the Gaussian and bending rigidities. Additionally we see that a positive Gaussian rigidity gives the membrane strong stability against very big noises. Finally, by plotting the curvature and Gaussian energy terms we can see if the membrane will undergo fission a moderate amount of time before the first fission event.

Lastly we also started to characterise the thermal fluctuations of our model. It is known since the 19th century that the red blood cells membrane fluctuate, which was named flickering. Nowadays we know that this flickering of the cell is due to the combination between the soft mechanical properties of the red blood cell membrane and temperature. How the membranes fluctuate and how the fluctuations relax has been studied and is well known, and to characterise our fluctuating membrane model we have studied the spectrum of the fluctuations. The results seem to vary from the experimental data but to match other non-local diffuse interface models. All this is expected to add up when introducing the fluid coupling to the system.

CONTENTS

Part I

Introduction

Chapter 1

Biological Introduction

Cells are the smallest unit of life. They suffer a set of stochastic and seemingly chaotic **events** and processes mashed together to form a living being. Kinetics of biological processes at the intra-cellular level are stochastic [1] and therefore intrinsically interesting to physicists. In a similar way to a person arising from the collective of all the cells that form them, a cell emerges from the combination of all its random components tailored in a specific way. So, to understand life and the human condition from the bottom up we have to understand all the parts that make us, and therefore, that make our cells.

The cells being the smallest unit of life is based on disregarding the virus as a living organism. After all, whether viruses are alive or not depends on the definition of what is life and this definition is bound to be arbitrary [2].

In this thesis we will choose a single component of the cell, but one that is present in all of them: the cellular membrane. The cellular membrane is what defines what is "the cell", giving it individuality. So, studying this key element we aim to explain several different phenomena using the same base model. However, before explaining in what phenomena of the membrane are we interested, first we will have to explain what is the cellular membrane.

1.1 The cellular membrane

The cellular membrane is maybe the only feature present in all cells. It is what defines the boundary of what is a cell and what is the rest of the world. Even though this wall does not give the metaphysical sense of self, without this wall there would be no self.

The cellular membrane is a dynamic, fluid structure which can expand for tens of micrometers even when it is composed of a lipid double layer of about 5 nanometers in thickness. Biological membranes are made out of a double lipid layer, also called lipid bilayer. Within each of these monolayers the different lipid molecules can flow through diffusion among its peers. The lipids that form the membrane exhibit

special properties like spontaneous assembly into bilayers. This happens because of a hydrophillic-hydrophobic polar structure of the lipid that makes the lipid molecule amphiphilic.

1.1.1 Function

The main function of the cellular membrane is to contain all the parts of the cell protected and organised, and by organised we mean roughly close together. Without the membrane we could not have cells and probably life as we understand would not be possible, as the different organelles and mechanisms would simply float away. This would not give the possibility of multiple mechanisms coming together and organizing into a self-replicating system. However, aside of working as a wall defining the outside world, the membrane has other functions for the cell.

Shape of the cell: The membrane deformation is key for many functions of the cell like movement, division, obtaining nutrients, or disposal of waste. To be able to perform these actions and more the membrane will have to be very flexible. This flexibility can be tuned by changing the composition of the membrane or by the introduction of specialised membrane-bound proteins. But not only biological membranes have to be flexible but also need to be robust. The shape of the cell is given in a lot of cases by a cytoskeleton under the membrane that gives shape and rigidity to the cell. This shape is also important for having proper internal structure, necessary in more complex cells.

Maintaining chemical balance: The chemical composition of the cytosol is of great importance to the cell survival. It is the job of the membrane to maintain the chemical composition of the cell, which usually is much different from the extracellular environment. On top of that it also has to let nutrients or required ions to enter the cell. It protects the cell by controlling what substances enter the cell and keeping inside what must remain, this is referred to as selectively permeability. To give a scale to the permeability we use the permeability coefficient as the number of molecules per area and time divided by difference in molecule concentration between the two sides of the membrane. Biological membranes have a high permeability coefficient for water of around 10^{-3}cm/s, a much lower coefficient for bigger molecules such as glucose of around 10^{-7}cm/s and extremely low for charged ions like Na^+, K^+ or Cl^- around 10^{-10}cm/s up to 10^{-12}cm/s [3]. The difference in orders of magnitude for this coefficient between different molecular species show how the membrane is designed to keep a chemical and specially an ionic balance between the inside and the outside.

Anchoring point for proteins and other structures: One of its most important functions is as attachment point for different cellular structures and systems for different cells, like the cytoskeleton, the cell wall, or any kind of membrane-bound protein. In **Figure 1.1** can be seen a sketch of a membrane with a wide variety of membrane bound proteins are represented, which will add functions to the membrane and to the

cell. The different proteins on the membrane surface specialise the membrane, from being merely the walls of the cell to regulating ionic concentration, anchoring, communication with other cells and a long etcetera. In the end most of the membrane specific tasks ar performed by membrane proteins and end up defining the functional properties of the membrane [4]. The number of possible extra functions of the cell are all the possible membrane proteins functions, although the few mentioned are the most prevalent ones.

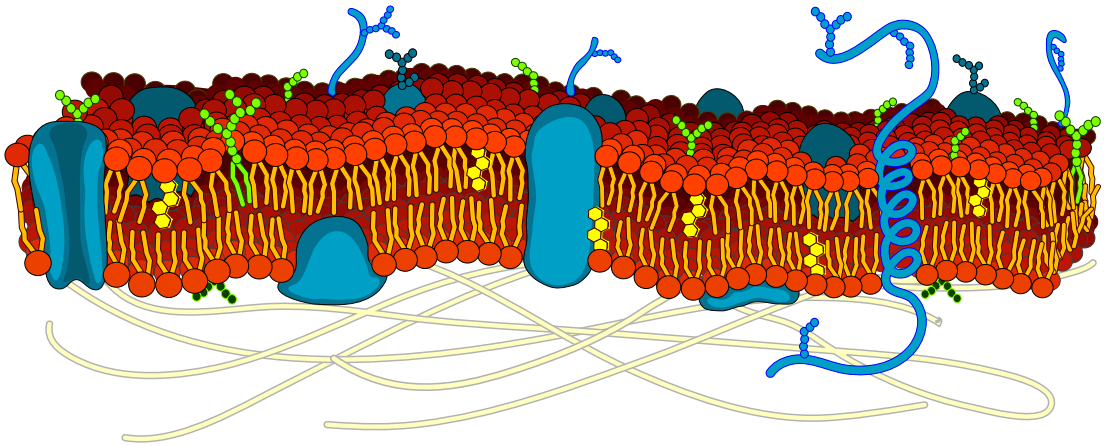

Figure 1.1: Diagram of a cellular membrane. In red and orange we can see the amphipathic molecules, usually phospholipids, that form the base of the membrane. Attatched to this membrane we can see how all kinds of proteins can be adhered to the membrane. Some only adhere to a monolayer, some to both, while others are anchored to the membrane but extend out. Image by LadyofHats, Public domain, obtained via Wikimedia Commons.

Signalling: An important job of the membrane is signalling, as when the environment changes the cell has to adapt and cells exchange information between them to be able to better react to changes. This cell to cell communication relies on the membrane having receptor proteins that are specialised in one kind of extracellular signal molecule. The binding to a receptor protein then initiates a specific intracellular signalling pathways that will initiate a specific response to the signal. Typical signals that eukaryotic animal cells receive include growth and division, cell differentiation into a new type of cell, survival, or death also called apoptosis [4].

1.1.2 Composition and structure

The composition of the cellular membrane consists on a special kind of lipids called amphipathic lipids, mainly phospholipids, glycolipids, and sterols. The lipid compositions of the inner and outer monolayers can be different and for different cells with different functions we will find variation in the composition of the lipids that form the

membrane. These amphipathic lipids consists of an elongated lipid with a head and a tail. The head is hydrophillic while the tail is hydrophobic and usually made up of fatty acid tails. This structure while may not give special properties to a single phospholipid molecule it does for a collective. When enough amphipathic lipids are present in a water solution, due to their hydrophobic-hydrophillic structure, they spontaneously assemble into structures like lipid bilayers or micelles [4].

Big part of the membrane composition depends on proteins, and the amount and types of proteins are highly variable. From Alberts et al [4] we can see a few examples of how much the proteins in the membrane composition can vary: from the the myelin membrane, which serves as electrical insulation in axons, less than 25% of the membrane mass is protein, to the the membrane of mitochondria and chloroplasts where approximately 75% of the mass is protein. In general cellular membranes will have about half of the membrane mass accounting for proteins. However this huge proportion of mass by the proteins is caused because the lipids that form the membrane are smaller and lighter than the proteins. So in number there will always be many more lipids than proteins in the membrane.

As stated before, the lipids on the membrane can flow and diffuse on the monolayer they are located in. The fluidity and diffusion of the bilayer will depend in the temperature and its composition, and in the event of a temperature change a cell can change the composition of its membrane lipids to maintain its fluidity. If the temperature falls beyond the critical temperature –for that specific membrane composition– the membrane will phase transition into a gel state, which is in general bad for any given cell.

1.1.3 Self-Assembly

Self-assembly of the membrane is the process by which an organised structure, in this case the membrane, is formed by simply having the components that form it together in a thermal bath. This happens because the energy of the system when forming the final structure is lower than the energy when all the components are individually floating in water. The difference in the total energy between the dis-organised and self-assembled state is what will drive the system to favour one of the two states. As the building blocks move randomly, driven through thermal fluctuations, they will attach and stick with the other building blocks when the combination lowers their total energy. Liposomes, micelles, bilayers, Langmuir-monolayers are different structures that minimize the energy of each amphipathic molecule by avoiding contact of the hydrophobic tails with water and ensuring the heads are in contact with water. This in turn minimizes the energy of the system, thus being energetically favorable state.

Different amphipathic lipid molecule shapes will assemble in different structure, an example of this can be seen in **Figure 1.2**, and as can be seen represented the shape

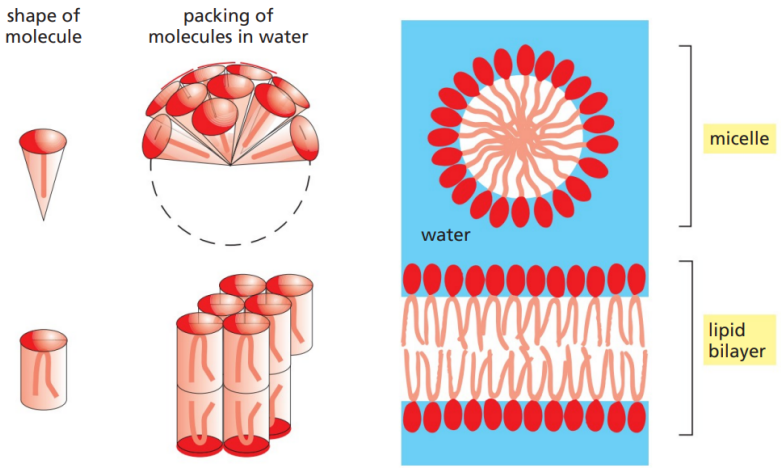

Figure 1.2: Two different self-assembled configurations for two different amphipathic lipid molecules. The shape of the molecule will give two different equilibrium configurations where the contact with water is maximised for the hydrophilic part and minimised for the hydrophobic part of the molecule. Adapted from Alberts et al. [4].

of the lipid molecule can decide in which way the molecules self-assemble. Moreover, even if two different kinds of lipids self-assemble both into bilayers, the shape of their lipid molecule can give different inherent mechanical properties to the membrane.

1.1.4 Active membranes

Life is an out of equilibrium ongoing process, we will go back to equilibrium the day we perish. This is reflected at the microscopic level by the cells spending energy to fulfil their needs, and that is why they need food to survive. This spending of energy is what characterises an out of equilibrium process.

The expense of energy is what categorises what is an active system, contrary to a system which does not require this expenditure of energy i.e. a passive system. From a thermodynamical point of view, active matter refers to a system where its constituents convert stored or ambient free energy into movement or force. Most of the field studies self-driven particles referred to as active particles. Each active particle consumes and dissipates energy, generally leading to motion [5]. However in the biological active matter field there is additional active systems that do not only consist of swimmers or active particles. These are the active membranes, where a biological membrane can exhibit also a consumption of energy to change its shape or properties [6, 7].

As stated before, cellular membranes can gain additional functions by adding proteins to their surface. In some cases this proteins work passively and change the membrane mechanics and behaviour just by being there. However, sometimes this proteins can only carry their work in the presence of energy sources, in the form of ATP. Such

"active" proteins give the name to the active membranes since J. Prost and R. Bruinsma coined the term [6]. In this first work on active membranes Prost and Bruinsma studied if the attaching and detaching of the cystoskeleton to the membrane could be adding extra fluctuations to the membrane. Red blood cells are also believed to have an active membrane along many other cells.

1.2 Red Blood Cells

Red blood cells are the cells that deliver oxygen in the vertebrate bodies through the circulatory system. Healthy red blood cells have a very recognisable shape called biconcave discocyte as can be seen in **Figure 1.3**. These cells are the ones that give blood its characteristic red colour as they are the most numerous kind of blood cell. Red Blood Cells (RBC) are the perfect cell to study the membrane thanks to its simple structure that relies a lot on its membrane properties. This simplicity arises from the fact that the human red blood cell, in contrast to the other cells, contains no organelles. Most cells have multiple structures specialised in a variety of functions, like the mitochondria (the powerhouse of the cell) or the Golgi apparatus (where proteins are collected and then dispatched from). The human red blood cell lacks all organelles, its function being oxygen delivery using the hemoglobin it carries inside. The flexibility characteristic to the red blood cell is required to be able to go through small micro-capillars. The cells and their membranes also have to be durable, as the cells need to survive 120 days in circulation.

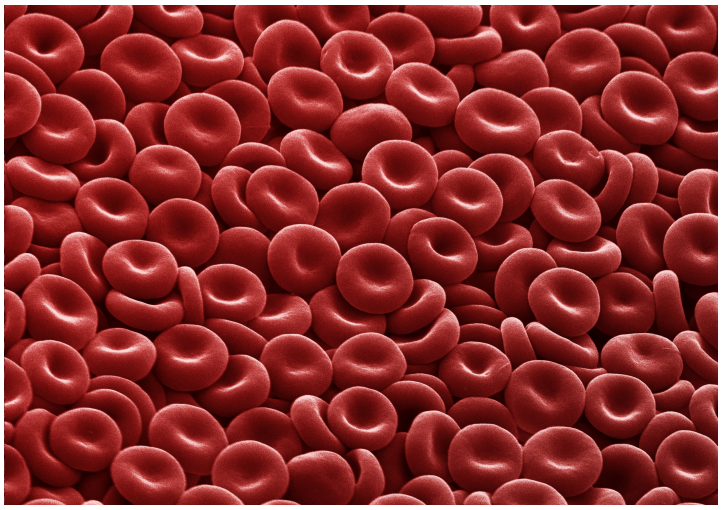

Figure 1.3: Red blood cells (or erythrocytes) with their normal biconcave discocyte shape, sometimes called discoids. Annie Cavanagh, CC BY-SA 4.0, via Wikimedia Commons

Its cytoplasm contains hemoglobin, a type of metalloportein containing iron to

which oxygen adheres by diffusion when the red blood cells pass through the lung capillars. In the case of human red blood cell, having no nucleus and no cytoskeleton, the cell function is to carry hemoglobin, which takes about 96% of the red blood cells dry content (excluding water) [8].

Due the simplicity in its structure, human red blood cells have been extensively used as models for the cellular membrane, and that is why this cell in particular will be interesting. Before going into the mathematical modelling, there are a few more quirks of the red blood cell that should be mentioned first.

1.2.1 Spectrin network

Red blood cells have a lattice of spring-like proteins attached to the membrane, the spectrin network. This network has a hexagonal lattice order as can be seen in a diagram in **Figure 1.4** and it consists of actin filaments and spectrin. In real cells there is gaps in the hexagonal network and usually is in a relaxed state, so the "springs" are not stretched. The spectrin network is only relevant under in-plain shear stresses, as a way to protect the integrity of the cell. The overall relevance of this spectrin network in the membrane mechanics of the red blood cell is still discussed [9, 10].

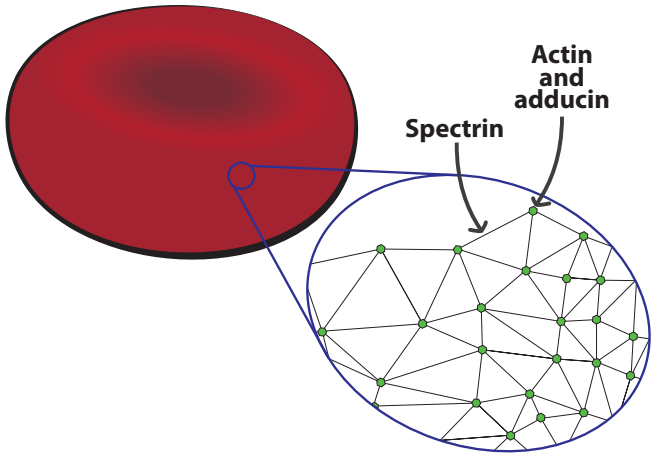

Figure 1.4: A red blood cell has a microscopic spectrin network attached to it that makes an approximately hexagonal lattice. The spectrin network is connected to the membrane at the vertices by proteins.

Experimental works for different values of cytoskeleton elasticity for healthy cells exhibit a faster shape evolution at higher cytoskeleton elasticity [9]. However, there seems to be no change in the final shape of the red blood cell, simply shorter time scales in the shape evolution [9].

1.2.2 Active nature of the red blood cell

It is also strongly believed that the red blood cell membrane spends energy, this is not completely proven but there are many experimental data that strongly point in that direction. In physics and in science, is hard to say that something is proven, however that does not mean it is not widely accepted [11, 12]. Mostly the only thing left to discover is which part of the membrane is the one expending this energy and for which function it is doing so.

The red blood cell membrane uses energy in form of adenosyne triphosphate, also known as ATP, for some kind of non-equilibrium process [12, 13]. It has been seen in experiments that in absence of ATP the red blood cell membrane can have a harder time maintaining its normal biconcave discoid shape [13]. Not all cells lose the shape but more do than in presence of ATP. The activity could be stabilising the shape of the membrane, or increasing its flexibility, deformability or other mechanical parameters.

The one thing most of the literature agrees, is that this non-equilibrium behaviour of the red blood cell membrane is not dominant. For example most of the fluctuations of the membrane seem to be of a passive thermal nature [10]. Therefore, there is no need to add the active nature of the membrane to study the behaviour of this cell.

It should be emphasised that there is no intention here to downplay how fascinating this facet of the red blood cell is. The active matter field is thriving and of great importance in condensed and soft matter, and special in biophysics. This field will be of great importance for the biophysics field future.

1.2.3 Diseases and illnesses that affect the membrane shape

The interest on the red blood cell is not only generated by the fact that it has a simple structure which makes it easy to model. On top of this, a number of illnesses and diseases affect the red blood cell directly. Alterations on the red blood cell can be studied from a physical standpoint as the function of this cell rely in its mechanical properties. Some of these diseases are malaria, sickle cell anaemia, or spherocytosis.

Malaria

Malaria is a life-threatening disease caused by parasites called Plasmodium that are transmitted to people through mosquitoes. The World Health Organisation estimates that in 2019 there were around 229 million cases of malaria worldwide and caused an estimated of 409 000 deaths in that year alone [14].

This parasite invades the red blood cell and eats the hemoglobyn that the cell carry. As the red blood cell is devoid of internal organelles and lacks the ability to synthesise proteins, in order to be able to survive and multiply inside the cell, the parasite needs to make modifications to the infected cell [15]. The parasite will add to the red blood cell membrane surface proteins that will enable the parasite to adhere to other cells [15].

Plasmodium goes to a great extent to remodel the infected cell: it looses its smoothness, becoming rough and the appearance of knobs on the erythrocyte membrane, as well as increased rigidity is caused by the parasite.

This increment on the rigidity of the membrane will be what will end up becoming deadly. As usually the red blood cells have to go through microcapillar smaller than themselves and need great deformations go through. Taking this into account, increasing the rigidity of the red blood cells can burst micro-capillars, which in the brain could be deadly or induce cerebral damage [16].

Sickle cell disease

First discovered in 1910 [17] the sickle cell disease is named after the sickle-shape it gives to the red blood cells. These sickle-cell diseases are different genotypes that produce similar characteristic syndrome of sickle-shaped cells. The different sickle-cell diseases are caused by a mutation in the β-globin gene, that makes haemoglobin. The most common type is sickle-cell anaemia, which refers specifically to the variant form of the gene known as β^S [18].

The mutation changes the molecular structure of the haemoglobin molecule, that is why this disease was coined as the first discovered molecular disease. The disease results in binding two chains of the haemoglobin molecule that results in the chaining of different haemoglobin molecules resulting in a kind of crystallization that generates a long polymer that grows up to fill the entire red blood cell. This long and rigid polymeric chain changes the final shape of the red blood cell, increasing the rigidity of the cell and difficulting the red blood cell task. Moreover it also promotes cellular dehydration, with physical and oxidative cellular stress [18]. The rigidity increase and the sickle-shape influence can be studied from a biophysical point of view, making the disease interesting to model.

Spherocytosis

Hereditary spherocytosis refers to a group of anaemias that are characterised by the presence of spherocytes, red blood cells that have developed a spherical shape [19]. The source of the shape-change from bi-concave disk shaped to sphere arises from a loss of cohesion between the lipid bilayer and spectrin network [20, 21]. This can produce a destabilisation of the bilayer which leads to release of lipid vesicles which in turn reduces the total membrane of a red blood cell. The loss of membrane is associated with defects in several membrane proteins [19]. The spherical red blood cells are mistaken by the spleen as old red blood cells and destroys them. This is how spherocytosis makes the affected person anaemic. The disease is of genetic origin, that is why it is an hereditary condition.

The spherical shape is less flexible compared to the biconcave discoid. The spherocytes are also more osmotically fragile, breaking easily with osmotic changes than

regular red blood cells. As most blood diseases and conditions hereditary spherocytosis ends up changing the membrane and the cell mechanical properties.

1.3 Dynamics of the membrane

A great deal of theoretical and experimental studies on membranes and cell shapes have been on equilibrium shapes [22, 23, 24]. Some processes like tube pearling, tubuling formation, shape morphology, etcetera can be studied with an static system. However, there is a limit of information that we can obtain from an static membrane. Static membranes can give only a limited set of information, mostly the surface, volume enclosed, and the static equilibrium shape.

By dynamics we refer to changes in the membrane born from interactions with the the external world or changes produced by itself that change the membrane completely. Adding an external field, division of membranes through fission, studying the temperature effects, are some examples of what we refer to by membrane dynamics.

Introducing external stimulus and looking at their changes and evolution we can obtain more information. The membrane could be stressed and poked directly using optical tweezers or micro-pipettes [25, 26]. More indirect methods like using a fluid flow as for example in a micro-channel [9] can be less invasive and used to see multiple cells in a row instead of having to focus merely on one. The dynamics of other processes like division can also tell us information of the membrane mechanical properties.

1.3.1 Deformation under shear flow

A basic way to induce stress and deformation to a single membrane without making direct contact with it is to put it under a fluid flow. To observe single cells deforming by a flow one would use a microfluidics channel and a microscope. An example of such experiments can be seen in **Figure 1.5**, adapted from [9].

The fluid tries to flow as it would in the absence of cell, however the cell presence will be an obstacle that will slow down the fluid advance. In the case of a rigid body the fluid would simply carry the object with it, however the cell is not a rigid object. In response to the obstacle the fluid will subject the cell to hydrodynamic forces, that instead of simply moving the cell will also deforming the membrane. This changes the cell shape as we can see in **Figure 1.5**, and the resulting shape will depend on the membrane properties, the fluid speed, and viscosity.

Therefore, the properties of the membrane can be studied by putting it in a controlled flow. How the membrane mechanical properties change can be studied by comparison of the different studied cells to cells with known properties or by mathematical modelling of which shapes should be obtained under different flows.

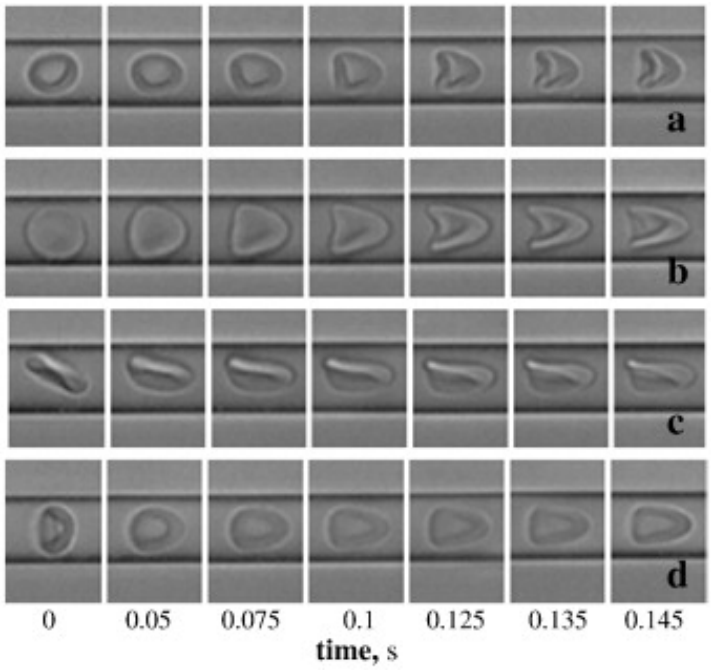

Figure 1.5: A variety of red blood cells moving through a micro-channel with the flow. In **a**, **b**, and **d** parachute-like shapes are obtained after enough deformation. Instead in **c** slipper-like shape is observed. Figure adapted from G Tomaiuolo and S Guido [9].

1.3.2 Topological transitions

Topology is the branch of mathematics that studies how mathematical functions (in our case surfaces) maintain some properties after a continuous deformation, regardless of how large this deformation is. When studying a surface and its shape one can define what is called a continuous deformation as a deformation that does not require to cut the surface, such as stretching, twisting, or bending. A topological transition then refers to an event in which the studied surface undergoes a discontinuous deformation such as opening or closing holes, tearing, gluing. For example, a deformation from a sphere to a torus (or doughnut) like in **Figure 1.6** requires a topological transition.

For cell membranes the most common topological transitions are fusion and fission. Fusion and fission are key in many processes, from mitosis to the transport of residues and proteins. There is no need to go from two spheres to one to have a membrane fusion process, as an example of fusion can be seen in **Figure 1.7.** Fission of the cellular membrane happens in organelle division and during endocytosis and it is necessary in many physiological functions like the release of neurotransmitters in the synapses and in muscle contraction [27]. Meanwhile, both fission and fusion are very important in the endoplasmatic reticulum membranes [28]. In fact one recent Nobel prize in

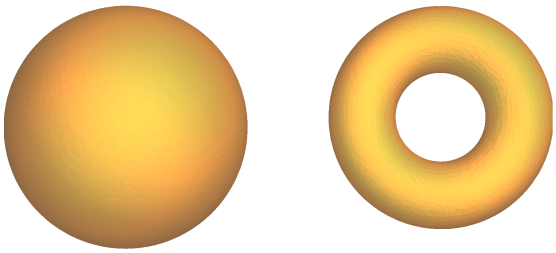

Figure 1.6: The change from a sphere to a torus requires a topological transition as we go from a continuous surface with no holes to a surface with a hole.

biology has been given for the study of the transport system on the Golgi apparatus, where vesicles are constantly incoming and outgoing. The Golgi apparatus, represented in **Figure 1.8**, is specially active in this topological transitions and the description and expansion of our understanding on this topic has been deemed deserving of a Nobel prize.

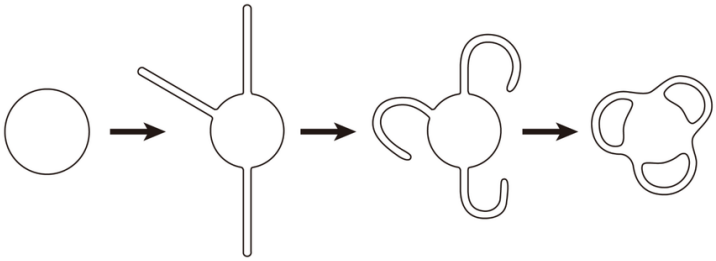

Figure 1.7: In cells there are many methods and processes in which a membrane may change its topology and genus. The pictured process is how tubules could give rise to cisternal fenestrations. Adapted from Glickand Nakano [29].

There are recent works on the relevance of this subject as the Topical Review "*The 2018 biomembrane curvature and remodeling roadmap*" [30] trying to predict which topics will be the most relevant on the research of biological membranes. In this article we can find that a third of the topics addressed where on the subject of fission and fusion.

1.3.3 Thermal fluctuations

While unmoving cells are usually referred to as having a static membrane, membranes are so flexible and have such a low rigidity that they move simply by temperature. The combination of the soft mechanical properties of the cellular membrane with its small width generates a very dynamic structure that undergo constant shape fluctuations

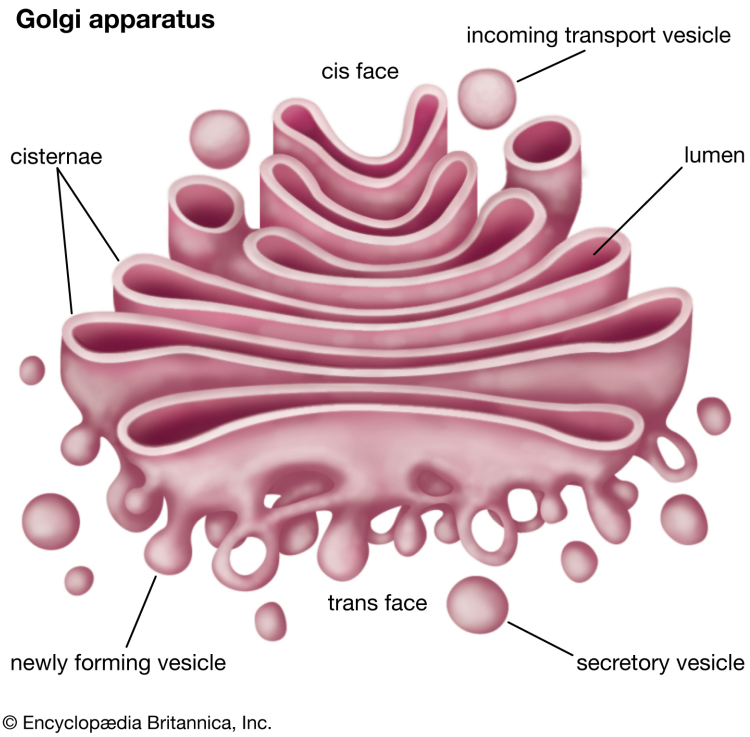

Figure 1.8: Topology transitions are constant in some systems like the Golgi apparatus. We can see a scheme of this cell organelle, formed by a biological bilipidic membrane. Topological changes are constant in this membrane. By courtesy of Encyclopædia Britannica, Inc., copyright 2018; used with permission.

mostly due to thermal noise. The random movement of the liquid molecules associated by the thermal noise can make the membrane fluctuate. The movement and oscillations of the membrane associated with temperature can also characterise the membrane mechanical properties.

The experimental study of membrane fluctuations to study the cell characteristics is typically done with red blood cells as its a simple cell without nucleus, which makes easier to study just the membrane. Some experiments on red blood cell deformation consist on using optical tweezers combined with the Fluctuation Dissipation Theorem [11, 12] or micro-pipette techniques [31]. But the red blood cell has also been studied by observing its thermal fluctuations, either in flickering microscopy (also called video microscopy) experiments [10, 32, 33, 34] where they use an optical microscope or with more sophisticated Diffraction Phase Microscopy [13, 35, 36]. These last approaches may have some restrictions in the information available to obtain but it also ensures that the results obtained are intrinsic to the membrane, independent of the experimental method and not altered by scale-dependent effects of the cell. We can see in Figure

1.9 an image of Diffraction Phase Microscopy of different red blood cells from [13].

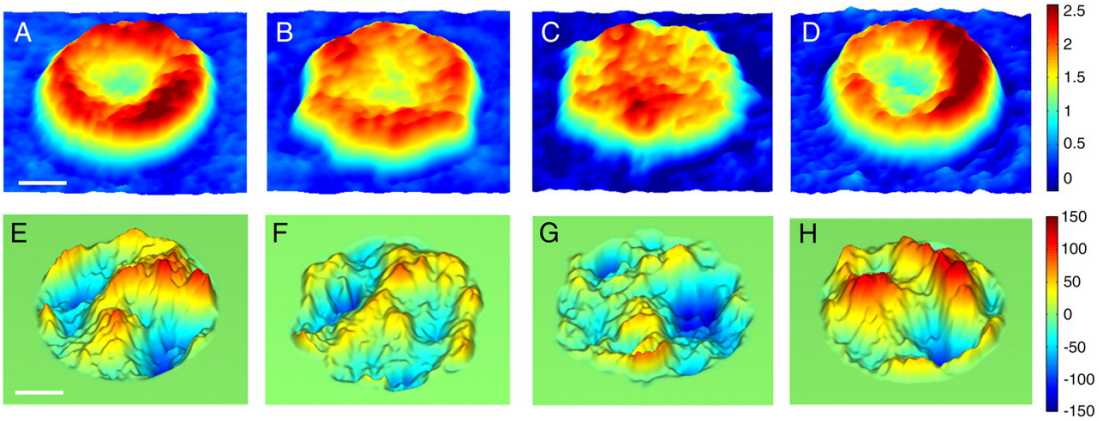

Figure 1.9: Different shaped red blood cells studied using diffraction phase microscopy. On top we have the shape of "top half" of the cell given by the membrane average position. On the bottom we have the fluctuation of the membrane position from respect its average position. Adapted from Y Park et al. [13].

In the end, temperature influences to a degree all events for the membrane: from its shape to its dynamics; and can promote or prevent a variety of processes. In some cases to reach a true equilibrium state you might need a little kick to start the evolution towards equilibrium. Sometimes even if a process might be energetically favourable it might be lost due to the noise that the temperature introduces. To top it all, one cannot simply avoid temperature effects by lowering it, as living beings need a comfortable temperature to be able to survive. And of course, studying living organisms is also limiting also how high the temperature can be so that the cell and membrane does not denature and break down.

Chapter 2

Membrane modelling

In this chapter we will explain the basis that will be used through all of the thesis. We want to model biological membranes and first of all we will start with a static membrane without external stimuli. Then using this model we will study different dynamics and phenomena by constructing on top of it.

2.1 Elasticity theory

Physical systems can be described by their energetics, as the forces acting in the system will point towards lowering its total energy. This can be easily done for point-like or hard bodies, defining the forces and energetics on its center of mass. However, for softer bodies we have to define the forces that happen at each point of the object.

The energetics of a surface that can deform will depend on all the points of the surface and its geometrical properties like area and volume. For example, a small water droplet is dominated by a surface tension which will try to minimise the droplet surface area. Depending on the surface tension coefficient between the water and the air and the surface tension between the water and the solid that contains it the final droplet shape will be different, as represented in **Figure 2.1**. Highly hydrophobic surfaces will give a round droplet as it tries to minimise its contact with the surface, meanwhile a highly hydrophilic surface will give a flat droplet.

2.1.1 Defining a surface

A membrane is at its core a surface that divides two different spaces. So, to properly define a membrane one needs an accurate explanation of a surface, its position, and its shape. These surfaces can be described with two different mathematical methods. Firstly by using an implicit form where we have a function $F(x,y,z) = 0$ which for the points (x,y,z) where the membrane is located the function is equal to zero. Secondly one can use the parametric form where one will have three different functions $x = f(u,v)$, $y = g(u,v)$, and $z = h(u,v)$ which determine a vector position $\vec{r}(u,v)$. Commonly

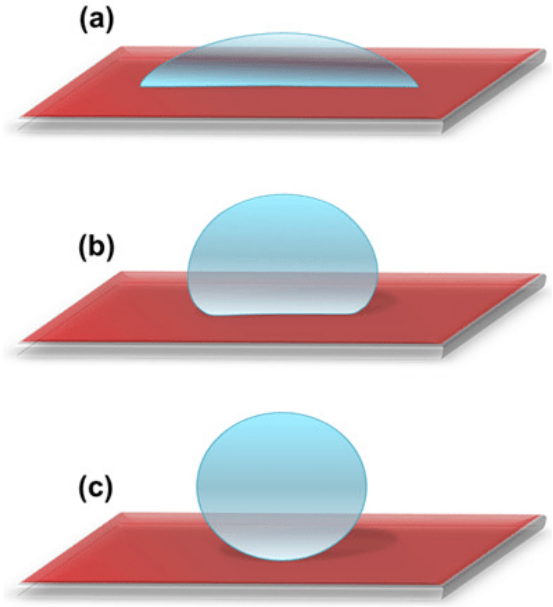

Figure 2.1: Wettability of water is defined by the surface tension coefficient between a material and water. The top **(a)** is a highly hydrophillic surface while the bottom **(c)** is a highly hydrophobic one. Adapted from Latthe et al. [37].

the parametric form is used by using (x,y) as the free parameters and then the function $z = h(x,y)$ as the height function of the surface. This makes so that one can work by simply using one function that gives the distance of the surface with respect to a (x,y) plane. This is the so-called Monge parameterisation which can only be used for surfaces that differentiable and are mostly flat and therefore are not multi-valued at any point of space. Reaching the final expression for this Monge parameterisation

$$\vec{r} = (u,v,h(u,v)) = (x,y,h(x,y)). \tag{2.1}$$

2.1.2 Bending energy

Not all interfaces are characterised by the surface tension. One can define the energetics of a surface in function of the position h of such surface. Lets start by defining a energy functional f as function depending on the position of the surface h and its derivatives

$$f = F\left(h(\vec{r}), \nabla h(\vec{r}), \nabla^2 h(\vec{r})\right). \tag{2.2}$$

The term $h(\vec{r})$ corresponds to the position of the membrane, the term $\nabla h(\vec{r})$ to its possible rotational orientation and $\nabla^2 h(\vec{r})$ to the curvature of the surface. The representation

of these deformations can be seen in **Figure 2.2** where translation bending and rotation are represented for a surface.

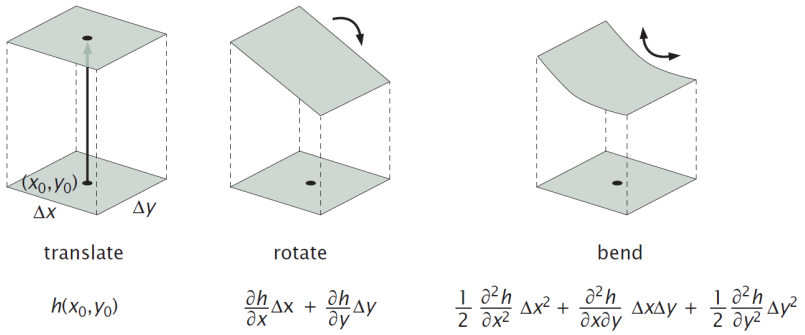

Figure 2.2: The terms in the expansion of the height function take a flat patch of the bottom reference plane and map it onto a patch of the deformed membrane. Adapted from [3].

The curvature at a given point of the surface can be defined by two circles that cross over each other at the given point like in **Figure 2.3**. However, as one can change arbitrarily the orientation of the plane where the circle is defined, there will be an infinite amounts of sets of two circles that can match the curvature at the point. However, there is only one set of two circles that will take two extreme values, one high and one low. Thus to define the curvature at a given point in the surface what one uses are the two orthogonal planes that give these two values. These are the so called principal curvatures

$$C_1 = \frac{1}{R_1} \quad , \quad C_2 = \frac{1}{R_2}. \tag{2.3}$$

Which are the eigenvalues of the curvature tensor **Q**. The curvature tensor is a 3×3 matrix but has rank 2, and thus it only has 2 nonzero eigenvalues. It is written as

$$Q_{ij} = -\hat{n}\partial_{ij}\vec{r}, \tag{2.4}$$

where $\hat{n}$ is the normal vector, $\vec{r}$ corresponds to the three dimensional position, and ∂_{ij} is used as an abreviation for two derivations respect to i and j where i, j can take x, y, z. This tensor **Q** can be written in the Monge parametrisation by taking equation (2.1) which defines a surface position as $\vec{r} = (x, y, h(x, y))$ leaving us with a curvature tensor **Q** as a 2×2 matrix that reads

$$Q_{ij} = \frac{\partial^2 h(x,y)}{\partial x_i \partial x_j}, \tag{2.5}$$

where $x_1 = x\ x_2 = y$.

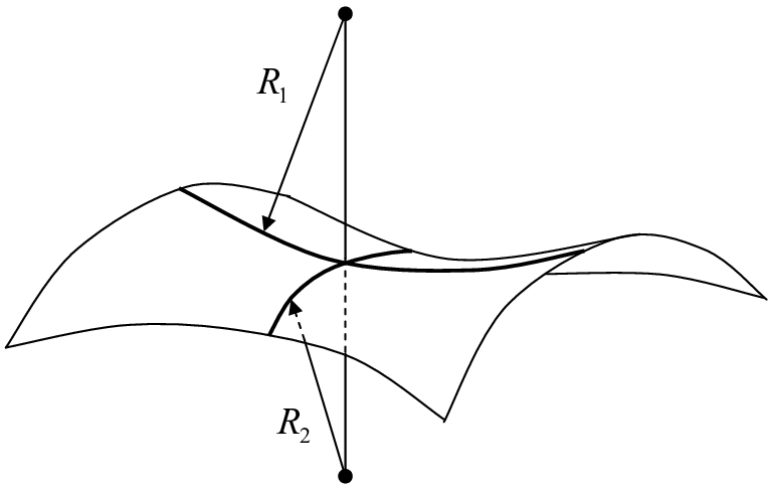

Figure 2.3: Diagram of a the two principal curvatures of a surface and the two corresponding radii of curvature that characterises it. Adapted from Hale [38].

Looking back at **Figure 2.2**, it would make no sense for the energetics of the surface to depend on position in space if we are not applying heterogeneous external fields. The same with the orientation as one expects that a surface can be rotated without any energy cost. Therefore from equation (2.2) the curvature term $\nabla^2 h(\vec{r})$ is the only one left, which represent all the curvature terms

$$f = aC_1 + bC_2 + cC_1^2 + dC_2^2 + eC_1C_2 + \mathcal{O}(C_i^3).$$

However, having an energy like this would imply that the energy cost of curving the surface in one direction is different than the other. For an homogeneous surface with no preferred direction it makes no sense. Therefore $a = b = 0$ and one is left with only the superior order terms, leading to

$$f = C_1^2 + C_2^2 + C_1C_2 + \mathcal{O}(C_i^3).$$

Therefore, the energy of the surface in the case of a constant surface area will depend on the curvature term squared and the crossed curvature terms. These, are the total and Gaussian curvatures respectively.

In the 70s Canham and Helfrich proposed the total curvature of a surface to model the biological membrane [22, 39] in combination with physical constraints. This total curvature C can be defined at any point of a surface by two radii of curvature like in **Figure 2.3** which is written as

$$C = \frac{1}{R_1} + \frac{1}{R_2}. \tag{2.6}$$

There is always the chance to work with the mean curvature H, which is proportional to the total curvature, and is written like

$$H = \frac{1}{2}\Big(\frac{1}{R_1} + \frac{1}{R_2}\Big). \tag{2.7}$$

With this expression we can compute the total curvature of any point on a surface, for any continuous surface can have its curvature at any point described by two radii of curvature, in our case named R_1 and R_2. An diagram representing the curvature of a point using two radii of curvature can be seen in **Figure 2.3**. Sometimes in the literature the bending energy is described using the mean curvature H. Although there is only a difference of a $1/2$ term it must be taken into account that these two expressions of the curvature are different.

There is a second curvature term that plays a role in the bending energy, and that is the Gaussian curvature, which is written as

$$K = \frac{1}{R_1} \cdot \frac{1}{R_2}. \tag{2.8}$$

This term is sometimes disregarded because, as the Gauss-Bonnet theorem states, its integral over a surface is constant and a topological invariant. Therefore this term will be taken into account only in cases where one membrane will either fission into two membranes or two are undergoing fusion into one.

We can write both of these curvature terms using the Monge parametrization. For a surface defined by $z = h(x,y)$ one needs to only define the total curvature C and the Gaussian curvature in terms of h, x and y. So, if h_i represents the derivative of h respect the parameter i where i can be either x or y, the total curvature is written as

$$C = \frac{(1+h_x^2)h_{yy} + (1+h_y^2)h_{xx} - 2h_x h_y h_{xy}}{\sqrt{(1+h_x^2+h_y^2)^3}}, \tag{2.9}$$

and the Gaussian curvature as

$$K = \frac{h_{xx}h_{yy} - h_{xy}^2}{(1+h_x^2+h_y^2)^2}. \tag{2.10}$$

Both of these equations can be simplified for a nearly flat surface [40]. Under this condition $h_x \ll 1$ and $h_y \ll 1$, and then the Gaussian and total curvature can be approximated to

$$C \approx h_{xx} + h_{yy}, \tag{2.11}$$

and

$$K \approx h_{xx}h_{yy} - h_{xy}^2. \tag{2.12}$$

Finally, using the curvature of a surface at any given point one can write the bending energy. This free energy depends on the squared curvature, giving no single sign of the curvature preference. For a surface Ω the bending energy is written as follows

$$F_B = \int_\Omega \Big(\frac{\kappa}{2}(C - C_0)^2 + \kappa_G K\Big) dS = \int_\Omega \Big(2\kappa(H - \frac{C_0}{2})^2 + \kappa_G K\Big) dS, \tag{2.13}$$

where C_0 is the spontaneous curvature, K the Gaussian curvature, κ the bending modulus, and κ_G the Gaussian (or saddle-splay) modulus. Both moduli represent the energy cost of changing the curvature term they accompany. The spontaneous curvature which refers to a possible intrinsic curvature of the surface. This can happen due to the molecular composition of the membrane lipids or due to attached proteins or other objects on the membrane surface that generate an intrinsic curvature. The spontaneous curvature can be written as the inverse of the spontaneous radius of curvature

$$C_0 = \frac{1}{R_0}, \tag{2.14}$$

where the spontaneous radius of curvature R_0 is the preferred radius of curvature that the membrane would take where it possible to do.

Usually, for interfaces, the bending term is of second order importance due to the surface tension. However, for biological membranes the surface area of the system cannot easily change and this practically eliminates the relevance of the surface tension. The bending energy is the base for the membrane energy, but the nature and composition of the membrane gives rise to additional physical constrains.

2.1.2.1 More on Gaussian curvature

The Gaussian curvature can be defined by a wide variety of ways. In this thesis will be defined by either by the radius of curvatures R_1 and R_2 (as seen in the previous section), the principal curvatures C_1 and C_2, or by the curvature tensor $\mathbf{Q}$. The curvature tensor can be seen in equation (2.5) and the principal curvatures in equation (2.3). The principal curvatures also match with the maximum *normal* curvature and the minimum *normal* curvature [41] and can also be obtained from the curvature tensor $\mathbf{Q}$.

As stated in the previous section, the curvature tensor $\mathbf{Q}$ is a rank 2, 3×3 matrix with three eigenvalues. One of the eigenvalues is zero and also has a determinant equal to zero [40]. The previously presented principal curvatures of the surface C_1 and C_2 will be the non-zero remaining eigenvalues. The Gaussian curvature then can be

written either as function of the principal curvatures like

$$K = C_1 C_2 \tag{2.15}$$

or as a function of the curvature tensor **Q** like

$$K = \sum_{i,j} \left[\left(Q_{ii} Q_{jj} - Q_{ij}^2 \right) \frac{1 - \delta_{ij}}{2} \right], \tag{2.16}$$

where i and j are the either x, y or z.

The intuitive idea of what the Gaussian curvature is has to be taken from what it tells us about a point on a surface S. While the curvature and mean curvature tells how is the local expansion of the surface near a given point, the Gaussian curvature talks about the overall shape of a region.

Given a point on a surface S the value of the Gaussian curvature will give four different types of points [41]:

- Elliptic if $K > 0$.
- Hyperbolic if $K < 0$.
- Parabolic if $K = 0$ with one of the principal curvatures that satisfy $C_i \neq 0$.
- Planar if $K = 0$ where both curvatures satisfy $C_i = 0$.

For an elliptic point both principal curvatures have the same sign, therefore all the curves that pass this point have a normal vector pointing towards the same side of the surface. This happens for example on all the points of a sphere.

For a hyperbolic point the curvatures are non-zero but have different signs. This means that there are curves whose normal vector points toward a different side of the surface. This happens on the saddle-splay points.

For a parabolic point there is one of the two principal curvatures that is zero, but the other one is not. This happens on a cylinder, as the principal curvature related to the circle is non-zero but the principal curvature that goes along the tube is flat and has curvature zero.

Finally for a planar point the Gaussian curvature is zero but both principal curvatures C_1 and C_2 will be zero. Obviously this is satisfied by a plane surface.

2.1.3 Gauss-Bonnet theorem

The Gauss-Bonnet theorem, as previously mentioned, states that the Gaussian curvature K of a given surface Ω has a constant sum if there is no topological transition. To be more precise, the sum is

$$\int_\Omega K \, dS = 2\pi \chi(\Omega), \tag{2.17}$$

where $\chi(\Omega)$ is the Euler characteristic of the surface Ω. This characteristic is a number that describes a given system –in this case one or multiple closed surfaces– by its number of holes and objects, which can be expressed as

$$\chi(\Omega) = 2(N - g), \tag{2.18}$$

where N is the number of objects and g its genus. Meanwhile the genus g describes the number of holes or handles. For example, a tea cup or a doughnut has $g = 1$ while a football or sphere, which has no holes, has $g = 0$. The Euler characteristic χ is different than the topological genus g in the sense that while the genus only describes the number of holes or handles, the Euler characteristic also takes into account the number of objects. This makes the characteristic χ more useful for studying fission and fusion of membranes.

From the theorem it can also be concluded that in the case that there is no topological transition, one could omit the Gaussian curvature term from the free energy. In this topologically invariant case the Gaussian term only gives a constant offset to the energy, and this will not change the shape or dynamics of the membrane. The only exception to this could be systems where the membrane gets very close to a topological transition, even if it does not finally occur.

2.1.4 Additional physical constrains

From the physical properties of the components that make the membrane two geometrical constrains arise that must be full-filled. One constrain affects the surface area of the membrane and the other affects the volume enclosed by the membrane. The addition of these two constraints will be what differentiates the bending energy from the complete energy that describes a basic cellular membrane.

2.1.4.1 Surface area

For other interfacial systems, like a droplet of oil in water, you can simply stretch the interface because you get molecules inside of the volume that will go to the newly stretched surface. However, in biological membranes we have a constant number of amphiphilic lipids, as the two bulks of fluid in either side of the membrane are water-based. Most cells can synthesise new amphiphilic lipids for the membrane, there are some exceptions like the red blood cell. The process for generating amphiphilic lipids takes a long time and is only useful in cases where a permanent change in surface area is necessary, like in cellular division (mitosis). However, if you take a membrane and suddenly deform it, the membrane will have no way to vary its number of lipids.

As a consequence to this, the amphiphilic molecules of the lipid bilayer have a rather constant distance among themselves, which is usually referred as the preferred area per lipid. We cannot compress them further because of the size of the lipid molecules

and we cannot stretch the membrane without having water molecules getting closer to the hydrophobic tails. Therefore this preferred area per lipid arises from the interplay between the lipid volume and the hydrophobicity of the amphiphilic tails. When stretching the membrane water can get closer to the hydrophobic tails, so it has a big energetic cost. This results in a huge elastic area compressibility modulus for the membrane [42].

Therefore, in the absence of amphiphilic molecules formation, it is very difficult for the total surface area of the cell membrane to change over time. As it also has a huge compressibility modulus the membrane can be treated as a two-dimensional in-compressible material. Both of this things in tandem give rise to the first physical constraint: the need of the membrane to maintain its surface area.

2.1.4.2 Enclosed volume

As explained in the first chapter, the membrane is well-known for its selective permeability. In normal conditions, water can pass through a cellular membrane having a coefficient permeability of around 10^{-3}cm/s but its mostly impermeable to ions with a permeability around 10^{-11}cm/s [3]. This ion impermeability usually is used to maintain a difference in ion concentration between the inside of the cell and the surrounding environment. The ionic imbalance generates an osmotic pressure between the cell and its exterior. Therefore, this osmotic pressure will tend to maintain the volume enclosed in the cell constant.

Thus, any water that enters the membrane must be compensated by water leaving the membrane at another point, making impossible to have a net flux of water leaving or entering the cell. This will be the second physical constraint that a closed biological membrane membrane will have to maintain: the conservation of the enclosed volume.

2.1.5 Complete membrane energy

Now, combining the bending energy equation and the physical constrains, the complete membrane energy can be written. First we will start with the topologically invariant case, taking into account the Gauss-Bonnet theorem we can forgo the Gaussian curvature term K and therefore end with

$$F_M = \int_A \Big(\frac{\kappa}{2}(C - C_0)^2 + \gamma_A \Big) dS + \int_V \Delta p \, dV, \tag{2.19}$$

where γ_A is a term similar to surface tension that will ensure the conservation of surface area, while Δp is the osmotic pressure term that will ensure the conservation of volume.

With this equation we can obtain the equilibrium shape of a membrane for a given surface area and enclosed volume. This can be measured with the surface-volume ratio, also called reduced volume. This reduced volume can be defined as the volume

enclosed by the membrane divided by the volume of a sphere with the same surface area as the membrane area

$$V_r = \frac{V}{\frac{4}{3}\pi(\frac{A}{4\pi})^{3/2}}, \tag{2.20}$$

where V is the membrane volume and A the area. Minimising the energy for a given reduced volume we can obtain the shape of the membrane as can be seen in **Figure 2.4** adapted from Canham [39]. For static membranes, the obtained equilibrium

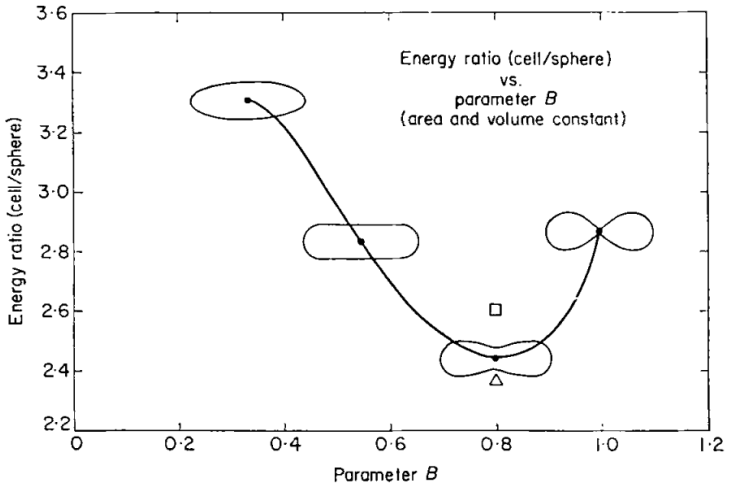

Figure 2.4: Bending energy ratio (cell/sphere) plotted against B, a parameter regarding the integrated membrane curvature. Adapted from Canham et al. [39].

shape depends entirely on this reduced volume. Different reduced volume values give different-shaped cells, however for a reduced volume close to a sphere the equilibrium shape ends up being very similar to a spheroid. The most interesting membrane shapes are found for reduced volume where we have a high surface area for a small enclosed volume.

If we are interested in studying topological transitions, we just have to add the Gaussian curvature term

$$F_{MK} = \int_A \Big(\frac{\kappa}{2}(C - C_0)^2 + \kappa_G K + \gamma_A\Big) dS + \int_V \Delta p \, dV. \tag{2.21}$$

This free energy can be used to describe the shape of cells and vesicles. However, while equations (2.19) and (2.21) work with all vesicles, it can not describe the shape of cells that have a rigid skeleton attached.

To obtain a stable film we will need a positive bending modulus $\kappa > 0$ as a negative bending modulus would imply that infinite curvature would be the most energetically

favourable state. The infinite curvature would mean the complete breakdown of the interface, so the bending modulus must always be positive. Meanwhile, the sign of the Gaussian (or saddle-splay) modulus can be either positive or negative. Membranes with equilibrium isotropic shapes such as spheres or planes have $\kappa_G < 0$, while films that result in saddle shapes will have a positive $\kappa_G > 0$ modulus [40].

Now, before starting to study cell equilibrium shapes or adding dynamics, is necessary a reliable and easy way to solve this system numerically. To this end we will be using a phase field methodology adapted to cellular membranes.

2.2 Phase field methodology

Born from the Ginzburg-Landau methodology phase field models are phenomenological continuum field models used to describe systems with phase separation, i.e. interfaces. Phase field modelization has already been extensively used for modelling of liquid-solid, liquid-liquid, and solid-solid interfaces. The method is mainly applied for phase transitions, like solidification [43, 44, 45] or order phase transitions in polycristalline materials [46, 47]. These methods have also been used to study other phenomenology than phase transitions like viscous fingering [48] or brittle fracture on solids [49]. Phase field methods are specially useful for computing systems with moving boundaries, as computing the explicit position of the boundary over time present difficulties that the phase field methodology circumvents.

More recently, in the past 20 years, it has also been used to study the cellular membrane [24, 50, 51, 52, 53, 54, 55, 56]. The methodology has been applied to study pearling instability [57], polymer induced tubulation [58], the deformation of a red blood cell inside a micro-channel flow [59, 60], or to study multi-component vesicles [61]. The phase field method can reproduce very accurately membrane morphology and dynamics of a cellular membrane. For these phase field models the membrane is taken as the boundary between two liquid phases, the intra-cellular and the extra-cellular liquid.

The phase field models consist on defining an order parameter which defines the phase in a point of space. In the case of the membrane phase field the order parameter ϕ defines which phase the point $(\mathbf{x},t)$ belongs to, either extra-cellular ($\phi = -1$) or intra-cellular ($\phi = +1$). What we are interested in is the membrane that will be defined by the diffuse interface, transition between the bulks $\phi = \pm 1$, that take values in the range $\phi \subset (-1,+1)$.

2.2.1 Diffuse interface

The interface of phase field models is explicitly chosen to have a diffusive behaviour. The advantages of this are that there is no need to explicitly track the exact position of the interface over time, which is a numerical problem not only hard to solve but

also computational consuming. However, to avoid tracking the position we will need to ensure that all the integrals over the membrane surface can be written as volumetric integrals over all the space. This will be the ultimate aim of defining the interface as a diffuse interface.

To this end, a hyperbolic tangent profile is chosen for the interface between two bulk phases of ϕ a representation can be seen in **Figure 2.5**. This function has been chosen

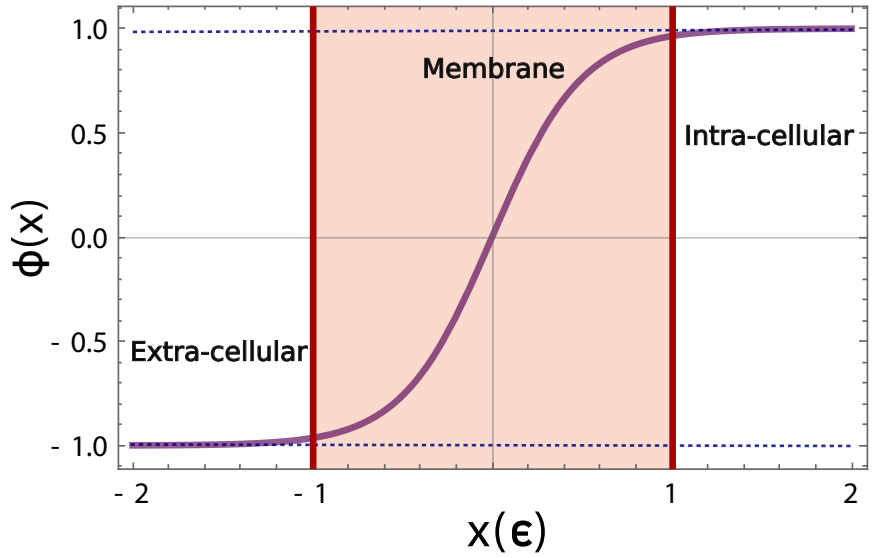

Figure 2.5: One dimensional behaviour of ϕ at a interface between two different fluids defined by $\phi = -1$ and $\phi = +1$. Each ± 1 phase corresponds to the bulk fluid at either side of the membrane.

because of a couple requirements that needed to be satisfied: i) the interface had to be a smooth transition (diffuse) ii) outside of the interface (in the bulk phases) the order parameter ϕ has to reach the values $\phi = \pm 1$ when $\mathbf{x} \to \pm\infty$ for the one-dimensional case. Both of these requirements are meet by the hyperbolic tangent.

Now that we know which shape we want ϕ to have at an interface, we can start defining the phase-field framework, and with that rewriting the free energy using ϕ.

2.2.2 Numerical definitions using phase field

In this section we will go over how can you use the order parameter $\phi(\mathbf{x})$ to define basic numerical parameters that we will use to write a free energy, this can be seen more in depth in [24, 62].

If we want to define the diffuse interface as an hyperbolic tangent we can use the distance to the interface $d(\mathbf{x})$ as the parameter for this hyperbolic function. We

parametrize the width of the diffuse interface with ε and we end like with

$$\phi(\mathbf{x}) = \tanh\Big(\frac{d(\mathbf{x})}{\sqrt{2}\varepsilon}\Big), \tag{2.22}$$

where $\sqrt{2}\varepsilon$ is the width of the interface. Meanwhile the expression of the distance to the interface $d(\mathbf{x})$ is

$$\partial_{ij}^2 d = \frac{\sqrt{2}\varepsilon}{1-\phi^2}(\partial_{ij}^2\phi + \frac{2\phi}{1-\phi^2\partial_i\phi\,\partial_j\phi}) = Q_{ij}. \tag{2.23}$$

Now using this distance $d(\mathbf{x})$ we can define many geometrical properties with a bit of creativity. As such, the normal vector to the surface can be expressed as

$$\hat{n} = \nabla d(\mathbf{x}). \tag{2.24}$$

Having the surface normal vector $\hat{n}$ one can define then the curvature tensor

$$Q_{ij} = \nabla_i n_j, \tag{2.25}$$

as how the normal vector changes along the surface is directly related to the curvature of such a surface. For example for a flat surface, which has zero curvature, we have a constant $\hat{n}$ that does not change while moving through the surface. This equation (2.25) then expresses how the curvature reflects how is the local expansion of the surface near a given point.

Now, using the curvature tensor Q we can write the curvature C and the Gaussian curvature K. The determinant of the curvature tensor Q is always zero [62], but using its trace we can write the curvature [62]

$$C = \mathrm{tr}[Q] = \mathrm{tr}[\nabla_{ij}^2 d_{ij}]. \tag{2.26}$$

The Gaussian curvature from equation (2.16) is a bit more complex being

$$K = \sum_{i,j}\Big[\Big(Q_{ii}Q_{jj} - Q_{ij}^2\Big)\frac{1-\delta_{ij}}{2}\Big].$$

The expression is focused on the non-diagonal elements of the tensor because it is related to the overall shape that the surface takes around a point and whether is plane, curved, or presents a saddle-splay shape.

One then can now go back to the definition of $\phi(\mathbf{x})$ as function of $d(\mathbf{x})$ and use that

to rewrite the curvatures with the phase field order parameter. The result is

$$C[\phi] = \frac{\sqrt{2}}{\varepsilon(1-\phi^2)}\Big(-\phi+\phi^3-\varepsilon^2\nabla^2\phi\Big), \tag{2.27}$$

and

$$K[\phi] = \frac{\varepsilon^2}{(1-\phi^2)^2}\Big(T_1+\frac{2\phi}{1-\phi^2}T_2\Big). \tag{2.28}$$

The terms T_1 and T_2 can be obtained from [62] and are computed from various derivatives of ϕ written for simplicity as ϕ_i where i is either $x\ y\ z$

$$T_1 = \phi_{xx}\phi_{yy}+\phi_{xx}\phi_{zz}+\phi_{yy}\phi_{zz}-(\phi_{xy})^2-(\phi_{xz})^2-(\phi_{yz})^2, \tag{2.29}$$

and

$$\begin{aligned} T_2 = {} & \phi_{xx}(\phi_y)^2+\phi_{xx}(\phi_z)^2+\phi_{yy}(\phi_x)^2+\phi_{yy}(\phi_z)^2+\phi_{zz}(\phi_x)^2+\phi_{zz}(\phi_y)^2 \\ & -2\phi_x\phi_y\phi_{xy}-2\phi_x\phi_z\phi_{xz}-2\phi_y\phi_z\phi_{yz}. \end{aligned} \tag{2.30}$$

The goal with the phase field is re-writing the bending energy as a volumetric integral rather than a integral over the membrane surface. To do this we can write the area differential as a volume differential by using a Dirac delta

$$dS = \delta(d(\mathbf{x}))\,dV. \tag{2.31}$$

Now we need to write the Dirac delta using the phase field. We can use the delta expression

$$\delta(d(\mathbf{x})) = \lim_{\varepsilon\to 0}\Big(\frac{3}{4\sqrt{2}\varepsilon}\mathrm{sech}^4\Big(\frac{d(\mathbf{x})}{\varepsilon\sqrt{2}}\Big)\Big), \tag{2.32}$$

using the derivative $f'(d(\mathbf{x}))$ of the phase field respect to $d(\mathbf{x})$ from [62] which is

$$f'(\frac{d(\mathbf{x})}{\varepsilon\sqrt{2}}) = \mathrm{sech}^2\Big(\frac{d(\mathbf{x})}{\varepsilon\sqrt{2}}\Big). \tag{2.33}$$

With the definition of the Dirac delta we can finally end with the surface differential expressed as a volume differential in the phase field

$$dS = \frac{3}{4\sqrt{2}\varepsilon}\Big(1-\phi^2\Big)^2 dV. \tag{2.34}$$

Now we can use equations (2.27), (2.28), and (2.34) to write the Canham-Helfrich energy using the phase field order parameter ϕ.

2.3 Membrane phase field formulation

Starting of with a membrane that does not undergo topological transitions in tandem with the Gauss-Bonnet theorem, one can start by skipping the Gaussian curvature term. The Canham-Helfrich free energy depends on the squared curvature, trying to minimise $C - C_0$ where C is the total curvature and C_0 the spontaneous curvature

$$F_{C_0} = \int_A \Big(\frac{\kappa}{2}(C - C_0)^2 \Big) dS, \tag{2.35}$$

where κ is the bending modulus. In addition to the curvature term, the terms proportional to γ_A and Δp guarantee area and enclosed volume conservation, respectively. Let start with the free energy (2.35) with an spontaneous curvature $C_0 = 0$ as the most simple case of a bending energy

$$F_B = \int_A \frac{\kappa}{2} C^2 dS. \tag{2.36}$$

To avoid tracking the interface, we will rewrite the energy (2.36) from a surface integral to a volume integral using (2.34). In addition, we will be substituting the expressions for the curvature C (2.27) obtained in the previous section. Using all this, we can write the bending energy as

$$F_B[\phi] = \int_{\mathrm{V}} \Big(\frac{3\sqrt{2}\kappa}{8\varepsilon^3} \big[-\phi + \phi^3 - \varepsilon^2 \nabla^2 \phi \big]^2 \Big) dV, \tag{2.37}$$

for $C_0 = 0$ and without the Gaussian curvature term. This first representation is quite simple, but as adding more things will make it more complex lets now define

$$\Phi[\phi] = -\phi + \phi^3 - \varepsilon^2 \nabla^2 \phi, \tag{2.38}$$

to ease writing the following free energies.

The case with a non-zero spontaneous curvature C_0 is slightly longer

$$F_{C_0}[\phi] = \int_{\mathrm{V}} \frac{3\sqrt{2}\kappa}{8\varepsilon^3} \Big(\Phi[\phi] - \varepsilon C_0 \big(1 - \phi^2\big) \Big)^2 dV. \tag{2.39}$$

With this expression we can compute a membrane that at its energy minimum is curved shape. The parameter C_0 has dimensions of length^{-1} and can take negative or positive values and as explained before is the inverse of the spontaneous radius R_0. Depending on the sign the preferred curvature will be in one direction or the other. Moreover C_0 cannot take a value of $C_0 = 1$ as the phase field would break down. However that is

an extremely large curvature with a spontaneous radius of $R_0 = 1/C_0 = 1$ which would imply a curvature of the membrane thickness length scale, which is extreme.

All in all, the complete membrane energy requires the conservation of area and volume and thus we have to add the Lagrange multipliers to reach a final energy of

$$F_M[\phi] = \int_V \frac{3\sqrt{2}\kappa}{8\varepsilon^3}\Big(\Phi[\phi] - \varepsilon C_0(1-\phi^2) + \gamma_A|\nabla\phi|^2 + \beta_V\phi\Big)^2 dV. \tag{2.40}$$

2.3.1 Bending energy with Gaussian curvature

Lets now do the same without removing the Gaussian curvature term. We can write the bending energy as two separate energies, the term with the square curvature and an energy term of the Gaussian curvature. Combining equation (2.39) with the following Gaussian energy term

$$F_K = \int_\Omega \kappa_G K dS,$$

the complete energy as a phase field can be obtained. To reach this one simply has to substitute dS for its volumetric expression as well as the phase field expression of K

$$F_K[\phi] = \int_V \kappa_G\Big(\frac{\varepsilon^2}{(1-\phi^2)^2}\Big(T_1 + \frac{2\phi}{1-\phi^2}T_2\Big)\Big)dV, \tag{2.41}$$

where the terms T_1 and T_2 have been presented in the previous section.

So finally with this term the complete energy equation in terms of the phase field can be written by combining equation (2.39) and equation (2.41) for a complete bending energy

$$F_{CK}[\phi] = F_{C_0}[\phi] + F_K[\phi]. \tag{2.42}$$

Although, as has been mentioned before, there will be no need yo use this final expression for systems that will not present topological transitions. See the Gauss-Bonnet theorem for details.

2.3.2 Temporal evolution

To compute the temporal evolution of the system, as we have a diffuse interface and two fluids, we will write the dynamic equation using the Fick law [63] writing the temporal evolution of the system as the gradient of a flux

$$\frac{\partial\phi}{\partial t} = \nabla\vec{J}, \tag{2.43}$$

where our flux $\vec{J}$ will be the gradient of the chemical potential μ so we have

$$\vec{J} = \nabla\mu = \nabla\frac{\delta F[\phi]}{\delta\phi}. \tag{2.44}$$

The chemical potential is computed from the adimensionalised free energy by a functional derivative defined in [64] as

$$\mu = \frac{\delta F[\phi]}{\delta\phi} = \frac{\partial F}{\partial\phi} - \nabla\cdot\frac{\partial F}{\partial(\nabla\phi)} + \nabla^2\frac{\partial F}{\partial(\nabla^2\phi)}, \tag{2.45}$$

which when computed for the case without the Gaussian curvature contribution gives us

$$\frac{\delta F_M[\phi]}{\delta\phi} = \frac{3\sqrt{2}\kappa}{8\varepsilon^3}\Big((3\phi^2-1)\Phi[\phi] - \varepsilon^2\nabla^2\Phi[\phi]\Big) - \gamma_A\nabla^2\phi + \beta_V. \tag{2.46}$$

Here we have a κ adimensionalised, as the phase field dynamic equation requires a dimension-less free energy for the dynamic equation. Here we already have the Lagrange multipliers for area γ_A and volume β_V introduced. How will we compute these multipliers and why are they introduced this way will be explained in the following section.

For now however, we can use this to write the dynamic equation as a phase field. The final dynamic equation is ends up being diffusive in nature as ends up being written as a Laplacian of the chemical potential μ, also known as a model B [65],

$$\frac{\partial\phi(\mathbf{x},t)}{\partial t} = M\nabla^2\mu = M\nabla^2\frac{\delta F_M[\phi]}{\delta\phi}, \tag{2.47}$$

where M the mobility coefficient of the phase field.

The mobility of the phase field M will work as the time-scale necessary for the formation and relaxation of the interface. This term will not be critical while we only work with the bending energy without additional external fields or influences. After we add external fields that affect the membrane we will have to ensure that the phase field dynamics do not alter the results.

The diffusive formulation of the dynamic equation enhances the conservation of volume. This kind of formulation where the dynamic equation has the functional derivative of the energy inside a Laplacian what Hohenberg and Halperin called a model B [65]. As there are no source or sink terms in the phase field dynamic equation (2.47) (which would have to be additive, outside the Laplacian) the initial order parameter ϕ phase field will be conserved.

2.3.3 Physical constraints and Lagrange multipliers

Just like in the real world, the computed cells will be required to conserve area and volume. To this end, Lagrange multipliers will be used. However, there are different methods to define and compute the Lagrange multipliers, and the different methods have different advantages.

First of all the expressions for the membrane surface area and enclosed volume using the phase field will have to be defined. The volume is the most straight-forward expression, as simply by integrating the ϕ parameter over the whole volume one obtains the difference of intracellular volume ($\phi = +1$) minus extracellular volume ($\phi = -1$). Therefore the volume to can be expressed as

$$V_\phi = \int_\Omega \phi(\mathbf{x}) dV. \tag{2.48}$$

One could also compute explicitly only the cell volume but, if the size of the system is constant over time, the difference between extracellular volume and the cell volume is also a constant.

The case of surface area is a bit more complex, as there is two different ways to define the area. First expression for the surface area is using the $\nabla\phi$, as the only place where $\nabla\phi \neq 0$ is in the interface. However we have to take into account that at different points of the interface we will have either positive or negative $\nabla\phi$. Taking this into account, as the positive and negative contributions would cancel each other out, we will use the absolute value $|\nabla\phi|$. Using the phase field an area expression can be built as

$$A_{\phi 1} = \int_\Omega \frac{3}{4\sqrt{2}\varepsilon} |\nabla\phi|^2 dV, \tag{2.49}$$

which is adimensional, like most parameters computed from ϕ.

The second expression for the surface area of the membrane uses the term $(1-\phi^2)$, as it is zero at the bulks where $\phi = \pm 1$ and is non-zero only in the interface. This can be exploited to compute the area with a second expression

$$A_{\phi 2} = \int_\Omega \frac{3}{8\sqrt{2}\varepsilon^3} (1-\phi^2)^2 dV. \tag{2.50}$$

This two expressions $A_{\phi 1}$ and $A_{\phi 2}$ are equals for the sharp-interface limit, where the width of the membrane tends to zero $\varepsilon \to 0$. This limit is where the Helfrich free energy perfectly equal to the free energy written as a membrane phase field. However, our numerical simulations will not be computed with a sharp interface, but with a diffuse one. Therefore we will have to be careful with both area expressions and ensure we have no problem with both of them. Moreover, we can use either $A_{\phi 1}$, $A_{\phi 2}$, or both to apply the area conservation.

Before computing the value of the Lagrange multiplier, we need to know how to add it to the dynamic equation of the phase field. In the complete free energy of the membrane obtained in equation (2.21) we simply had

$$\int \gamma_A dS + \int \Delta p dV.$$

So we shall translate this into the phase field energy and into our dynamic equation. As stated, thanks to the diffusive formulation we can usually do without the Lagrange multiplier for volume. Moreover, in cases where we do not study a whole membrane we will omit these multipliers for both area and volume. When we study a patch of membrane we will have a membrane that reaches up to the walls of the system, whether we use Periodic Boundary Conditions or not we can turn off the Lagrange multipliers because the rest of the membrane and the cell can be taken as a reservoir of area and volume. We can simply take for granted that any variation in area or volume in our system would be compensated at another point of the cell membrane.

2.3.3.1 Explicit integral

The most strict method is using the dynamic equation to obtain the variation of area over time $\partial_t A$ and setting it to zero [66]. We start first from the expression of the dynamic equation written as

$$\frac{\partial \phi}{\partial t} = M\nabla^2\Big(\frac{\delta F_B[\phi]}{\delta \phi} + \gamma_A \nabla^2 \phi\Big). \tag{2.51}$$

We want to ensure the area does not change, so we must satisfy $\partial_t A = 0$. To obtain $\partial_t A$ from equation (2.51) we will be using the area expression $A_{\phi 1} \approx \int_\Omega |\nabla \phi|^2 dV$. So by using (2.51) we can obtain the equation of $\partial_t A$ by doing a bit of work. First we will start by the derivation of both sides of the equation

$$\nabla\Big(\frac{\partial \phi}{\partial t}\Big) = \nabla D\nabla^2\Big(\frac{\delta F_B}{\delta \phi} + \gamma_A \nabla^2 \phi\Big),$$

followed by multiplying it all with $\nabla\phi$

$$\nabla\phi\Big(\nabla\Big(\frac{\partial \phi}{\partial t}\Big)\Big) = \nabla\phi D\nabla\nabla^2\Big(\frac{\delta F_B}{\delta \phi} + \gamma_A \nabla^2 \phi\Big).$$

Now, as area can be computed by integrating over the volume we have to integrate both sides of equation

$$\int \nabla\phi\Big(\nabla\Big(\frac{\partial \phi}{\partial t}\Big)\Big) dV = D\int \nabla\phi\Big(\nabla\nabla^2\Big(\frac{\delta F_B}{\delta \phi} + \gamma_A \nabla^2 \phi\Big)\Big) dV.$$

If time t is independent of space, which it is, we can do a permutation to move the ∇ inside the temporal derivative, and the left hand-side of the last expression can then be rewritten as

$$\int \Big(\frac{\partial(\nabla\phi)^2}{\partial t}\Big)dV = \frac{\partial A}{\partial t},$$

and taking into account that we must satisfy $\partial_t A = 0$ we end up with

$$0 = \int \nabla\phi \Big(\nabla\nabla^2\Big(\frac{\delta F_B}{\delta\phi} + \gamma_A\nabla^2\phi\Big)\Big)dV. \tag{2.52}$$

Finally we can solve for a constant γ_A and obtain an explicit Lagrange multiplier for the area conservation

$$\gamma_A = -\frac{\int \nabla\phi\cdot\nabla(\nabla^2\frac{\delta F_B}{\delta\phi})dV}{\int \nabla\phi\cdot\nabla[\nabla^2(\nabla^2\phi)]dV}. \tag{2.53}$$

We can compute this Lagrange multiplier at each time step and use it on the dynamic equation to maintain the surface area. This Lagrange multiplier is the best one we can get, however the multiple Laplacians and derivatives to compute make it a bit time-consuming. Therefore we shall decide during the testing phase of coding a new system we shall study how the surface area behaves over time. We can start with a more simple method to compute the multiplier, but if the system seems to strain the Lagrange multiplier too much we will switch to the explicit integral computation.

2.3.3.2 Penalty approach

One method to compute the Lagrange multiplier is the penalty approach. For this method we use a reference value to the variable we are trying to maintain constant, for example the area, and we penalise changes to the parameter we want to maintain constant. To do this we use a simple equation, for the area $A(t)$ at a given time t and a reference value for the area A_0 we have

$$\gamma = \alpha(A(t) - A_0), \tag{2.54}$$

where α is a constant of positive value which defines how hard this conservation condition is enforced. We want to be able to use the maximum value of α that does not break down the numerical computation.

The penalty approach is a simple and fast method to compute the Lagrange multiplier. Is less precise than an explicit method however, in cases with no extreme deformations, the penalty approach can be more than enough while offering faster computation times. Also in the case of using multiple Lagrange multipliers the penalty approach simple and fast computation is ever more necessary when extra firepower is necessary but you do not want to slow too much the simulations.

2.3.3.3 Volume Conservation

The volume conservation usually is maintained by the diffusive formulation of the dynamic equation. With this formulation, if there is no big noise source or any intense interaction between the phase-field and another field, there is no need to use a Lagrange multiplier to conserve the volume. The volume is computed using equation (2.48) and to ensure that the volume is being conserved throughout the simulation its evolution over time will be computed.

However, for high strain cases the simulation will need extra help. For those cases we will add to the dynamic equation the following [50]

$$\frac{\partial \phi}{\partial t} = M\nabla^2(\frac{\delta F_B}{\delta \phi} + \beta). \tag{2.55}$$

Similar to the area case we can use a penalty approach, just that in this case the Lagrange multiplier β is weighted with ϕ. This Lagrange multiplier β is adding ϕ to all the points in the system equally. This contribution is trying to compensate for any global change in volume by summing a small contribution to all points in space. This small contribution is expected to then diffuse and reach the region where the leaking of volume is happening.

The added contribution will be either positive or negative depending on whether the initial value of equation (2.48) decreases or increases. The only method we used when we have introduced a volume Lagrange multiplier is the penalty approach. Therefore by computing the value of volume at each time-step we can compute the volume Lagrange multiplier with the difference between the volume at a given point of time $V(t)$ and the volume at the start of the simulation V_0

$$\beta = C_\beta(V(t) - V_0). \tag{2.56}$$

The constant C_β is, as for the area case, a constant that defines how hard are we enforcing the conservation, and if taken too high the simulation will diverge.

2.3.3.4 Choosing the method to be used

Choosing which method and how many Lagrange multipliers to use will be dictated by testing the limits of each new model. Moreover, to ensure that the chosen method is good enough we track the area and volume of all simulations to ensure that no big variations happen. Variations of less than 5% are taken as good enough if they plateau, although minimising this deviations to the lowest possible value is of great importance.

For each method that we present in this thesis there will be a brief discussion on the method used to compute the Lagrange multipliers. The grade of difficulty to main-

tain the geometrical constraints during those simulations will also be addressed and explained.

2.4 Computing stationary membranes

2.4.1 Shape evolution

The dynamic equation of the membrane can be used to obtain the equilibrium shape of a membrane under no external influences. To do this, we start with a starting shape that has a given surface area A and volume V. This area and volume have a particular ratio of A/V that will have to be maintain constant through the simulation. So, as there are different shapes that have the same ratio A/V the simulation over time will go from the initial shape to the equilibrium one over time. This can be done in 2D and 3D, with or without spontaneous curvature, and taking into account the Gaussian curvature if we desire.

The first shape that one studies is usually the most simple one, which in the case of a closed surface would be a sphere. Starting with an spheroid we get little evolution. This happens because the sphere is the maximisation of enclosed volume V for a given area A and there are no other shapes that can comply this constraint as all other shapes would require either to reduce the volume or increase the area. We can see in **Figure 2.6** how over time there is no change for a spheroid either in 3D or 2D simulations. In the top images of the **Figure 2.6** how the diffuse interface is formed from the hard step profile at the start. It can also be seen in the bottom images of 3D simulations how the sphere also starts very rough, because of the space resolution of the simulated 3D lattice, but evolves to a very smooth surface. This smoothness comes also from the formation of the diffuse interface, which can give the interface a better resolution than the defined Cartesian lattice. So to study shape transformations produced by the minimisation of the surface curvature it will be necessary to start with bodies that are not spherical.

In the case of working with an ellipsoid this changes. The ellipsoid changes to a final shape depending on its area-volume ratio. This ratio in the end depends on the ratio between the two ellipsoid semi-axis. For a regime the ellipsoids evolve into a biconcave discoid shape, same shape as the red blood cell. We can see the evolution of a 2D and 3D ellipsoid to a biconcave discoid in **Figure 2.7**.

The first interfaces studied between two fluid bodies were of in-miscible fluid droplets, which usually exhibit a surface tension dominated energy. Our results end up differing a lot from what you obtain for surface tension surfaces. For droplets one would always expect to obtain a spherical shape, as area does not have to be maintained constant and the energy is minimised by minimising this surface area. Therefore, all the results we can see here when using the bending and membrane energy as in **Figure 2.7** are very different that what you would expect for a case dominated by the surface tension.

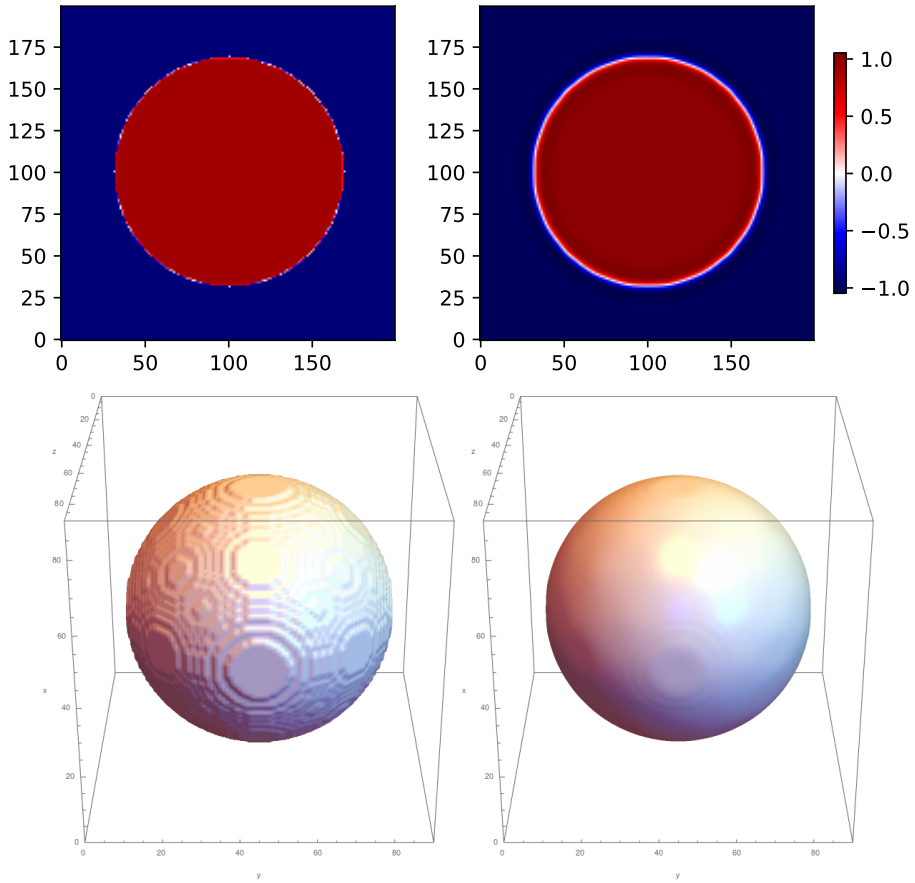

Figure 2.6: Spheroidal cell evolution. On the left we have the initial conditions and on the right we have the final stationary shape. First two images are the colormap of ϕ where red indicates $\phi = +1$ and blue $\phi = -1$. The 3D representation interpolates and plots the surface where $\phi = 0$.

Most equilibrium shapes change with the introduction of the spontaneous curvature C_0. With this term the bending energy will minimise so that the total curvature is as close to C_0 as possible. This is obvious when looking at the bending energy from equation (2.19) where, to minimise the total energy the curvature term

$$\kappa(C - C_0)^2$$

pushes the membrane curvature to get as close to $C = C_0$ as the constraints allow. The spontaneous curvature in general arises from imbalances between the two layers of the lipid bilayer. This can happen due to one of the surfaces being charged, or having dipolar molecules attached to it, or simply by having proteins that push one side of the

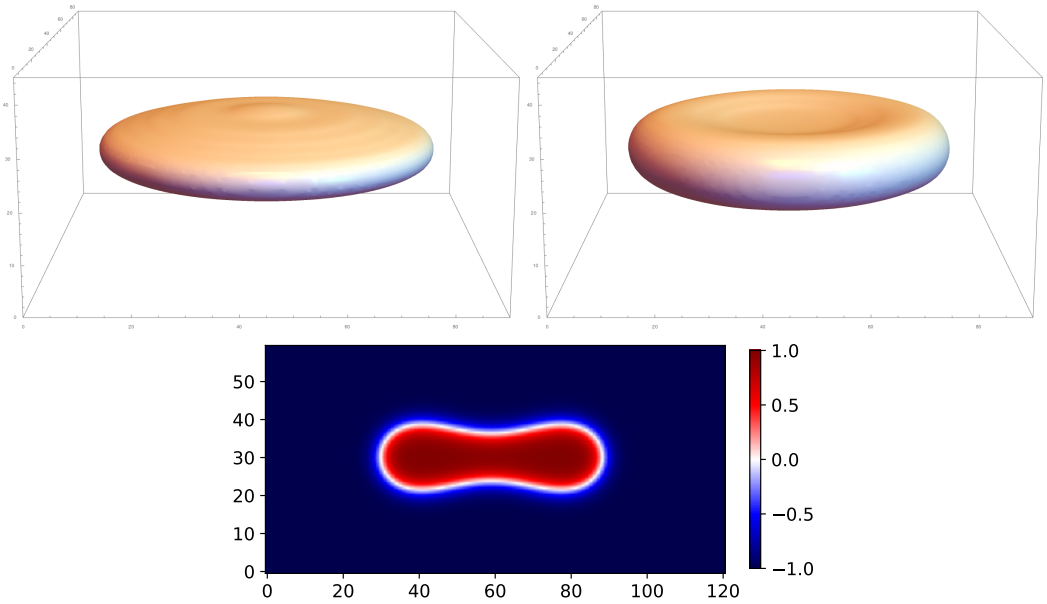

Figure 2.7: Top: Biconcave discoid shape obtained from an starting ellipsoid in 3D. Bottom: biconcave discoid shape in 2D the colormap refers to the value that the order parameter ϕ takes. The result is like taking a radial slice from the 3D cell shape.

membrane [6].

2.4.2 Parameters evolution

The temporal evolution of the phase field, and therefore of the membrane shape, is driven with the minimisation of the membrane free energy. Therefore changes in shape can be explained by the change of the bending energy, as the membrane changes to try to minimise the sum of the curvature squared. We can see how the bending energy of a membrane changes over a simulation in **Figure 2.8**. The bending energy goes down as the initial shape deforms into a final less curved shape, while maintaining the geometrical constraints.

We also have to track the evolution of the area and volume to ensure it maintains a rather constant value over time. An example can be seen in the bottom of **Figure 2.8**. The first big change in area and energy comes from the formation the formation of the interface, which at the start was a step-function and had to evolve to a smooth diffuse interface. From there, we can see how the change in area is minimum. Meanwhile the volume barely fluctuates around the starting value of the simulation, as the formation of the diffuse interface does not have anything to do with the total volume of the order parameter.

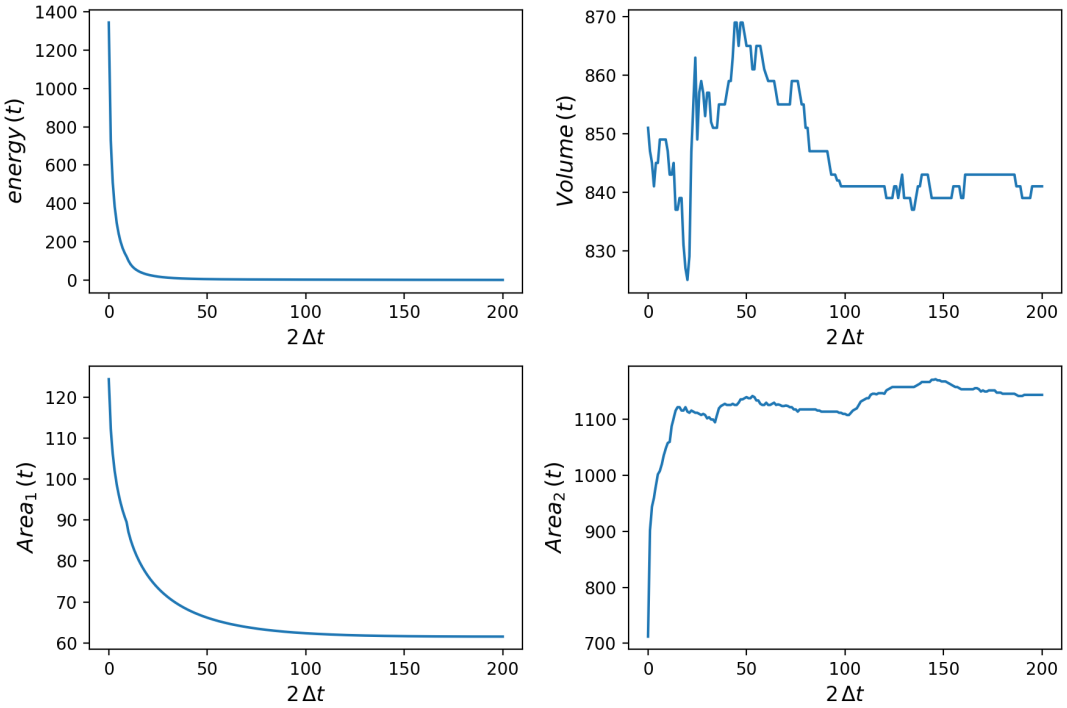

Figure 2.8: Bending energy, the two Area representations from equations (2.49) and (2.50) and the volume from equation (2.48) over time for a simulation of a simple static cell going from ellipsoidal to discoid shape.

In the end there will always be a variation from the initial volume and area, the point is that we try to make this variation as close to the numerical fluctuations as possible. Also, with the cells reaching equilibrium shape we expect a plateau in both of these parameters if the Lagrange multipliers are working as intended. There will be a competition between the force produced by the bending energy, the force produced by the Lagrange multipliers, and any other interaction added to the system.

All in all, a thorough study of stationary shapes of cells and vesicles has been already studied using a membrane phase field [24, 57, 58, 62]. This section has been just an introduction to what can be done with static membranes, but to look for more in-depth research one should go to the literature. In this thesis following chapters we will expand on this model and study dynamics in various ways: fluid flow, topological transitions, fluctuations, and combinations of all these dynamics.

2.5 Formulation with physical units

Before starting this section we have to point out a couple of facts of using phase field models. First of all, we start from a normal free energy written as the integral of a

energy density. This equation for the free energy is translated to a phase field formalism without any other change than to write it as a volume integral like in equation (2.40). This formulation as a volume integral is done to avoid having to track the interface position.

From that phase field free energy we then write the dynamic equation like equation (2.47). To compute this dynamic equation we use the functional derivative of the free energy $\delta F/\Delta\phi$. However if we look at the units of equation (2.47)

$$\frac{\partial\phi(\mathbf{x},t)}{\partial t} = M\nabla^2\frac{\delta F[\phi]}{\delta\phi},$$

one can clearly see that, as ϕ has no units, therefore $\delta F/\Delta\phi$ must also have no units. We have adimensionalized the energy modulus κ that goes into the dynamic equation (2.47). This is the standard procedure for a phase field model, however we know that in the end ϕ is representing a concentration and that we could have the whole system with consistent units. Whether they are real units or internal units for the simulation. So in this section we shall introduce back the units to the equations that we are using and see how to work with an order parameter that has units.

2.5.1 Energy derivative with units

We mostly work with a dimensionless order parameter ϕ. While this works perfectly and can be used to explain the cellular membrane and other systems, if we look at some parameters defined through ϕ we start to see that they are not what we would expect. All that is lacking is simply a couple of scaling constants, which do not change any results but nonetheless we will look into it for completitude.

To understand the implications of using a dimensionless order parameter (the one we are calling ϕ) lets look at some of the parameters we compute with it. First of all, if we look at the energy of the membrane in equation (2.39) we can see that, given the dimensions of all the constants, the energy has the expected units of energy given by the bending modulus κ. However lets look at at the chemical potential. The traditional definition of the chemical potential in thermodynamics is that it represents how much energy you need to add or subtract particles from the system. This would have units of J/N_p where N_p is the number of particles. However, if we compute the chemical potential of using ϕ we have

$$\frac{\delta F_M}{\delta\phi} = \frac{3\sqrt{2}\kappa}{8\varepsilon^3}\Big[(3\phi^2-1)(\phi-\phi^3+\varepsilon^2\nabla^2\phi)-\varepsilon^2\nabla^2(\phi-\phi^3+\varepsilon^2\nabla^2\phi)\Big]. \tag{2.57}$$

Instead what we get is units of pressure, as the only units with dimensions are κ and ε

we end up with

$$\Big[\mu[\phi]\Big] = \left[\frac{\delta F_M}{\delta \phi}\right] = \frac{[\kappa]}{[\varepsilon^3]} = \frac{\mathrm{J}}{m^3} = \mathrm{Pa}. \tag{2.58}$$

However some thermodynamical consistency is maintained, as we can see that the Gibbs-Duhem relation still has consistent units

$$dp = d\mu\, d\phi, \tag{2.59}$$

which has units of

$$[p] = [\mu\phi] = Pa.$$

The goal is not to cast doubt on models that use dimensionless order parameters, but to understand where this mismatches between the expected and the actual result arise from. In the end we will keep on working with the dimensionless ϕ, but here we will have a guide to follow in case we are interested on rewriting a model to include a dimensional order parameter.

2.5.2 Giving dimensions to the order parameter

Usually with phase field you work with adimensional order parameter, energy, etcetera. However, here we will check how do you give the proper dimensions to all the parameters and variables with cohesion. First step will be defining a new order parameter with dimensions, which we will name ψ. The dimensions of ψ will be of a concentration of particles

$$[\psi] = \frac{N_p}{V} = \frac{N_p}{m^3}, \tag{2.60}$$

where N_p refers to number of particles and m to meters (or length in general). So with this dimensions we can define an energy functional

$$F[\psi] = \frac{3\sqrt{2}\kappa}{8\varepsilon^3} \int \Big(-R\psi + U\psi^3 - \varepsilon^2 K\nabla^2\psi \Big)^2 dV, \tag{2.61}$$

where R, U, and K are three phenomenological constants that ensure $C_n \times \phi^n$ have the same dimensions for each power of n. These constants will have the units so that the product $C_n \times \phi^n$ gives Joules as a result. Therefore we know they must have the following units

$$[R] = \frac{m^3}{N_p}, \quad [U] = \frac{m^9}{N_p^3}, \text{ and } \quad [K] = \frac{m^3}{N_p}. \tag{2.62}$$

We will also take that these constants can be written as function of the others and we will use R as the variable

$$U = f(R^3) \quad K = f(R), \tag{2.63}$$

however, this will only be used to simplify a couple proves. We can mostly go with R U and K without any complication.

The energy written as either $F[\psi]$ or $F[\phi]$ have the same dimensions of Joules, however the matching when using either parameter ends when computing the chemical potential. Now that we defined how to write the energy using ψ we compute chemical potential using this new order parameter

$$\mu_\psi = \frac{\delta F[\psi]}{\delta \psi} = \frac{3\sqrt{2}\kappa}{8\varepsilon^3}\Big[\Psi\big(-R+3U\psi^2\big) - \varepsilon^2 K\nabla^2\Psi\Big], \tag{2.64}$$

where

$$\Psi = -R\psi + U\psi^3 - \varepsilon^2 K\nabla^2\psi, \tag{2.65}$$

taking into account R, U, and K units from equation (2.62), we can clearly see how the order parameter we have a dimensional term proportional to R, one to $U\psi^2$, and to K which all give the same units of m^3/N_p. Then when using ψ we get a chemical potential with the expected units of

$$\Big[\mu_\psi\Big] = \frac{[\kappa][R]}{[\varepsilon^3]} = \frac{J}{N_p}. \tag{2.66}$$

We can see with this how if we define the order parameter as a concentration and work with additional phenomenological constants R, U, and K we can write a thermodynamically consistent phase field model. This adds extra work that does not give new insight on the physics but nonetheless can be written. Gibbs-Duhem is fulfilled by this order parameter as

$$dp = \psi d\mu \tag{2.67}$$

if we take the proposed units $[\psi] = \frac{N_p}{V}$ this thermodynamic relation also gives us the correct units for μ_ψ

$$[\mu_\psi] = \frac{Pa}{[\psi]} = \frac{Pa\,m^3}{N_p} = \frac{J}{N_p}. \tag{2.68}$$

Moreover, if we approximate the dimensionless order parameter to $\phi \approx R\psi$ we can get the same unit-wise correct chemical potential using the chain rule

$$\frac{\delta F[\psi]}{\delta \psi} = \frac{\delta F[\phi]}{\delta \phi}\frac{\partial \phi}{\partial \psi} = \frac{\delta F[\phi]}{\delta \phi}R. \tag{2.69}$$

Part II

Stream function membrane phase field model

Chapter 3

Stream function formulation

3.1 Membrane deformation in a flow

The biological membrane is specially known to be flexible and deformable. This produces a body shape very responsive to external forces, and specifically the forces produced by a fluid flow.

Outside of the turbulent flow, a fluid flow in absence of any obstacle has a very particular profile depending on the characteristics of the system. A moving wall in contact with a fluid induces the fluid to move with it, faster for the fluid closer to the wall, which is known as Couette flow. A pressure gradient can push fluid down a channel, faster in the centre and slower as you approach the channel walls, known as Poiseuille flow. When an obstacle is introduced to a flow like this however, the flow is disturbed and the flow will react to this disturbance by generating a force on the obstacle. For an immovable obstacle the disturbance on the flow is very high and the forces generated on the obstacle are high too. But not all obstacles have to be neither rigid nor immovable. That is where the case of a biological membrane on a flow enters the stage.

The biological membrane in contrast to an immovable obstacle can be pushed and moved, and is very easy to deform. In this case the membrane is still an obstacle, but will be a free and elastic obstacle. It will perturb the flow to a much lesser degree, but as the membrane is very flexible and deformable the forces that the fluid exerts on the membrane will be enough to generate huge deformations and shape changes. This can be a great tool to study biological membranes, as the flow characteristics like flow speed are easily controlled with good precision. Therefore it can be a great tool with very high reproducibility, that can be used to compare different membranes and cells under the same conditions.

Specifically, red blood cells are of great interest because by understanding better its mechanical properties can improve diagnosis or treatment of blood-related diseases

[67, 68, 69]. There are many experimental works on the deformations of red blood cells in micro-fluidic conditions [70, 71, 72]. The goal is to model the red blood cells so that under the same conditions the simulations replicate the experimental data. There is interest in modelling these experiments, as being able to perfectly replicate them can give insight into how to diagnose illnesses or characterise membranes.

Previous works on this topic have been based on Lattice Boltzmann Methods [60, 73, 74] which are difficult and complex to implement. Other models are particle-based methods like Smoothed Dissipative Particle Dynamics [75, 76] which simplify the membrane and fluid with mesoscale particles much bigger than the molecules that actually form them. Lastly, there are also models based on use of the Green function or Dirac delta like immersed boundary method [77] or the boundary integral method [78, 79, 80]. All of these have their pros and cons, but in search for a simpler method a new one will be introduced.

3.1.1 Navier-Stokes equation

The Navier-Stokes equations will be the ones used to model the fluid hydrodynamics. The Navier-Stokes equations are based on the balance between the momentum conservation and mass conservation of a Newtonian fluid (a fluid with viscosity independent of shear). The equation in question can be expressed by applying Newton second law to fluid motion, with the assumption that the stress in the fluid is the sum of a diffusing viscous term and a pressure term

$$\rho\left(\partial_t \vec{v} + \vec{v}\cdot\nabla\cdot\vec{v}\right) = -\nabla P + \eta\nabla^2\vec{v} + f, \tag{3.1}$$

where ρ is the density, P is the pressure, η is the viscosity of the fluid, and f is a volumetric force. On the left handside in equation (3.1) we have the convective acceleration term $\partial_t\vec{v} + \vec{v}\cdot\nabla\cdot\vec{v}$, also known as the inertial term. On the right hand-side we have the diffusion term $\eta\nabla^2\vec{v}$, the pressure gradient ∇P, and the external volumetric forces f. The complete Navier-Stokes equation (3.1) works for both liquid and gaseous fluids. To differentiate between both kind of fluids we take the liquid incompressibility condition that can be expressed in terms of the velocity as

$$\nabla\cdot\vec{v} = 0. \tag{3.2}$$

The condition in equation (3.2) equates to a fluid that has a constant value of density along all the volume. This is what is expected of normal liquids in most day to day situations and even more so in biological conditions that will be studied here.

Although the Navier-Stokes equations are well-known and extensively used, however there is no easy solution to this differential equations. The Navier-Stokes equation is no simple equation, as it comprises one of the Clay Mathematics Institute millennium

problem [81]. The prove of existence and smoothness of Navier–Stokes solutions or the breakdown of Navier–Stokes solutions on 3D carry a prize of 1 million US$ prize for a solution or a counterexample. This is so because the Navier-Stokes equations are never completely integrable.

3.1.2 Reynolds number

To characterise the behaviour of a liquid flow the Reynolds number is usually used, which is an adimensional number comprised by the ratio of inertial forces to viscous forces. This is an adimensional parameter with the following expression

$$Re = \frac{\rho v L}{\eta}, \tag{3.3}$$

where η is the dynamic viscosity of the fluid, ρ its density, v the flow speed, and L the characteristic length of the system.

For high values values of the Reynolds number the inertia dominates and we have a turbulent flow. This flow will be chaotic, with vortex and extreme vorticities. This is how the wind usually flows, or how smoke moves, or how the water at a river flows. For lower Reynolds numbers viscous forces dominate and we have what its called a laminar flow. This kind of flow is characterised by its more smooth and less erratic behaviour.

But what value is a big or small Reynolds number? For high Reynolds number the turbulent regime starts at around $10^3 - 10^4$ depending on the system. Meanwhile, low Reynolds regime is usually considered from $Re = 0.1$ downwards.

Blood may exhibit different Reynolds numbers. In an artery we have a very wide channel which may even behave as a turbulent flow, while for the much smaller micro-capillars we have a low Reynolds flow. In these cases the characteristic length L that defines our Reynolds would be the diameter of the blood veins.

As we are interested in the behaviour of cells inside a micro-channel, which have a very small section, we will be interested in the low Reynolds limit.

3.2 Stream function phase field

As presented in Chapter 2 phase-field methodology models successfully vesicles and simple cells like red blood cells [24, 50, 51, 52, 54, 57, 58, 61]. This phase-field methodology has been expanded to model membranes coupled to a fluid flow in the past. The phase-field method reproduces accurately the membrane morphology and dynamics under a flow in combination with the Lattice-Boltzmann method [55, 60, 73, 74]. Previous work has focused on giving exhaustive phase diagrams of red blood cells morphologies both in 2D [79, 80] and in 3D [75, 82] where aside from deformation, other dynamics like *tumbling* are studied.

The dimensionality of the study is also relevant, as a vesicle and a red blood cell are indistinguishable in 2D. In 3D the cytoskeleton made by a spectrin-network attached to the red blood cell membrane gives the membrane resistance to in-plane shear. This can be very important in some health disorders like hereditary spherocitosis [20, 21]. The dimensional difference, although might not be important for the membrane shape under normal conditions, can be of great importance for the results of some parameters or scalings. While lacking the in-plane shear can make it challenging to give quantitative results with 2D simulations, extensive previous qualitative research on healthy red blood cell in a micro-channel has been proven successful. This is even more obvious when comparing with experimental results for different values of cytoskeleton elasticity for healthy cells [9] where the same shapes as in 2D simulations [60] are obtained.

In this section a methodology in 2 dimensions to simulate membranes coupled to a flow will be presented, where the approach relies directly upon basic fluid mechanics equations. Consequently, this methodology is ideal to further extensions such as including more sophisticated constitutive equations for instance, Maxwell or Oldroyd viscoelasticity. This is far from straightforward using, for example, Lattice-Boltzmann method. Some possible extensions for this model will be time-dependent flows, inertial flows and even a 3D formulation of this same methodology.

To avoid some difficulties of solving the Navier-Stokes equations one can use instead the vorticity and the stream function. An additional benefit of this will be fulfilling the incompressibility condition regardless of the accuracy of the solving method.

3.2.1 Stokes equation coupled to the phase field

As explained in the previous section, the flow of fluids, both liquid and gas, can be explained using the the Navier-Stokes Equation (3.1). This equation is based on the conservation of momentum for a substance that, under a pressure and/or volumetric force responds by adopting a velocity profile with a given distribution $\vec{v}$. Usually the volumetric force is gravity, but in this model this term will be ignored because at the length-scale of a cell inside a micro-channel gravity should not play an important role.

This equation has to be coupled to the membrane, so the fluid flow is deformed by the membrane presence using a phase field. To that end we introduce a term depending on the membrane chemical potential μ and the phase field ϕ [83]

$$\rho\left(\partial_t\vec{v}+\vec{v}\cdot\nabla\cdot\vec{v}\right) = -\nabla P+\eta\nabla^2\vec{v}-\phi\nabla\mu. \tag{3.4}$$

This term $\phi\nabla\mu$ is a force density which will couple the energetics of the membrane represented by μ with the fluid flow that is characterised by P and $\vec{v}$. There is some discussion on the literature [84] on whether this term should be written as $\phi\nabla\mu$ or $\mu\nabla\phi$, however there seems to be no big effect on the results and no conclusion has been reached.

However this equation is for a generalised fluid, and we are interested in liquids, the most big difference between gas and liquid is the incompressibility condition, which requires $\nabla \cdot \vec{v} = 0$. Also, at the low Reynolds limit as the viscous forces dominate over inertia thus the inertial term $\rho \delta_t \vec{v}$ will be negligible. Taking both of these things into the Navier-Stokes equation (3.1) one ends up with the so-called Stokes equation,

$$0 \quad = \quad -\nabla P + \eta \nabla^2 \vec{v} - \phi \nabla \mu, \tag{3.5}$$

which in this case is also coupled to the membrane phase-field through the $\phi \nabla \mu$ term.

3.2.2 Stream function formulation

This model will couple the previous membrane phase field model to the fluid equation. Similar to previous chapters, we start from the Helfrich free energy, which for convenience will be rewritten

$$F = \int_A \Big(\frac{\kappa}{2} C^2 + \gamma_A \Big) dA + \int_V \Delta p \, dV, \tag{3.6}$$

where C is the total curvature [22, 39] which has an associated energy scale that is the bending modulus κ. In addition to the curvature term one has the Lagrange multipliers γ_A and Δp that will guarantee area and enclosed volume conservation, respectively.

We can write the energy in terms of the phase field order parameter ϕ as seen in Chapter 2. For the case of a fluid flow, we will introduce two Lagrange multipliers for area, as the fluid stretches the membrane and it is harder to conserve area. We then have the following free energy for the membrane written as a phase field,

$$F[\phi] = \int_V \Big(\frac{\kappa}{2} \big[-\phi + \phi^3 - \varepsilon^2 \nabla^2 \phi \big]^2 + \gamma_1 \varepsilon^2 (\nabla \phi)^2 + \gamma_2 (1 - \phi^2)^2 + \beta \phi \Big) dV, \tag{3.7}$$

where γ_i are two Lagrange multipliers to ensure area conservation and β is the Lagrange multiplier to ensure volume conservation, which have been discussed in Chapter 2.

As stated in the previous chapter, with this formulation, we can write an equation for time evolution of the phase field

$$\partial_t \phi(\bar{\mathbf{x}}, \bar{t}) = M \nabla^2 \mu, \tag{3.8}$$

where M the mobility coefficient of the phase field and ∂_t denotes the partial derivative with respect of time and

$$\mu = \frac{\delta F[\phi]}{\delta \phi} \tag{3.9}$$

is the chemical potential written as a functional derivative [64] of the energy equation (3.7).

Equation (3.8) minimizes the Canham-Helfrich energy in absence of fluid, so we need to couple the latter equation with the velocity field. As the fluid drags the cell we have

$$\partial_t \phi = M\nabla^2\mu - \vec{v}\cdot\nabla\phi, \tag{3.10}$$

where the velocity field $\vec{v}$ is affecting directly the membrane where it is present $\nabla\phi$. The bulks of ϕ will be unaffected as $\nabla\phi$ is only different than zero at the membrane. This equation coupled with equation (3.5) will be the two necessary equations to represent a cell moving in a flow, with the cell presence distorting the fluid flow.

We should not forget that the hydrodynamics in 2D is noticeably different from 3D due to its even longer range. However, this is not a problem in our study because the behaviour of the Oseen tensor in our system is dominated by the characteristic finite size of our micro-channel.

Generally the most obvious method to compute equation (3.10) would be to solve the fluid velocity $\vec{v}$. This is not trivial as the velocity is different at each point of space, and is influenced by the obstacle that the membrane is. Moreover, it is also necessary to compute the pressure P at each point in space. As solving neither of this is easy, instead of brute-forcing our way through $\vec{v}$ and P we rephrase Equation (3.5) in terms of the vorticity $\vec{\omega}$ and the stream function $\vec{\xi}$, defined respectively as

$$\vec{\omega} = \nabla\times\vec{v}, \qquad \nabla\times\vec{\xi} = \vec{v}. \tag{3.11}$$

In 2 dimensions the vectors vorticity $\vec{\omega}$ and stream function $\vec{\xi}$ have only one non-zero component thus we define $\vec{\omega} = (0,0,\omega)$ and $\vec{\xi} = (0,0,\xi)$ so, hereafter, we will work only with their unique non zero scalar component. With these two relations between ξ, ω, and the velocity v, we can find the relation between ω and ξ by using the vector identity

$$\nabla\times(\nabla\vec{A}) = \nabla(\nabla\cdot\vec{A}) - \nabla^2\vec{A} \tag{3.12}$$

giving the Poisson equation

$$\nabla^2\xi = -\omega. \tag{3.13}$$

With this equation we can relate the vorticity with the stream function. Now we need a relation between one of these two and the phase field. If we take the curl of Equation (3.5), we find

$$0 = -\nabla\times(\nabla P) + \mu\nabla\times(\nabla^2\vec{v}) - \nabla\times(\phi\nabla\mu),$$

using again Equation (3.12) and the vector identities

$$\nabla\times(\nabla P) = 0 \qquad \text{and} \qquad \nabla\times(\phi\nabla\mu) = (\nabla\phi)\times(\nabla\mu), \tag{3.14}$$

we find another Poisson equation to explain the vorticity behaviour

$$\nabla^2\omega = \frac{1}{\eta}\left(\nabla\phi \times \nabla\mu\right) = \frac{1}{\eta}\left(\partial_y\mu\,\partial_x\phi - \partial_x\mu\,\partial_y\phi\right). \tag{3.15}$$

This equation connects the flow behaviour with the membrane by the presence of the terms $\nabla\phi$ and μ. Now, we have the vorticity ω and stream function ξ connected, and the vorticity connected to the membrane influence. The last thing we need is to connect the membrane to the fluid, as we explained before we can change the dynamic equation. The evolution of the phase field ϕ from equation (3.10) can be written using the stream function ξ by using its definition from the velocity $\vec{v}$. So writing the dynamic equation of the phase field in terms of ξ and with the two Poisson equations to solve ξ and ω we end up with a system of the three equations,

$$\begin{aligned}
\partial_t\phi &= M\nabla^2\mu - (\partial_y\xi\,\partial_x\phi - \partial_x\xi\,\partial_y\phi),\\
\nabla^2\omega &= \frac{1}{\eta}\left(\partial_y\mu\,\partial_x\phi - \partial_x\mu\,\partial_y\phi\right),\\
\nabla^2\xi &= -\omega.
\end{aligned} \tag{3.16}$$

With these three equations we can compute numerically the evolution of a membrane inside a fluid flow. The simplicity of the model stems from the coupling of an equation for the membrane and an alternative description of the fluid based on integrating the two Poisson equations for the stream function ξ and the vorticity ω. Moreover, this system of equations fulfils the incompressibility condition regardless of the accuracy of the solving method.

3.2.3 Bending and phase-field time-scales

We add a new time-scale, the hydrodynamic one, which is much faster than the bending one, we need to make sure that the phase field does not create artefacts when interacting with the fluid flow. The formulation is written in a way that we expect the diffuse interfase to have a proper shape at all times. Initially the interfase has an hyperbollic tangent shape, when the flow starts this shape will be altered as we are taking it out of equilibrium. However, we need it to not completely lose shape due to the applied external dynamics. We need a mobility M that guarantees that the relaxation do not alter the simulation results. Quantitatively, the value of M is such that the membrane deformation time-scale $\tau_\kappa = \eta l^3/\kappa$ is 10^5 times slower than the phase field time-scale $\tau_\phi = \varepsilon^2/M$.

3.2.4 Heterogeneous Viscosity and viscosity contrast

Up until now we have considered the viscosity as a constant parameter, but this methodology does not require to restrict the viscosity to a simple constant. Using the order

parameter of the phase field we can compute a heterogeneous viscosity that depends on the liquid phase.

For a simple viscosity modelling we can introduce two viscosities, one for the outer fluid and one for the internal fluid (with respect to the membrane). To do this one can use the following expression

$$\eta(\mathbf{x}) = \frac{\eta_{liq}(1-\phi(\mathbf{x}))}{2} + \frac{\eta_{cell}(1+\phi(\mathbf{x}))}{2}, \tag{3.17}$$

where η_{liq} would be the viscosity for the bulk that we will take as external fluid $\phi = -1$ and similarly for the liquid inside the cell we will have the viscosity η_{cell} that will be applied to $\phi = +1$.

If there is interest on working with membrane viscosity one could go and use the following expression

$$\eta(\mathbf{x}) = \frac{\eta_{liq}(1-\phi(\mathbf{x}))}{2} + \frac{\eta_{cell}(1+\phi(\mathbf{x}))}{2} + (\eta_{mem} - \frac{\eta_{liq}}{2} - \frac{\eta_{cell}}{2})(1-\phi(\mathbf{x})^2), \tag{3.18}$$

however research on this topic is scarce and this third viscosity η_{mem} will not be used in this thesis. Still we could use the last viscosity representation but using $\eta_{mem} = (\eta_{cell} + \eta_{liq})/2$ to study a system with different viscosities for only the liquid phases.

Now on the topic of having two different viscosities for the intracellular and extracellular liquid, usually in the bibliography one refers to this as the viscosity contrast [85]. The viscosity contrast is simply the ratio between the viscosity of the cytosol and the viscosity of the surrounding fluid $\zeta = \eta_{cell}/\eta_{liq}$. The most basic model will work with a viscosity contrast $\zeta = 1$, that is simply a homogeneous viscosity taking the same value for the cell and for the liquid. With this model we can work with any viscosity contrast, but for starters we will be working with $\zeta = 1$. If no mention of which viscosity contrast was used for any results then one can assume that $\zeta = 1$ was taken.

3.2.5 Boundary conditions for the equations

The system of equations is fixed, and will not change whether we want to simulate a Couette flow, a Poiseuille flow or any kind of flow at all. So for all the types of flows we have to solve the same system of equations (3.16). Therefore, the difference in the resulting flow pattern will not arise from the system of equations we are solving but from the boundary conditions of the equations. To be more specific it will depend on the value that the vorticity and stream function take at the walls of the channel. Here we will show which values this boundary conditions have to take for Poiseuille and Couette flow.

Poiseuille Flow

The Poiseuille flow is produced inside a channel or pipe where we have a pressure drop between the ends of the channel. The fluid will flow from high to low pressure, and the velocity will be proportional to the pressure gradient. We can see the characteristic Poiseuille flow velocity profile in **Figure 3.1 (a)**.

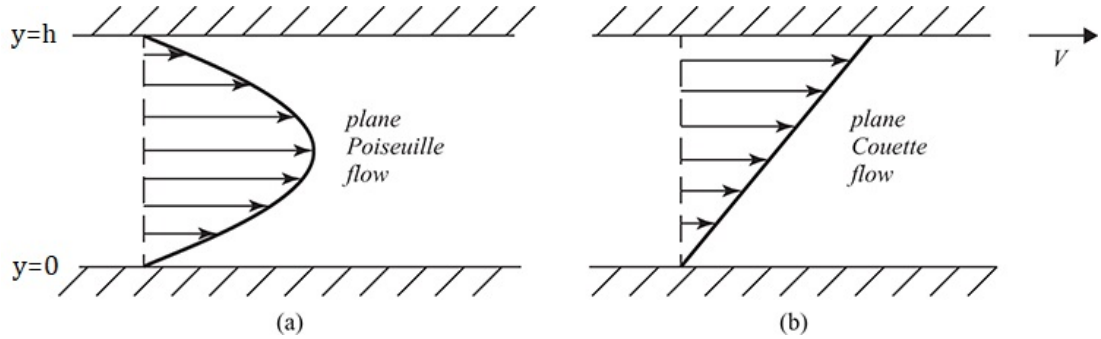

Figure 3.1: Profile for the velocity of (a) a Poiseuille flow and (b) a Couette flow.

For a Poiseuille flow, we use the analytical velocity profile to obtain the expressions for the vorticity and the stream function in absence of a cell. With these equations we can obtain the boundary condition of these equations at the walls of the channel:

$$v_x(y) = -\frac{dP}{dx}\frac{1}{2\eta}y(h-y) \Rightarrow \begin{cases} \xi(h) = -\frac{dP}{dx}\frac{h^3}{6\eta} \\ \xi(0) = 0 \\ \omega(h) = -\frac{dP}{dx}\frac{h}{\eta} \\ \omega(0) = \frac{dP}{dx}\frac{h}{\eta} \end{cases}, \tag{3.19}$$

where h is the channel height and $\frac{dP}{dx}$ as the pressure gradient.

Couette Flow

Taking the no-slip condition, one takes the fluid in contact with a wall to be stuck to the wall. Thus if the wall moves the fluid will move with it and if the wall is not moving the fluid in contact with the wall will not move. For fluid between two walls separated by a distance h where the top wall is moving at a velocity v_{wall}, one obtains the so-called Couette flow. The Couette flow velocity profile and is represented in **Figure 3.1 (b)**.

Due to the no-slip condition for the velocity boundary condition with both walls, we know that the top fluid will be moving at speed v_{wall} while the bottom fluid will be stationary. Solving this brings us the velocity expression $v_x(y) = v_{wall}\frac{y}{h}$ which we can

use to compute both ξ and ω and then compute their values at the walls

$$v_x(y) = v_{wall}\frac{y}{h} \Rightarrow \begin{cases} \xi(h) = h\,v_{wall}/2 \\ \xi(0) = 0 \\ \omega(h) = -v_{wall}/h \\ \omega(0) = -v_{wall}/h \end{cases} . \tag{3.20}$$

3.2.6 Lagrange multiplier with fluid flow

In Chapter 2 we introduced the Lagrange multipliers and how to compute them, and the idea that there are two different expressions for the area when working with a phase field model

$$A_1 = \int \frac{3}{4\sqrt{2}\varepsilon}|\nabla\phi|^2 dV \quad \text{and} \quad A_2 = \int \frac{3}{4\sqrt{2}\varepsilon}(1-\phi^2)^2 dV,$$

which are equal at the $\varepsilon \Rightarrow 0$ limit. However, the explicit Lagrange multiplier showed was computed from a dynamic equation that did not account for the term $\vec{v}\nabla\phi$.

Following the same procedure to obtain the explicit Lagrange multiplier of Chapter 2 we can obtain the explicit Lagrange multiplier for a dynamic equation that has a convective term added. Starting from a dynamic equation with a flow term, using F_B from equation (2.37), we have

$$\frac{\partial\phi}{\partial t} = \nabla^2\Big(\frac{\delta F_B[\phi]}{\delta\phi} + \gamma_A\nabla^2\phi\Big) - \vec{v}\cdot\nabla\phi, \tag{3.21}$$

one has to ensure the area does not change, so the Lagrange multiplier must satisfy $\delta_t A = 0$. As in Chapter 2 to obtain $\delta_t A$ from equation (2.51) one needs to use the area expression $A_{\phi 1} \approx \int_\Omega |\nabla\phi|^2 dV$. So from equation (3.21) one needs to arrive to the expression $\delta_t A$. Starting with the derivation of both sides of the equation one obtains

$$\nabla\Big(\frac{\partial\phi}{\partial t}\Big) = \nabla\Big(M\nabla^2\Big(\frac{\delta F_B}{\delta\phi} + \gamma_A\nabla^2\phi\Big) - \vec{v}\cdot\nabla\phi\Big),$$

that has to be multiplied on both sides of the equation by $\nabla\phi$ to obtain

$$\nabla\phi\Big(\nabla\Big(\frac{\partial\phi}{\partial t}\Big)\Big) = \nabla\phi\nabla\Big[M\nabla^2\Big(\frac{\delta F_B}{\delta\phi} + \gamma_A\nabla^2\phi\Big) - \vec{v}\cdot\nabla\phi\Big].$$

Now, as area can be computed by integrating over the volume we have to integrate both sides of equation

$$\int \nabla\phi\Big(\nabla\Big(\frac{\partial\phi}{\partial t}\Big)\Big)dV = \int \nabla\phi\Big(\nabla\Big[M\nabla^2\Big(\frac{\delta F_B}{\delta\phi} + \gamma_A\nabla^2\phi\Big) - \vec{v}\cdot\nabla\phi\Big]\Big)dV,$$

which is the same expression obtained in Chapter 2 with the addition of the term $\vec{v}\cdot\nabla\phi$ If time t is independent of space, which it is, we can do a permutation to move the ∇ inside the temporal derivative. With that the left hand-side of the last expression can then be rewritten as

$$\int \Big(\frac{\partial(\nabla\phi)^2}{\partial t}\Big)dV = \frac{\partial A}{\partial t},$$

and taking into account that we must satisfy $\delta_t A = 0$ we end up with

$$0 = \int \nabla\phi\Big(\nabla\Big[M\nabla^2\Big(\frac{\delta F_B}{\delta\phi} + \gamma_A\nabla^2\phi\Big) - \vec{v}\cdot\nabla\phi\Big]\Big)dV. \tag{3.22}$$

Finally we can solve for a constant γ_1 and obtain an explicit Lagrange multiplier for the area conservation where $\mu = \delta F_{Bending}/\delta\phi$

$$\gamma_1 = \frac{\int(-\nabla\phi\cdot\nabla(\mathbf{v}\cdot\nabla\phi) + M\nabla\phi\cdot\nabla\nabla^2\mu)dV}{M\int\nabla\phi\cdot\nabla\nabla^4\phi\,dV}. \tag{3.23}$$

The final expression while similar to the one obtained in Chapter 2 shows an additional parameter dependent on the term $\vec{v}\cdot\nabla\phi$. This multiplier is enough to conserve the area for zero or low speed simulations but to explore the high velocity flows further precision was necessary.

Following Qiang Du, *et al.* [50] we have extended the Lagrange multiplier for the area and added one for the volume. This approach is accurate in the range of low to moderate velocities used in our work. As the first Lagrange multiplier is obtained for the first area expression we add a second Lagrange multiplier for the other expression and implement it with a simpler penalty approach. This second area multiplier does not need to be as accurate as the first as it just only gives additional support to the area conservation

$$\gamma_2 = C_\gamma(A(t) - A_0),$$

where C_γ is the weight given to this penalty for the area.

Finally a Lagrange multiplier for the volume conservation is also added with a penalty approach

$$\beta = C_\beta\Big(V(t) - V_0\Big),$$

where C_β is the weight given to this penalty.

3.2.7 Characterisation

With the present model we can compute a simulation where a biological membrane will flow and deform accordingly to the type of flow and its characteristics. However the aim is to go deeper, not only obtaining shapes of cells but to quantify and analyse the results as best as possible.

To this end we use the information in the results to compute additional parameters. The first thing we do is study the influence of the cell on the channel flow. To do this we compute the difference between the vorticity ω and the stream function ξ of a simulation respect to ω_0 and ξ_0, which are analytical vorticity and the stream function in absence of a cell. We call this the deviations of the stream function $\xi - \xi_0$ and deviations of the vorticity $\omega - \omega_0$.

These parameters show the influence of the cell on the flow and how far away it goes. Moreover we can also see if the changes on the flow are symmetric or not. It is possible to even get some insight on the stability of the current shape from looking at these deviations. However one can go further beyond this by computing their squared integral, computing two observables

$$\mathcal{W} = \int_{\text{channel}} (\omega - \omega_0)^2 dV, \tag{3.24}$$

$$\mathcal{X} = \int_{\text{channel}} (\xi - \xi_0)^2 dV, \tag{3.25}$$

that allow tracking of the deformation history of the membrane. The theory behind this is based on Wu [86] who showed that the vorticity integrated throughout the channel is conserved in two-dimensional incompressible flows. This even hold in the presence of immersed solid bodies. Therefore, we know that while $\mathcal{W}$ and $\mathcal{X}$ are not conserved the membrane is being deformed and when these observables stay constant the cell is already at its equilibrium shape and behaves as a solid rigid from the fluid perspective. We integrate the square as we are not interested in the sign of the deviation.

More parameters to characterise the membrane can be computed from the model. Other more traditional parameters as the shear stress tensor and the membrane influence on pressure can be computed. The shear stress tensor can be computed using the flow velocity as, [56]

$$\sigma_{ij} \equiv \nabla_i v_j - \nabla_j v_i. \tag{3.26}$$

The pressure field is obtained from the Gibbs–Duhem relation for constant temperature [60]

$$dP = \phi d\mu. \tag{3.27}$$

This relation does not give us the complete pressure field but we can use μ to compute the influence of the cell on the pressure. We find what is traditionally seen in solid obstacles on flows: that the pressure is bigger behind the cell and lower in front of it (taking as the flow as moving forwards with respect to the cell).

3.3 Numerical implementation

We have defined then a model that can compute the evolution of a biological membrane in a fluid flow. Now, how do we implement it? We will be working in a 2-Dimensional space, and we will define this space as a grid like in the **Figure 3.2**. The grid points are separated by the spatial resolution Δx, which we always take as equal in both dimensions x and y. Usually we will use $\Delta x = 1$ and chose a cell size to have enough resolution to describe deformations of the membrane.

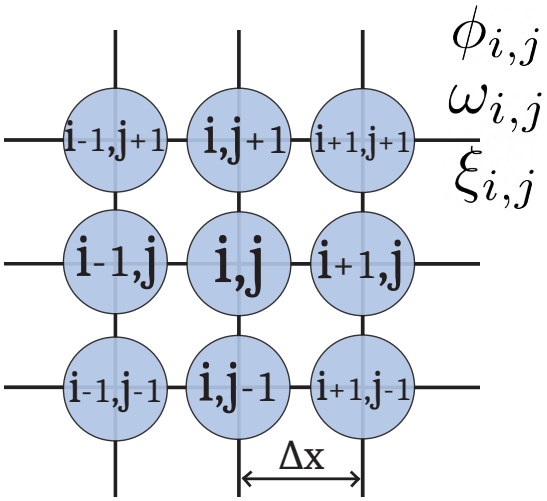

Figure 3.2: Sketch of the grid for a simulation. Each field ϕ, ω, and ξ have a value assigned at each point of the grid.

In this space we will have three different fields to compute which interact with each other. So at each point in space we will have the information of the phase field $\phi_{i,j}$, the vorticity $\omega_{i,j}$, and the stream function $\xi_{i,j}$. We will have to compute the evolution of each of these fields. The final code used for solving these can be seen in Appendix A and also in the GitHub repository we share [87] where we solve iteratively the system of equations (3.16).

We start all the simulations with an ellipsoid which has the reduced volume of a discocyte shape. This initial shape will evolve to a discocyte and will flow due the interaction with the stream function field.

3.3.1 Centre of mass

Computing the centre of mass and corrections for the stream function model is easy under normal conditions. We can use the definition of centre of mass changing the

density for the order parameter ϕ

$$\mathbf{r}_{CM} = \frac{1}{\int_{\mathcal{V}} dV\, \phi(\mathbf{x})} \int_{\mathcal{V}} dV\, \phi(\mathbf{x}) \cdot \mathbf{x}. \tag{3.28}$$

This consists of a simple integral over all the system volume of the product between ϕ and its position $\mathbf{x}$ and normalising using the volume integral over ϕ alone. This method is what will be used in most computations of the centre of mass that can be seen in this thesis. It is the most simple and under normal conditions reliable, for static or low velocity simulations it works perfectly, however this is not always the case.

As has be seen in equation (3.16) the influence of the membrane on the fluid is computed using gradients of ϕ. However, the influence of the membrane on the flow extends from the membrane location further away. This happens because the membrane in ϕ leaves a infinitesimal "shadow" and the bulk right behind the cell is not exactly $\phi = -1$ but something like $\phi = -0.999$. This shadow is what transmits the influence of the cell to the liquid, but even if it is small in intensity it can be big under fast flows. That is why to get the best estimation for the centre of mass position we will be computing equation (3.28) only for values of $\phi > 0.95$.

3.3.2 Choosing Membrane width

The width of the membrane is defined in our model by the parameter ε and if possible we will take always the smallest value that gives good results, usually $\varepsilon = 1$. However, with the fluid-coupled system $\varepsilon = 1$ sometimes lacks good resolution in the vorticity and stream function fields. In this cases we are using $\varepsilon = 2$ and increasing the overall size of the system to ensure that the width of the membrane does not affect the phenomenology. This is very important because in real life the membrane width is orders of magnitude smaller than in simulations. Therefore, we have to be careful not to work with systems which membrane width is comparable to any other characteristic length of the cell.

3.4 Generalisation of the model

An advantage of the presented model is the ease to add or modify the flow. Here we will see a couple of expansions to different hydrodynamic behaviours and dimensions.

3.4.1 Inertial flow

The low Reynolds flow has been taken because that is the conditions found in a microchannel and in most of cellular biology. However, that is not a requirement for this kind of formulation. There are some situations like blood flow in arteries or small inertial effects that would require to add the inertial contribution to the flow. We can

study medium and high Reynolds numbers by adding the flow inertial term. Instead of working with the Stokes equation we shall work with the Navier-Stokes equation.

Starting again from the Navier-Stokes equation for an incompressible flow ($\nabla\cdot\vec{v}=0$)

$$\rho\partial_t\vec{v} \quad = \quad -\nabla P+\eta\nabla^2\vec{v}-\phi\nabla\mu, \tag{3.29}$$

where again we couple the fluid flow to the membrane presence with the term $\phi\nabla\mu$. This fluid will be coupled to the membrane by adding to the dynamic equation the fluid velocity field $\vec{v}$

$$\partial_t\phi = M\nabla^2\mu-\vec{v}\cdot\nabla\phi, \tag{3.30}$$

this equation remains unchanged from the low-Reynolds modelling. Again we will be using the vorticity ω and the stream function ξ

$$\vec{\omega}=\nabla\times\vec{v}, \qquad \nabla\times\vec{\xi}=\vec{v}.$$

This two vectors in a 2D system have only a non-zero component, $\vec{\omega}=(0,0,\omega)$ and $\vec{\xi}=(0,0,\xi)$ and they can be related through the velocity and the identity

$$\nabla\times(\nabla\vec{A})=\nabla(\nabla\cdot\vec{A})-\nabla^2\vec{A}$$

giving the same Poisson equation as for the low Reynolds case

$$\nabla^2\xi=-\omega. \tag{3.31}$$

Thus the first two equations of the system of equations will have no change. The only remaining equation to be obtained is the one for the vorticity, which will be the one to carry the influence of the inertia.

To get this last equation we start as before by doing the curl of equation (3.29) in which

$$\nabla\times(\nabla P)=0 \qquad \text{and} \qquad \nabla\times(\phi\nabla\mu)=(\nabla\phi)\times(\nabla\mu),$$

thus leaves us with

$$\nabla\times(\rho\partial_t\vec{v})-\nabla\times(\nabla^2\vec{v})=\frac{1}{\eta}(\nabla\phi\times\nabla\mu). \tag{3.32}$$

We can permute the curl operators to obtain

$$\rho\partial_t(\nabla\times\vec{v})-\nabla^2(\nabla\times\vec{v})=\frac{1}{\eta}(\nabla\phi\times\nabla\mu), \tag{3.33}$$

with $\nabla\times\vec{v}=\vec{\omega}$ and the fact that we have only a non-zero component for the vorticity

$\vec{\omega} = (0,0,\omega)$ we reach the final equation

$$\frac{\rho}{\eta}\partial_t \omega - \nabla^2 \omega = -\frac{1}{\eta}(\nabla\phi \times \nabla\mu). \tag{3.34}$$

The only change we find in the final system of equations is in the vorticity equation, which instead of being a Poisson equation, one reaches the thermal conduction equation.

With this equation for the vorticity, one can then compute a high Reynolds flow as instead of solving the Stokes equation this equation encompasses the whole Navier-Stokes equation. This is the only equation that changes in the system, thus if we want to compute high-Reynolds fluid or work with visco-elasticity one can use the following system of equations

$$\begin{aligned} \partial_t \phi &= M\nabla^2\mu - (\partial_y\xi\,\partial_x\phi - \partial_x\xi\,\partial_y\phi), \\ \frac{\rho}{\eta}\partial_t\omega - \nabla^2\omega &= -\frac{1}{\eta}(\nabla\phi)\times(\nabla\mu), \\ \nabla^2\xi &= -\omega. \end{aligned} \tag{3.35}$$

We can see how in this case one obtains the kinematic viscosity, which is defined as $\nu = \eta/\rho$. This parameter is sometimes used in fluid dynamics as the fraction η/ρ appears frequently. Thus it is no surprise for this to appear in our inertial system of equations.

3.4.2 Temporal-dependent flow

Using the stream function formulation one can easily adapt the fluid flow to any flow profile that has an analytical expression. One possibility is to use a flow velocity profile that is time-dependent. For example from a flow that gets faster or slower over time to even a oscillating flow.

First of all there is no need to change the phase field equations, as these are uncoupled of the fluid except in the dynamic equation where one has the $\vec{v}\nabla\phi$ term. So, if we change the computation of the fluid velocity field properly, the membrane will experience its effects and nothing will need to be changed. Therefore, one needs to update only the two remaining parameters, the vorticity ω and the stream function ξ.

However, the final system of equations (3.16) needs no change, what we have to change are the boundary conditions. This time-dependent flows can be used in tandem with other model expansions like the inertial flow from the system of equations (3.35).

3.4.2.1 Oscillating Boundary conditions

Having the analytical expression of the velocity profile that one wants to simulate, as stated before to obtain such boundary conditions one simply needs to compute its curl (for the vorticity) and integral (for the stream function).

The case of an oscillating or time-dependent flow is no different. As an example for a sinusoidal flow that changes its flow direction for a frequency w one can compute the boundary conditions for both a Poiseuille and a Couette flow.

Poiseuille Flow

$$v_x(y,t) = \sin(wt)\Big[-\frac{dP}{dx}\frac{1}{2\eta}y(h-y)\Big] \Rightarrow \begin{cases} \xi(y=h) = -\sin(wt)\frac{dP}{dx}\frac{h^3}{6\eta} \\ \xi(y=0) = 0 \\ \omega(y=h) = -\sin(wt)\frac{dP}{dx}\frac{h}{\eta} \\ \omega(y=0) = \sin(wt)\frac{dP}{dx}\frac{h}{\eta} \end{cases}, \tag{3.36}$$

Couette Flow

$$v_x(y,t) = \sin(wt)\Big[v_{wall}\frac{y}{h}\Big] \Rightarrow \begin{cases} \xi(y=h) = \sin(wt)h\,v_{wall}/2 \\ \xi(y=0) = 0 \\ \omega(y=h) = -\sin(wt)v_{wall}/h \\ \omega(y=0) = -\sin(wt)v_{wall}/h \end{cases}. \tag{3.37}$$

3.4.2.2 Different temporal-dependent flows

If other kind of temporal-dependence is required one would have to simply follow the same procedure: at the time-dependant function to the flow velocity equation and simply derive again the boundary conditions. For example, one could have a Poiseuille flow that starts slow but accelerates up to a certain speed at a time $t = 2T$

$$v_x(y,t) = \tanh(t/T)\Big[-\frac{dP}{dx}\frac{1}{2\eta}y(h-y)\Big] \Rightarrow \begin{cases} \xi(y=h) = -\tanh(t/T)\frac{dP}{dx}\frac{h^3}{6\eta} \\ \xi(y=0) = 0 \\ \omega(y=h) = -\tanh(t/T)\frac{dP}{dx}\frac{h}{\eta} \\ \omega(y=0) = \tanh(t/T)\frac{dP}{dx}\frac{h}{\eta} \end{cases},$$

or a flow that suddenly doubles in velocity but just momentarily between the times T_1 and T_2 where $H(t)$ is the Heaviside step function

$$v_x(y,t) = \big(1+H(t-T_1)-H(t-T_2)\big)\Big[-\frac{dP}{dx}\frac{1}{2\eta}y(h-y)\Big] \Rightarrow$$
$$\Rightarrow \begin{cases} \xi(y=h) = -\big(1+H(t-T_1)-H(t-T_2)\big)\frac{dP}{dx}\frac{h^3}{6\eta} \\ \xi(y=0) = 0 \\ \omega(y=h) = -\big(1+H(t-T_1)-H(t-T_2)\big)\frac{dP}{dx}\frac{h}{\eta} \\ \omega(y=0) = \big(1+H(t-T_1)-H(t-T_2)\big)\frac{dP}{dx}\frac{h}{\eta} \end{cases}.$$

As the boundary conditions are only dependant on space derivatives we simply need to multiply the Boundary conditions by the temporal dependence we want to simulate. Therefore adapting this model to use temporal-dependent flows is trivial work and very easy to numerically implement.

3.4.3 Generalisation to 3D

The proposed model has been exclusively written for a 2D system, however an expansion to three dimensions is possible. Although is usually understood that the stream function only works for a 2D system, that is not accurate. It is true that in 2D the stream function formalism is straightforward, however that does not mean that expansion to 3D is impossible. In the literature there are various works that deal with this [88, 89, 90].

In the end we have one more degree of freedom, and the 3rd dimension makes so that the vorticity $\vec{\omega}$ and the vector stream function $\vec{\xi}$ cannot be said to have only one non-zero component. Solving the Navier stokes equation by the use of a vector potential, which we can call stream function is still possible. The most difficult part of all would be to define the proper Boundary Conditions for this new stream function, which will not be as straightforward as in 2D. Therefore, the final system will be similar to the system of equations (3.16), but working with vectorial fields instead of scalar ones

$$\begin{aligned} \partial_t \phi &= M\nabla^2\mu - (\nabla \times \vec{\xi})(\nabla\phi), \\ \nabla^2\vec{\omega} &= \frac{1}{\eta}(\nabla\phi)\times(\nabla\mu), \\ \nabla^2\vec{\xi} &= -\vec{\omega}. \end{aligned} \tag{3.38}$$

This system of equations is very similar to the 2D one, and as such all the expansions to the 2D model can be applied to the 3D case. Obtaining the Boundary Conditions will be less trivial than for the 2D case but nonetheless one can work with time-dependent flows and inertial flows in 3D.

Chapter 4

Membranes in a Poiseuille flow

4.1 Poiseuille flow in a narrow channel

The Poiseuille flow occurs when a pressure gradient is applied between the two ends of a pipe or a channel. This is the flow best used to describe the fluid flow inside a micro-channel or a micro-capillar of our circulatory system, which we aim to do in this section. The circulatory system ranges from centimetres radius arteries to capillars and micro-capillars. Inside micro-capillars we get a low Reynolds flow, or a Stokes flow, as the presented model in this channel.

The red blood cell morphology is very well known inside channels that are slightly bigger than the cell, both from experiments [91, 92] and simulations [60, 73] alike. This particular confinement gives varying shape regimes for different flow speeds. Example of experiments on red blood cells in this conditions can be seen in **Figure 4.1** and the aim in this section is to replicate and explain this membrane morphologies.

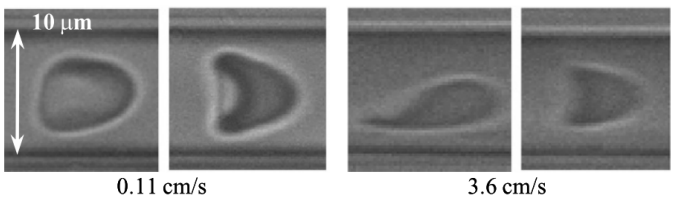

Figure 4.1: Experimental results adapted from Guido et al. [91]. Images of red blood cells flowing in micro-channels of diameter 10 μm at different velocities.

For this particular confinement, solving the presented model results for a red blood shaped cell can be seen in **Figure 4.2** for a variety of flow speeds. For this given confinement and viscosity contrast ζ, the shape deformation of the cell induced by the fluid depends entirely on the flow speed. In **Figure 4.2** we can see how with changing

velocity the cell exhibit different shape regimes which are known as normal discocytes, slippers, and parachutes.

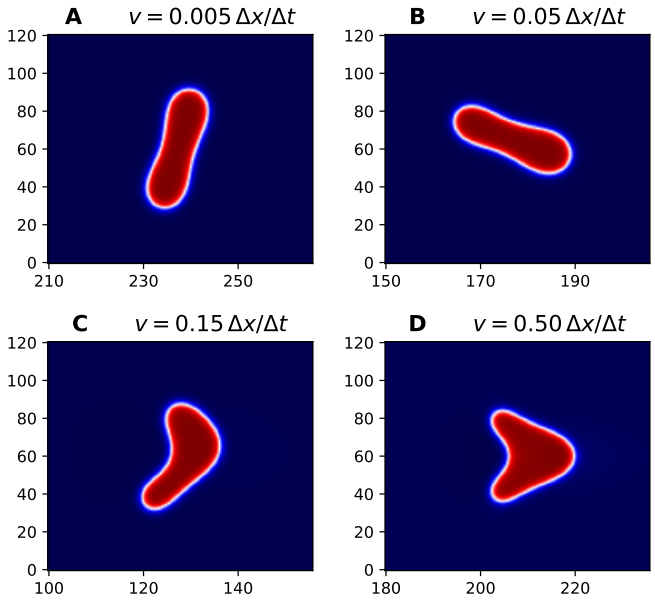

Figure 4.2: Cell morphologies in confined channels. **A-D**: Different flow speeds from slower to faster with $b/a = 1.5$ where b is the channel height and a the cell size.

For very slow flows we have that the discocyte shape is maintained like in **Figure 4.2A**. In this case the cell mostly flows along very slowly without any apparent deformation caused by the flow. When the speed is starting to increase we have a change in the shape regime to what is called the *slipper* shape (**Figure 4.2B-C**). This slipper shape is characterised for an asymmetry respect to the centre of the channel, and one half of the cell getting bigger than the other. The final shape regime for red blood cells is the highest velocity regime where the cells develop the so-called *parachute* morphology, as seen in **Figure 4.2D**. In this regime the bending energy becomes subdominant and the velocity field in the channel is the dominant mechanism of deformation. The different regimes span a wide array of velocities, involving 2 orders of magnitude to go from the slowest to the fastest.

All this shapes have been obtained and studied previously and that is why they are the perfect way to prove the accuracy of a new model. In particular the results match pretty well with previous phase field models of membranes in a flow [60, 73, 74] in which a Helfrich model for the membrane was coupled with a lattice-Boltzmann description of the flow. This helps support the path taken to solve the hydrodynamics of the system.

We can get a rough approximation of the real values of the different parameters that characterise the simulation. In **Table 4.1** we can see the values that these parameters take for simulations where the cell is approximately $a = 65\Delta x$ long. These are approximate values to what the internal units of the numerical results take. One has to take into account that even if the internal units for time are Δt the simulations themselves advance much less time at each temporal iteration. Usually each time step in the simulation advances $0.01\Delta t$, this changes for simulations with higher rigidity where we have to decrease the time increment. Moreover changing the cell size in a simulation would require re-scaling of these units.

	x, y	t	κ	η
Internal Units	Δx	Δt	1 EU	1 EU $\cdot \Delta t/(\Delta x)^3$
Real Units	0.1μm	10^{-5}s	$2.8 \cdot 10^{-19}$J	$2.8 \cdot 10^{-3}$Pa$\cdot s$

Table 4.1: Units translation for a simulation with a cell of size $a = 65\Delta x$ and the bending rigidity of a red blood cell, EU refers to Energy Units. Depending on the resolution of the simulation the conversion changes.

To obtain the real life scale of the simulations we have to decide a target size of membrane to be simulated, in this case we take the red blood cell membrane as our goal. The scaling parameters are then taken by fixing the space and energy modulus to values that correspond to one real red blood cell. In this case we are taking the value reported by Timo Betz et al. [12].

Then, using those fixed parameters and comparing with the velocities that parachutes, slipper, and discoids take in a micro-channel, we can obtain the velocity and with that Δt. After obtaining the time scale, energy scale, and length scale we can simply obtain the viscosity as shown at the table. This is the enslaved parameter that will depend on all the decisions that have been taken up until this point. This approach on obtaining the real units would be difficult to implement for flows with little or no experimental data, as comparison with experiments is crucial to obtain the time-scale Δt. However, this does not mean that we have to re-calculate the units when changing the channel size.

The units from **Table 4.1** can be used for any simulation of a Poiseuille flow where the red blood cell measures $a = 65\Delta x$ regardless of the value that any other parameter take.

4.1.1 Hydrodynamic characterisation

The computed system of equations (3.16) consist of the phase field ϕ the vorticity ω and the stream function ξ. To study the influence of the cell on the flow and vice-versa we represent all this parameters in **Figure 4.3** where a parachute shaped cell is obtained. If we look at the cell influence on the flow, when looking at the flow velocity

in **Figure 4.3 C** where the velocity vector field is plotted, we see almost no change from what we would expect for a Poiseuille flow. Even in the region where the membrane is present there seems to be no change on that region for neither the velocity nor ξ. This lack of change reflects that the cell is mostly flowing along with the liquid, influencing the actual flow only barely. That is why to get to see the influence of the cell on the flow one studies the deviations of ξ respect to an ideal Poiseuille without any obstacles in **Figure 4.3 D**.

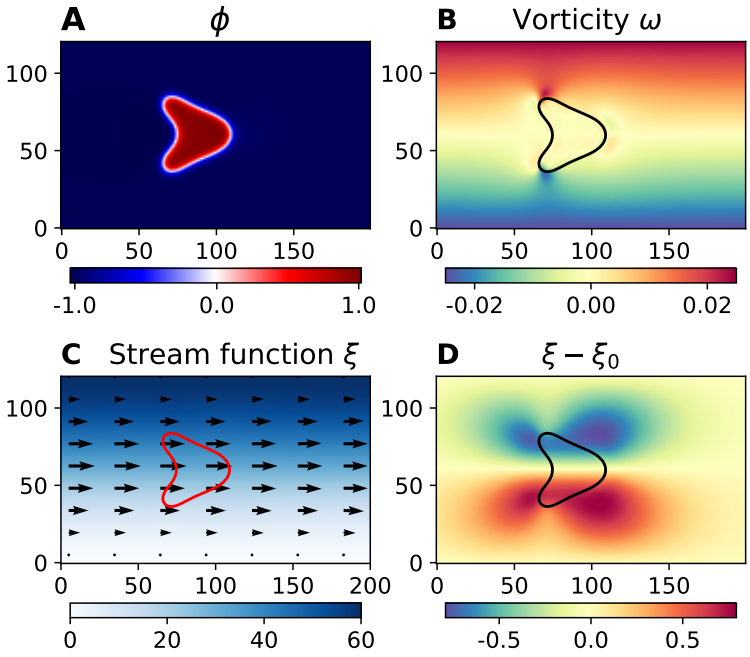

Figure 4.3: Poiseuille flow with slight confinement exhibiting parachute morphology. **(A)** Order parameter; **(B)** Vorticity; **(C)** Stream function and velocity field; and **(D)** Deviations of the stream function ξ with respect to an empty channel ξ_0. Simulation of a channel sized $400\times121\Delta x$ and a flow speed of $0.5\Delta x/\Delta t$.

The plot $\xi - \xi_0$ does not only shows us that there is in fact influence of the cell on the flow but also shows us the spatial reach of this influence. This information will be useful to ensure that the simulations are big enough to avoid self-interaction of the membrane with itself through the hydrodynamics combined with periodic boundaries in the direction of the flow.

The deviations of the stream function $\xi - \xi_0$ shown in **Figure 4.3** are for a symmetric parachute but many equilibrium shapes are asymmetric. For an asymmetric shape, as can be seen in **Figure 4.4 A**, the stream function deviations change slightly and lose their symmetry. Even after losing symmetry the spatial reach of the influence of the cell (seen through $\xi - \xi_0$) does not seem to increase. Here in **Figure 4.4 B** the

vorticity deviations $\omega - \omega_0$ can also be seen, which have been not shown until now. The cause is –as can be seen in **Figure 4.4 B**– that while the influence of the cell on the stream function seems to have a long spatial reach, this is not the case for the vorticity deviations. Instead, the deviations $\omega - \omega_0$ seem to be focused in areas with the larges curvature of the membrane and do not travel very far in space. So even if the vorticity deviations $\omega - \omega_0$ are present, when interested in ensuring no cell self-interaction, it seems more important to look at the stream function deviations $\xi - \xi_0$.

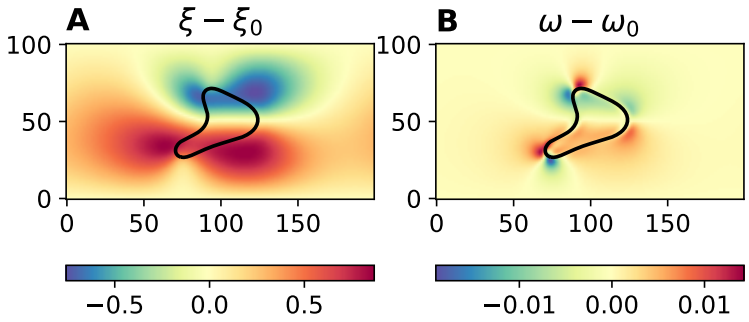

Figure 4.4: Asymmetric parachutes. Cell-induced **(A)** stream function and **(B)** vorticity deviations. Note how the stream function deviations are significant at distances comparable to the cell size. Flow speed $v = 0.5\Delta x/\Delta t$ and size of channel 200×101.

However, as has been explained in Chapter 3, ξ and ω deviations are not the only hydrodynamic parameters that we can compute. In **Figure 4.5** we can see the influence of a parachute shaped cell on the velocity and pressure, and the shear stress tensor. In comparison to an ideal Poiseuille flow we can see how the fluid velocity in the centre of the channel slows down because of the cell presence. As the fluid is incompressible and due to the fact that far from the cell the flow rate is the same, if the fluid in the centre of the channel where the cell is located is slowing down it will have to find another way. That is why the fluid has to go around the cell and therefore why the velocity close to the wall is higher than for a Poiseuille in absence of cell. The vertical component of the flow velocity $v_y - v_{y0}$ agrees with the previous description of what the liquid is doing, circling around the cell with a more complex swirl around the cell edges where the vorticity is highest.

The patterns in $v_x - v_{x0}$ of **Figure 4.5** also can be explained using the pressure field. As the pressure behind the cell increases because of the fluid slow down produced by the cell the pressure in front of the cell will decrease. The patterns on velocity influence by the cell can be understood more clearly by looking at the pressure. As there is a high and a low pressure regions inside the fluid, there will appear a flow going from high pressures to low pressures. After developing the parachute shape, the cell remains symmetric and travels rigidly with the fluid, consistent with previous simulations [59].

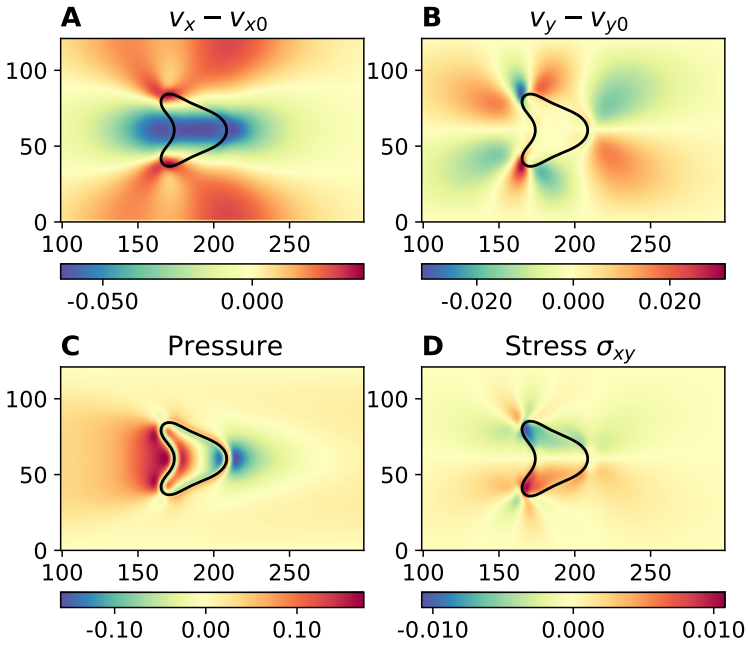

Figure 4.5: Symmetric parachute. **(A)** Deviations of the horizontal velocity with respect to ideal Poiseuille; **(B)** Deviations of the vertical velocity; **(C)** pressure variation by the cell; **(D)** Shear stress. Same simulation parameters as in Fig. 4.3.

Finally, it is also possible to see the shear stress produced on the cell membrane using the transverse component of the shear stress tensor σ_{xy}. The absolute value of stress it is maximum at the cell tips, as the membrane presence diverting fluid towards the tips (**Figure 4.5A**) to go around the cell. This also the reason for the increases of the vorticity at the parachute tips that can be seen in **Figure 4.3**. All in all looking at the stress and its direction we can see how the cell tips are being pressed towards the centre of the channel, that is why the top side has a negative value for σ_{xy} and the bottom side of the cell a positive value. When comparing the stress and pressure plot it can be observed that regions with large pressure correspond to regions with a lower shear stress.

For slipper-shaped cells, or any kind of non-symmetric cell shape, the results vary qualitatively. As can be seen in **Figure 4.6** a slipper shaped cell tends to align towards one half of the channel, this in turn changes how the fluid adapts to the presence of the cell. While looking at the velocity one can see that the cell is still slowing down the fluid at the centre of the channel in this case the fluid is having a preferred side in which to circle around the cell. Most flow changes then will happen in the side at which the cell is tilted towards. As a consequence, at the front (right side) of the cell, both the pressure and the shear stress are large.

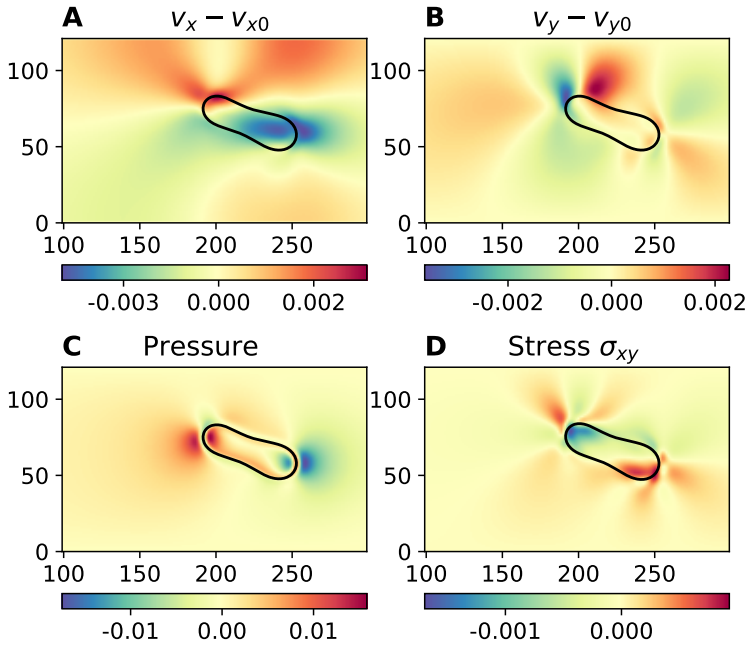

Figure 4.6: Slippers. **(A)** Deviations of the horizontal velocity with respect to an empty channel; **(B)** Deviations of the vertical velocity with respect to an empty channel; **(C)** Fluid pressure; and **(D)** Shear stress. Simulation of a channel sized $400\times121\Delta x$ and a flow speed of $0.05\Delta x/\Delta t$ and a viscosity of $\eta = 1$.

4.1.2 Stability analysis

How a simulation reaches the stationary solution can be studied with $\mathcal{W} = \int(\omega - \omega_0)^2 dV$ and $\mathcal{X} = \int(\xi - \xi_0)^2 dV$ which are equations (3.24) and (3.25) respectively. These observables allow us to track the deformation history of the cell. In **Figure 4.7** the square of vorticity and stream function deviations evolution over time can be observed. In this Figure both $\mathcal{W}$ and $\mathcal{X}$ have very similar behaviours. At the start of the simulation one can see a big decrease in both parameters, when the changes on the cell membrane shape are faster and more dramatic and a slow down to a plateau as the cell membrane reaches its final equilibrium shape. Thus, we can use $\mathcal{W}$ and $\mathcal{X}$ as measurse of the elastic deformation of the cell and the dissipation caused by friction between the cell and the flow.

For now these parameters seem to only point the characteristic time to reach the stationary solution, but we could use it for systems with time dependence or where shapes are not completely stationary. In an oscillating flow with an inertial flow, the variation of these parameters could give insight to the visco-elasticity of the membrane.

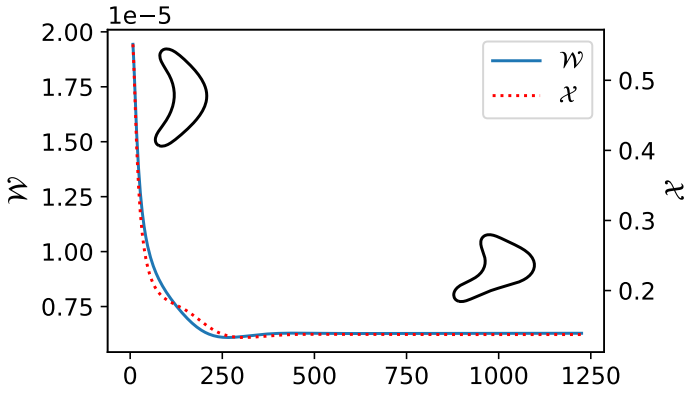

Figure 4.7: Time evolution of the integrated squared cell-induced stream function $\mathcal{X}$ and vorticity $\mathcal{W}$ deviations with respect to an empty channel. These observables capture quantitatively the effect of the cell shape on the flow until the system reaches the steady state. Same simulation parameters as in Fig.4.4.

4.2 Poiseuille in wide channels: anti-parachute and tumbling

In this section, we present results for channels whose width is several times larger than the size of the cell. For very wide channels we have that the central region of the channel is more akin to a constant flow velocity than a varying one when looking at the cell length-scales. This happens because the velocity profile of a Poiseuille flow is a parabola, and this parabolic profile flattens at the centre of the channel.

In the case of a parachute we have a channel of similar size to the cell. For a parachute shape we have a cell which has a very different fluid velocity at each point of its volume. However this does not happen when the channel becomes several times the size of the cell. We see how at the centre of the channel we have a region of approximately constant speed and, consequently, lower shear stress and higher Reynolds number.

4.2.1 Anti-parachute shape

This lower level of confinement brings many changes respect to the previous results. First, we find that when starting with a cell centred in the channel the cell evolves a shape we called "anti-parachute" shape, which can be seen in **Figure 4.8**. This shape is meta-stable, depending on the parameters of the simulation we can find a perpetually stable anti-parachute or we can find it becoming unstable and evolving into a slipper shaped cell. In **Figure 4.8 AB** we see an anti-parachute shaped cell and the final result of a simulation in which the shape became unstable and changed shape. This anti-parachute is unstable for medium-width channels or for very high speeds.

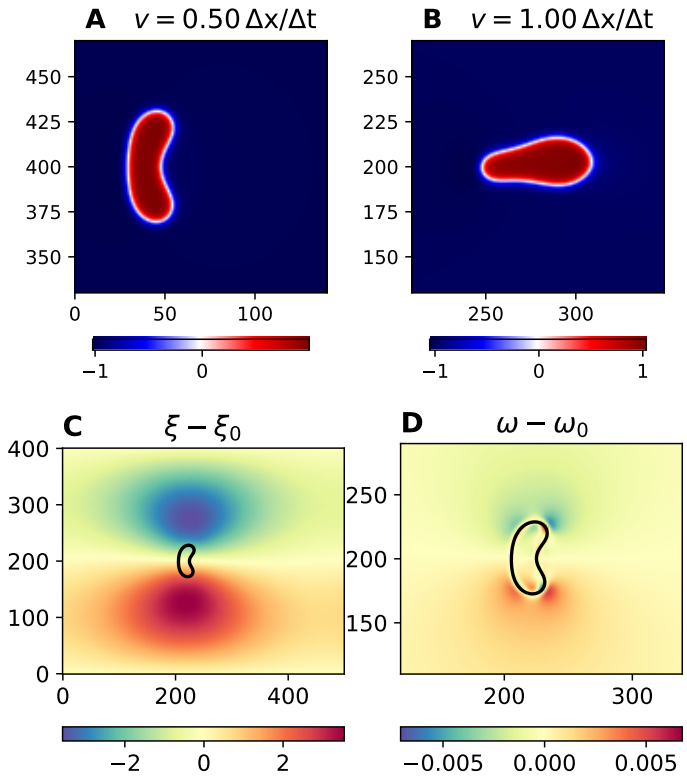

Figure 4.8: Anti-parachutes. **A-B** Snapshot of a cell in a fast flow inside a wide channel. Cell-induced **(C)** stream function and **(D)** vorticity deviations (flow speed of $v = 0.5\Delta x/\Delta t$). Channel sizes: **A** 600×800 **B,C,D** 500×400. Width-cell ratios: **A** $b/a = 12$, **B, C, D** $b/a = 6$ where b is the channel height and a the cell size.

In **Figure 4.8 C-D** we can see how different is the deviation of the stream function and the vorticity in comparison to a more confined channel. In this case the influence on the stream function reaches much further but has a lower gradient, decreasing slowly. However the deviation of the vorticity is much more similar to a more confined channel.

To understand the anti-parachute shape first we have to look at what happens for a normal parachute shaped cell. The parachute has a very different fluid velocity at each point of its membrane, and the cell ends up getting the shape of the velocity profile. Thus, the parachute ends up having an approximately parabolic shape due to the flow velocity profile along the channel. This is in part due to the rather large variation of fluid velocity along the cell, as the channel is almost the same size as the cell. Thus the velocity gradient is rather high at all points of the membrane for this channel confinement.

However, for very wide channels the velocity gradient is much lower. The fluid

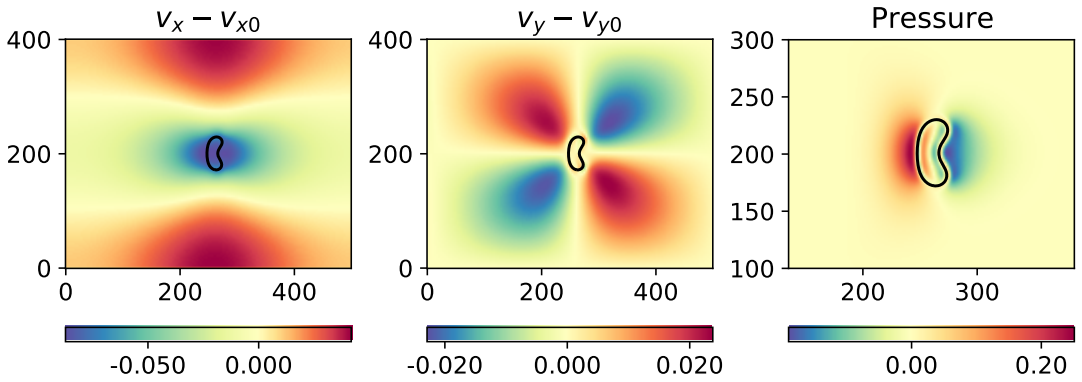

Figure 4.9: The anti-parachute hydrodynamic influence on the flow. Channel sizes: 500×400. Width-cell ratio: $b/a = 6$ where b is the channel height and a the cell size. Speed $= 0.5\ \Delta x/\Delta t$.

velocity change through the cell membrane happening much more slowly, for wide enough channels we could even approximate it to constant. In that constant-speed region the deformation on the membrane is different because here we have a flat obstacle that is feeling the same flow speed at all points of the membrane. In these wide channels as centre is a constant-speed region if the membrane were to deform in a way to have the same shape as the velocity profile it would remain flat. Instead, as the fluid is circling around the membrane to avoid the obstacle that ends pressing the edges of the cell inwards, giving it the anti-parachute shape. The cell edges are pressed towards the flow direction similar to what can be seen in **Figure 4.9** on the velocity changes $v_y - v_{y0}$. This force bends the cell in the opposite direction of a normal parachute shape resulting in the shape displayed in **Figure 4.8A**. The cell is generating a resistance proportional to its cross-section so it is normal for the flow to deform the obstacle in a way that reduces this cross-section as represented in **Figure 4.10**. However, this is only happening because the flow speed is approximately equal across the cross-section of the membrane.

In this special case the bending contribution becomes subdominant and the only two players in the interface shape are the hydro-dynamical forces and the area conservation. While the area conservation is forced by the membrane properties, the flow is trying to minimise the parameter $v_y - v_{y0}$ seen in **Figure 4.9**. And to this end decreases the cross-section of the cell while maintaining the area.

4.2.2 Stability analysis

The anti-parachute shape is a meta-stable shape, meaning that under certain conditions the shape is eventually lost. This happens at channels that are not wide enough or for very high flow velocities. The anti-parachute starts to oscillate in the centre of

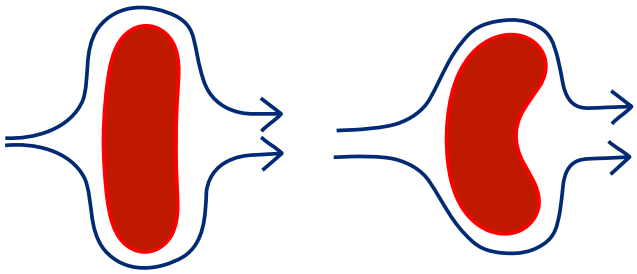

Figure 4.10: Sketch of how the fluid circles around a cell. We can see by comparing the two shapes how the anti-parachute shape has a lower cross-section and produce a lower drag.

the channel and eventually in one of the oscillations it slips and leaves the centre. It then evolves into a slipper-shape like in **Figure 4.8 B** and travels back to the centre of the channel. This behaviour can be studied using the integrated squared vorticity deviations $\mathcal{W}$ from equation (3.24) which reads

$$\mathcal{W} = \int_{\text{channel}} (\omega - \omega_0)^2 dV.$$

As shown in **Figure 4.11** $\mathcal{W}$ starts dropping fast but finds a temporary plateau, however this simulation being at a very high flow speed the shape is lost until it finds a second and last plateau with the final stable shape. The longer the membrane maintains anti-parachute shape the longer the plateau becomes, matching the longevity of the shape.

Using the model we have obtained simulations where the anti-parachute is quickly lost like in **Figure 4.11** and other simulations where the anti-parachute survived the entire computation and seemed to be able to survive indefinitely. Following the result of Ref. [86], we conclude that the the anti-parachute morphology behaves as a solid object (conserved vorticity) during that transient time.

Usually the final result after losing the meta-stable shape of the anti-parachute includes a slipper shape parallel to the flow like in **Figure 4.8 B**. However in **Figure 4.11** a tilt with respect to the channel direction can be observed. It should be pointed out that the results display variability and the presentation of the results tries to reflect that. On the one hand, the cell is close to the centre but still tilted with respect to the centre. Also, simply due to the evolution of that particular simulation, finding the final equilibrium position takes much longer than the others.

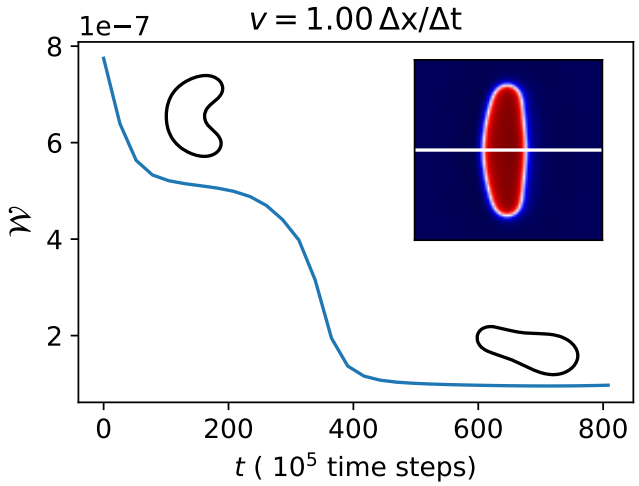

Figure 4.11: The sum of the squared deviation of the vorticity ω over time. Each plateau corresponds to a given membrane shape that is also represented. Inset of the initial conditions, shaped as an ellipsoid with the reduced volume of a discocyte with a white line showing the centre of the channel. Size of the channel 500×400 and $b/a = 12$ where b is the channel height and a the cell size.

4.2.3 Non-centred cells on a wide channel

The results shown are based on cells that are very close to the centre of the channel when the flow starts. The initial conditions were not perfectly centred, to avoid possible computational meta-stability of the results, and thus the cell was displaced $1\Delta x$ from the centre. However, one could argue that this would not be the average starting position of a cell inside a wide channel in an experiment. So, study on what happens when you start away from the centre has to be done.

This exactly is what is represented in **Figure 4.12**. The first panel **A** represents the y position of the centre of mass of the cell over time and the shape of the cell at different points of time. It can be seen how the cell develops an elongated shape and travels with a rather constant speed to the centre of the channel, where it develops a slipper shape. When looking at the parameter $\mathcal{W}$ in **Figure 4.12 B** one can see that is very different from other previous Figures. In this case the change on this parameter is slowly changing over time, as the cell shape changes continuously from the initial elongated slipper-ish shape to the final one, while it approaches the centre.

4.2.4 Tumbling

So far, we have studied the case with a viscosity contrast $\zeta = 1$ however, the observed behaviour can be lost at high viscosity contrasts. In 2D simulations for high viscosity contrasts, the so-called tumbling dynamics can be obtained [80, 82]. In **Figure 4.13**

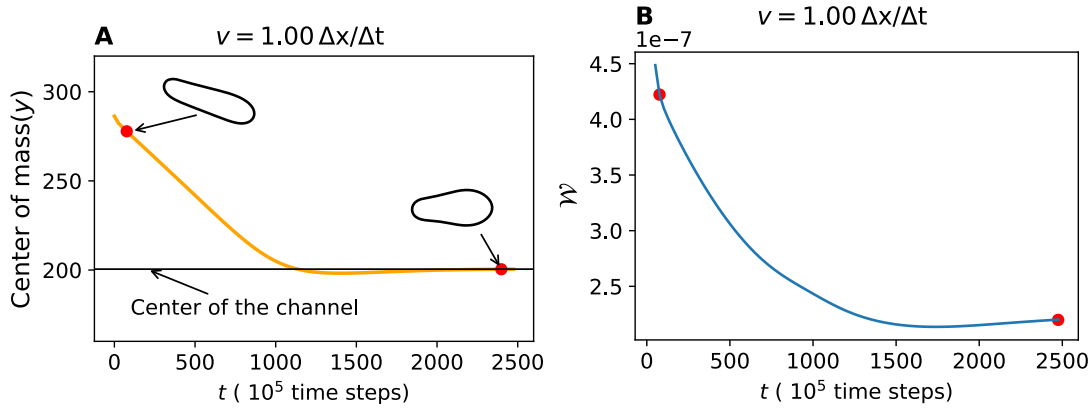

Figure 4.12: Time evolution of the centre of mass of a cell located initially displaced with respect to the centre of the channel. The orientation as well as the location change continuously with time. Size of channel 400×400. Width-cell ratio $b/a = 6$ where b is the channel height and a the cell size.

we reproduce this sort of behaviour using a viscosity contrast of $\zeta = 6$. We choose this viscosity contrast because it is similar to the contrast between a red blood cell cytosol and the blood plasma/water. With this viscosity contrast and an un-centred initial conditions for the cell we can see the tumbling effect. The initial position for the membrane is displaced from the centre so the symmetry is broken and the tumbling mechanism can operate right away. If we started centred we would have to wait for the anti-parachute state to break before seeing tumbling.

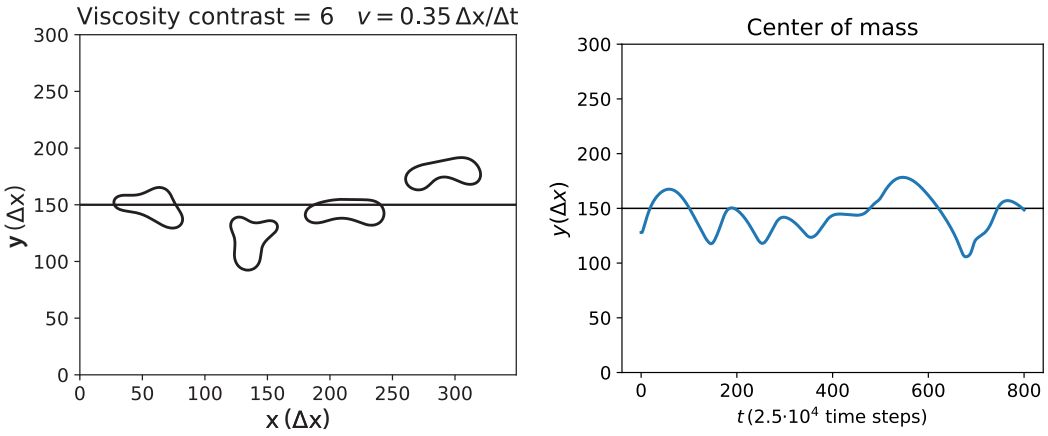

Figure 4.13: Cell evolution over time, from left to right there is represented different snapshots advancing time. There is a black solid line indicating the centre of the channel. Simulation of 301×350 with a width-cell ratio $b/a = 4.5$ where b is the channel height and a the cell size.

The perpendicular position of the centre of mass can also be seen in **Figure 4.13** as

a function of time, where we see big changes and swings from one half of the channel to the other one. As reference on how big this displacements from one side of the channel to the other are, we have to take into account that the cell has a size of about $65\Delta x$. Taking this cell size into account and looking at **Figure 4.13** we can see that the displacements go around 100-150 Δx thus the displacements of the tumbling dynamics are big in comparison with the cell.

The tumbling effect can also be seen using $\mathcal{W}$ and $\mathcal{X}$ which are represented in **Figure 4.14**. When the cell tumbles its shape changes greatly, and between tumbling and tumbling sometimes there is a short amount of time where the cell looks rather stable before restarting the tumbling. This is reflected in **Figure 4.14** on both $\mathcal{W}$ and $\mathcal{X}$ where we can see peaks at each tumbling motion and valleys and plateaus when the cell travels without further deformation.

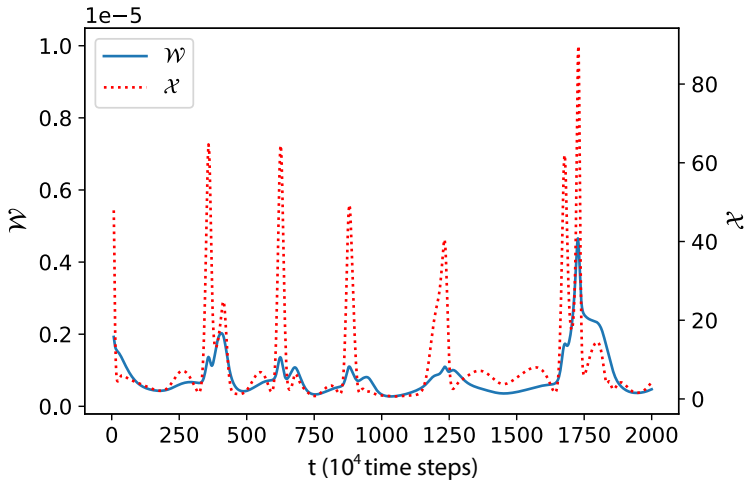

Figure 4.14: $\mathcal{W}$ and $\mathcal{X}$ over time t for a simulation with tumbling present.

Studying this phenomenology it is easier to get more insight on the parameters $\mathcal{W}$ and $\mathcal{X}$ and their differences. Between both variables $\mathcal{X}$ looks more reactive, firing sometimes even when little to no change happens, however it also represents that something is happening before $\mathcal{W}$ does. That is why $\mathcal{X}$ can be more useful for real-time tracking of when events are going to happen while $\mathcal{W}$ is more stable and can be better to simply analize and compute statistics about the state of the system.

4.3 Poiseuille super-confined

We have studied the confinement level where the channel is bigger than the cell. So now lets see a higher confinement level with a channel whose section much smaller than the cell. In **Figure 4.15** we can see the results for a cell double the size of the

channel, thus a channel width to cell ratio of $b/a = 0.5$. Here we can see how the stream function and the vorticity behave with this highly confined case.

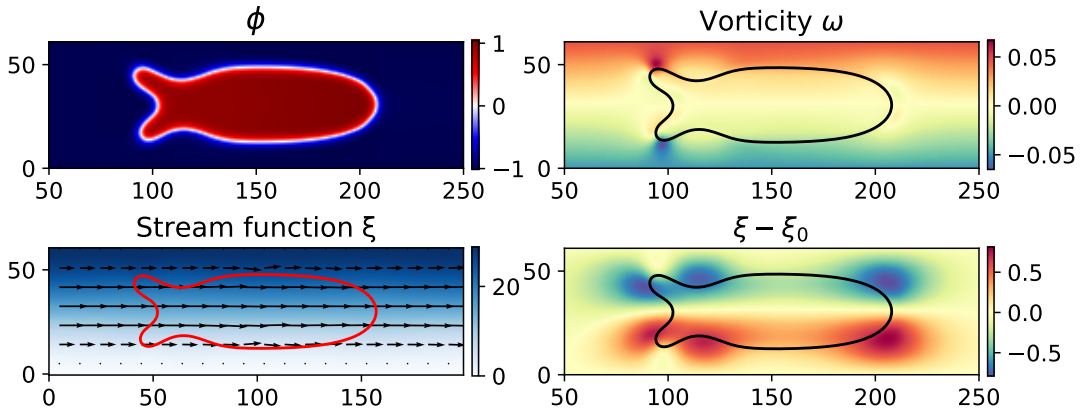

Figure 4.15: Super confined cell takes a squid-like shape under some parameters. Simulation parameters: cell size $120\Delta x$ channel size 60×300 Poiseuille speed $=0.20\Delta x/\Delta t$.

The resulting shape of the membrane still depends on the velocity of the fluid, however the results obtained differ greatly from the shapes obtained for a wider channel. We can see how the cell shape change with varying velocity in **Figure 4.16**.

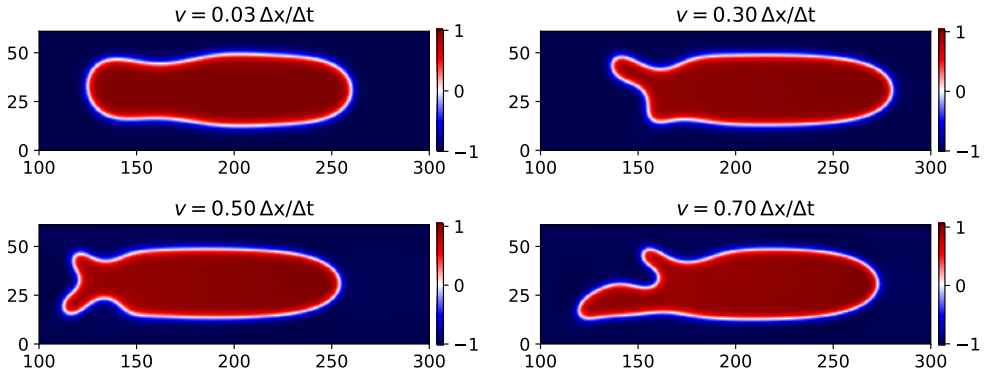

Figure 4.16: Super-confined simulations at varying speeds. Simulation parameters: cell size $120\Delta x$ channel size 60×300.

There are experimental results with which we can compare our results. We can see that the simulations show similar results when compared to the experimental results of Guido and Tomaiuolo [91] as numerical results from Freund [93] in **Figure 4.17**. The results only partially match the experimental ones, however we expect a better match when simulating a cell with the reduced volume closer to those cells in the experiment. The confinement level will also be very important to obtain the same membrane shape.

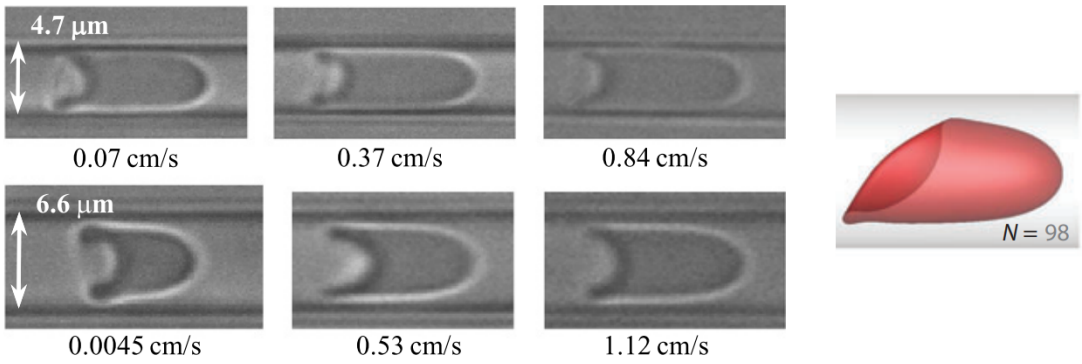

Figure 4.17: Left: Experimental results adapted from [91] for Red Blood Cells in small microchannels. Images of RBCs flowing in vitro in microcapillaries of diameter 4.7 and 6.6 μm at different velocities. **Right:** Simulation of a super-confined red blood cell, adapted from Freund [93].

4.3.1 Hydrodynamic characterisation

The hydrodynamic parameters computed for the super confined case in **Figure 4.18** are quite similar to the parachute case in **Figure 4.5**. In the super-confined case the results, as expected, are more compressed together but share similarities with the parachute results. The membrane shape from **Figure 4.18**, match very well with previous simulations by Freud. If one looks at the profile that one gets from cutting in half the cell simulation in **Figure 4.17**. The indentation coming from the backside of the cell is less accentuated, hinting towards being a lower flow speed than Freud results.

Size of the cell is highly important in simulations of this kind, as the little tentacles seen in 2D that the membrane is producing are close in size to the width of the interface. If we go for a cell that is too small we will not be able to see this shapes properly as we can lose some crucial details.

All in all, the confinement level changes completely the diagram shape of a biological membrane when compared with the previous section. We had already a membrane cell under confinement, but increasing this confinement changes the final result immensely.

4.3.2 Channel size effect

The change from confined to super-confined is gradual as can be seen in **Figure 4.19**. There one can see the colormap of the velocity changes produced by the cell in the direction of the flow. The results for the less confined channels (the bigger ones) show a more or less homogeneous slow down of the fluid inside the cell in the centre of the channel. However, as we decrease the channel height the decrease of the flow speed stops being homogeneous inside the cell, and is maximum at the front and the back.

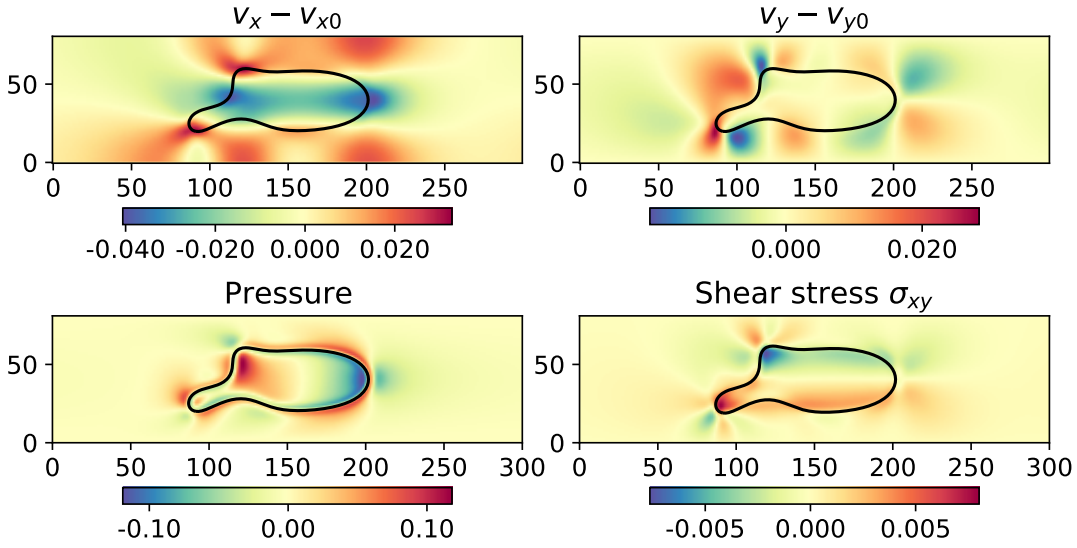

Figure 4.18: Super confined cell. **(A)** Deviations of the horizontal velocity with respect to an empty channel; **(B)** Deviations of the vertical velocity with respect to an empty channel; **(C)** Fluid pressure; and **(D)** Shear stress. Simulation of a channel sized $300\times81\Delta x$ and a flow speed of $0.25\Delta x/\Delta t$ and a viscosity of $\eta = 1$ and consisted of $4\cdot10^7$ iterations.

For the most confined cases like $H = 80$ from **Figure 4.19** it can be clearly seen that the slow down of the fluid is concentrated at the front and the back, but the fluid picks up speed while inside the cell.

Moreover, the parachute shape is lost also gradually with the change in channel height. Seems that the super-confinement accentuates asymmetry in the equilibrium cell shape.

In these simulations the interaction between the wall and the membrane is not treated specially. Because of the diffuse interface, we see that the membrane will not approach the channel wall as it would require to squezee and tighten the width of the interface. Therefore we cannot have the cell approach the channel walls to more than 2ε, which in this simulations where $\varepsilon = 2\Delta x$ that the most the membrane will approach the wall.

4.4 Conclusions

In this chapter we prove the validity of the newly introduced mathematical formulation for two-dimensional deformable cells flowing in a channel. This model is based on low-Reynolds flow by the use of the Stokes equation combined with the well-known membrane phase-field models. The simplicity of this model its one of its biggest strengths and arises from the coupling of the membrane phase field with the liquid flow through the stream function ξ and the vorticity ω. To numerically compute the evolution of the

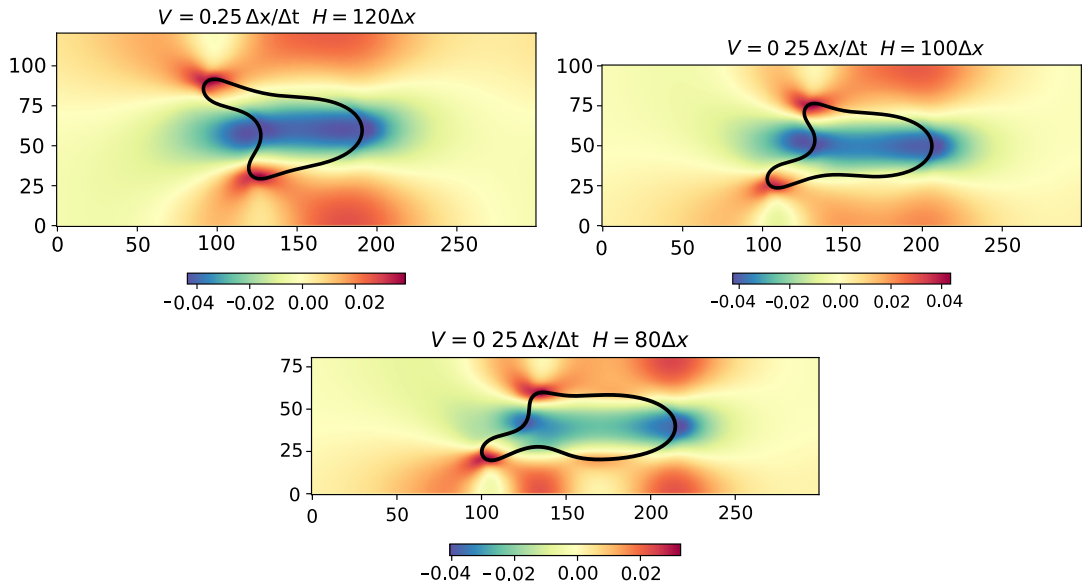

Figure 4.19: Velocity deviation $v_x - v_{x0}$ colormap for a constant velocity but different channel sizes. The shape of the cell membrane is also plotted.

system, aside from solving the previously presented membrane phase field, one needs to simply solve two Poisson equations to compute the liquid behaviour.

There are some well-known shapes that red blood cells take inside a confined micro-channel that have been studied thoroughly in the literature: the parachute, the slipper, and the discoid shapes. To prove the validity of the model this shapes have been the first to be replicated, by simulating red blood shaped cells inside a micro-channel slightly bigger than the cells itself.

Then the cells have been studied aside from their final shape, by exploiting the hydrodynamic parameters that we introduced to solve the flow, the stream function ξ and the vorticity ω. By studying the deviations of these parameters with respect a channel with an ideal Poiseuille flow without any obstacle inside one can study the flow deformation and the stability of the cell. One of the most important results is the ability to study the convergence and stability of a cell shape and position by studying the squared integral of the deviations for the stream function and vorticity $\mathcal{X}$ and $\mathcal{W}$.

After ensuring the veracity of the results the model and the methodology have been applied to study different confinement levels: the super-confinement of a channel smaller than the cell inside and the very low confinement of a channel around ten times the size of the cell.

For the very wide channels a novel meta-stable shape has been obtained: the anti-parachute. This shape is only obtained because for a very wide channel (in comparison to the size of the cell) the Poiseuille flow gets an approximately constant velocity at

the centre of the channel. Although under specific conditions this shape is maintained forever, this shape however is lost after a time for simulations where the channel is medium-sized or the velocity is too high. The anti-parachute shape should be able to be obtained experimentally, although it requires a very centred cell and a very ideal flow, so it might be very hard to achieve. With the viscosity contrast, which measures the ratio of the inner and outer viscosities, tumbling has also been achieved, replicating known results for 2D cell simulations where tumbling is obtained at high viscosity contrast [80, 82].

Finally, cells in a super-confined channel have been studied, where the channel was smaller than the cell size. In this case, the shapes obtained are very different from all the previous shapes, and more or less agree with previous experiments [91] and simulations [93]. However it seems that for these confinement levels, the model is not as lenient when not exactly matching the reduced volume and the confinement levels of the experiments. This is apparent when slightly changing the size of the cell, its reduced volume, or the confinement, leading to very big changes in final shape of the cell.

Chapter 5

Membranes in a Couette flow

5.1 Couette flow

When one has a fluid contained between two walls and one of this walls moves one gets a Couette flow, sometimes called a simple shear flow [94]. The fluid in contact with the walls is stuck to them, this is called the no-slip boundary condition. In the Poiseuille flow the consequence of this is that the fluid at the walls is not moving, as the walls are usually still. However, in the case of having a moving wall, due to the no-slip boundary condition, the fluid in contact with the wall moves with the wall at the same speed. This fluid moving with the walls generates the Couette flow, where one can find a linear velocity profile where the velocity value decreases from the moving wall with distance. As the expression of the velocity profile for a Couette flow is known, one can implement it to a simulation with the model presented in Chapter 3. Using the boundary conditions shown in Chapter 3 one obtains the flow as seen in **Figure 5.1**.

Such flow is a good approximation to what a red blood cell experiences inside a rheometer. For example a plate rheometer consists of two parallel discs, one of which rotates, and the space between the two discs is filled with liquid. The rheometer then measures the torque required to rotate the disc. Because of the friction with the fluid requires an amount of energy to rotate the disc and how difficult it is to do so is proportional to the fluid viscosity. This is the motivation behind studying the effects of a Couette flow for a red blood cell.

There are only 2 parameters of the Couette flow that characterise the flow locally: the flow velocity at that given point and the velocity slope or velocity gradient ∇v. We refer as velocity slope to how rapid the velocity changes with distance to the wall. For a Couette flow moving towards the x axis the velocity slope is the derivative in the perpendicular direction to the flow $\partial v_x/\partial y = v_{wall}/H$. Then, we will not only characterise the cell deformation and movement in a Couette flow based on the velocity of the flow at the centre of mass, but also by this velocity slope. In conclusion, for two cells inside

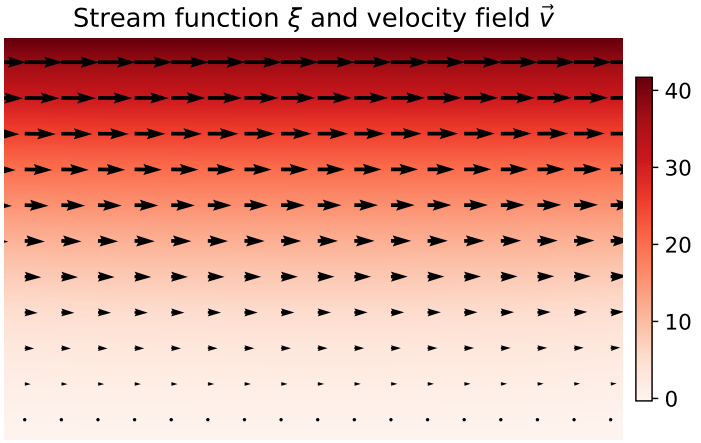

Figure 5.1: Velocity vector field and stream function colormap for a Couette flow. For a top wall moving we can see how the velocity increases from the bottom wall up to the top one, where the fluid reached $v = v_{wall}$.

two different Couette flows, even if they are located in a point where the velocity is the same, their response will not be equal due to the difference in the gradient $\partial v_x/\partial y$.

5.2 Membrane stationary shape

We can see in **Figure 5.2** some simulations where, for a channel of the same height, we change the flow speed and therefore velocity slope. A red blood cell in a constant Couette flow seems to always align in the same direction regardless of the flow velocity. However, it seems like the angle of inclination of the cell respect to the flow direction changes for different flows. This can be seen in **Figure 5.2** when changing the v_{wall} of a cell for a constant system size thus changing the velocity slope. Another thing that changes greatly is how much it deviates from a normal discocyte shape to a more squished disc.

Additionally one can change the velocity gradient. For various simulations where the parameter v_{wall} is the same but the height of the channel differs one can see slight differences in the final cell shape. For simulations with a constant wall velocity of $v_{wall} = 0.6$ but where the size of the channel H is changed, like in **Figure 5.3**, one can see differences in the final cell shape.

In general we know that the higher the flow speed the higher the hydrodynamic stress on the membrane caused by the flow. In the Couette flow case this hydrodynamic stress appears as a stretching of the cell, an elongation of the cell and the disappearance of the discoid valley in the centre of the cell. From what can be seen in **Figure 5.3**, it seems that the velocity gradient v_{wall}/H also increases the stresses on the membrane, as the cell original discoid shape is lost. Moreover, there seems to be a dependence

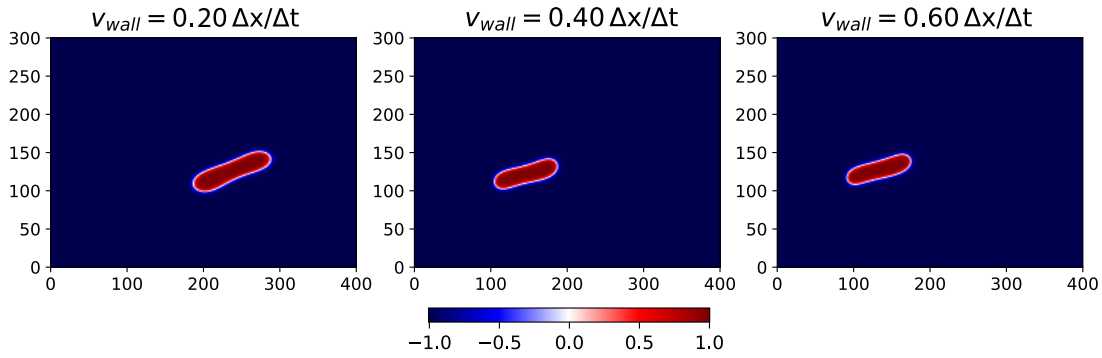

Figure 5.2: Cell morphologies for Couette flow with the top wall of the channel moving. Shapes for different flow speeds from slower to faster changes only slightly for a given channel height $H = 140$.

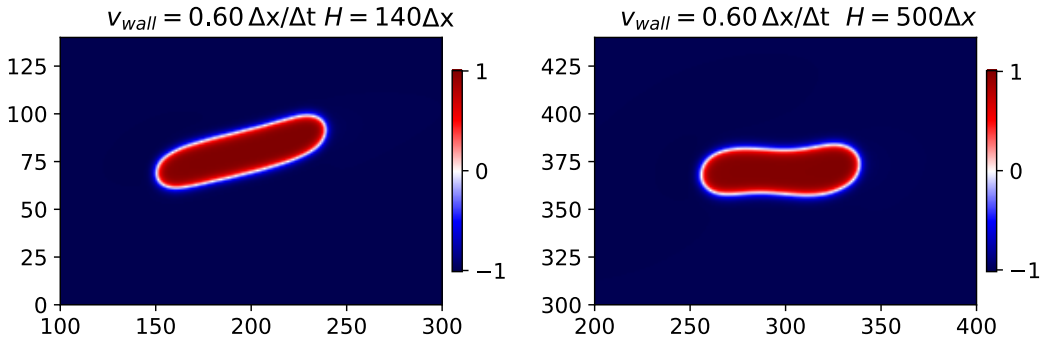

Figure 5.3: Different cell shapes in a Couette flow by changing the velocity gradient towards the wall $\partial v_x/\partial y$. This is done by changing the channel height H.

between this velocity gradient and the tilt of the angle that the cell takes with respect the flow direction.

5.3 Stationary position and lateral migration

Depending on the starting position of the cell or vesicle, for Couette simulations there seems to appear a net displacement perpendicular to the flow direction, a lateral migration produced by a lift force, as can be seen in **Figure 5.4**. We can observe for different simulations that, for cells starting far away from the moving wall, the cell moves perpendicularly to a specific stationary vertical position. After the initial rotation and deformation at the start of the simulation, that can see in the top plots of **Figure 5.4**, the membrane starts going up. When approaching to its stationary position it can be seen **Figure 5.4** that the perpendicular velocity slows down to a stop. During this process the cell membrane does not deform nor change shape greatly. Seeing this behaviour repeatedly for any starting position, it can be said that there is an stationary

position for any given Couette flow.

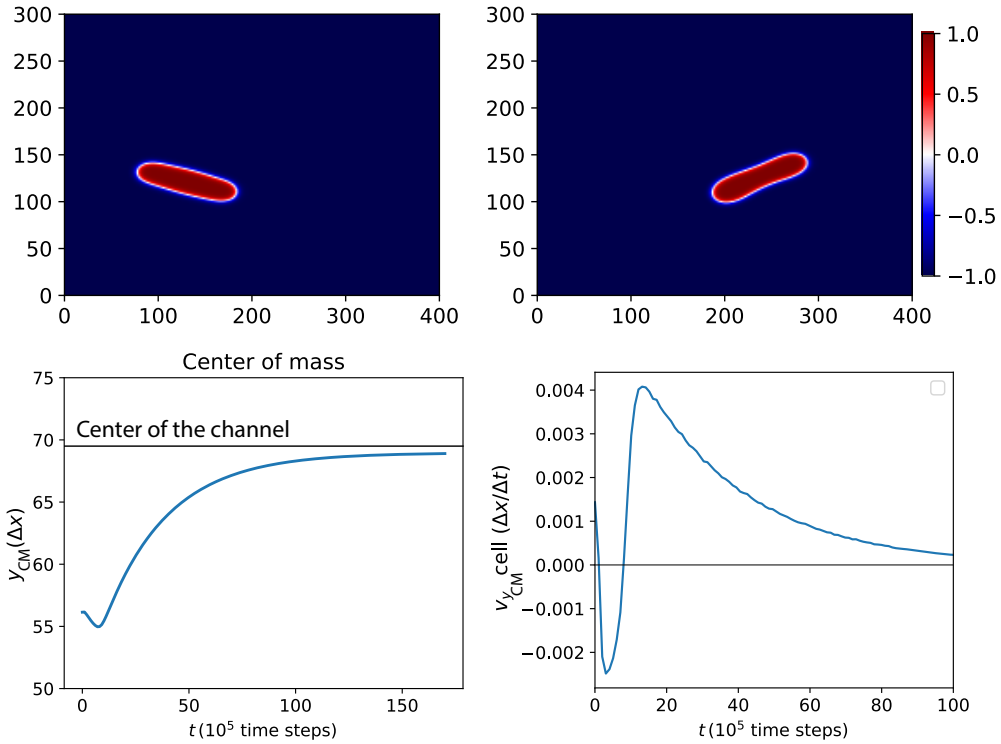

Figure 5.4: Cell rotates and then moves upwards. Top-left the cell just after starting the simulation and at the right the cell after rotating due to the Couette flow. Bottom plots are the position and speed of the cell centre of mass for a simulation of channel height $139\Delta x$ and velocity $v_{wall} = 0.2\Delta x/\Delta t$. Initial downward displacement corresponds to the rotation of the cell up to the final alignment.

This perpendicular displacement (or lateral migration) is not only found in simulations that have a constant Couette flow, but is also observed for oscillating Couette flow where the flow changes direction over time as a sinusoidal function. An example of an oscillating simulation can be seen in **Figure 5.5**. Therefore, this perpendicular displacement is not a time-reversible process but an irreversible one.

We can see the lift for a

From literature we know that a lift force is known to appear for neutrally buoyant rigid bodies in both Poiseuille and Couette flows which is called *inertial lift* or Segré-Silberberg effect [94]. This is studied for low Reynolds numbers and they start with the Stokes equation, similarly to our simulations here, but the resulting lift force only appears when doing a perturbation expansion. Their first-order correction takes inertia into account [94] thus explaining why in a low-Reynolds flow they obtain this inertial lift. So even at very low Reynolds one would need to be computing the inertial

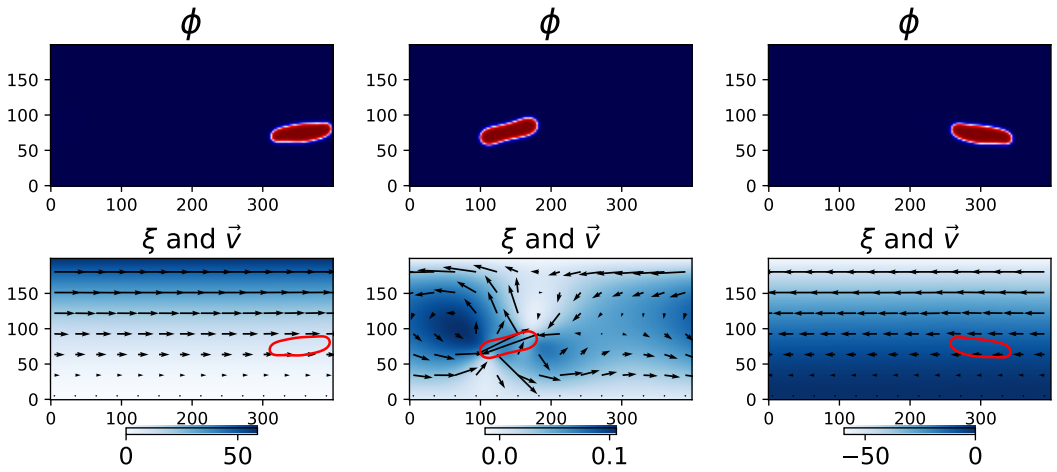

Figure 5.5: Oscillating simulation with a Couette flow that behaves sinusoidal over time. We can see from left to right how the simulation going to the right stops and changes direction and goes to the left. The intensity of the velocity is proportional to the value of the stream function ξ so the value of the colorbar can be used as a guide.

contribution to obtain the inertial lift, thus the effect that we are seeing here has a different source. This different effect is related to the shape that the cell takes and has been studied by Olla [95]. There is a non-inertial lift force that seems to depend on the distance to the wall, the orientation and length of the particle and the viscosity contrast. After Olla, there was more research on the lateral migration of vesicles and this non-inertial lift. This lift force has been referred to by Lorz et al. as "anomalous lift force" [96]. This force has different expressions at different distances from the wall, depending on whether the cell or membrane is very close to the wall, at an intermediate distance, or at a long distance. We will see a couple of these expressions in the following subsections.

5.3.1 Dependence on the reduced volume

In this chapter, up until now, we have only seen results for cells that have the same reduced volume as a red blood cell, giving it red blood cell shape when no flow is applied. But, one could question if changing this reduced volume to more spherical values can change the results of the stationary position in a Couette flow. We can refresh the expression for the reduced volume that we introduced in equation (2.20)

$$V_r = \frac{V}{\frac{4}{3}\pi(\frac{A}{4\pi})^{3/2}}, \tag{5.1}$$

where V is the membrane volume and A the area.

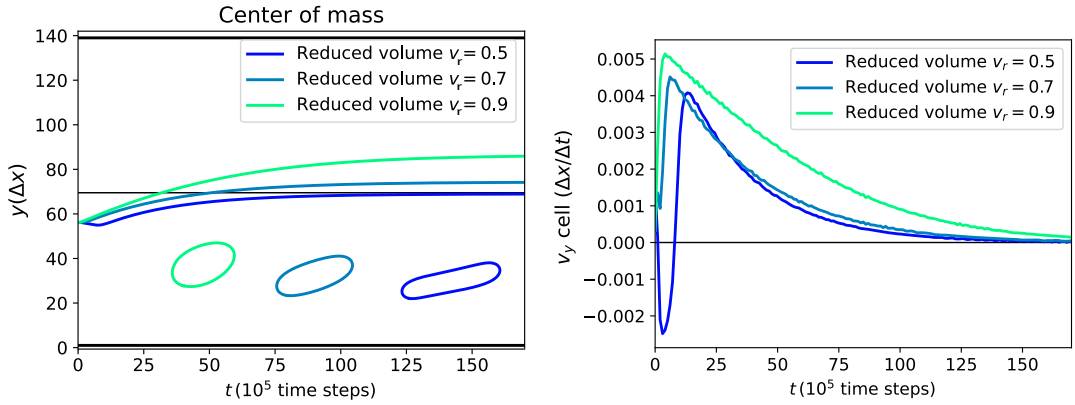

Figure 5.6: Vertical component of the position and velocity of the centre of mass of the cell. This vertical component is referred to the one perpendicular to the fluid flow. Different reduced volume v_r cells. Channel walls are represented as thick black lines, the thin black line represents the centre of the channel.

We can see the results of this in **Figure 5.6** where we are increasing the reduced volume by increasing the enclosed volume but maintaining the same surface area while maintaining the rest of the parameters constant. Thus, we are not changing neither the velocity v_{wall} nor the velocity gradient. The dependence of this displacement with the reduced volume is apparent in both the velocity of the cell and the stationary position. While the stationary position change in **Figure 5.6** is small for the two cells of lower reduced volume, small enough that one could say its purely numerical, the more spherical cell show that this trend seems to depend on the reduced volume.

For the velocity plot of **Figure 5.6** it seems that the closer the reduced volume gets to one of a sphere we get the faster the cell moves to its stationary position. This could be because the starting position for the spheroid is farther away than for the other cases.

This results go in line with the literature, as Abkarian et al. [97] report a lift force for a Couette flow that depends on the viscosity of the fluid η, the radius R of the vesicle, the distance h from the substrate, and a monotonous decreasing function $f(1-V_r)$ of the reduced volume

$$F_L = \eta\dot{\gamma}\frac{R^3}{h}f(1-V_r). \tag{5.2}$$

This expression uses the shear rate $\dot{\gamma}$ instead of the wall speed v_{wall}, but in the end both are proportional to the other. This force is studied for vesicles that are closely spherical and start adhered to the bottom wall of the channel.

At intermediate distances between the wall and the vesicle the lift force seems to

behave differently [98]

$$F_L \propto \eta \dot{\gamma} \frac{R^4}{h^2}, \tag{5.3}$$

which has also been observed in numerical simulations of 2D vesicles by Meßlinger et al. [99].

5.3.2 Viscosity contrast

This stationary position of the cell not only changes with the reduced volume v_r but also changes with its mechanical properties, like the viscosity contrast. Thus the next step we have taken is to introduce a difference between the viscosity of the cell fluid and the channel fluid. This is represented with the viscosity contrast ζ which, as seen previously, takes an expression of

$$\zeta = \frac{\eta_{cell}}{\eta_{liquid}}. \tag{5.4}$$

The distance with the wall at the stationary position changes with the viscosity contrast ζ as seen in **Figure 5.7**. For a viscosity contrast of $\zeta = 1$ we find that the cell mostly flows towards the centre of the channel and stays there. The stationary position is not exactly the centre of the channel, but is around the centre with a slight variation. However, this behaviour will change a lot with the viscosity contrast ζ. With increasing ζ we find an increasing stationary position, up to having the cell reaching the top wall of the channel in some cases, this behaviour can be seen in **Figure 5.7**.

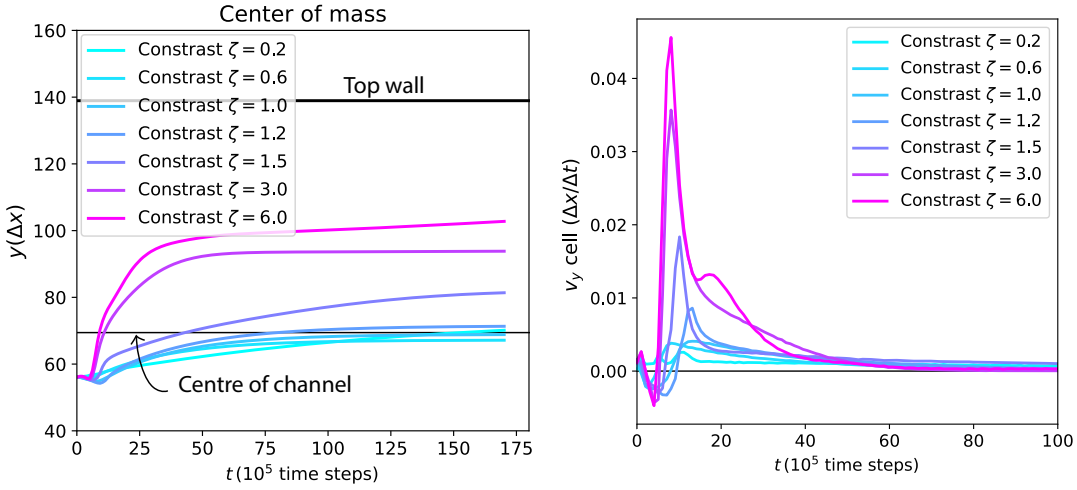

Figure 5.7: Vertical component of the position and velocity of the centre of mass of the cell. This vertical component is referred to the one perpendicular to the fluid flow. Plots are the same reduced volume v_r but different contrasts ζ. Channel walls are represented as thick black lines, the thin black line represents the centre of the channel.

For many of the lower contrasts values like all lower than $\zeta = 1$ and some even for ζ a bit higher than 1, one can see their stationary positions to be around the centre of the channel. Meanwhile for increasing contrast ζ the stationary position of the cell quickly jumps close to the moving wall, with the cell even reaching a physical contact with the wall. For the simulations of **Figure 5.7**, for the simulation where the centre of mass reaches values around 100, the cell cannot move more vertically as the cell is already touching the wall. The cell represented in the plot is there to show how at that height of the centre of mass the cell is in contact with the horizontal line on top, which corresponds to the top wall of the channel. There seems however to be a force depending on the viscous contrast as with higher contrast the cell still gets a bit further up.

The dependence of viscous contrast ζ with what looks like a hydrodynamic force can be also be observed in the right plot of **Figure 5.7** which shows the perpendicular velocity v_y of the cell centre of mass. This velocity has a peak which depends strongly on the contrast ζ, and in this case the dependence between the result and the viscosity contrast is more apparent, as the lowest viscosity contrast of $\zeta = 0.2$ has the lowest value while the highest contrast the higher speed. However, it is not clear if the velocity dependence arises purely from the viscosity contrast. There is the chance that it has something to do with the fact that the faster cells also are the cells that start farther away from their stationary position.

5.4 Tumbling

We can sometimes observe tumbling in a Couette flow for viscosity contrasts higher than $\zeta = 1$. while the position of the centre of mass over time in **Figure 5.2** show continuous approximately straight lines, sometimes we find that for high ζ tumbling is observed. In Couette this is not as easy to induce as in Poiseuille. In the latter by simply having a big channel with high contrast one can observe tumbling by breaking the flow symmetry by positioning the cell outside of the centre of the channel. However, there is not this kind of central symmetry in Couette, and there is no obvious method to induce tumbling even if the viscous contrast is high enough to produce it.

In **Figure 5.8** one can see a plot of the y position of the centre of mass over time. At each jump in the plot, there is a tumbling event for that particular simulation, which sketch of how it goes can be seen as an inset on the plot. Even if the tumbling seems less frequent for a cell inside a Couette flow, it seems that once it starts tumbling the cell does not stabilise again and just keeps tumbling for a long time.

5.5 Conclusions

The previously presented stream function membrane phase field model is shown to simulate properly a Couette type of flow. A channel with a Couette flow will be charac-

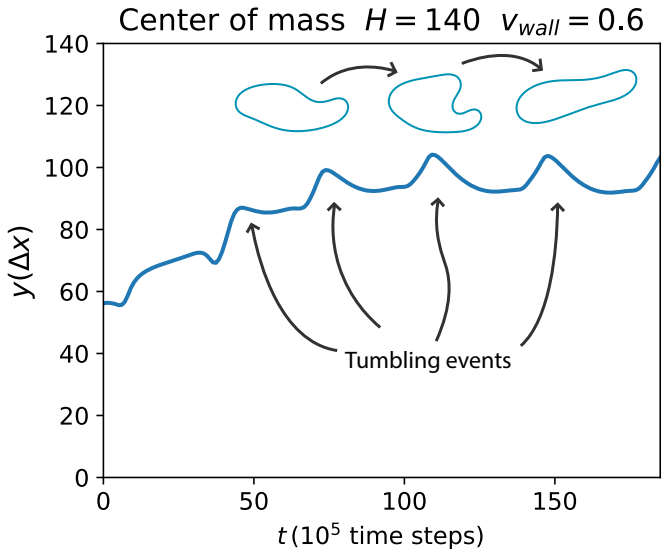

Figure 5.8: A simulation with a viscosity contrast $\zeta = 2$ and a channel height $H = 140\Delta x$ where the cell tumbles as well as displacing upwards. Each sudden peak in the vertical component of the cells position indicates a tumble of the cell.

terised by two parameters: *i)* the velocity of the moving wall v_{wall} *ii)* the rate at which the velocity increases when approaching the wall. This last term will be the velocity derivative in the perpendicular direction to the flow which, for a Couette flow, has a value of $\partial v_x/\partial y = v_{wall}/H$.

At first sight it seems that the cells in a Couette flow simply align in a very specific way, which looks dependant on the flow characteristics. However if one looks closely and for long enough, it can be seen that the cells seem to display a lift. This lift has a different source to other lateral migration effects in Couette flow like the Segré-Silberberg effect, also known as inertial lift. For the Segré-Silberberg case one needs the inertial contribution of the Navier-Stokes equations to obtain the lift, even at low Reynolds numbers. Therefore, as the simulations in this chapter do not contain the inertial term, we can say that the source of this lift is different than the Segré-Silberberg effect. The lift seems to behave as the lift proposed by Olla and others [95, 98] where the force depends with the distance to the wall, the fluid viscosity, the cell size, and the reduced volume.

This lift does not lasts forever, as cells in a Couette flow display an stationary position (or distance) with respect to the walls. The final stationary position and the speed at which the cell moves perpendicularly depend on both the reduced volume of the cell and the viscosity contrast. In fact, for high viscosity contrasts one finds that the cell will go up towards the top moving wall until it cannot move more vertically as the cell is already touching the wall.

Moreover, the viscosity contrast also induces sometimes a tumbling regime to the cell, although it seems to be less frequent than for Poiseuille flows. The reason might be the fact that tumbling in Poiseuille flows the rate of change in the flow velocity along the channel is parabolic. This change is faster and more sudden when moving perpendicular to the the channel. As the velocity profile of a Couette flow is linear, and therefore its derivative constant taking a value of $\partial v_x/\partial y = v_{wall}/H$, the cell might be in a more stable shape at all positions inside the channel.

Part III

Helfrich models

Chapter 6

Gaussian curvature and fission

6.1 Membrane fission in cells

There is a fair amount of research on cellular membrane deformation and morphology. However in comparison, there is little understanding on topological transitions of biological membranes [23, 30, 100]. In these topology-dependent events the Gaussian curvature plays a great role.

Usually, by using the Gauss-Bonnet theorem (seen in Chapter 2) one can avoid the Gaussian curvature contribution to the bending energy. This theorem states that the integral of the Gaussian curvature over a surface is proportional to the surface Euler characteristic [101]. For a surface Ω the Gauss-Bonnet theorem states that

$$\int_{\Omega} K\, dS = 2\pi\chi(\Omega), \tag{6.1}$$

where $\chi(\Omega)$ is the Euler characteristic as we have already seen in Chapter 2 and is a topological invariant. Therefore, the energy contribution of the Gaussian curvature is a constant unless the topology of the system changes. The Euler characteristic describes the system by the number of holes g and objects N like

$$\chi(\Omega) = 2(N-g), \tag{6.2}$$

so we will need either a change on the number of closed membranes or the number of holes to change the Gaussian contribution. However, topological transitions are necessary in biology and happen constantly in some systems. For example many viruses are enveloped by a lipid membrane which mediates the fusion of the virus with the host cell membrane; like the HIV-1, herpesviruses, the Ebola virus [102], and coronaviruses [103] like SARS-CoV-2. Life requires the cellular division or the formation of vesicles

to either transport food or waste. Therefore we have a big motivation to study fusion and fission.

Fission and fusion have both different mechanics and requirements to happen, therefore it would be better to focus the study on one of the two. Here we will focus on membrane fission, and the most common fission event being the formation of vesicles. For membrane fission a requirement across the board is a big curvature on the area that is going to fission. This big curvature can arise with a wide variety of methods, from hard rods pushing the membrane to ion imbalance between the two sides of the membrane to curvature inducing membrane proteins. For all the cases where we do not have an actual object or structure pushing the membrane, we can model this curvature generation using the spontaneous curvature.

On top of the necessity of inducing a local curvature in the area where the membrane will undergo fission, the final fission is often mediated by very specific proteins, although this is not always the case. In some cases instead of having specific proteins to produce the fission a large spontaneous curvature can suffice to produce fission [104, 105, 106]. This can be accomplished by interactions among membrane-bound proteins [104] or by a osmotically induced pearling instability [105]. Protein-mediated fission has been extensively researched. For example the dynamin superfamily [30, 107, 108, 109] or the ESCRT machinery [102, 110, 111] are two different sets of proteins that mediate in budding and fission. In mitochondrial division a major component is the dynamin Drp1 while other dynamins are considered helpful or be necessary for some fission processes.

Thus, due to its biological relevance, there is more than enough motivation to pursue the study of topological transitions in membranes. Even if we addressed the Gaussian curvature in the Canhan-Helfrich model in Chapter 2 we shall do a brief overview before going into the numerical implementation and results.

6.1.1 Vesicle formation

Vesicle formation –or vesiculation– is the process with which vesicles are created from a former and bigger membrane. As we have seen in previous chapters a vesicle is a structure consisting of a lipid membrane enclosing liquid or cytoplasm. We can find vesicles inside or outside cells, as it is how cells dump waste outside of the cell by secretion process also called by exocytosis. Vesicle formation is a fundamental process in many biological systems. Some examples of systems that rely on the formation of vesicles are the Golgi apparatus [112, 113], the synaptic system [114, 115], or enveloped viruses [102, 116].

For example in the synaptic nerve terminals we have neurons generating neurotransmitter and enclosed inside vesicles. These vesicles are released by exocytosis in the synaptic nerve terminals [114]. In the Golgi apparatus there is a constant release of

transport vesicles filled with proteins that are carried to their destinations inside the cell where they are required. Vesicles, like the cell membrane, can be further functionalised or signalised by using membrane proteins attached to their lipid bilayer.

The 2013 Nobel Prize in Physiology or Medicine was awarded to James Rothman, Randy Schekman and Thomas Südhof for expanding on the role and function of cell vesicles, especially in yeasts and in humans, and overall their discoveries on machinery regulating vesicle traffic [117]. So we can say with confidence that the mechanisms of vesicle formations are relevant in the cells life and in research.

6.2 Modelling the Gaussian contribution

As we have seen in previous chapters, phase-field approaches are suitable to model the dynamics of membranes. The Gaussian curvature is an intrinsic property of the surfaces, however thanks to the Gauss-Bonnet theorem we could go on without giving it too much attention. No matter the dimensionality the Gaussian curvature has an influence on the membrane shape and dynamics [118]. Remembering the Gauss-Bonnet theorem, it states that the energy contribution of the Gaussian curvature is a topological invariant. Therefore, if the Euler characteristic from equation (6.2) of the system (the number of holes and objects) does not change, we can ignore this contribution. The Gaussian curvature is quite complex to compute numerically, and there is not as much research as for membranes that do not undergo topological transitions. For a phase field model the Gaussian curvature has not been computed up until now. However, it is necessary to study fusion and fission so we will be computing the Gaussian contribution to study topological transitions.

In Chapter 2 we already introduced the bending and membrane energy, the total and Gaussian curvatures, and how to write them all as a phase field, lets do a quick overview of the Gaussian part. We start from the complete bending energy for the total curvature C (related to the mean curvature by $H = C/2$) and the Gaussian curvature K we have

$$F = \frac{\bar{\kappa}}{2}\int_{\Gamma}(C - C_0)^2 ds + \bar{\kappa}_G \int_{\Gamma} K ds, \tag{6.3}$$

where $\bar{\kappa}$ and $\bar{\kappa}_G$ are the bending modulus and Gaussian modulus, C_0 is the spontaneous curvature and the integral is calculated over the whole membrane surface Γ.

Let us expand on the Gaussian curvature term. This term can be defined using the curvature tensor $Q_{\alpha\beta}$ of the surface as

$$K = \sum_{\alpha,\beta}\left[\left(Q_{\alpha\alpha}Q_{\beta\beta} - Q_{\alpha\beta}^2\right)\frac{1-\delta_{\alpha\beta}}{2}\right], \tag{6.4}$$

more on this Gaussian curvature has been addressed in Chapter 2. The curvature tensor can be defined using the vector normal to the surface normal vector $\hat{n}$ as

$$Q_{\alpha\beta} = \nabla_\alpha n_\beta. \tag{6.5}$$

This tensor represents changes in the orientation of the normal vector along the surface. These changes are directly related to the curvature of such a surface. This curvature tensor in turn can be defined in terms of the gradients of the order parameter ϕ as [62],

$$Q_{\alpha\beta} = \frac{\sqrt{2}\varepsilon}{1-\phi^2}\left[\partial_{\alpha\beta}\phi + \frac{2\phi}{1-\phi^2}\partial_\alpha\phi\partial_\beta\phi\right], \tag{6.6}$$

where $\partial_\alpha = \partial/\partial x_\alpha$, and $\partial_{\alpha\beta} = \partial^2/\partial x_\alpha \partial x_\beta$.

Now, similarly as in the second chapter, we can write the bending free energy as a sum of the bending energy term and the Gaussian energy term. The resulting free energy will be $F = F = F_{SC} + F_G$, where F_{SC} is a bending free energy for a spontaneous curvature C_0 written as a phase field, as seen in previous chapters is

$$F_{SC} = \kappa \int_\Omega \left((\phi - \varepsilon C_0)(\phi^2 - 1) - \varepsilon^2\nabla^2\phi\right)^2 dV, \tag{6.7}$$

where $\kappa = 3\sqrt{2}\bar{\kappa}/16\varepsilon^3$ and $C_0 = c_0/\sqrt{2}$. Meanwhile, the energy density for the Gaussian curvature contribution will end up looking like

$$\begin{aligned} F_G &= \frac{\kappa_G}{2\varepsilon^2}\int_\Omega \tilde{K} dV = \frac{\kappa_G}{2\varepsilon^2}\int_\Omega K(1-\phi^2)^2 dV \\ &= \frac{\kappa_G}{2\varepsilon^2}\int_\Omega \sum_{\alpha<\beta}(1-\phi^2)^2\left[Q_{\alpha\alpha}Q_{\beta\beta} - Q_{\alpha\beta}^2\right] dV, \end{aligned} \tag{6.8}$$

where $\kappa_G = 3\sqrt{2}\varepsilon\bar{\kappa}_G/4$.

Both energy terms determine the complete bending energy of the system. The time evolution of the phase-field is set according to the Cahn-Hilliard dynamics, also known as model B, since the volume is supposed to be locally conserved [24, 56, 57, 58, 119, 120]. The variations of the free energy with respect to ϕ must then be subjected to diffusion, yielding a dynamic equation for the phase-field governed by [24],

$$\frac{\partial\phi}{\partial t} = \nabla^2\left(\frac{\delta F_{SC}}{\delta\phi} + \frac{\delta F_G}{\delta\phi}\right). \tag{6.9}$$

This dynamic equation can be written explicitly in terms of the phase field order

parameter ϕ which results in

$$\begin{aligned}\frac{\partial\phi}{\partial t} &= \kappa\nabla^2\left((3\phi^2-1-2\phi\varepsilon C_0)\Phi-\varepsilon^2\nabla^2\Phi+\sigma[\phi]\nabla^2\phi\right)\\ &\quad-\kappa_G\nabla^2\left(\frac{12\phi}{1-\phi^2}F_{K_1}+\frac{2(3\phi^2+1)}{(1-\phi^2)^2}F_{K_2}\right),\end{aligned} \tag{6.10}$$

where, as in previous chapters, $\Phi=(\phi-\varepsilon C_0)(\phi^2-1)-\varepsilon^2\nabla^2\phi$. In this final expression for the dynamic equation the bending and the Gaussian contributions can be differentiated by their energy moduli κ and κ_G respectively. The terms F_{K_i} represent the Gaussian curvature effect and are

$$F_{K_1}=\partial_{\alpha\alpha}\phi\partial_{\beta\beta}\phi-(\partial_{\alpha\beta}\phi)^2,$$

and

$$F_{K_2}=\partial_{\alpha\alpha}\phi(\partial_\beta\phi)^2+\partial_{\beta\beta}\phi(\partial_\alpha\phi)^2-2\partial_{\alpha\beta}\phi\partial_\alpha\phi\partial_\beta\phi.$$

This is the model we derived in the article [121]. The final dynamic equation (6.10) should be looked at closely. We can see the first term, the bending contribution, is the same that we obtain in Chapter 2. Meanwhile the new term is the Gaussian contribution, which is proportional to the Gaussian bending modulus κ_G and many derivatives of ϕ. In the denominator of the Gaussian contribution we have a couple of terms $(1-\phi^2)$ which will go to zero at the bulks. This can make tricky to compute the Gaussian contribution, but not impossible. To do this we will use Residue Theorem, but we will go more into detail in the following section.

6.2.1 The Gaussian modulus

The energy contribution of the Gaussian curvature to the membrane energetics is mediated, similarly to the bending modulus κ for the curvature, by the Gaussian (or saddle-splay) modulus κ_G

$$F_B=\int_\Gamma\frac{\bar{\kappa}}{2}(C-C_0)^2ds+\bar{\kappa}_G\int_\Gamma Kds. \tag{6.11}$$

This modulus will define whether it will be energetically favourable for a membrane to fission or not. Lipid bilayers, depending on the values of the Gaussian and bending moduli, exhibit different stable configurations. The biological membrane could either be *(i)* topologically stable, *(ii)* favour fission into multiple membranes, or *(iii)* favour the generation of holes and channels within the membrane without dividing.

On the actual value that the Gaussian modulus takes in biological membranes there are no direct experimental measurements of this Gaussian modulus. However there is work and interest on measuring it and new methods are proposed to such end although

still require trial [122]. What can be done are indirect measurements of this modulus. Some of those indirect measurements give a negative value of about $\bar{\kappa}_G \approx -15 K_B T$ [123], and molecular dynamics simulations give similar results [124]. This value would set that the bending and Gaussian moduli would have a similar order of magnitude but the Gaussian modulus would be negative instead. The negative sign implies that the energetic term of the Gaussian curvature favours fission, since fission increases the Euler characteristic as can be seen in equation (6.2). Increasing the Euler characteristic would in turn increase the negative contribution to the total membrane energy, minimising the total energy.

6.2.2 Lagrange Multiplier with Gaussian contribution

The Lagrange multiplier for area has to be computed differently as before. In this case we will not need additional Lagrange multipliers for area nor volume as the dynamics are slower and less stressful for the membrane. Thus the conservation of both area and volume is easier to maintain. The parameter $\sigma[\phi]$ is a Lagrange multiplier that depends on the field ϕ and assures area conservation [62]. One can determine $\sigma[\phi]$ in a similar manner to how we showed in Chapter 2, but in this case the functional derivative of the bending energy does not only contain the curvature contribution but also the Gaussian contribution

$$\sigma[\phi] = -\frac{\int_\Omega \nabla\phi \cdot \nabla[\nabla^2\left(\frac{\delta F_{SC}}{\delta\phi} + \frac{\delta F_G}{\delta\phi}\right)]dV}{\int_\Omega \nabla\phi \cdot \nabla[\nabla^2(\nabla^2\phi)]dV}. \tag{6.12}$$

We end up with the same results as the explicit computation of the Lagrange multiplier of Chapter 2 with the change of the free energy functional derivative of the energy to a sum of two functional derivatives.

6.3 Numerical implementation

Computing this things will not be trivial, as the Gaussian contribution of the dynamic equation (6.10) has in the denominator two terms that go as $(1-\phi^2)$ which will go to zero at the bulks. The denominator going to zero will diverge to infinity, so we will have to be smart and careful to be able to compute this numerically. To such end we will use the complex plane, something similar to the Residue Theorem, with which we can exploit the complex plane to compute a integral that diverges at a point.

6.3.1 Technical details

To compute the system, we define a 3D grid space with an equal distance between the points in the grid of $\Delta x = \Delta y = \Delta z$. In this grid we can compute the temporal evolution using an Euler method for the integration of time with the appropriate time step of $dt = 10^{-5}$, small enough to avoid artefacts [125].

The initial conditions for the membrane we choose a cylindrical shape of radius R and length L whose base is in contact with the wall of the domain where we are using zero flux boundary conditions. We will give the system a few time-steps to produce the diffuse interface before start computing the Gaussian contribution of the system. Moreover, to lead the deformation we introduce a spontaneous curvature term C_0 which will have a constant value all over the space. However, by design, this spontaneous curvature will only act on the membrane.

The tricky part is computing the contribution

$$\frac{12\phi}{1-\phi^2}F_{K_1} + \frac{2(3\phi^2+1)}{(1-\phi^2)^2}F_{K_2},$$

as in the bulk $(1-\phi^2) \to 0$ and this would go towards infinity. However, adding a very small imaginary contribution to ϕ. With the complex order parameter field $\phi_{\mathbb{C}}$ we can compute the two contributions

$$\frac{\phi_{\mathbb{C}}}{(1-\phi_{\mathbb{C}}^2)}$$

and

$$\frac{(3\phi_{\mathbb{C}}^2+1)}{(1-\phi_{\mathbb{C}}^2)^2}$$

without the denominator diverging. After that we simply take the real part of the result and with that we can compute the Gaussian contribution to the chemical potential $\delta F_G/\delta\phi$.

The work presented in this chapter consists of three dimensional calculations using an Euler integration for the integration of the energy functional derivative. This is the same integration as of previous chapters, with the difference being that the functional derivative $\delta F/\delta\phi$ has been computed as

$$\frac{\delta F}{\delta\phi} = \frac{\delta F_B}{\delta\phi} + \frac{\delta F_G}{\delta\phi},$$

where the Gaussian functional derivative has been computed by the addition of a small imaginary contribution. As the previous chapter we also use a finite-difference scheme for the spatial discretisation. The Euler integration method for the temporal derivatives has been computed with the appropriate time step of $dt = 10^{-5}$, small enough to avoid artefacts [125].

6.4 Fission of membrane tubes

There are countless membrane shapes that could be used to study the vesicle formation process. Some of them can make the fission easier or more difficult, as depending on

the initial shape of the membrane you can have a big energy barrier to surpass to reach the equilibrium state. For example, a flat infinite membrane is very hard to induce to form vesicles, even when it is energetically favourable, as the membrane needs very high curvature to fission and a flat membrane has by definition zero curvature. Therefore, we will study a shape that has more affinity with the vesicle fission than a flat membrane.

Contrary to a flat membrane, for which even a very high spontaneous curvature will not induce spontaneous deformation, a membrane tube is very sensitive to the spontaneous curvature term. It is known that for a membrane tube in the presence of a constant spontaneous curvature you obtain a pearled tube as has been seen in simulations [57, 126, 127] and experiments [128, 129] This pearling instability does not fission the tube if you only compute the curvature contribution of the bending energy. The membrane pearls are connected by very thin membrane necks that avoid the complete fission of the membrane. So, we can exploit this system morphology to study vesicle formation from tubes.

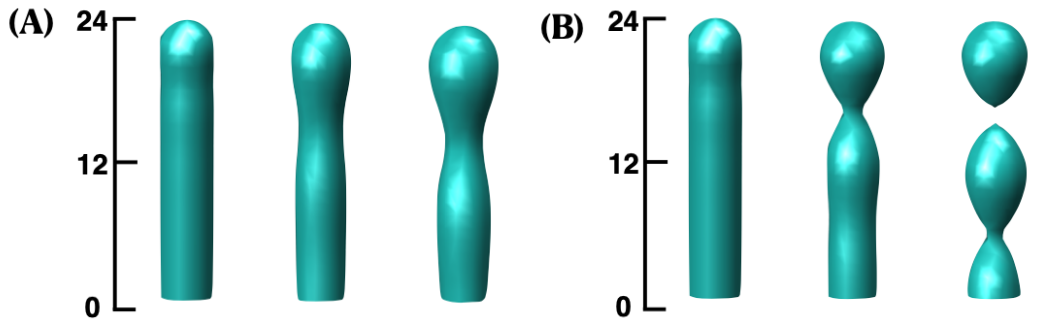

Figure 6.1: Time evolution of the interface $\phi = 0$, the time increasing from left to right. (A) without considering Gaussian curvature ($\kappa_G = 0$). (B) Considering the Gaussian curvature contribution with $\kappa_G = -10$, the last snapshot depicts the exact moment when the vesicle breaks from the main membrane. The parameters used were $R = 5$ and $L = 26$ in grid units, $\kappa = 1$, and $C_0 = -0.3$.

We will start with a short membrane tube, so that the tube divides from one into two closed membranes. We can see the difference in Figure 6.1 when **(A)** the Gaussian curvature term is not included in the free energy, and **(B)** solving the complete dynamical equation (6.10) including the Gaussian contribution. For the case **(A)** when the Gaussian curvature is not considered ($\kappa_G = 0$) a single neck forms, but there is no fission of the membrane. In the Figure 6.1 **(B)** we can see the membrane up to the instant where the membrane splits in two, which can be easily seen in the Gaussian energy contribution which drops. The addition of the Gaussian contribution makes fission

energetically favourable and a vesicle is formed from the initial cylinder for a Gaussian modulus of $\bar{\kappa}_G \approx -\bar{\kappa}$ [130].

This model has no problem with multiple fission events. To study this we will start with a longer cylinder. In **Figure 6.2** we can see the results for a cylinder of length $45\Delta x$. In this Figure we are seeing the axial cut of the three-dimensional cylinder, to be able to plot both the initial and final state of the membrane. The vesicles formation of a long tube is sequential, going one at a time. This can be easily seen in the **Figure 6.2** (b) where the Gaussian energy can be seen to drop four times, each of these drops happen at the time that a fission occurs. The Gaussian energy can be seen to rise before dropping, however why stated that the model is based on minimisation of the energy, so why is this happening? Well, this rise on the Gaussian contribution energy is lead trough the curvature term bending energy (6.11). The deformation that the membrane is undergoing lowers the term $(C-C_0)^2$ from equation (6.11) more than the increment that the Gaussian term suffers. Therefore, thanks to the curvature C getting closer to the spontaneous curvature value C_0 the total bending energy is dropping even when the Gaussian contribution is increasing.

The first vesicle start at the tip of the cylinder and this follows downwards to the last one. Shape changes start simultaneously through the entire tube, however the rate at which they are pearling is not equal. This happens because the spherical cap of the tube is promoting the pearling instability leading to faster pearling near the tip. When seeing **Figure 6.3** where we have the sequence of a very long tube it can be more easily seen that the spherical cap of the cylinder is promoting the pearling deformation. This happens because the tip is already more curved than the rest of the cylinder, so it deforms faster into a bud, which due to the Gaussian contribution fissions from the tube. Therefore, we have a interplay between the time that takes to pearl the tube and the time that takes to fission it. In our model, fission is practically instant in comparison to the pearling time-scale and that is why before reaching a tube with two pearls we already have the vesicle formed.

We can see a similar process in the experiments of Sanborn et al [105] in **Figure 6.4**. In these experiments they have membrane tubes attached to a Giant Unilamelar Vesicle (GUV). They induce a change in ion concentrations to produce an osmotic shock to the system. This osmotic shock pearls the tube and ends up cutting the pearls into individual vesicles. In this case they have a faster time scale to pearl the tube than to scission the vesicles from it.

6.4.1 Volume and area conservation

When looking at both **Figure 6.2** and **Figure 6.3**, one can realise that the enclosed volume by the membranes and the total surface area of the system is not conserved. This is necessary for systems in which the initial and final shapes do not maintain the

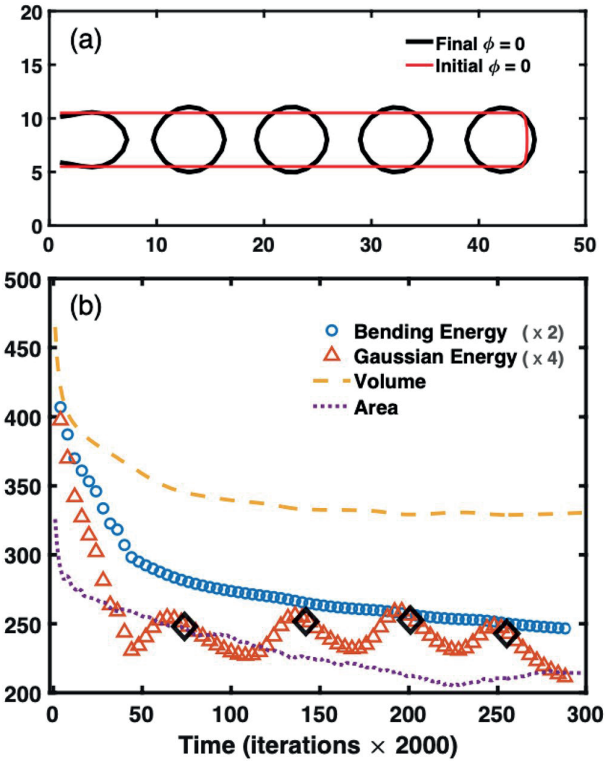

Figure 6.2: Time evolution of a longer tube with Gaussian curvature. (A) Contour plots on the plane x,z of the initial (red) and final (black) $\phi = 0$. (B) Time variations of the volume (yellow dashed line), the area (red dotted line) and both energy contributions. The open black diamonds represent the times where bifurcations occur. The parameters used were: $R = 6$ and $L = 45$, $\varepsilon = 1$, $\kappa_G = -10$ and $C_0 = -0.5$.

reduced volume. We have already addressed the fact that these geometrical parameters should be conserved, but they should be conserved over an entire closed membrane. Here we have a membrane tube that is connected to the system boundary, considering that this tube should be connected to a much larger membrane, which is acting as a reservoir of both surface area and volume. So, if the tube has extra volume that needs to get rid of, or needs extra membrane to produce the vesicles, it can dump or take from the rest of the cell and membrane.

On the conservation of area and volume, while it is true that it is not necessary to conserve the global volume and area, its another story for the area and volume of the vesicles after fission. In this case, the model maintains size and surface area over time of the multiple vesicles. This is more apparent in **Figure 6.3** where from the first formed vesicle to the last we have a long simulation time but still the size of the first vesicle seems to hold up. It is not trivial that the model would behave like this, as it

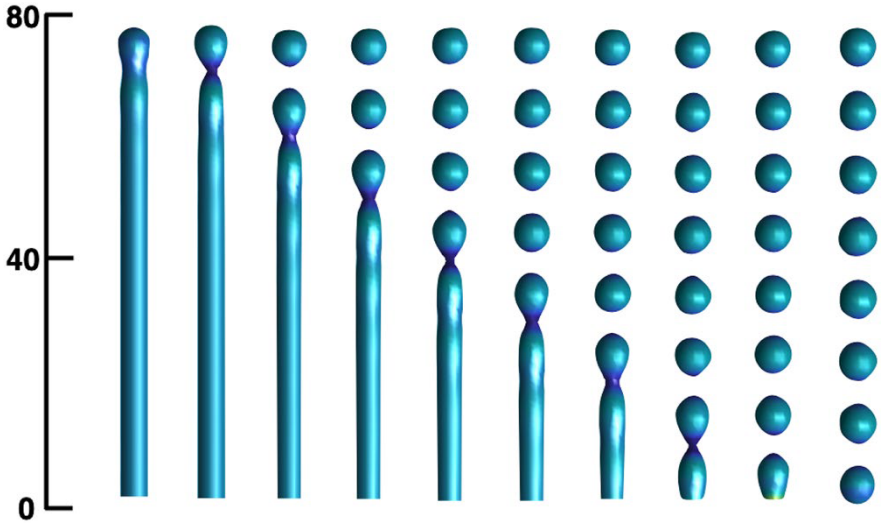

Figure 6.3: Snapshots of the evolution of the pearling instability in a long cylinder. Vesicles fission in sequence from the tip to the base. The parameters used were: $R = 6$, $L = 75$, $\varepsilon = 1$, $\kappa = 1$, $\kappa_G = -10$ and $C_0 = -0.5$.

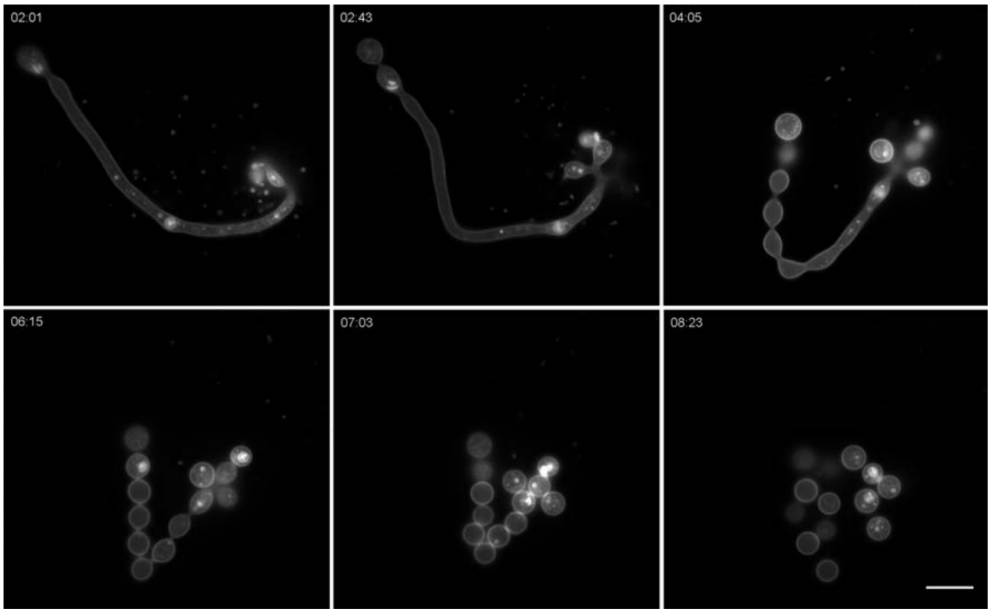

Figure 6.4: Adapted from Sanborn et al [105]. Selected epifluorescence images from a movie obtained for GUVs. GUVs are subjected to an initial negative osmotic gradient by dilution in deionized water. The images are taken 45 min after the dilution when osmotic gradient has reversed due to evaporation of bulk water. Scale bar is 10 μm.

could be possible in a phase field model to have the different droplets cannibalise one another to grow. However, it is necessary for the formed vesicles to maintain size for the simulation to be physically and biologically realistic.

6.4.2 Dispersion relation

To understand the pearling instability and the influence of the Gaussian curvature on this instability we will make use of the dispersion relation. To obtain the dispersion relation, we start with the effects of small perturbations around a flat interface. For perturbations at the interface, therefore $\phi = 0$, taking plane waves in the shape of $\phi = \phi_0 e^{i\mathbf{q}\cdot\mathbf{x}-\omega t}$ where, for small amplitudes, $\phi_0 \ll 1$. Considering isotropic perturbations we can take all this into the complete dynamic equation (6.10) to obtain the following dispersion relation

$$\begin{aligned}\omega(q) = {} & 3q^2\kappa\left[(1-2\varepsilon^2 C_0^2)+12\delta\varepsilon C_0\right] \\ & -9q^4\kappa\varepsilon^2\left[2(1+4\delta\varepsilon C_0)\right]-9q^4\kappa\sigma+27q^6\kappa\varepsilon^4.\end{aligned} \tag{6.13}$$

Here, δ represents terms of order $\mathcal{O}(\phi^2)$. As we can see in equation (6.13), the Gaussian contribution of the dynamic equation (6.10) is not present in the dispersion relation. The main contribution to the instability comes from the first term in the dispersion relation. This term depends on the spontaneous curvature, which will dominate and decide whether the pearling instability happens or not. Therefore, the Gaussian contribution does not alter the region of unstable wavelengths. We can see how the dispersion relation behaves for different spontaneous curvatures C_0 in **Figure 6.5**.

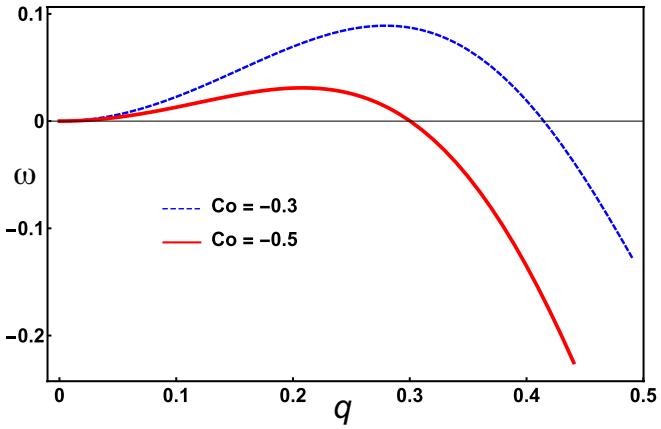

Figure 6.5: Dispersion relation with different values of spontaneous curvature. The parameter values are: $\kappa = 1$, $\varepsilon = 1$, $\delta = 0.001$ and $\sigma = 0.1$.

We can compute the critical length of the instability, by using $l_c = \pi/q_c$ where q_c

is the critical wave-length. The critical wave-length q_c is taken as the value of q taken when $\omega(q) = 0$ for a q greater than zero. We can see how q_c changes with C_0 in **Figure 6.5**. This critical length l_c gives the spatial scale for the pearling instability, which in turn will give us the scale of the size of the produced vesicles. For example we obtain for $C_0 = -0.3$ that $l_c \approx 7.6$ and for $C_0 = -0.5$ that $l_c \approx 10$ which is in agreement with the vesicle sizes obtained. For instance, in **Figure 6.3** eight vesicles can be formed in a tube of length $L = 75$ and a spontaneous curvature of $C_0 = -0.5$, as the critical length is $l_c \approx 10$ in this case.

6.4.3 Gaussian modulus phase diagram

As stated before, we have three possible stable results for a membrane when taking into account the Gaussian bending modulus κ_G. We can have either fission for a negative κ_G big enough in relation to the bending modulus κ. If κ_G is negative but not big enough respect to κ we will have a stable membrane with no fission. Lastly, for positive κ_G we will result with a multiple self-connected membrane, where many holes are developed by the membrane but it does not fission. This last case we end up with a continuous single membrane with multiple holes.

This all depends on the sign of κ_G and the ratio κ_G/κ. A representation of the resulting phase diagram can be seen in **Figure 6.6**, where we also have represented the equation

$$8\varepsilon^4\kappa + \kappa_G = 0 \tag{6.14}$$

which defines the transition between the two phases for negative Gaussian modulus. Equation (6.14) is obtained from Helfrich and Harbich [130] and then translated to our diffuse membrane model.

This phase diagram is obtained for a geometry that helps the formation of vesicles and their scission. The resulting phase diagram would change for different membrane geometries. For example, starting with a flat infinite membrane the end result for any κ_G would still be a flat membrane. With the Gaussian contribution and spontaneous curvature you can only do so much. If the system is set up so that fission requires a big energy contribution before happening, sometimes the spontaneous curvature can be not enough to bring the system to the minimal energy state. However, there are mechanics to surpass this difficulties and a specific case will be addressed in the following chapter.

6.5 Conclusions

A model to study membrane fusion and fission is presented. This model is developed by addition of the Gaussian term to the bending energy of a three-dimensional membrane phase field. This is done by expanding on already existing membrane phase-field models [24, 50, 59, 131], which has been used to study a variety of systems based on the

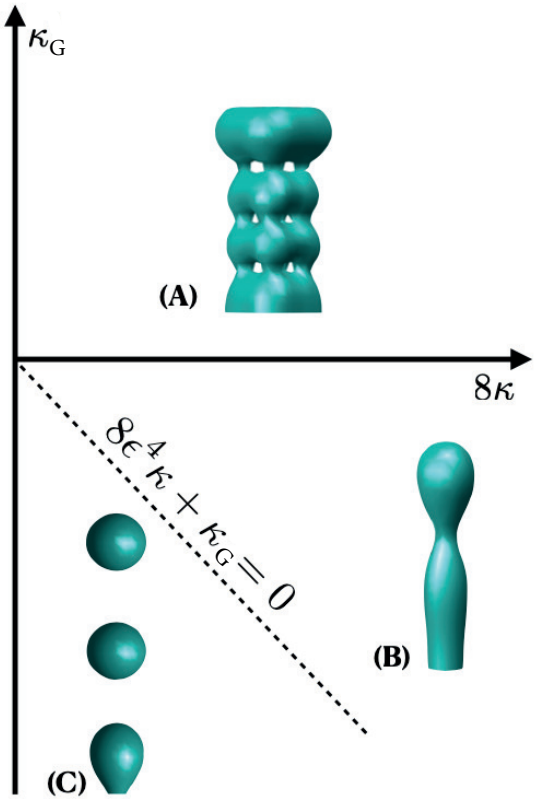

Figure 6.6: Membrane shape diagram for the (κ, κ_G) landscape with $\varepsilon = 1$. (A) Multiple self-connected membrane with positive κ_G, (B) neck formation without fission for $\kappa_G > -8\kappa$, and (C) vesicle formation with a magnitude of $\kappa_G < -8\kappa$.

Helfrich theory for cellular membranes [22]. This novel phase field model can be used to explore fission events and other topological transformations of membranes, where the Gaussian curvature is relevant.

The model has been applied to the study of the pearling mechanism on tubes, where a spontaneous curvature on the membrane transforms a membrane tube in an array of spherical beads still attached together. Pearling instability has been already studied in simulations [57, 126, 127] and experiments [128, 129]. However the results reported here show how the inclusion of the Gaussian curvature term leads to the fission of the pearls from the tube. However, this only happens for some values of the Gaussian modulus κ_G

Moreover, we have obtained the dispersion relation that can be used to obtain the preferred size of the vesicles given a spontaneous curvature. Both the size of the final vesicles and the size predicted by the dispersion relation match. With increasing spontaneous curvature one obtains smaller vesicles, as the relation between curvature and

radii is inverse like $C_0 = 1/R_0$.

Therefore, fission and vesicle formation from a membrane tube can be modelled using this methodology. Not only that but this model can be used to study what would happen if the Gaussian bending modulus were positive instead of negative. A positive Gaussian modulus could be a way to model what happens in the Golgi apparatus where membrane fenestration creates "handles" and holes at some areas of the organelle. In the case of the cell not finding a mechanism to reverse the sign of this energy modulus then one can say with certainty that the Golgi apparatus is going against the Gaussian curvature. The only way to do this would be by working against the Gaussian energy term with the use of molecular motors to create its characteristic handles and channels even with a negative Gaussian bending modulus κ_G. In any case, the study of the membrane fission dynamics is crucial to be able to identify the mechanisms that drive the topological transformations in the Golgi apparatus and membranes in general.

Chapter 7

Vesicle formation induced by thermal fluctuations

7.1 Introduction

Vesicles are a biological component that are crucial for many biological processes, e.g. transport vesicles [132], secretory vesicles [133], and endocytosis [134]. Many of these biological processes require to create and destroy vesicles constantly. Even red blood cells are known to loose membrane when they became old through shedding of microvesicles and leading to a change in the surface-volume ratio [135]. Thus, there is great interest in getting insight on the mechanics of vesicle formation (or vesiculation).

In the previous Chapter 6 the vesiculation of a membrane tube was studied. The membrane tube is a geometry that aids the formation of vesicles and the fission of the membrane into multiple vesicles [121] and that is why such geometry was chosen. However, there are some membrane geometries that instead of aiding the vesicle formation they hinder the membrane evolution towards vesiculation like for example a flat membrane.

Prior to vesiculation the membrane will change shape and form buds through a process which is, very originally, called budding. These buds are deformations of the membrane and they look like a membrane sphere fused with the rest of the membrane line in the representation of a bud in **Figure 7.1**. These mushroom-like deformation of the membrane are what typically happens prior to the vesicle scission from its original membrane where the attachment point to the main membrane is cut.

A perfectly flat membrane example is a geometry that hinders this budding process as this geometry lacks any curved region, which difficulties membrane budding and therefore difficulties vesiculation. However, in nature vesiculation happens in wide

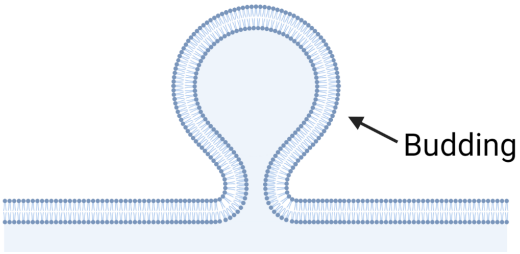

Figure 7.1: Schematic of a bud formed through the budding of a biological membrane.

variety of situations and with plenty of membrane geometries for the "mother" membrane. Therefore there is much to gain in studying which mechanism can promote –or even induce– the formation of a vesicle from a non-favourable geometry.

This is exactly what will be addressed in this chapter by using thermal fluctuations as a mechanism to promote vesicle formation. By adding a thermal noise of enough intensity, one would expect to be able to deform the membrane enough as to randomly be able to obtain a membrane shape that could vesiculate. Or maybe there is a energy wall that is impeding the flat membrane to change shape and form buds, in which case the thermal energy might help cross this barrier to achieve success. Using the previously shown model that introduces the Gaussian curvature term to the energy, one can study this topological transitions properly.

In previous experimental works, temperature has been used to produce fission of vesicles in Giant Unilamelar Vesicules (GUVs) [136] although they used the first order phase transition in GUVs between their gel and fluid membrane states. For long it has been known that vesicle formation is temperature-dependent [134, 137] but here will be studied the energetics and the dynamics of vesiculation and its dependence on temperature.

7.2 Model

The basis for this model will follow the Canham-Helfrich free energy explained in Chapter 2 as well as the addition of the Gaussian curvature energy term from the previous chapter. Then the most important parameters will be the total curvature C, the Gaussian curvature K and the two physical constraints: a conservation of the total area of the surface and of the volume contained within. This free energy is written as following

$$F = \int_A \left(\frac{\bar{\kappa}}{2}(C - C_0)^2 + \bar{\kappa}_G K + \gamma_A \right) dA + \int_V \Delta p \, dV, \tag{7.1}$$

where C is the total curvature, K the mean Gaussian curvature, C_0 is the spontaneous curvature.

In this chapter we will not forgo the Gaussian contribution as we are interested in studying the formation of vesicles. This process changes the number of objects in the system, a big closed membrane will split into multiple closed membranes. This in turn changes the Euler characteristic, thus the system will be undergoing topological transitions.

As in previous chapters, the minimisation of this free energy in equation (7.1) will be computed numerically by using a phase field model. The resulting free energy as a phase field will be split into two different contributions $F = F_{C_0} + F_G$, where F_{C_0} is a bending free energy for a spontaneous curvature, which reads

$$F_{C_0} = \kappa \int_\Omega \left((\phi - \varepsilon C_0)(\phi^2 - 1) - \varepsilon^2 \nabla^2 \phi\right)^2 dV, \tag{7.2}$$

where $\kappa = 3\sqrt{2}\bar{\kappa}/16\varepsilon^3$ and $C_0 = c_0/\sqrt{2}$. And, as we have seen in the previous chapter, the energy density for the Gaussian curvature contribution will end up looking like

$$F_G = \frac{\kappa_G}{2\varepsilon^2} \int_\Omega \sum_{\alpha<\beta} (1-\phi^2)^2 \left[Q_{\alpha\alpha} Q_{\beta\beta} - Q_{\alpha\beta}^2\right] dV, \tag{7.3}$$

where $\kappa_G = 3\sqrt{2}\varepsilon\bar{\kappa}_G/4$. This contribution has already been presented in Chapter 2 and Chapter 6. For the sake of convenience let us refresh a couple of concepts on the curvature tensor. The curvature tensor can be defined using the vector normal to the surface normal vector $\hat{n}$ as

$$Q_{\alpha\beta} = \nabla_\alpha n_\beta. \tag{7.4}$$

This tensor represents changes in the orientation of the normal vector along the surface. These changes are directly related to the curvature of such a surface. This curvature tensor in turn can be defined in terms of the gradients of the order parameter ϕ as [62],

$$Q_{\alpha\beta} = \frac{\sqrt{2}\varepsilon}{1-\phi^2} \left[\partial_{\alpha\beta}\phi + \frac{2\phi}{1-\phi^2} \partial_\alpha \phi \partial_\beta \phi\right], \tag{7.5}$$

where $\partial_\alpha = \partial/\partial x_\alpha$, and $\partial_{\alpha\beta} = \partial^2/\partial x_\alpha \partial x_\beta$.

We can compute the dynamic equation by doing the functional derivative of both of the free energy contributions

$$\frac{\partial \phi}{\partial t} = \nabla^2 \left(\frac{\delta F_{C_0}}{\delta \phi} + \frac{\delta F_G}{\delta \phi}\right). \tag{7.6}$$

This dynamic equation can be written explicitly in terms of the phase field order

parameter ϕ which results in

$$\begin{aligned}\frac{\partial\phi}{\partial t} &= M(\kappa\nabla^2\left((3\phi^2-1-2\phi\varepsilon C_0)\Phi-\varepsilon^2\nabla^2\Phi+\gamma\nabla^2\phi\right)\\ &\quad-\kappa_G\nabla^2\left(\frac{12\phi}{1-\phi^2}F_{K_1}+\frac{2(3\phi^2+1)}{(1-\phi^2)^2}F_{K_2}\right)),\end{aligned} \tag{7.7}$$

where $\Phi=(\phi-\varepsilon C_0)(\phi^2-1)-\varepsilon^2\nabla^2\phi$. In this dynamic equation the bending and the Gaussian contributions can be differentiated by their energy moduli κ and κ_G respectively. There is no need for a volume Lagrange multiplier as the dynamic equation is written as a diffusive equation (also known as model B), however we introduce a Lagrange multiplier for area γ. The terms F_{K_i} represent the Gaussian curvature effect and are

$$F_{K_1}=\partial_{\alpha\alpha}\phi\partial_{\beta\beta}\phi-(\partial_{\alpha\beta}\phi)^2,$$

and

$$F_{K_2}=\partial_{\alpha\alpha}\phi(\partial_\beta\phi)^2+\partial_{\beta\beta}\phi(\partial_\alpha\phi)^2-2\partial_{\alpha\beta}\phi\partial_\alpha\phi\partial_\beta\phi.$$

7.2.1 Thermal fluctuations without fluid coupling

To add a thermal behaviour to the membrane it will be necessary the use of noise. The noise will represent the displacement generated by the random impacts of molecules on to the membrane due to their random Brownian motion. Those impacts will displace constantly the membrane from its average position as sketched in **Figure 7.2** moving different points of the membrane to different directions and displacements. This noise cannot be chosen lightly and a few things have to be taken into consideration, however the method will be independent on the explicit free energy taken so the equations will be written in a more general way.

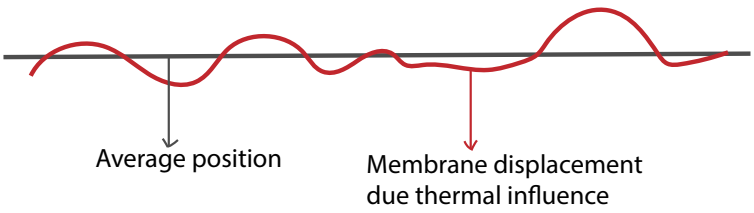

Figure 7.2: Sketch of a membrane shape due to thermal displacement.

So there are many ways to add a noise to a dynamic equation, either additive or multiplicative correlated or uncorrelated et cetera. However, as we are interested in a

thermal behaviour this will constrain how can we add up this noise.

Thermal fluctuations, which are generated by thermal noise, are uncorrelated thorough space and time, also known as delta-correlated. This means that when comparing two different points of space the fluctuations over a long enough time require to have no correlation between them, therefore being independent. So it is necessary to have a noise that its intensity independent of time and space. From the Fluctuation Dissipation Theorem we can obtain the relation between the noise variance and the temperature via its auto-correlation which, for a noise ξ, takes the form

$$\langle \xi(\mathbf{x},t)\xi(\mathbf{x}',t')\rangle = \frac{2k_BT}{\kappa}\delta(\mathbf{x}-\mathbf{x}')\delta(t-t'), \tag{7.8}$$

where k_B is the Boltzmann constant and T the temperature. Its inverse dependence on the bending modulus κ comes from the fact that a higher rigidity reduces the thermal fluctuations of a membrane. Similarly sometimes in the literature one defines an effective temperature that encompasses both T and κ and changes on the rigidity are taken as changes on the effective temperature. The noise will be delta-correlated in time and space, which means that there will be no correlation for the noise value between two different points of time or space. This noise will be acting on the membrane position through the order parameter ϕ.

Therefore the noise ξ will be an uncorrelated white noise with a mean $\langle\xi\rangle = 0$, a standard deviation σ as Gaussian probability distribution,

$$P(\xi) = \frac{1}{\sqrt{2\pi\sigma^2}} exp\Big(-\frac{(\xi - \langle\xi\rangle)^2}{2\sigma^2}\Big), \tag{7.9}$$

This probability density distribution is represented in **Figure 7.3**. Probability densities must vanish at $\xi \to \pm\infty$ as their integral over all the space must be equal to one. The variance is the first moment of a single random variable X is defined by

$$\sigma^2 \equiv \langle[\xi - \langle\xi\rangle]^2\rangle \tag{7.10}$$

and is the measure of how much the values of X deviate from the mean value $\langle X\rangle$ [138] which is also represented in **Figure 7.3**. Thus the intensity of the noise can be measured with the variance σ^2 and from the Fluctuation Dissipation theorem we know that for a thermal noise this variance will be proportional to the temperature by

$$\sigma^2 = \frac{2k_BT}{\kappa}. \tag{7.11}$$

This variance, as we said before, is the measure of how much the values of ξ will deviate from the mean, which in this case is zero. Thus we can identify in equation

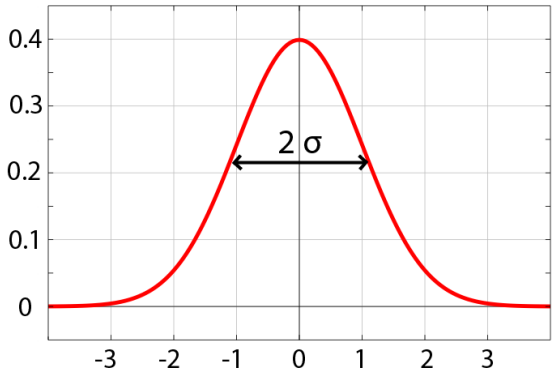

Figure 7.3: Gaussian probability distribution and its standard deviation σ. In the case of a thermal noise this σ will be proportional to the temperature.

(7.8) that the magnitude of the auto-correlation is the variance σ^2. Therefore we can modulate the intensity of this noise via the standard deviation σ of the Gaussian distribution.

Now to add this delta-correlated noise into the system. One has to take into account that we are working on a phase field model, and that the position of the membrane is obtained for the points in space with $\phi = 0$. Using this and the fact that the system interface will relax fast to the hyperbolic tangent profile one can simply add a noise to the ϕ value around the points of the diffuse interface where $-1 < \phi < 1$. This would be written like

$$\frac{\partial \phi(\mathbf{x},t)}{\partial t} = M\Big(\nabla^2\Big(\frac{\delta F[\phi]}{\delta \phi}\Big) + \xi(\mathbf{x},t)(1-\phi^2)/\varepsilon^2\Big), \tag{7.12}$$

where $\xi(\mathbf{x},t)$ is a noise that has a different value at each point in space and is multiplied by $(1-\phi^2)$ so that only the points of the membrane are perturbed while the fluid bulks are left alone.

This noise directly added to the order parameter ϕ as it is a Gaussian distributed noise with mean zero the value of ϕ at a given point can either go up or down. So for a membrane point where ξ increases the value of ϕ positively, one shall see that point of the membrane to move from the vesicle inside ($\phi = 1$) outwards to the external fluid ($\phi = -1$) and vice-versa. That is how this phase field noise translated to spatial fluctuations of the membrane.

In other phase field models involving liquids and interfaces the noise has been defined for the flux of a volume of fluid. To to this one writes the dynamic equation like a divergence of a flux and then introducing the noise inside this divergence [139, 140] like $\nabla\xi(\mathbf{x},t)$. However we are not studying a flow, we are studying the vibration of a

membrane inside a motionless fluid. Therefore no gradient nor divergence has been considered for the noise.

Although the noise has a Gaussian distribution with a mean zero, the conservation of volume and area can be violated. That is because for the distribution having mean zero translates to an the average of the displacements is zero over long periods of time. However between two points in time one could see a variation of either volume or area. In this chapter we should distinguish from the start between general area/volume conservation (for the whole system) and the area/volume conservation of each single vesicle.

The general area however will be maintained by the Lagrange multiplier γ_A, so one should only worry about volume for noises that are not too extreme. The general volume and area conservation depends first of all on the noise intensity, so all volume conservation will end up breaking down for noises that are too intense. To understand the influence of the noise on the general volume conservation we have to understand that each point of the membrane gets a different ϕ displacement. As the noise is only applied on the volume of membrane, the bigger a vesicle we have the lower the ratio of "membrane" to "intracellular volume" we have. This is due to the fact that the ratio of the surface area vs enclosed volume gets bigger for smaller vesicles, as the width of the membrane is constant. If the interface occupies a space of similar volume to the enclosed intracellular volume one will have problems of volume conservation very easily. Thus, the bigger the vesicle, the bigger the number of points that are influenced by the noise and the closer the average of all these fluctuations is to zero. This makes so having big enough vesicles should correct the largest part of the volume fluctuations.

Therefore for big simulations is easy to ensure the general conservation of volume and surface area for the whole system. However, this is more difficult to ensure for each individual vesicle, as its size will depend on the spontaneous curvature of the membrane in most cases the resulting vesicles are small. This could be addressed by adding complex Lagrange multipliers to the model, however with the model as is one can study whether vesiculation happen or not, its energetics, and the dynamics that bring a membrane to vesiculate. The proper modelling of the vesicles after they have scissioned from the mother membrane would add little or nothing given our goals.

7.3 Vesicle formation promoted by thermal fluctuations

Vesicle formation can be studied by using the complete bending energy that takes also into account the Gaussian curvature term. However, for some geometries we will find that even for values of the Gaussian rigidity modulus κ_G that should produce fission, sometimes nothing happens. This is due to the fact that while some geometries promote fission, like a membrane tube as seen in the previous chapter, some others do the opposite and difficult the fission of the membrane. An example of this is a flat infinite

membrane, where the curvature is zero and even if the membrane has a spontaneous curvature C_0, there is a barrier of energy that you need to surpass to be able to reach fission. Therefore for cases where fission brings the system to a lower energy configuration, if geometry is not promoting the fission, the membrane will need another way to promote fission. This is where the temperature can come in and play a role.

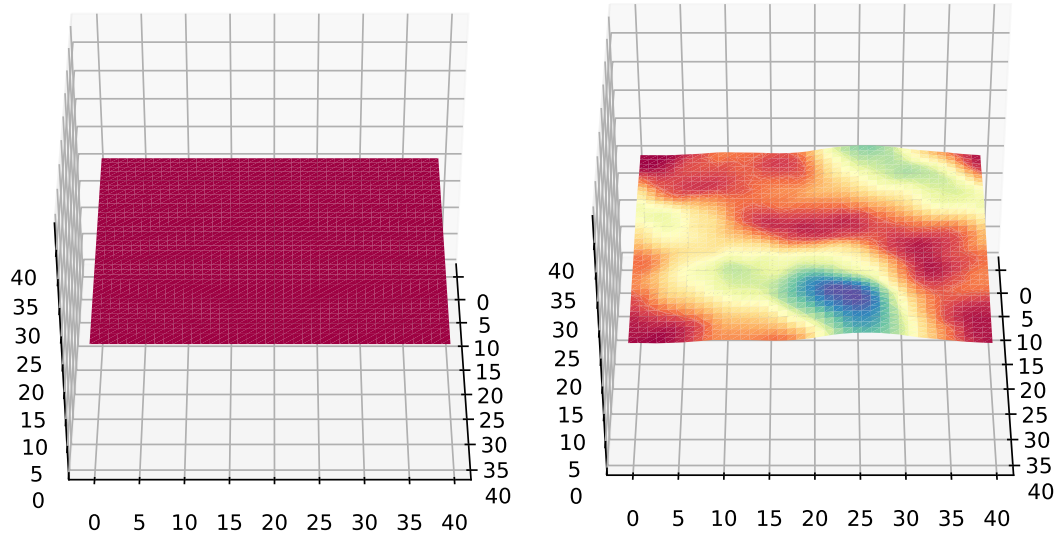

Figure 7.4: Left: Snapshot of a flat membrane under conditions where fission is energetically favourable, however due to the starting geometry we see no change over time on the membrane shape. The parameters used $T = 0$, $\varepsilon = 1$, $\kappa = 1$, $\kappa_G = -10$ and $C_0 = -0.5$. **Right:** Snapshot of a fluctuating flat membrane under conditions where fission is energetically favourable and with low temperature. The parameters used $T = 1.33 \cdot 10^{-5}(IU)$, $\varepsilon = 1$, $\kappa = 1$, $\kappa_G = -0.5$ and $C_0 = -0.25$.

Thermal energy can be measured with the k_B Boltzmann constant and the relation

$$E_T = k_B T, \tag{7.13}$$

where k_B a value of $k_B = 1.38065 \cdot 10^{-23}\text{J K}^{-1}$ [141]. If we introduce a Gaussian white noise on the membrane position, we can mimic the temperature. With enough thermal energy we expect the membrane to have enough energy to produce fission. This will depend on the interplay between temperature and the bending and Gaussian rigidities κ and κ_G respectively. If the temperature is not enough, for a given spontaneous curvature C_0, κ and κ_G we will find that even though the membrane can fluctuate the fluctuations will not be enough to bend the membrane enough so that a bud can be produced. If a bud is produced even for a short amount of time, the Gaussian contribution will scission the membrane in two producing a vesicle.

This process can be modelled using our stochastic phase field model with the additional Gaussian contribution. However, our goal with this method is not to simulate physics that model perfectly the dynamics of the vesicles after scission as we are only interested in the process that brings us to the fission event itself. The true wonder is to obtain vesicle formation starting with a geometry that difficults fission.

From Chapter 6 we know that, for a Gaussian curvature modulus that satisfies $\kappa_G > -8\varepsilon^4\kappa$ (for the phase field bending and Gaussian moduli) we know that we can get fission. When adding temperature to the flat membrane one could start to see fluctuations that take the shape of something like **Figure 7.4 B**. In this case we have a flat membrane in the presence of a white noise generating thermal fluctuations. This thermal fluctuations however are not big enough to produce vesicle formation.

If we keep cranking up the temperature for a given C_0 and κ_G and κ we shall find vesiculation. This vesiculation process is a random process, so it can be hard to know for sure if with more time a simulation would actually fission or would not. Therefore an amount of time has to be chosen so that is long enough as to be able to say that if no vesiculation has happened up to that point then vesiculation is not possible for that combination of parameters.

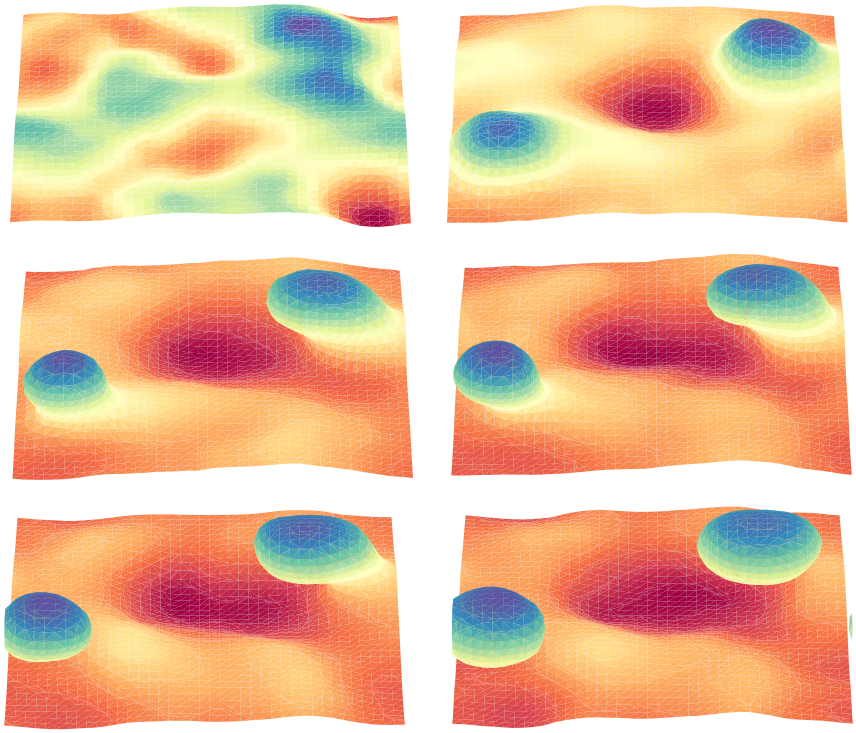

Figure 7.5: The parameters used $T = 3.6 \cdot 10^{-5}(IU)$, $\varepsilon = 1$, $\kappa = 1$, $\kappa_G = -5.0$ and $C_0 = -0.25$.

With enough temperature we change phase into the vesiculation phase, where we can obtain vesicles from a flat membrane like in **Figure 7.5**. If we keep the simulation running we can see vesicles keep forming until they fill all the simulated space. However, the simulated vesicles after detachment do not behave rigorously. In the end we have small volumes with a Gaussian white noise, which has an average value of zero but still this white noise makes so that the vesicles volume fluctuates over time, even is the average over time of change is zero. This is why one has to take into account that this model and simulations intend to simulate and study the process up to fission, including the fission itself, but has no interest in continuing the simulation much longer.

One could expand the model so that the scissioned vesicles behave more rigorously, however this would be complex and computationally costing. This would require do distinguish between local volume conservation for each vesicle, and the phenomenology would not change. The phenomenology of this system is all contained by the presented model for this kind of geometry. It has been proven that the even a membrane with a geometry unfavourable for fission, if it is combined with a temperature, one can obtain fission and vesicle formation. The only remaining question left is how the phase space looks in function of the free parameters, and how the transition between vesicle formation phase and fluctuating phase looks like.

7.3.1 Positive Gaussian modulus

Changing the sign of Gaussian modulus κ_G to a positive one completely changes the results. Getting the system to vesiculate seems impossible, even for unrealistically high noise the Gaussian contribution can hold the membrane together. The morphology of the membrane also changes, for very big noises like in **Figure 7.6** we can see huge deformations and valleys much bigger than the vesicles produced with negative Gaussian modulus κ_G but without losing the membrane coherence.

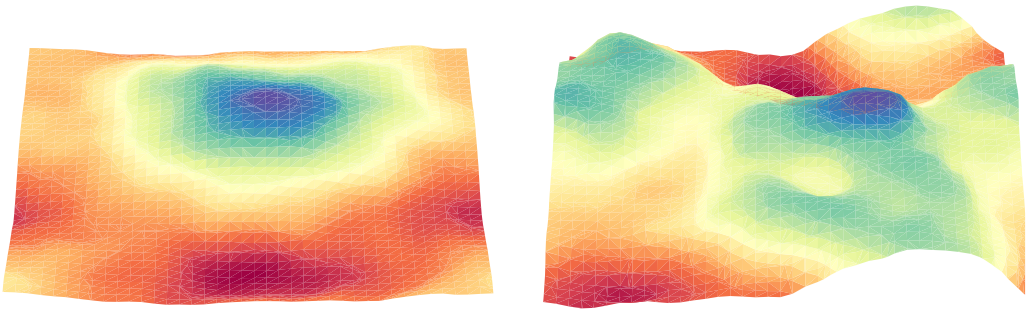

Figure 7.6: Left: Membrane fluctuating with T=$6.4 \cdot 10^{-5}$IU and $C_0 = -0.25$. **Right:** Membrane fluctuating with T=$256 \cdot 10^{-5}$IU and $C_0 = -0.25$. Little matters the intensity of the noise, for positive Gaussian modulus we find no topological transitions. For very high noises the membrane curves and stays curved, but does not go further than that.

Some of the temperatures introduced in **Figure 7.6** are two orders of magnitude over the previously simulated temperatures. Nonetheless, even if the spontaneous curvature term would prefer to have spheres of radius $R_0 = 1/C_0$ it seems to not matter how much thermal energy we introduce. In the end the Gaussian term seems to dominate the fate of the membrane, holding it together and not reaching by far not even the formation of a bud.

Usually the Gaussian contribution is thought of only influencing the system when small membrane necks and other shapes close to topological transitions happen. However, the results obtained seem to suggest that the Gaussian term is changing radically how the membrane deforms at all stages and membrane geometries, at least for thermal fluctuations.

The lack of vesiculation makes sense given the Gauss-Bonnet theorem, which as seen in Chapter 2 states that

$$\int_{\Omega} K\,dS = 2\pi\chi(\Omega), \tag{7.14}$$

where $\chi(\Omega)$ is the Euler characteristic as we have already seen in Chapter 2 and is a topological invariant. Therefore, the energy contribution of the Gaussian curvature is a constant unless the topology of the system changes. The Euler characteristic describes the system as

$$\chi(\Omega) = 2(N - g), \tag{7.15}$$

where N is the number of objects and g is the number of holes. Given that the Gaussian energy term is

$$\kappa_G \int_{\Omega} K\,dS,$$

and κ_G is taken positive in these cases, one would expect that increasing the number of holes would lower the energy of the system. And even if the configuration is hard to achieve the high temperatures used should be giving the necessary energy to produce any membrane deformation necessary.

Therefore, maybe the most intriguing of all is not reaching a self-connected membrane like we see in Chapter 6. One would expect with this level of noise to maybe go through topological transitions but in the direction of increasing the number of holes and thus decreasing the Euler characteristic and the Gaussian contribution. This might be point to the plane membrane being a geometry even worse for obtaining multiple self-connected membranes than for vesicle formation, and maybe this could be even quantified.

7.3.2 Vesiculation Phase diagram

The parameters that play a role in whether fission happens or not are the temperature T, the bending and Gaussian modulus κ and κ_G and the spontaneous curvature C_0.

However, from the equation

$$8\varepsilon^4\kappa + \kappa_G = 0, \tag{7.16}$$

we know that the important factor on the moduli values is the ratio between them κ_G/κ. So using this we can reduce the number of parameters by one, down to three: T, κ_G/κ, and C_0.

If we want to plot the phase diagram as a function of the three free parameters we would need to do a 3D plot, and that could be hard to read. Therefore, one way can be to plot the phase diagram of two free parameters fixing the third one. We can see a phase diagram for a fixed spontaneous curvature $C_0 = -0.25$ and $C_0 = -0.10$ in **Figure 7.7**.

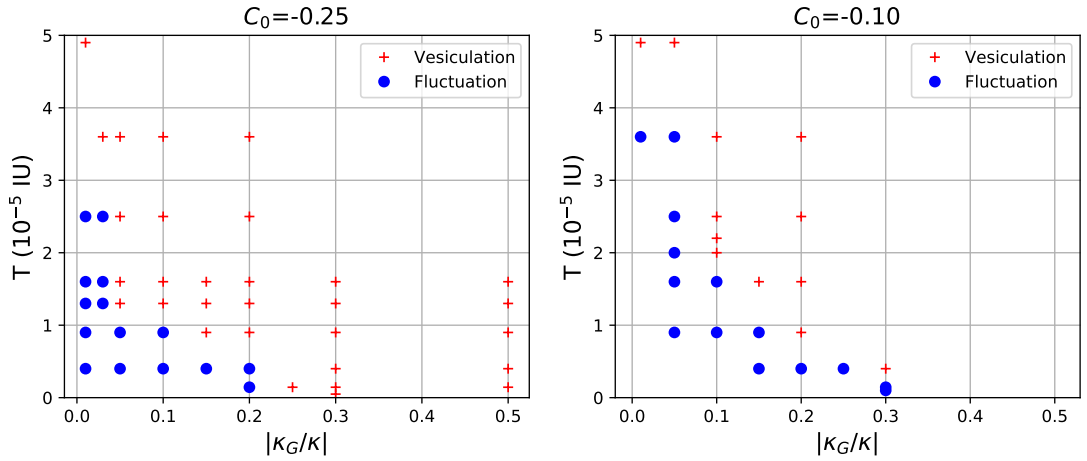

Figure 7.7: Phase diagram of vesicle formation from a flat membrane depending on temperature T and the energy moduli ratio κ_G/κ for a fixed spontaneous curvature C_0. The simulations had a size of $40 \times 40 \times 44$ and a membrane width of $\varepsilon = 1$.

The spontaneous curvature value helps the vesiculation process. The bigger C_0 the bigger the drop in energy between a flat surface (with curvature zero) and the a spherical vesicle of literally any curvature value, as it will reduce the bending energy contribution

$$\kappa(C - C_0)^2.$$

We can see when comparing the two plots in **Figure 7.7** that when decreasing the spontaneous curvature to $C_0 = -0.10$ there are areas in the phase diagram that change phase. It is be more pronounced for lower energy moduli ratios of κ_G/κ.

What we are seeing in the results is that there is an energy barrier that one has to surpass to obtain vesicle formation. This energy barrier is being surpassed with the temperature. So for any combination of C_0 and $|\kappa_G/\kappa|$ there is a energy barrier

of a given magnitude, which decreases when increasing either C_0 or $|\kappa_G/\kappa|$. So for a given energy barrier we are seeing in the phase diagrams of in **Figure 7.7** how we need a minimum temperature to be able to pass from the fluctuating phase into the vesiculating phase.

7.3.3 Estimating the real temperature

In this chapter we will be using the internal computational units (IU) for the parameters. This is due the fact that those are the actual numbers running inside the simulation, and a translation from internal units to real units involves estimation and approximation to a degree. So it is more accurate to give the parameters with their internal units. However, let us see which kind of temperatures are we simulating and how do we obtain them.

For the estimation on the temperature we will be using the Mean Square Displacement (MSD) $\langle|h|^2\rangle$. To this end we need to compute the exact position of the membrane over time. We will do this by interpolating the position $\phi(x,y)=0$ to obtain $h(x,y)$. For a flat membrane is easy as we only need to go through the direction z until finding the ϕ value closest to zero for each position (x,y). This value z will be our height $h(x,y)=z(x,y)$.

With this information we can use the following equation [142]

$$\langle|h|^2\rangle \approx \frac{A\,k_B\,T}{4\pi^3\kappa}, \tag{7.17}$$

where $A=L^2$ is the surface area of the system and L its length. However, previous literature report a slightly different expression for this [34]

$$\langle|h|^2\rangle = \frac{k_B T}{2\pi\kappa} q_{min}^{-2} = \frac{A\,k_B\,T}{8\pi^3\kappa}, \tag{7.18}$$

where q_{min} is the lower cutoff wave-vector and has a value $q_{min}=2\pi/\sqrt{A}$. We will stick with the first one but it should be pointed out that there could be an extra factor 2.

Using this expressions we can compare the numerically obtained $\langle|h|^2\rangle$ with the temperature T and the bending modulus κ. So, we can easily know A and $\langle|h|^2\rangle$ from a simulation and we can also fix κ. Therefore we can find the thermal energy of the system from equation (7.17)

$$k_B\,T = 4\pi^3\kappa\frac{\langle|h|^2\rangle}{A}, \tag{7.19}$$

this will be independent on the scale that we are simulating. The importance is not if we are simulating a $L=400\mu$m or $L=1\mu$m system in length, but the ratio between the surface area and the MSD. Moreover, the final temperature depends strongly on the rigidity κ. The bending modulus can take a wide range of values, from $\kappa\approx 10k_BT_a$ to

	$T = 0.1 \cdot 10^{-5}$ IU	$T = 1.6 \cdot 10^{-5}$ IU	$T = 3.6 \cdot 10^{-5}$ IU
$\kappa = 10 k_B T_a$	28 K	444 K	1000 K
$\kappa = 70 k_B T_a$	225 K	3600 K	8100 K

Table 7.1: Temperatures from IU to Kelvin for different internal values and different rigidities measured in $k_B T_a$ where $T_a = 298$K and k_B is the Boltzmann constant.

$\kappa \approx 100 k_B T_a$ where $T_a = 298$K. From this expression we can see that for a membrane with double the bending modulus κ we will need double the temperature to have the same MSD.

So to understand if the simulated temperatures are too high we take a simulation with a fairly high temperature where we define that $T_{internal} = 3.6 \cdot 10^{-5} IU$. From that simulation we study the MSD and obtain it to be $\langle |h|^2 \rangle = 0.5 \Delta x^2$ for a flat square membrane of area $A = 40 \times 40 = 1600 \Delta x^2$. Introducing this information in equation (7.19) results in

$$k_B T \approx 0.39 \kappa. \tag{7.20}$$

Therefore, the final temperature for this simulation will depend in whether are we simulating soft giant unilamelar $\kappa_{GUV} = 10 k_B T_a$ vesicles or a bit more sturdier red blood cells $\kappa_{RBC} = 70 k_B T_a$. The resulting thermal energy for each κ_{GUV} and κ_{RBC} respectively is

$$k_B T \approx 4 k_B T_a,$$

and

$$k_B T \approx 27 k_B T_a.$$

So depending on the bending modulus of the membrane κ at $T_{internal} = 3.6 \cdot 10^{-5} IU$ we are simulating around $T = 1000$K and $T = 8100$K. This is a huge range of temperatures available to simulate depending on κ. However, the results here range mainly from $T_{internal} = 0.1 \cdot 10^{-5} IU$ up to $T_{internal} = 1.6 \cdot 10^{-5} IU$, which result in the wide temperature ranges represented in **Table 7.1**. Looking at the temperature range form this table one can see that our results do not seem to represent adequate temperature ranges for more rigid membranes, like the ones of red blood cells. So our simulations can be used to represent a range of real biological membranes of low-medium bending rigidity κ with realistic temperatures.

With these results we can plot the region where water is liquid in the previous phase diagram. Looking at **Figure 7.8** we can see how depending on the bending modulus we should look at different regions. With this we can look for a given bending if a transition to vesiculation or fluctuation regimes is possible by changing T, C_0, or κ_G.

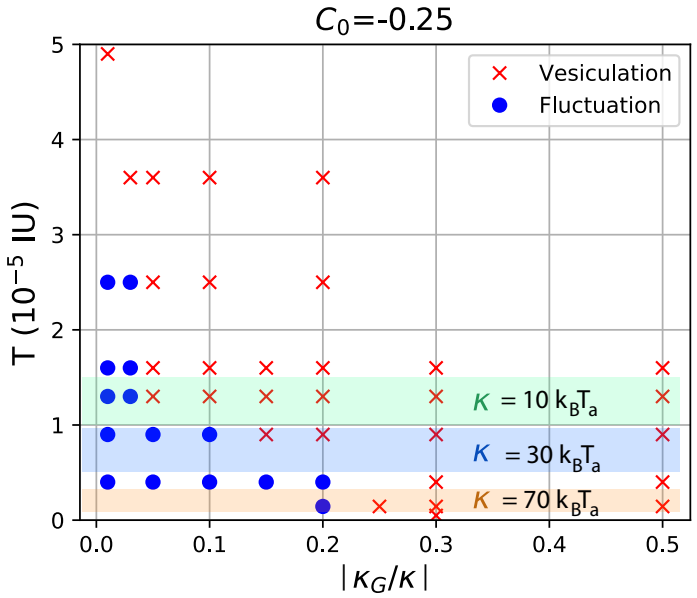

Figure 7.8: Phase diagram of vesicle formation depending on temperature T and the energy moduli ratio κ_G/κ for a fixed spontaneous curvature C_0. In colours we find different regions where water is liquid depending on the bending modulus κ. Simulations size of $40 \times 40 \times 44$ and membrane width $\varepsilon = 1$.

7.3.4 Energy evolution

Overall these simulations are driven mainly through the decrease in the Gaussian energy term F_G from equation (7.3), which we can see how it decreases over time in **Figure 7.9**. This energy term starts decreasing once the first vesicles fission from the main membrane. However, there seems to be an energy barrier to surpass, so the simulations that do not have a high enough temperature cannot get to lower their Gaussian energy term.

There is also the Curvature term per unit area (or curvature energy density) plotted in **Figure 7.9**. This term is obtained from F_{C0}/A by using equation (7.2) and the surface area of the membrane. This term in general decreases or remains constant, depending on whether we have vesicle formation or not. In simulations where we have a normal vesiculation process the vesicles formed get a curvature closer to C_0 than when they where flat ($C = 0$) and thus reduce the term $(C - C_0)^2$ from the free energy.

So let us address the reason for studying the energy density of the curvature term instead of the total energy term. To understand it we should look at **Figure 7.10** where the Curvature term integrated over all the space is plotted next to the area evolution. We can see how both energy and area increase almost identically. This

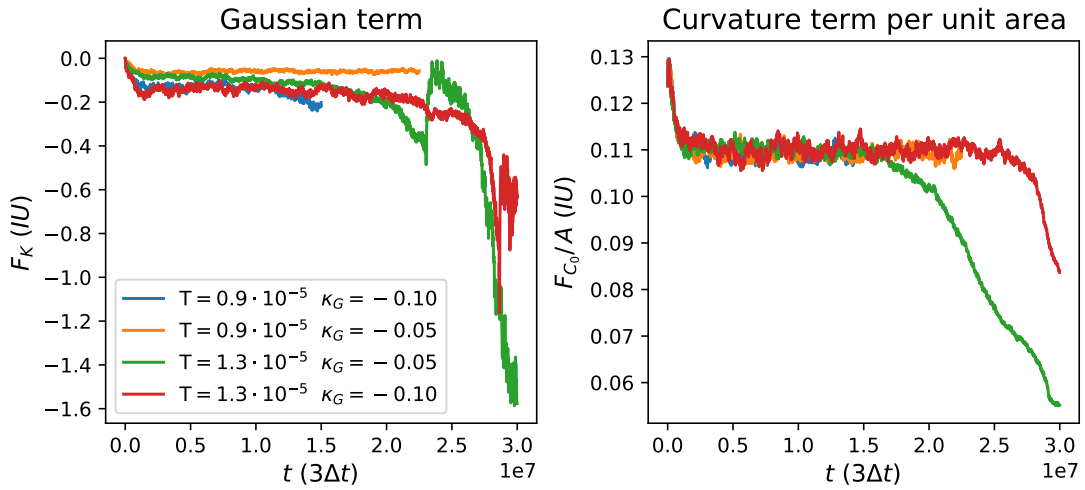

Figure 7.9: Evolution over time of the two energy contributions for a series of simulations, in some there is vesiculation and in some there is not. From the bending free energy we have the Gaussian energy term and the Curvature term energy density. In the plot there are both simulations where vesiculation occurs and some simulations where it does not.

happens because in the end having membrane has an energy cost in the Curvature term of the free energy, thus any increase in surface area increases the Curvature term of the free energy. Meanwhile, the Gaussian energy term due to the Gauss-Bonnet theorem is proportional to the number of objects and holes as seen in equation (7.14). Therefore the Gaussian energy contribution should not increase due an increase in area. In conclusion the best way to understand the evolution of the membrane in a vesiculation scenario where area is not conserved is to plot the complete Gaussian term and the Curvature term per unit area.

Finally we have studied the chemical potential term squared $\int \mu^2 dV$ where the chemical potential is defined with the functional derivative

$$\mu = \frac{\delta F}{\delta \phi}$$

and is represented in **Figure 7.11**. This term clearly shows that the changes on the membrane are driven by a very specific thermal energy, we can see a clear offset on μ^2 at each different temperature. The value of this offset is clearly related to the temperature of the system and all simulations at the same temperature overlap as can be seen in **Figure 7.11**. In cases where there will be vesiculation this term starts climbing up, before vesiculation starts.

Different values of κ_G will make so that the energy contribution of each vesicle

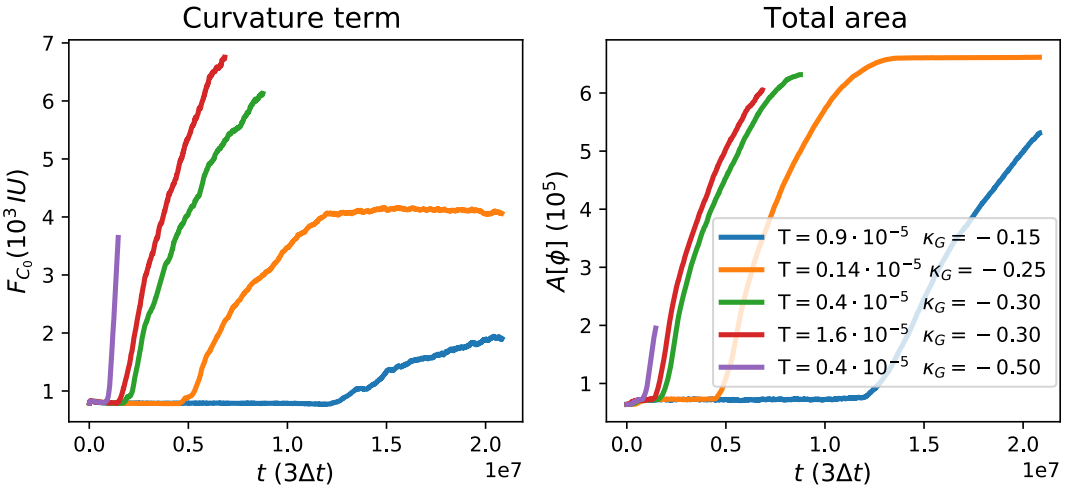

Figure 7.10: Evolution over time of the complete Curvature energy term and the membrane area. This system has a reservoir of area so it can increase or decrease the area to be able to create vesicles.

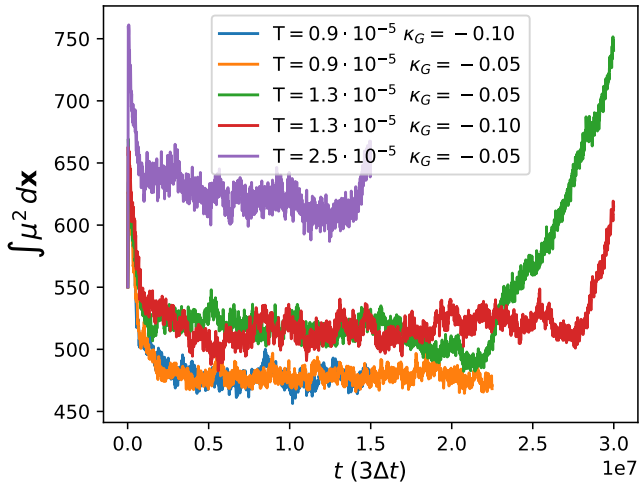

Figure 7.11: Evolution over time of the chemical potential squared or μ^2 for different simulations. In the plot there are both simulations where vesiculation occurs and some simulations where it does not.

created is bigger. Thus the slope of the Gaussian energy term over time will depend on both temperature T and the Gaussian modulus κ_G. The effect of κ_G on the simulations that vesiculate can be seen in **Figure 7.12**. In this Figure one can see how the rate of change over time of the energy is very dependent on the Gaussian modulus κ_G.

The temperature can be seen to change also that rate between the two simulations of **Figure 7.12** that share the same modulus $\kappa_G = -0.30$. However, κ_G seems to be more influential on the energy terms than the temperature.

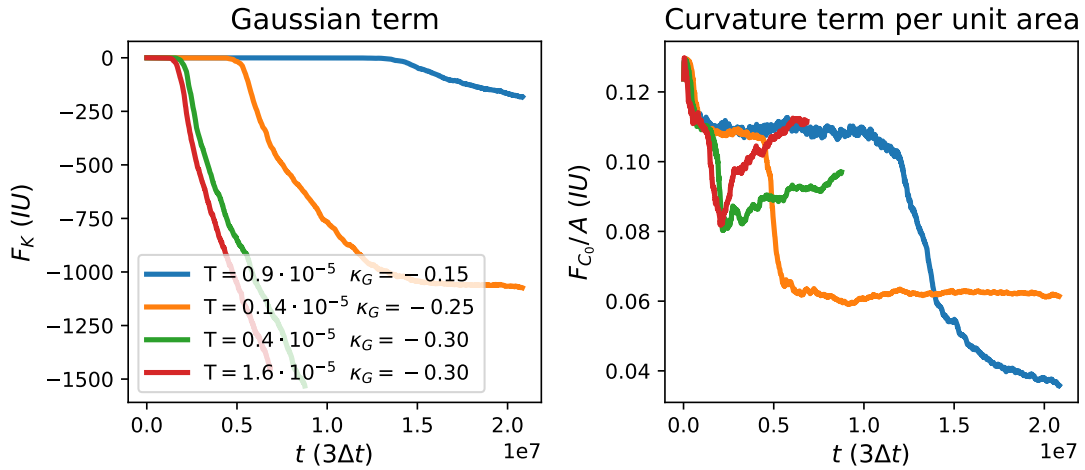

Figure 7.12: Evolution over time of the two energy contributions for a series of simulations. From the bending free energy we have the Gaussian energy term and the Curvature term. In all simulations there is vesiculation and the main change in the rate at which the energy changes is mediated by the Gaussian modulus κ_G.

For the curvature energy density in **Figure 7.12** we can see a similar behaviour as in previous plots for all the range of κ_G. In some cases the curvature term climbs back again. In these cases the κ_G is so big that its dominating over the curvature term and the vesicles deform in non-spherical ways to try to fit more vesicles.

In **Figure 7.12** one can also see how after a long time of vesiculation the Gaussian and Curvature energy terms stop changing and plateau again. This happens because in these simulations that have been left to run a long time the system reaches a point where all the space is full of vesicles and there is no room to put any more.

7.3.5 Turning off the noise

The noise (or temperature) is necessary to kick-start the fission process, however there is no need to maintain it after a certain point. Even for simulations where there has still not been a single fission event, if the membrane is already curved enough due to the temperature, even after turning off the noise it will end in multiple fission events.

Another consequence of the noise is that the vesicle shape and dynamics are a bit rough. One can see edges that one would not expect under normal circumstances as the resulting vesicles sometimes deform into rough shapes. This can be seen in the left plot of **Figure 7.13**. This happens because the vesicles are rather small and when in

comparison with the thermal fluctuations the latter are big enough to deform a lot the vesicles. As the fluctuations are rather big at the size scale of a vesicle, it also makes more difficult to conserve area and volume and, most importantly, to be dominated by the bending. However as stated earlier, the point of these simulations is not to have a rigorous description of the vesicles after the fission but to study the process that leads to fission.

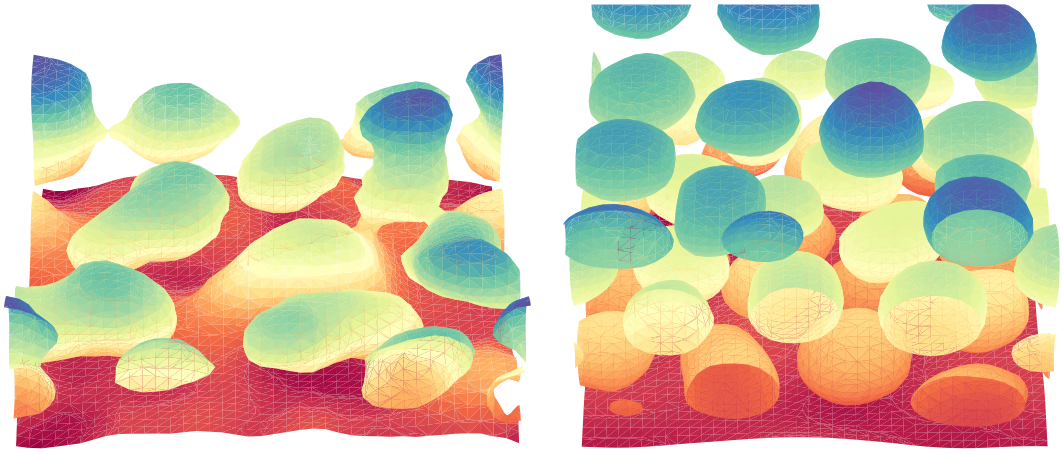

Figure 7.13: When thermal noise is present the membrane shape has more rough edges and might stick to new vesicles if there is no more room left. After turning the noise off, the vesicles take their preferred spherical shape.

To prove that this weird behaviour after fission is due to the noise and not to mistakes in the computation or the model we study what happens if we turn the noise off mid-way through a simulation. One can see that after an initial kickoff where the membrane starts to be deformed enough to generate vesicles, even if turning off the temperature one will still get vesiculation. We can see this case in **Figure 7.13**, where after reaching a point where the membrane starts to generate vesicles we turn off the temperature and the vesicles behave more properly and vesiculation continues. This happens because the fluctuations made the system reach a much better geometry to fission and until reaching the steady state more vesicles will be formed only due to the Gaussian energy contribution.

7.4 Conclusions

There are some geometries that are harder to deform than others. A flat infinite membrane for example is one, as even with a high spontaneous curvature the membrane does not deform and stays in the meta-stable flat state. But only studying fission of geometries that aid the vesiculation process seems limiting.

Thus, here we study the vesiculation of a flat membrane by introducing a thermal noise to the membrane. This thermal noise is used to promote vesiculation, as if we introduce big enough fluctuations the system is able to start the vesiculation process. In the end the thermal energy related to this noise by k_BT is helping the system overcome an energy barrier and achieve a lower energy state.

For vesicles with a positive Gaussian modulus κ_G there is no intensity of noise (or temperature) that can make the system vesiculate. This does not change even when increasing the spontaneous curvature, which makes even more energetically favourable to have spherical vesicles of radius $R_0 = 1/C_0$. We also do not observe the membrane to use this thermal fluctuations to create handles or passages to become what we have called in the previous chapter a multiple self-connected membrane like we see in Chapter 6. One would expect with this level of noise to maybe go through topological transitions by increasing the number of holes. The increase in the number of holes would decrease the Euler characteristic and therefore the Gaussian contribution. This might be point to the plane membrane being a geometry even worse for obtaining multiple self-connected membranes than for vesicle formation.

A phase diagram for a couple of different spontaneous curvatures are obtained as function of the temperature T and the ratio of the bending and Gaussian modulus κ_G/κ. This is done to show how the spontaneous curvature, the temperature and the ratio κ_G/κ facilitate or hinders vesiculation. The temperature shows to module if vesiculation will be able to happen or not for a given ratio κ_G/κ. The results clearly show how higher spontaneous curvatures help the vesiculation process by lowering the energy barrier to overcome, however also changing the final size of the produced vesicles.

The model does not perfectly model the physics of the resulting vesicles, as the noise can be big enough to make their area and volume fluctuate. This could be fixed by making the model more complex, however we see no point in doing it. The spirit of this work is to study whether vesiculation can happen or not given some mechanical parameters and use it to further our knowledge of vesiculation processes and mechanisms in nature.

We have studied the energetics of fission and one can see how the Gaussian term decreases during vesiculation, as-well as the curvature term at the start. Moreover we have discovered how the chemical potential squared is useful in predicting both the temperature and whether vesiculation will happen or not. This is so because this term is a very straight line that is proportional to the temperature and only deviates from this plateau if vesicle formation will happen.

One could expand the model so that the scissioned vesicles have a more rigorously description, with a better conservation of area and volume for each formed vesicle. However, this would be complex and computationally costing and is out of the scope

of our work, as our main goal is to study how the vesicles are created. This would require do distinguish between local volume conservation for each vesicle, and the phenomenology would not change. The phenomenology of this system is all contained by the presented model for this kind of geometry. It has been proven that the even a membrane with a geometry unfavourable for fission, if it is combined with a temperature, one can obtain fission and vesicle formation.

Chapter 8

Flickering and fluctuation spectra

8.1 Thermal fluctuations in membranes

The combination of the soft mechanical properties of the cellular membrane with its small scale generates a very dynamic structure that undergo constant shape fluctuations mostly due to thermal noise. This quasi two-dimensional interface of the cell is in some cases crucial for the function of such organism, like the case of the red blood cells or the muscle tissue cells. However, due to its nanometric thickness the study its properties and dynamics can be difficult but their fluctuating behaviour can be exploited to characterise and extract information about the cell. The experimental study of membrane fluctuations to study the cell characteristics is typically done with Red Blood Cells (RBC) as its a simple cell without nucleus, which makes easier to study just the membrane. Moreover there is a big interest in this cell as the active behaviour of the red blood cell seems modify how the membrane fluctuates.

Some experiments on red blood cell deformation consist on using optical tweezers combined with the Fluctuation Dissipation Theorem [11, 12] or micro-pipette techniques [31]. But the red blood cell has also been studied by observing its thermal fluctuations, either in flickering microscopy (also called video microscopy) experiments [10, 32, 33, 34] where they use an optical microscope or with more sophisticated Diffraction Phase Microscopy [13, 35, 36]. These last approaches may have some restrictions in the information available to obtain but it also ensures that the results obtained are intrinsic to the membrane, independent of the experimental method and not altered by scale-dependent effects of the cell. Recent studies on red blood cells are focused on disease diagnosis through understanding of the cell mechanics [67, 68, 69].

8.1.1 Experimental works

There are many experimental works studying the thermal fluctuations of the red blood cell membrane and other works on induced fluctuations studying the response of the

red blood cell. Most of these studies have the main goal to study the active nature of the red blood cell membrane or to obtain mechanical properties of the cells, like the bending rigidity κ. To understand better the fluctuating nature of the red blood cell lets look at data from the literature on red blood cell membrane fluctuations.

8.1.1.1 Flickering microscopy

Flickering microscopy is the experimental technique where red blood cells are filmed using a microscopy and using image detection software one tracks and studies the position of the membrane over time. This technique is completely passive and do not involve interaction with the studied cell.

In **Figure 8.1** we can see the results from Rodríguez-García et al. [10] where they study the membrane fluctuations of membranes with different rigidities. In these results one can see the scale of the average membrane displacements h over all the points in membrane where Δh is the standard deviation measuring how big they are. To change the rigidity of the red blood cells they either drug them with stiffening drugs (**Figure 8.1 C**) or deplete them of ATP (**Figure 8.1 B**).

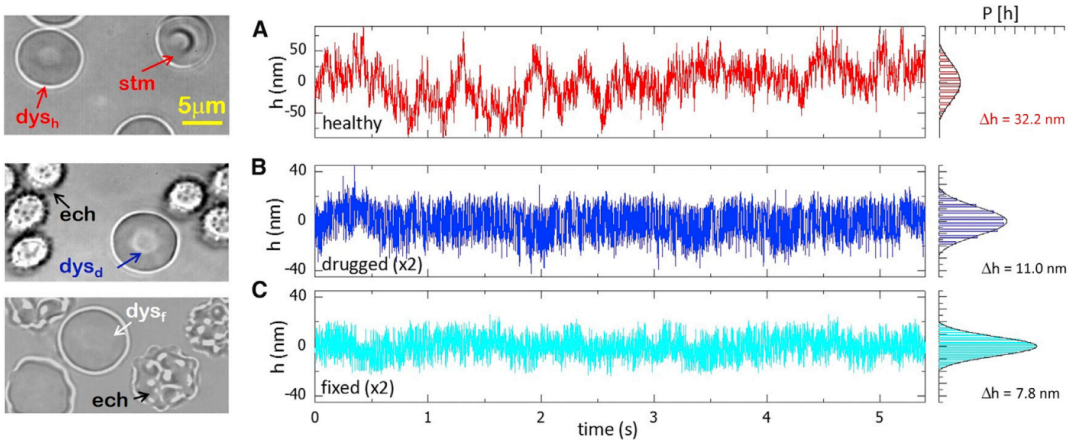

Figure 8.1: Characteristic membrane-fluctuation time traces tracked at an arbitrary point in the equatorial profile of RBCs. The data correspond to RBCs with a discocyte shape at different activity states. (A) A healthy flicker (dys$_h$) upon cytoskeleton activity. (B and C) Passive cases include drugged RBCs (dys$_d$) after ATP depletion in PBS buffer (B) and cells fixed with glutaraldehyde (dys$_f$) (C). Although most RBCs in the passive conditions appeared as nonfluctuating speckled echinocytes, some retained their discocyte shape and continued to fluctuate (dys$_d$ and dys$_f$). The normalised histograms at right represent the probability distributions of the membrane displacements averaged over all the points in the equatorial profile (Δh is the standard deviation). Adapted from Rodríguez-García et al. [10].

The changes in rigidity are shown to change the standard deviation of the fluctuations, therefore decreasing the average amplitude of the membrane fluctuations (de-

creasing how much they move). They report Gaussian distributions for the membrane displacements h when looking at a single point in the membrane in all cases.

8.1.1.2 Quantitative Phase Imaging

While flickering microscopy can only measure the position of the cell equator, Diffraction Phase Microscopy (a quantitative phase imaging technique) measures the position of each point of the membrane for a single side of the cell, giving a 2D map of the membrane position. In Popescu et al [143] we see an example of use of this technique adapted in **Figure 8.2**.

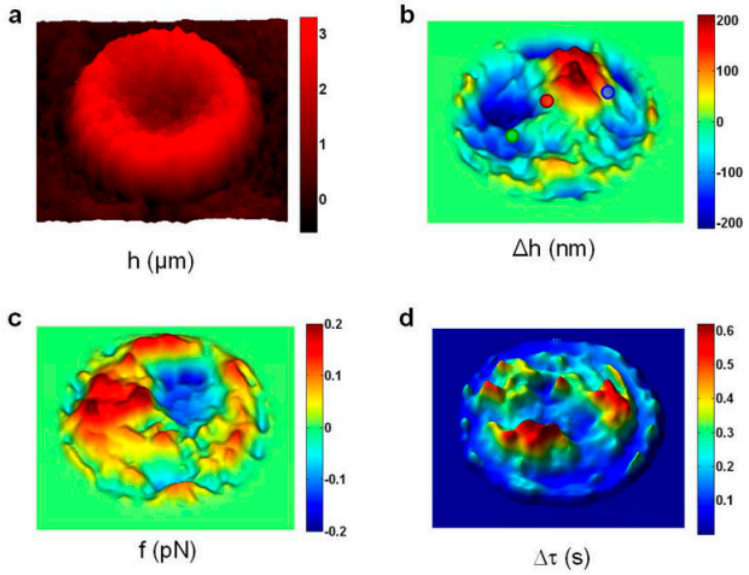

Figure 8.2: Dynamic images of RBCs provided by the DPM instrument. (a) Physical map of a normal RBC. (b) Instantaneous displacement map of the cells in panel a shows areas with relatively little displacement over time (red circle), while other areas show net positive (blue circle) or negative (green circle) displacement over the course of these measurement. (c) The instantaneous restoring force f and (d) the temporal (τ) coherence map. Adapted from Popescu et al. [143].

This technique gives similar results to microscopy flickering but the data is more complete, being a whole 2D displacement map instead of only the cell equator. However, it is more challenging to implement. Nonetheless, data obtained from these experiments properly show how soft is the membrane of the red blood cells. One can see in **Figure 8.2a** how bumpy the membrane is, instead of an idealised smooth surface, and that is because of the temperature coupled to this soft mechanical properties of the membrane.

8.1.1.3 Optical tweezers

Using optical tweezers one can manipulate the red blood cells. For example in Turlier et al [11], as can be seen in **Figure 8.3**, they fix four beads to a red blood cell and manipulate them using optical tweezers. They do both experiments and simulations and **Figure 8.3** is a simulation that is mimicking their experimental setup. What they do in this work is fixing the position of three of the beads in space and move the fourth one.

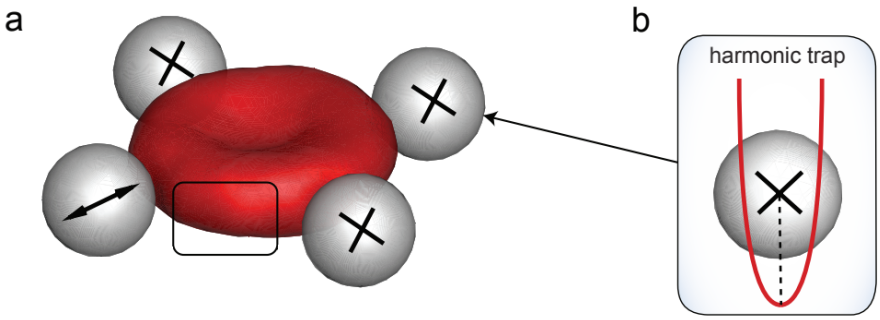

Figure 8.3: Simulations mimicking the experimental conditions. (a) Simulation setup with a RBC and four beads attached. Three beads (marked by crosses) are used as handles via a harmonic potential, while the fourth probe bead (marked by a two-side arrow) is sinusoidally driven to measure the mechanical response or let free for monitoring its fluctuations. (b) Illustration of a bead, whose centre-of-mass is held in a harmonic potential. The harmonic potential mimics the optical tweezer trap in experiments and assumes the same strength for this trap. Adapted from Turlier et al [11].

With the fourth bead they can either let it free and measure its position to analyse membrane displacement at that single point the bead is attached or move it by using an optical tweezer. Using the optical tweezer they induce fluctuations to the membrane using this moving bead, and measure the required strength to move the bead.

8.2 Model

8.2.1 Topologically invariant Helfrich membrane with noise

As in the previous chapters, the model is based in the well known Canham-Helfrich energy [22, 39] for a 2D surface with two physical constraints: a conservation of the total area of the surface and of the volume contained within. For convenience lets rewrite the free energy for a membrane without surface tension

$$F = \int_A \left(\frac{\kappa}{2}(C - C_0)^2 + \bar{\kappa} K + \gamma_A \right) dA + \int_V \Delta p \, dV, \tag{8.1}$$

where H is the mean curvature, K the mean Gaussian curvature, H_0 is a possible spontaneous mean curvature. The equation previously been shown but is repeated here for convenience. To simplify the results and to have one less free parameter the spontaneous mean curvature will be taken as zero. There is γ_A and Δp which are the Lagrange multiplier that ensures the area and volume conservation respectively and κ the bending modulus of each curvature. In addition, taking into account that the mean Gaussian curvature is a topological invariant, as stated by the Gauss-Bonnet theorem [144], its contribution is constant. Therefore the Gaussian curvature K will not be taken into account during the formulation.

This will be the total energy used for the computation of the temporal evolution, therefore we will not be taking into account any kind of cytoskeleton or spectrin network effect. The reason being that an attached spectrin network will be considered to just add an in-plane shear resistance having a negligible influence on bending resistance. Therefore, as the scales of thermal deformations is small and there is no big nor fast shape transitions in the system the elasticity and shear resistance from the cytoskeleton will be neglected.

As can be seen in Chapter 2 the Canham-Helfrich bending free energy written in function of our order parameter ϕ, as done by Campelo and Hernández-Machado [24], leads to the following free energy

$$F[\phi] = \frac{\kappa}{2}\int_{\mathrm{V}} \Big(\big[-\phi + \phi^3 - \varepsilon^2\nabla^2\phi \big]^2 + \gamma_A \varepsilon^2 (\nabla\phi)^2 \Big) dV, \tag{8.2}$$

for a membrane of width ε. Again, as the dynamic equation will be written as a model B there is no need to use the Lagrange multiplier for volume conservation. The final dynamic equation for this chapter will be the same as the one obtained in Chapter 7

$$\frac{\partial\phi(\mathbf{x},t)}{\partial t} = M\Big(\nabla^2\Big(\frac{\delta F[\phi]}{\delta\phi}\Big) + \xi(\mathbf{x},t)(1-\phi^2)/\varepsilon^2\Big), \tag{8.3}$$

however in this case, the free energy $F[\phi]$ will forgo the Gaussian curvature term. Details on the noise $\xi(\mathbf{x},t)$ are mostly addressed in Chapter 7. There is a function added to shorten the result, which is $\Phi[\phi] = (-\phi + \phi^3 - \varepsilon^2\nabla^2\phi)$ as in previous chapters. The system following this equation will conserve its volume thanks to its diffusive formulation and the area by the Lagrange multiplier γ_A.

How we introduce this noise will be of great significance for the model, as we have to make sure it does not break neither of the system constraints while mimics a thermal behaviour. As in Chapter 6 noise term ξ will be a Gaussian white noise with mean zero and also has to be delta-correlated in space and time. From the Fluctuation Dissipation Theorem, and from Chapter 6 we obtain the relation between the noise variance and

the temperature via its auto-correlation. We rewrite the equation for convenience, which takes the form

$$\langle \xi(\mathbf{x},t)\xi(\mathbf{x}',t')\rangle = \frac{2k_BT}{\kappa}\delta(\mathbf{x}-\mathbf{x}')\delta(t-t'), \tag{8.4}$$

where k_B the Boltzmann constant and T the temperature of the system. Consequently, as the noise auto-correlation (8.4) is equal to the variance σ^2 for $\mathbf{x}=\mathbf{x}'$ and $t=t'$, obtaining the direct relation $\sigma^2 = 2k_BT/\kappa$. Therefore we can modulate the intensity of this noise via the standard deviation σ of the Gaussian distribution.

We have to keep in mind that is a noise for the position of the interface and the interface is defined by the points of space which take values $-1<\phi<1$. Thus the noise is only applied at the membrane points thanks to the term $(1-\phi^2)$ of equation (8.3). As stated in Chapter 6, in other phase field models the noise has been defined like a noise for the flux of a volume of fluid and therefore introducing the noise inside this divergence [139, 140]. However we are introducing a spatial non-conserved noise, which overall will balance itself out across the membrane but is not conservative by itself. The aim of this noise is to simply mimic a change in position on a membrane point due to temperature. Finally during the computation of the evolution the state of the system is printed every some tens of thousand of time-steps. Therefore the change generated by the noise at each time-step does not enter into the analysis of the evolution, just its accumulative effect over a moderate time length.

8.3 Power Spectrum

To understand the underlying mechanics of a fluctuating system, we can study its displacements in the Fourier space to study the fluctuation separated in wave-vectors. The power spectrum represents the weight that each wave vector q has when we decompose the membrane fluctuations in simple waves.

We work with the membrane displacement from its equilibrium position $h(x,t)$. Transforming this membrane displacement $h(x,t)$ to the Fourier space, results in $h(q,t)$ where q is a wave-vector or wave number of a fluctuation. Then the power spectrum will be computed by averaging over time t the product of membrane displacement $h(q)$ times its conjugate so

$$\langle h(q)h^*(q)\rangle_t = \langle h_q h_{-q}\rangle, \tag{8.5}$$

as in this case $h^*(q) = h(-q)$.

However, before starting to compute the power spectrum of the numerical results, lets see from the literature and by analytical means which spectra can one expect for a biological membrane. From literature we know that –in the limit of small fluctuations

and for a infinitely large membrane– is known to usually be

$$\langle |h_{\mathbf{q}}|^2 \rangle = \frac{k_{\mathrm{B}}T}{\kappa q^4 + \gamma q^2}, \tag{8.6}$$

as can be seen in Brochard and Lennon famous article on red blood cell flickering [145] although this expression can vary for more complex membranes [146]. So, knowing which is the final result let us see how one obtains this.

8.3.1 Prove of the Power Spectrum with the Oseen tensor

For this prove we use the relaxation rate $\omega_{\mathbf{q}}$, for a membrane displacement that behaves in the Fourier space as

$$h(q,t) = h_0 e^{-i\mathbf{q}\mathbf{x}+\omega_{\mathbf{q}}t}, \tag{8.7}$$

where a fluctuation with a mode q will decay with a time-scale following the relaxation rate $\omega_{\mathbf{q}}$. Thus the time-scale of the relaxation for a fluctuation will be $\tau_q = 1/\omega_{\mathbf{q}}$.

Starting off from the over-damped Langevin equation for the equation of motion of a membrane for the displacement h and transform it to Fourier space. The first half of the derivation follows Turlier and Betz work [142]. The starting Langevin equation

$$\dot{h}(\mathbf{x},t) = \int d^3\mathbf{x}' \Lambda(\mathbf{x}-\mathbf{x}') \Big[-\frac{\delta \mathcal{H}}{\delta h(\mathbf{x}',t)} + \xi(\mathbf{x}',t) \Big], \tag{8.8}$$

with thermal noise ξ and the Oseen tensor Λ and the functional derivative of the Hamiltonian $\mathcal{H}$ in the Monge representation. Doing the Fourier transform of this equation leads to

$$\dot{h}_{\mathbf{q}}(t) + \Lambda_{\mathbf{q}}(\kappa \mathbf{q}^4 + \gamma \mathbf{q}^2) h_{\mathbf{q}}(t) = \Lambda_{\mathbf{q}} \xi_{\mathbf{q}}(t). \tag{8.9}$$

Now the term multiplying $h_{\mathbf{q}}$ can be identified as the relaxation rate $\omega_{\mathbf{q}}$. For membrane coupled with the fluid by Navier-Stokes through the diagonal part of the Oseen tensor in the Fourier space $\Lambda_{\mathbf{q}} = 1/4\eta\mathbf{q}$ for a viscosity η. Therefore the relaxation rate is

$$\omega_{\mathbf{q}} = (\gamma \mathbf{q} + \kappa \mathbf{q}^3)/4\eta = \Lambda_{\mathbf{q}}(\gamma \mathbf{q}^2 + \kappa \mathbf{q}^4). \tag{8.10}$$

This is the relaxation rate obtained by Brochard and Lennon [145] and is also known as the Slow Mode. Introducing it to the Langevin equation

$$\dot{h}_{\mathbf{q}}(t) + \omega_{\mathbf{q}} h_{\mathbf{q}}(t) = \Lambda_{\mathbf{q}} \xi_{\mathbf{q}}(t). \tag{8.11}$$

Now transforming to frequencies by Fourier ends giving a displacement h in the frequency space as

$$h_q(\omega) = \frac{\Lambda_{\mathbf{q}} \xi(\omega)}{-i\omega + \omega_q}.$$

This last expression leads to the Power Spectrum or Power Spectral Density by

$$\langle |h_q(\omega)|^2 \rangle = \frac{\Lambda_{\mathbf{q}}^2 \langle |\xi(\omega)|^2 \rangle}{\omega^2 + \omega_q^2}, \tag{8.12}$$

getting the Spectrum of the frequency by integrating the modes or vice-versa. This is combined with the auto-correlation of a thermal noise obeying the Fluctuation Dissipation Theorem gives [142]

$$\langle \xi_{\mathbf{q}}(t) \xi_{\mathbf{q}'}(t') \rangle = 2k_B T \Lambda_{\mathbf{q}}^{-1} \delta(\mathbf{q} + \mathbf{q}') \delta(t - t'). \tag{8.13}$$

Combining all of the above we reach the modes Power Spectrum

$$\langle |h_q h_{-q}| \rangle = \int_{-\infty}^{\infty} d\omega \frac{\Lambda_{\mathbf{q}}^2 \langle |\xi(\omega)|^2 \rangle}{\omega^2 + \omega_{\mathbf{q}}^2} = \frac{2k_B T \Lambda_{\mathbf{q}}}{\omega_{\mathbf{q}}}, \tag{8.14}$$

that finally leads to the expression

$$\langle |h_q h_{-q}| \rangle = \frac{2k_B T}{\gamma \mathbf{q}^2 + \kappa \mathbf{q}^4}. \tag{8.15}$$

So following this procedure we obtain the same equation (8.6).

8.4 Parametrisation

To study the spectrum of the simulated membrane we have to define how do we obtain the membrane position. The easiest geometry to study will be circular cells. It will be easier to study this membranes as the parametrisation will be simpler, as it is much easier to define the radial position of each point in the membrane for a circle than a discoid. In addition, for a circle it will be also easier to define the distance between two points in the membrane than for any other shape.

The parametrisation chosen for a 2D circular membranes is represented in **Figure 8.4B**, where the position of the membrane is described by $r(t, \theta)$ where θ is the angle between the point position and the axis origin. For the case of a 3D discoidal membrane the same parametrisation will be used, however only the equator of the membrane will be obtained and analysed, similar to how it is done in flickering microscopy experiments [10].

The points θ_i and θ_{i+1} will be spaced by $\Delta\theta$. Even though the parameter used is an angle θ the angular distance $\Delta\theta$ will be proportional to a distance on the membrane d by $d \simeq \Delta\theta \cdot r$. Therefore the angle θ can be used as the coordinate for position as well as for distances on the membrane.

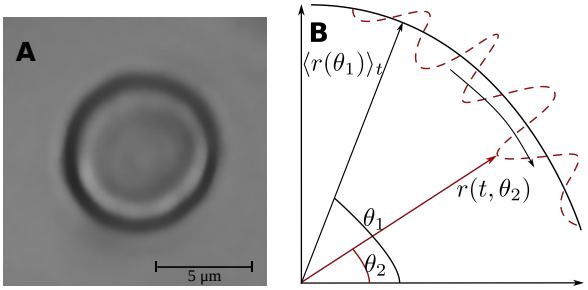

Figure 8.4: **A** Image obtained in a flickering microscopy experiment of a Red Blood Cell with a discoidal shape. **B** Sketch of the parameters used to describe the membrane shape for a circular symmetry cell.

With the position of the membrane defined, one can define then the displacements of the membrane h respect its average position as

$$h(\theta,t) = r(t,\theta) - \langle r(\theta)\rangle_t. \tag{8.16}$$

For this, the mean of the position r over the time $\langle r(\theta)\rangle_t = \frac{1}{\mathrm{T}}\sum_{i=0}^{\mathrm{T}-1} r(\theta,t_i)$ is used. With this displacement parameter, one can mimic the analysis of the experimental works so the comparison of the results is straightforward.

To obtain the position of the membrane and the evolution over time of such the data is interpolated to obtain the position of the point $\phi = 0$. As the interpolation is done on a well-behaved smooth field the interpolation should give a proper result in terms of accuracy. Similarly, in flickering microscopy experiments a video is obtained with the cell shape over time and the position of the interface, the membrane, is computed from the image.

8.4.1 Correlation and spectrum

To get an insight into the fluctuations properties it is necessary a range of mathematical tools to study these random displacements. Most of the information obtained of the membrane characteristics will be obtained by studying the spectral profiles of the membrane displacement h.

The Power Spectrum or Power Spectral Density of the modes q is computed as

$$\left\langle \left|h(q)\right|^2 \right\rangle = \sum_i \left|h(q,t_i)\right|^2, \tag{8.17}$$

where $h(q,t)$ is the Fourier Transform of the original computed $h(\theta,t)$ using a Fast Fourier Transform (FFT) algorithm. The Fourier transformation is be defined as

$$h(q,t) = \mathrm{FT}_\theta[h(\theta,t)] = \frac{1}{S}\int_S h(\theta,t)e^{-2\pi i q\theta}d\theta, \tag{8.18}$$

for a membrane of surface S. Where q is the fluctuation mode, defined from λ/λ_0 where λ is the wavelength of the fluctuation and λ_0 the lowest wavelength possible in a circular cell $1/2\pi\langle r\rangle$. Therefore q just takes integer values. This unit-less mode q can be easily related to a wavelength via $q/\langle r\rangle$ as the shapes studied have circular symmetry.

The correlation function can also be used to study the reach of the influence of a single fluctuation. The auto-correlation function –or simplified as correlation in this chapter– along a surface with S spatial points is defined as

$$\langle h(\theta',t)h(0,t)\rangle_\theta = \frac{\frac{1}{\mathrm{S}}\sum_{i=0}^{\mathrm{S}-1}\left(h(\theta_i,t)-\langle h(t)\rangle_\theta\right)\left(h(\theta_i+\theta',t)-\langle h(t)\rangle_\theta\right)}{\sigma_\theta^2(t)}, \tag{8.19}$$

which is normalised using the variance σ_θ^2 of the random variable h over the parameter θ. The variance is defined as ${\sigma^2}_\theta(t) = \frac{1}{\mathrm{S}}\sum_{i=1}^{\mathrm{S}}\left(h(\theta_i,t)-\langle h(t)\rangle_\theta\right)^2$.

Additionally the dependence of the correlation with the frequency can be studied by Fourier Transforming the correlation to $\langle h(\theta',\omega_j)h(0,\omega_j)\rangle_\theta$. This is done by applying a Fast Fourier Transform (FFT) to the data and results can be seen in the Numerical Results section. The frequencies $\omega_j = j/(\Delta t\,\mathrm{T})$ are defined as fractions of the total time elapsed $\Delta t\,\mathrm{T}$, and Δt is the constant time resolution between t_i and t_{i+1} where $t_i = i\Delta t$.

Moreover, the correlation can also be computed via the relation between Power Spectra and correlation established by the Wiener-Khinchin theorem

$$\langle h(\theta',t)h(0,t)\rangle = \mathrm{FT}_q^{-1}\left[\left\langle\left|h(q)\right|^2\right\rangle\right], \tag{8.20}$$

where FT^{-1} stands for the inverse Fourier Transform. This method is the usual way of obtaining the correlation and will be the method used in the results section, as it can be useful for correcting some fluctuating modes q that are related to noise.

8.4.2 Corrections and filters

As the nature of these simulations is noisy and stochastic, some some corrections to improve the clarity of the results will be used. In this subsection each correction will be explained, when has it been used and which criteria has been followed. A total of two different corrections have been used.

The first the erasing of the fluctuating modes $q = 0$ and $q = 1$ of the displacement h [32, 34]. The mode $q = 0$ is erased because is the mode related a change of the total area of the membrane, as we constrain changes in this parameter, the contributions to this wave-vector come only from small fluctuations around the initial value of total area. The mode $q = 1$ is erased because its the mode related to the movement of the centre of mass of the system, which is not a shape fluctuation. The variation of both the area and position value is very small during the simulation, with a standard

deviation an order of magnitude below the simulated spatial resolution. Even though, the spectrum of these modes is non-zero because of the constant variation at each time-step ends stacking up.

The second correction has been the use of a Low-pass Filter applied to the Power Spectrum aiming to erase the noise without altering its shape. The most important criteria is to never change the dependence of the Power Law exponent that characterises the Spectra. The filter for smoothing the low$-q$ regime has to be applied with the data in the Fourier space to avoid artificial results of the spectra as previously mentioned by Brandt *et al.* [147]. Therefore no filter is applied directly to the correlation. Results of the simulation analysis before any filter is applied can be seen in the Numerical Results section.

8.4.3 Equatorial loss in a 3D membrane

For experiments on 3D membranes it is impossible to obtain the position of all the surface points of a cell or vesicle. Usually one finds that has to study either a single point, a curve –like the equator–, or a patch of the membrane. This, can be proven to change the power spectrum by a q^{-1} factor, and is what will be called here the equatorial loss.

Through flickering microscopy experiments one can see how the dependence obtained of the power law exponent gives q^{-3} [33, 148] instead of q^{-4} as in the theoretical expression equation (8.6). This effect arises from the fact that these kind of experiments just analyse the equator of the cell, which ends up being just a single line on the surface of the membrane. This single line does not have to behave the same exact way as the whole membrane, which has more restrictions like volume and area conservation. It can be proven this drop of a q^{-1} factor, starting from a mode $\mathbf{q}$ that belongs to a 2-Dimensional space and which square modulus is $\mathbf{q}^2 = q^2 = q_x^2 + q_y^2$. By integrating one of the two components, in this case q_y as

$$\langle |h(q_x, y=0)|^2 \rangle = \int_0^\infty dq_y \langle |h_\mathbf{q}|^2 \rangle = \int_0^\infty dq_y \frac{k_\mathrm{B}T}{\gamma(q_x^2+q_y^2) + \kappa(q_x^2+q_y^2)^2}. \tag{8.21}$$

For simplicity lets consider two cases: **a)** in which the membrane is tension-less $\gamma = 0$ and the second one, **b)**, in which the bending modulus is zero $\kappa = 0$.

a) Tensionless membrane $\gamma = 0$, purely bending

By removing the surface tension one reaches

$$\langle \left|h(q_x, y=0)\right|^2 \rangle_{\sigma=0} = \int_0^\infty dq_y \frac{k_\mathrm{B}T}{\kappa(q_x^2+q_y^2)^2} = \frac{k_\mathrm{B}T}{\kappa} \int_0^\infty dq_y (q_x^2+q_y^2)^{-2}, \tag{8.22}$$

which has a solution

$$\frac{k_B T}{\kappa}\int_0^\infty dq_y (q_x^2+q_y^2)^{-2} = \frac{k_B T}{\kappa}\Big[\frac{q_y}{2q_x^2(q_x^2+q_y^2)} + \frac{1}{2q_x^3}\arctan(\frac{q_y^2}{q_x^2})\Big]_0^\infty$$

$$\langle\big|h(q_x, y=0)\big|^2\rangle|_{\sigma=0} = \frac{k_B T}{2\kappa q_x^3}\frac{\pi}{2}. \tag{8.23}$$

This is the result for a case where if we look a the Power Spectrum for a normal membrane, if we take into account a single line on the 2D surface we lose a q_x^{-1} contribution.

b) Purely surface tension case $\kappa = 0$

Similarly starting with

$$\langle\big|h(q_x, y=0)\big|^2\rangle_{\kappa=0} = \int_0^\infty dq_y \frac{k_B T}{\gamma(q_x^2+q_y^2)} = \frac{k_B T}{\gamma}\int_0^\infty dq_y (q_x^2+q_y^2)^{-1} \tag{8.24}$$

which has a result

$$\frac{k_B T}{\gamma}\int_0^\infty dq_y (q_x^2+q_y^2)^{-1} = \frac{k_B T}{\gamma}\Big[\frac{1}{q_x}\text{arctg}(\frac{q_y}{q_x})\Big]_0^\infty$$

which results in an arc-tangent which has a value zero at $q_y = 0$ and for $q_y = \infty$ gives $\pi/2$

$$\langle\big|h(q_x, y=0)\big|^2\rangle_{\kappa=0} = \frac{k_B T}{\gamma q_x}\frac{\pi}{2}. \tag{8.25}$$

This way is proven that the loss of a q_x^{-1} contribution does not only happen for a bending membrane, but also for a surface tension case. Therefore this is a global result of taking into account a single line on the 2D surface. One also has to take into account that the equator line does not require either to conserve area nor volume as its the whole surface which has this constraints. Therefore a single line on such surface, the equator included, is effectively non-conservative.

8.5 Numerical Results

The results of the numerical integration and the computed temporal evolution can be observed in **Figure 8.5A** for a 2D simulation for starting conditions of a circular cell and in **Figure 8.5B** for a 3D simulation of a discocyte shaped cell. The results resemble the data from flickering microscopy experiments [10, 32, 33, 34, 148], as can be observed by comparing **Figure 8.5A** and **Figure 8.4A**.

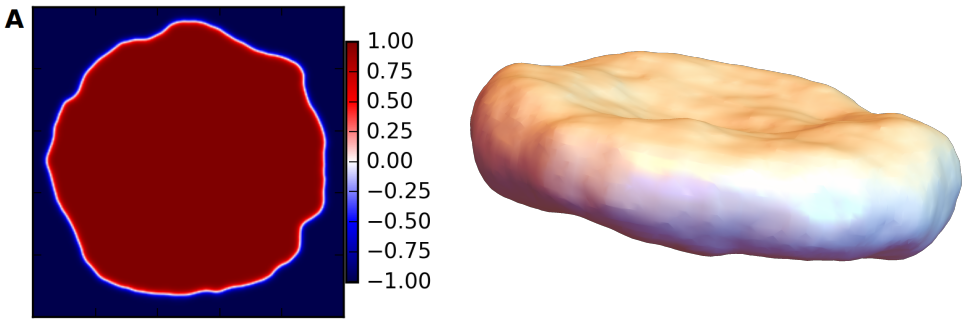

Figure 8.5: A Snapshot of a 2D simulation of a circular membrane with thermal noise in a lattice of 250×250 points. Colorbar corresponds to the value of the the phase field order parameter ϕ. **B** Snapshot of a 3D simulation of a discoidal membrane within a lattice of $90 \times 90 \times 45$ points.

8.5.1 2D Results

From the displacement of the interface h over time one can obtain the results from **Figure 8.6** where equations (8.17) and (8.20) averaged over time are represented for a 2D circular cell. The Power Spectrum of **Figure 8.6A** presents two different behaviours when using log-log scale. The power spectrum consists of a plateau in the small-q regime, followed by a small peak at the maximum mode q and then falls as a straight line which will be called high-q regime. The small-q regime is not influenced by a surface tension term as this is a tension-less simulation. Therefore this region develops a plateau either because of finite-size effects or because of not having a long enough simulation.

The high-q regime is characterised by a straight line, which in the in a log-log representation implies a Power-Law behaviour q^{β}, where β is the slope of the straight line in log-log representation. By fitting the Power Spectrum in this high-q regime to obtain the exponent β. The obtained dependence is q^{-5} with an exponent $\beta = -5.0 \pm 0.1$. The obtained spectra for all the different simulations are good enough with just one simulation worth of data to fit the exponent of the high-q regime. Being able to fit the results and obtaining a good and clear dependence is very relevant as many experimental works simply draw a straight line alongside the results as data is not good enough to obtain a good fit.

The dependence obtained is different to the one in equation (8.6). This happens due to the non-local behaviour of the phase field methodology, which gives the q^{-5} fluctuation spectra. This has been seen in previous works on phase field membranes when studying relaxation of a deformed membrane [59]. Using the same method of membrane studying relaxation it has been shown that when coupled with Navier-Stokes the spectrum changes to a dependence q^{-4} like in Brochard and Lennon [145].

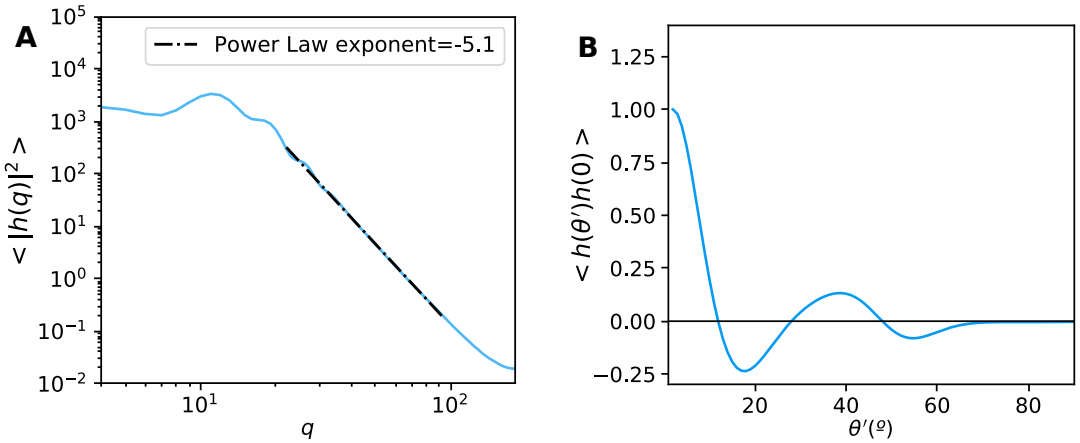

Figure 8.6: **A** Power Spectrum of a 2D simulation of a circular membrane after using a Low-pass filter. The discontinuous line is the fitted Power-Law. **B** The correlation obtained using the Wiener-Khinchin theorem from the spectrum.

Therefore we know from the literature that our resulting power spectrum would change from q^{-5} to q^{-4} like in equation (8.6) by introducing an hydrodynamic coupling to the membrane [59].

The correlation in **Figure 8.6B** is computed by the use of the Wiener Khinchin theorem to be able to profit from the filter applied to the Power Spectrum as explained before. From **Figure 8.6B** one can see how the influence of a fluctuation is transmitted along the surface of the membrane. After the initial fluctuation, an anti-correlated region appears, probably due to the pull by the local area and volume conservation. This peak and valley is repeated until the fluctuation dies out with enough distance. These results come from a single simulation with a given set of parameters, but its traits and characteristics are replicated in various simulations using similar parameters.

8.5.2 Results before filtering

Before obtaining the final results shown previously in this section, one applies the two corrections already mentioned in Section 8.4.2. Here some results before applying the corrections and filters will be shown. Using the raw data for the membrane position over time one can directly proceed to compute the correlation and the spectrum obtaining the results in **Figure 8.7**.

Looking at **Figure 8.7** the presence of a noise can be seen in the Power Spectrum at the low-q plateau. This is thought to be result of the finite-system effects plus the randomness of the events. This noise leaks to the correlation giving a result of a correlation that fluctuates around zero for longer distances. To obtain the final results a Low-pass filter will be used to erase such noise in the spectra. The filtering of this noise

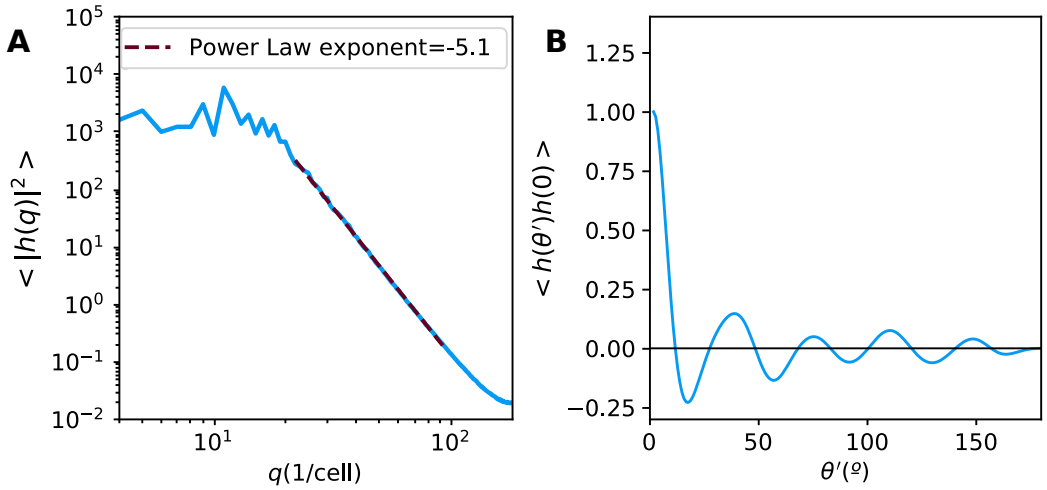

Figure 8.7: **A** Normalised Correlation and Power Spectrum of a simulation without the low-pass filter. The discontinuous line of the spectrum curve is the fitted Power Law. **B** The correlation obtained from the spectrum.

in the spectra and the removal of the modes $q = 0, 1$ will change completely the final correlation.

8.5.3 Dependence on frequency

One can compute the power spectrum and correlation as a function of the frequency ω instead of time t. To do this one would simply do the time Fourier Transform of the spectrum $\langle |h(q,t)|^2 \rangle$ or of the displacements $h(q,t)$. The results can be seen in **Figure 8.8**, where even if we applied the previously mentioned filters, noise is still apparent in the results. This is so because in the end we lack the average over time that we were doing up until now to be able to plot the different frequencies ω.

The Power Spectrum plateau of the low-q regime has a dependence with frequency as can be seen in Figure 8.8**A**. This could mean that system-size effects could have a dependence on frequency. Also, the Power-Law exponent its not exactly -5 for all the frequencies neither does give a -4 dependence. This dependence is hard to study as with the plateau advancing, in some cases comprising almost all of the spectrum. So with the increasing frequency the proportion of Power-Law-like behaviour shortens, and the harder it is to get a good fit for a power-law.

Moreover at high q when one reaches the order of $q = 100$ the resolution effects of the lattice start to kick in making the study of the Power-Law with the frequency more difficult. The resolution problems appear much sooner when decomposed in frequencies in comparison to for example **Figure 8.7**. As expected when integrating over all the frequencies to obtain the Power Spectrum just in function of the wave-vector we recover the previous result from **Figure 8.7**.

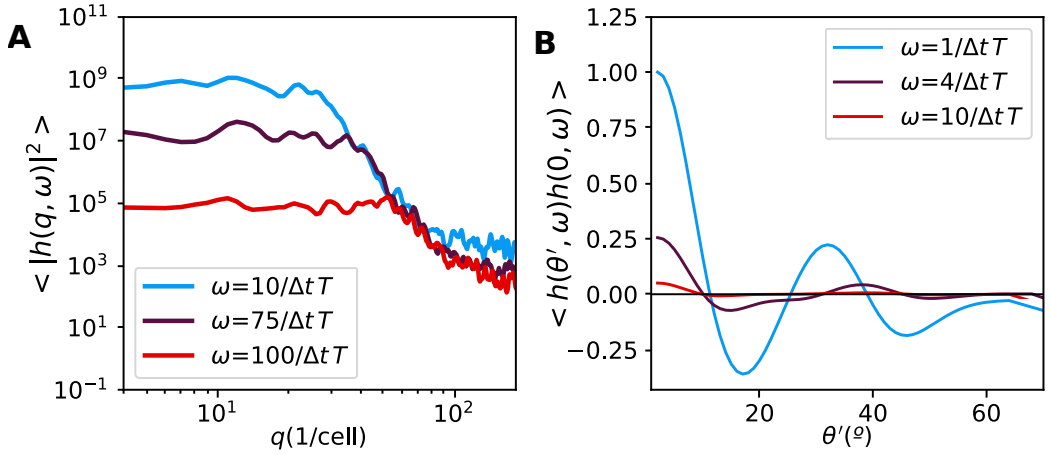

Figure 8.8: **A** Spectrum of the modes q for different frequencies ω with a Low-pass filter applied, parameter T is the total number of time-steps of the simulation, in this case $T = 10^8$. **B** The normalised distance correlation in function of ω obtained from the spectrum.

The distance correlation represented in function of a frequency ω can be seen in **Figure 8.8B**. The frequency dependence of the correlation and obtained results that qualitatively resemble the ones from Brochard and Lennon and Park *et al.*. The shape of the curve is maintained although there is a drop in the correlation value with increasing frequency ω.

8.5.4 3D Results

As already shown in **Figure 8.5** this model can be used to simulate membranes and cells in three dimensions and we can choose any shape, whether discoid or spheroid like in **Figure 8.9**.

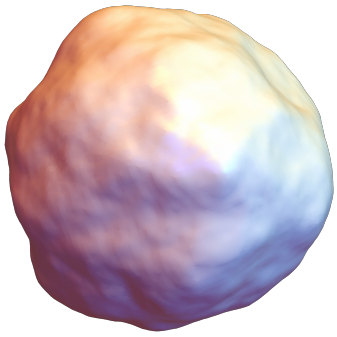

Figure 8.9: Snapshot of a 3D simulation of a spheroid in a $90 \times 90 \times 90$ lattice.

In the case of spheres the parametrisation used are spherical coordinates. Still the studied variable was the angle θ as has more resemblance with the other data studied

and behaves similarly. However the spherical angle $\phi \subset [0, \pi]$ has a weirder behaviour as it has no periodic boundaries.

In the case of studying the equator fluctuations of the 3D discocyte-shaped membrane, as in RBCs experiment of flickering microscopy, we obtain the results in **Figure 8.10**. As with the 2D results the Figure represents Equation (8.17) and equation (8.20). The results of the analysis for a Spheroidal cell in **Figure 8.10** are similar to the ones of the discocyte-shaped cell. These results are obtained for the displacement h of the equatorial plane of the spheroid. Therefore what we are doing here is computing the Spectrum of a single line along the membrane.

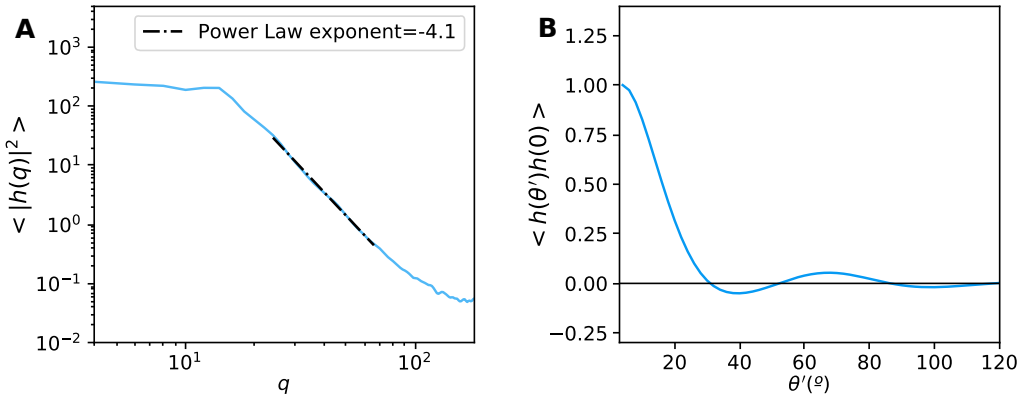

Figure 8.10: **A** Power Spectrum of a 3D simulation of a circular membrane after using a Low-pass filter. The discontinuous line is the fitted Power-Law and the obtained exponent value. **B** The correlation obtained using the Wiener-Khinchin theorem to the filtered spectrum.

The Power Spectrum in **Figure 8.10A** has the most relevant changes in comparison with the 2D simulation results. While one could expect that the system should fall with a power-law exponent q^{-5} as the 2D simulation the 3D case falls as q^{-4}. However, this is not due to recovering the behaviour of equation (8.6) but due to another effect. Then, as the membrane behaves like the previous 2D simulations, we expect that by introducing an hydrodynamic coupling to the membrane, our resulting power spectrum would change from q^{-5} to q^{-4} [59].

The change in the spectrum is related to what we have called the equatorial loss and derived it in Section 8.4.3. This is done by integrating over one component of the modes $\mathbf{q}^2 = q_x^2 + q_y^2$ and looking at the remaining component. The change of a q^{-1} contribution when studying the equator of a 3D membrane is an effect that also happens in experimental results of flickering microscopy [33, 148]. In experiments the dependence obtained of the power law exponent gives q^{-3} [33, 148] instead of the expected dependence q^{-4} predicted from the equipartition theorem [145]. Meanwhile

the correlation in **Figure 8.10B** is similar as the 2D case but for a simulation with a lower noise intensity. The high statistical variability seem to make the anti-correlation less intense.

8.6 Phase Field model Power Spectrum

For small interface width ε we have that the order parameter ϕ is proportional to its chemical potential which in turn due to Gibbs-Duhem equation is proportional to the pressure p. Therefore, we can change from the phase field parameter ϕ to the pressure p and make an asymptotic expansion to obtain the macroscopic equations of the system [149]. With this equations we obtain the relaxation rate ω_q [59] and use it to obtain the Power Spectra.

We have a membrane which is subjected to a thermal noise ξ, whose fluctuations relax following the macroscopic equations of the pressure p around the membrane and its velocity v

$$\nabla^2 p = 0 \tag{8.26a}$$

$$\Delta p = 2\gamma H - 4\kappa H(H^2 - K) - 2\kappa\nabla_S^2 H \tag{8.26b}$$

$$v = -\frac{M}{2}(\nabla p^+ + \nabla p^-). \tag{8.26c}$$

Where the equation for Δp derived by Zhong-Can and Helfrich [150], which presents a surface tension γ, and ∇_S^2 is the Laplacian on the membrane surface. We will also be taking the ansatz that for a single mode of deformation will decay in an exponential way with the following profile

$$h = h_0 e^{i\mathbf{q}\mathbf{x} - \omega_\mathbf{q} t} \tag{8.27a}$$

$$p = p_0 + A e^{i\mathbf{q}\mathbf{x} + kz - \omega_\mathbf{q} t}. \tag{8.27b}$$

This profiles are for a system where the direction z is the normal direction to the membrane and the wave-vector k defines how the pressure falls along the bulk in this normal direction and $\mathbf{x}$ is the plane along the membrane and $\mathbf{q}$ its wave-vector. With the two previous sets of equations we can solve ω_q.

From equation (8.26c) and equation (8.27a). The velocity can be written as $v = \dot{h}$ where h is the membrane displacement from equilibrium, this plus the profile for the pressure from Eq. 8.27b ends up giving

$$\omega_q h_0 = \frac{M}{2} A 2k e^{kz}. \tag{8.28}$$

This last equation gives the relation between the relaxation rate and the pressure profile in the normal direction to the membrane. Therefore the next step is studying the

relation between the normal and tangential pressure profiles With the pressure profile p we can obtain its Laplacian

$$\nabla^2 p = A\exp\left[i\mathbf{q}\mathbf{x} + kz - \omega_q t\right](-q^2 + k^2)$$

which when set equal to zero gives

$$-q^2 + k^2 = 0 \tag{8.29}$$

for $\mathbf{q}^2 = q^2$. For the last macroscopic equation, Δp, we use the small scale deformations approximation, giving a curvature $H \simeq -\delta_x^2 h = q^2 h$ therefore

$$\Delta p = A\exp[i\mathbf{q}\mathbf{x} + kz - \omega_\mathbf{q} t] \simeq 2\gamma q^2 h + 2\kappa_c q^4 h - 4\kappa_c q^6 h^3.$$

Supposing that at low curvatures the lower contribution order is much larger that the following one we can reduce the curvature contribution to just the first one.

$$Ae^{kz} = 2h_0(\gamma q^2 + \kappa_c q^4) \tag{8.30}$$

Finally we just solve for ω_q using the last 3 equations, giving the relaxation rate

$$\omega_q = 2M\,|\mathbf{q}|(\gamma\mathbf{q}^2 + \kappa\mathbf{q}^4) = 2M\,(\gamma q^3 + \kappa q^5)\,. \tag{8.31}$$

This relaxation rate, different than Brochard and Lennon Slow mode [145], will be one of the factors changing the final result of the Power Spectrum. The difference between both relaxation rates is due to the Navier-Stokes coupling. Now that we have this relaxation rate for a non-local Helfrich fluctuation we have to obtain its spectra.

Now following one of the previous methods to obtain the power spectrum we shall obtain the new power spectrum, starting from the Langevin equation of an over-damped membrane. Without the Navier-Stokes coupling the equation is

$$\dot{h}_\mathbf{q}(t) + \omega_q h_\mathbf{q}(t) = \xi_\mathbf{q}(t),$$

where $\dot{h}$ is the temporal derivative of the displacement h. We now Fourier transform this equation to frequency and solve for $h_\mathbf{q}(\omega)$ and obtain the Fluctuation Spectrum as function of the frequency ω and the mode q

$$h_\mathbf{q}(\omega) = \frac{1}{(-i\omega + \omega_q)}\xi_\mathbf{q}(\omega),$$

$$\langle |h_\mathbf{q}(\omega)|^2 \rangle = \langle h_\mathbf{q}(\omega) h_{-\mathbf{q}}(\omega) \rangle = \frac{\langle \xi_\mathbf{q}(\omega)\xi_{-\mathbf{q}}(\omega)\rangle}{\omega^2 + \omega_q^2}.$$

For this we need the noise spectrum $\langle \xi_{\mathbf{q}}(\omega)\xi_{-\mathbf{q}}(\omega)\rangle$ that we will obtain with the noise correlation in time and space from Fluctuation Dissipation Theorem in Fourier space

$$\langle \xi_{\mathbf{q}}(t)\xi_{\mathbf{q}'}(t')\rangle = 2k_B TM\delta(\mathbf{q}+\mathbf{q}')\delta(t-t'). \tag{8.32}$$

Combined with the previous obtained relaxation rate the modes power spectrum is

$$\langle |h_{\mathbf{q}}|^2\rangle = \langle |h_{\mathbf{q}}h_{-\mathbf{q}}|\rangle = \int_{-\infty}^{\infty} d\omega \langle |h_{\mathbf{q}}(\omega)|^2\rangle,$$

which after integrating gives,

$$\langle |h_{\mathbf{q}}|^2\rangle = \frac{k_B T}{\gamma q^3 + \kappa q^5}. \tag{8.33}$$

The noise spectrum $\langle \xi_{\mathbf{q}}(\omega)\xi_{-\mathbf{q}}(\omega)\rangle$ and the relaxation rate ω_q will be different depending on the coupling of the Navier-Stokes equations, that is the reason the spectrums in equation (8.6) and equation (8.33) are different.

8.7 Conclusions

At first sight, the additive white noise to the order parameter of the phase field seems to mimic the thermal fluctuations present at a membrane. We obtain a q^{-5} fluctuation spectra due to the non-local behaviour of the phase field methodology. This has been seen in previous works on phase field membranes when studying relaxation of a deformed membrane [59] and in the same work is shown that when coupled with Navier-Stokes the spectrum changes to a dependence q^{-4} like in Brochard and Lennon [145]. Therefore we know from the literature that our resulting power spectrum would change from q^{-5} to q^{-4} by introducing hydrodynamic coupling to the membrane [59]. However, adding the hydrodynamic coupling is not trivial using a membrane phase field with a coherent and thermal noise.

This begs the question, if the main difference is the hydrodynamic coupling, are there membranes that somewhat are uncoupled from the fluid? It is not necessary to be either coupled or completely uncoupled, but maybe porous membranes or other membranes that are somewhat uncoupled to the hydrodynamics could have a behaviour between q^{-5} to q^{-4}.

There is a methodology to analyse and study the fluctuating interface computed with the phase field model like they do in flickering microscopy. Some behaviour observed in experimental data is reproduced by the simulations, like what has been referred here as the "equatorial loss".

Part IV

Conclusions

Chapter 9

Conclusions and the future

9.1 Conclusions

This thesis was driven to study the dynamics of membranes and the interplay between the membrane mechanical properties with external perturbations. The goal is to further our understanding on the influence of the membrane mechanical properties during different phenomena both by analytical and numerical means. This is done in hopes that this better understanding could be applied for real-life applications either for membranes characterisation or clinical diagnosis.

To this end we have studied membranes by expanding on previous membrane phase field models. We will be starting by studying membranes inside a fluid flow and with this purpose we will be solving the Navier-Stokes equation. We develop a new methodology more simple to implement and to understand by using the stream function and the vorticity. With this stream function formulation we can also use new ways to characterise the hydrodynamic interaction between cell and fluid. New shapes like the "anti-parachute" have been obtained using our model. We also study a non-inertial lift that occurs for red blood cell shaped membranes in a Couette flow.

Then we implement the Gaussian curvature to the free energy of the membrane, which is necessary to study topological transitions. Topological transitions in membranes are of great importance in biology, and with our model have been able to reproduce the fission of a membrane tube in presence of a spontaneous curvature. Then we move to study how temperature can promote topological transitions by introducing a thermal noise. There are some geometries that without this thermal noise do not undergo topological transitions. This effect has been studied and we have found a phase transition between a topologically constant state and a state that undergoes fission. We then focus on the study of the membrane fluctuations without topological transitions.

All our results revolve around membranes in non-equilibrium conditions and the stationary state under those conditions. Thorough the thesis we have studied the in-

terplay between the membrane and external influences, like the temperature or a fluid flow.

9.1.1 Part II - Stream Function Membrane Phase field Models

Chapter 3: Stream function formulation

A membrane interacting with the fluid is a sensible goal, as membranes are immersed in fluid. However, most models to compute a membrane inside a fluid are highly complex to implement. Thus, to avoid some complications of solving the Navier-Stokes equations we have used the vorticity ω and the stream function ξ. With this we can solve easily a 2D system of a membrane and a fluid interacting with each other. An additional benefit of this method will be fulfilling the incompressibility condition regardless of the accuracy of the solving method; also physical scales are explicit in the model. The implementation of this model in 2D results in the integration of two Poisson equations; one for the stream function ξ and other for the vorticity ω. This model results in the final system of equations seen in equation (3.16). With these three equations we will compute all the results of membranes in flows.

Both hydrodynamic variables ω and ξ have been found to give insight to the fluid and membrane interactions and influence one on the other. And there is no loss for using them, as the pressure and velocity can be computed within this framework. With this vorticity and stream function we propose $\mathcal{W} = \int(\omega - \omega_0)^2 dV$ in equation (3.24) and $\mathcal{X} = \int(\xi - \xi_0)^2 dV$ in equation (3.25) as two scalar parameters that are useful for the study of the stability of the membrane and its convergence to a stationary state.

A very important advantage of the model is its adaptability. Any kind of flow that has an analytical expression for its velocity (even if it changes over time) can be simulated. Although commonly thought not possible, one can expand this model to three dimensions by using a vector potential stream function $\vec{\xi}$ with a bit of work on the Boundary Conditions. We show how this model can be expanded and adapted to

- Inertial flows (see Section 3.4.1)

- Time-dependent flows, like oscillating flows (see Section 3.4.2)

- Expanded to three dimensions (see Section 3.4.3)

The expansions to inertial flow and the 3D case we have to update the system of equations to solve, while time-dependent flow only relies on changing the Boundary Conditions. As the new systems of equations are similar to each other with a bit of work all these expansions can be combined with each other if needed.

The main points of the model are

- A model for membranes inside a low Reynolds flow has been developed. Using the stream function ξ and the vorticity ω one can solve the membrane-flow system using a set of three equations (3.25).
- The system of equations (3.25) is easy to implement, consisting of a dynamic equation for the phase field plus two Poisson equations to solve the stream function ξ and the vorticity ω.
- The formulation makes changing the different mechanical parameters of the membrane and flow very easy. Moreover, the incompressibility condition is ensured to be fulfilled regardless of the solving method accuracy.
- With $\mathcal{W} = \int(\omega - \omega_0)^2 dV$ and $\mathcal{X} = \int(\xi - \xi_0)^2 dV$ one can study numerically how the system reaches the stationary state.
- The proposed model is very easy to expand in a variety of ways. The system of equations for inertial flow is derived and shown. Time-dependentd flows can also be studied using this methodology.
- The system can be adapted to 3D by generalising the stream function into a vector potential.

Chapter 4: Membranes in a Poiseuille flow

In Chapter 4 we provide proof of the validity of the newly introduced mathematical formulation for two-dimensional deformable cells flowing in a channel. There are some well-known shapes that red blood cells (RBC) take inside a confined micro-channel that have been studied thoroughly in the literature: the parachute, the slipper, and the discoid shapes. This shapes have been the first to be replicated to prove the validity of the model by simulating RBC-shaped inside a micro-channel slightly bigger than the cells itself. All the mentioned shapes –the parachute, slipper, and discoid shapes– are reproduced with our model for high-velocity to low-velocity regimes.

Aside of the cell shape morphology we study the cells by exploiting the hydrodynamic parameters that we introduced to solve the fluid flow, the stream function ξ and the vorticity ω. By studying the deviations of these parameters with respect a channel with an ideal Poiseuille flow (without any obstacle inside) one can study the flow deformation, the cell deformation, and its stationary position. One of the most important results is the ability to study the convergence and stability of a cell shape and position by studying the squared integral of the deviations for the stream function and vorticity $\mathcal{W}$ and $\mathcal{X}$ presented in equations (3.24) and (3.25) respectively. These two parameters change while the cell is still not in its stationary position or the membrane is still

deforming to its stationary shape. We study this behaviour in the evolution form the starting initial conditions up to parachute and slipper shapes.

After ensuring the veracity of the results the same model and methodology have been applied to study two different confinement levels: the super-confinement of a channel smaller than the cell inside and the very low confinement of a channel around ten times the size of the cell.

For the very wide channels a novel meta-stable shape has been obtained: the *anti-parachute*. This shape requires the cell to start at the centre of the channel, although there is no need for a perfect centering. This shape is only obtained because for a very wide channel (in comparison to the size of the cell) the Poiseuille flow has a big enough region at the centre of the channel with an approximately constant velocity. Under specific conditions this shape is maintained forever, however this shape is lost after a time for simulations where the channel is medium-sized or the velocity is too high. All this points to the anti-parachute shape being a meta-stable shape.

The anti-parachute shape should be able to be obtained experimentally, although it requires a very centred cell and a very ideal flow, so it might be very hard to achieve.

There is also the parameter known as viscosity contrast, which measures the ratio between viscosity of the cell internal liquid divided by the viscosity of the surrounding liquid. To further prove the validity of the model previous results for 2D cell simulations where the cell tumbles for high viscosity contrasts [80, 82] is also replicated using these wide channels.

Finally, cells in a super-confined channel have been studied, where the channel was smaller than the cell size. In this case, the shapes obtained are quite different to parachutes and slippers, and agree with previous experiments [91] and simulations [93]. For these range of confinements, the resulting shape is very sensitive to changes in reduced volume and confinement.

To summarise, for cells in a Poiseuille flow

- Reproduce known experimental and numerical results, including parachute and slipper shapes, to prove the validity of the stream function formulation.
- Show that the parameters $\mathcal{X}$ and $\mathcal{W}$ can be used to study the convergence of a membrane cell to its stationary state.
- A novel meta-stable cell called anti-parachute is obtained, which we predict that could be reproduced in experiments (although with difficulty).

- Show tumbling for high viscosity contrasts (where the viscosity of the cell internal liquid is greater than the viscosity of the surrounding liquid)

- Super-confined cells, where the channel is much smaller than the cell inside them, are studied and the shapes resemble previous experimental and numerical works.

Chapter 5: Membranes in a Couette flow

Having a moving wall in an otherwise still fluid generates what is called a Couette flow. This flow can be induced for example by moving a cylinder inside a recipient with fluid and cells, as for example in a blood rheometry. Thus studying what happens in this type of flow has real life relevance.

The previously presented stream function membrane phase field model is shown to simulate properly a Couette type of flow. A channel with a Couette flow will be characterised by two parameters: *i)* the velocity of the moving wall v_{wall} *ii)* the rate at which the velocity increases when approaching the wall (the gradient). This last term will be the velocity gradient, which is non-zero only in the perpendicular direction to the flow and, for a Couette flow, has a value of $\partial v_x/\partial y = v_{wall}/H$.

At first sight it seems that the cells in a Couette flow simply align in a very specific way, which looks dependant on the flow characteristics. However if one looks closely and for long enough, it can be seen that the cells display a net movement perpendicular to the flow, this is called lateral migration. This displacement does not lasts forever, as cells in a Couette flow display an stationary position (or distance) with respect to the walls. The final stationary position depends on both the reduced volume of the cell and the viscosity contrast. In fact, for high viscosity contrasts one finds that the cell will go up towards the top moving wall, and only stop its perpendicular displacement by collision with the wall itself.

Moreover, the viscosity contrast also induces sometimes a tumbling regime to the cell, although it happens with less frequency than for Poiseuille flows. The reason might be the fact that tumbling in Poiseuille flows the rate of change in the flow velocity along the channel is parabolic. This change is faster and more sudden when moving perpendicular to the the channel. Due the velocity profile of a Couette flow being linear its gradient is constant and takes a value of $\partial v_x/\partial y = v_{wall}/H$. This constant gradient along all the points of the cell seems to be more stable against tumbling than the parabolic velocity profile of a Poiseuille flow.

To summarise, for cells in a Couette flow

- Stationary shapes can be characterised by both the velocity of the moving wall v_{wall} and the velocity gradient $\partial v_x/\partial y = v_{wall}/H$.

- Cells display a stationary position respect to the wall, to which the cell will move perpendicularly to the flow until reaching it. This is also known as lateral migration and the stationary position depends on both the reduced volume of the cell and the viscosity contrast.
- The lateral migration comes from a non-inertial lift. The results reproduce previous theoretical [95] and numerical results [99].
- May display tumbling, however with less frequency than Poiseuille flows.

9.1.2 Part III - Helfrich models

Topological transitions in membranes are of great importance in biology and by addition of a Gaussian curvature term in the energy we can study both fission and fusion. As fusion of cells is a more complex mechanism, we started with membrane fission. The most common fission event is vesicle formation, which will be the biological process that we will take for reference.

Chapter 6: Fission purely by the Gaussian curvature term

By addition of the Gaussian term to the bending energy a three-dimensional membrane phase field model with the ability to properly study topological transitions is presented. This is done by expanding on already existing membrane phase-field models [24, 50, 56, 58, 59, 119, 120, 131], which has been used to study a variety of systems based on the Helfrich theory for cellular membranes [22]. More specifically, in this chapter fission of membrane tubes is studied.

When one has a membrane tube with an intrinsic spontaneous curvature a process known as pearling happens. The pearling instability consists on a membrane tube that becomes an array of spherical beads attached together by very small tethers, visually similar to a pearl-necklace. Pearling instability has been already studied in simulations [57, 126, 127] and experiments [128, 129] here we started by reproducing this pearling instability.

The results reported here show how the inclusion of the Gaussian curvature term leads to the fission of the pearls from the tube. We study the area and volume variation, as we have this membrane attached to a reservoir so it can either give or suck volume and membrane if necessary. The energetics of the process is also studied. We see how the Gaussian term increases between fission events, and when the fission happens it falls. This increase in energy is driven then through the curvature energy term, which decreases enough as to drive this increase in the Gaussian energy. Fission is reported to start at the spherical tip of the tube and travel downwards. This happens because the spherical tip of the tube is working as a catalyst for the pearling, and thus as the first pearl is produced at the tip this in turn helps forming the second pearl next to the first

one and so on. Thus, we prove that fission and vesicle formation can be studied using this methodology.

Additionally, we have obtained the dispersion relation that can be used to obtain the preferred size of the vesicles given a spontaneous curvature. Both the size of the final vesicles and the size predicted by the dispersion relation match. With increasing spontaneous curvature one obtains smaller vesicles, as the relation between curvature and radii is inverse like $C_0 = 1/R_0$.

With all this, we study the phase diagram and the dynamics of vesiculation in function of the bending modulus κ and the Gaussian (or saddle-splay) modulus κ_G. The Gaussian modulus is measured as a negative parameter in experiments and therefore we start there. For negative Gaussian modulus, the results depend on whether the Gaussian modulus is big enough in comparison to the bending modulus. For a big Gaussian modulus the membrane undergoes fission splitting in a number of vesicles that will depend on the length of the tube and the spontaneous curvature. However, if the Gaussian modulus is too small compared to the bending modulus no topological transition will occur, even if we are computing the Gaussian energy term in the simulation.

For a positive Gaussian modulus the membrane also undergoes topological topological transition, but it is not the fission of the tube into several vesicles. In this case due to the Gauss-Bonnet theorem and the Euler characteristic the Gaussian energy term favours the creation of membrane handles and passages. This leaves us with what we call multiple self-connected membrane.

With all this, we predict that a positive Gaussian modulus could be a way to model what happens in the Golgi apparatus where membrane fenestration creates handles and holes at some areas of the organelle. In the case of the cell not finding a mechanism to reverse the energy modulus sign then one can say with certainty that the Golgi apparatus has to go against the Gaussian curvature. The only way to do this would be by working against the Gaussian energy term with the use of molecular motors or other active mechanisms. This is the only way, with a negative Gaussian bending modulus κ_G, to create the characteristic handles and holes. In any case, the study of the membrane fission dynamics it is crucial to be able to identify the mechanisms that drive the topological transformations in the Golgi apparatus and membranes in general.

To summarise, in this chapter on membrane fission

- Expanded the membrane free energy by adding the Gaussian curvature term one can study topological transitions.
- Fission of a membrane tube into multiple vesicles is studied. To this end we take advantage of the pearling instability, which coupled with a high enough Gaussian modulus κ_G produces multiple vesicles.

- The Gaussian energy is found to increase until the fission event where it falls. The increase in energy is driven through the bending energy due to the spontaneous curvature which decreases more than what the Gaussian term increases.
- A dispersion relation is obtained, which we can use to compute the size of the formed vesicles depending on the spontaneous curvature applied.
- We reproduce Helfrich prediction for a shape diagram in function of the bending modulus κ and Gaussian modulus κ_G. This diagram displays three regimes: *i)* a multiple self-connected membrane for positive κ_G *ii)* no fission for negative κ_G that is relatively lower than κ *iii)* fission of the tube for big and negative κ_G.
- We propose that the mechanisms that regulate the Golgi apparatus shape could be trying to change the value of κ_G to obtained the desired shape at different regions of the organelle.

Chapter 7: Fission promoted by thermal noise

There are some geometries that are harder to deform than others. A flat infinite membrane for example is one, as even with a high spontaneous curvature the membrane does not deform and stays in the meta-stable flat state. It is limiting to only study fission of geometries that aid the vesiculation process.

Thus, here we study the vesiculation of a flat membrane by introducing a thermal noise to the membrane. This thermal noise is used to promote vesiculation, as if we introduce big enough fluctuations the system is able to start the vesiculation process. In the end the thermal energy related to this noise by K_BT is helping the system overcome an energy barrier and achieve a lower energy state.

For vesicles with a positive Gaussian modulus κ_G there is no intensity of noise (or temperature) that can make the system vesiculate. This does not change even when increasing the spontaneous curvature, which makes even more energetically favourable to have spherical vesicles of radius $R_0 = 1/C_0$. We also do not observe the membrane to use this thermal fluctuations to create handles or passages to become what we have called a multiple self-connected membrane like we see in Chapter 6. One would expect with this level of noise to maybe go through topological transitions by increasing the number of holes. The increase in the number of holes would decrease the Euler characteristic and therefore the Gaussian contribution. This might be point to the plane membrane being a geometry where its more difficult to obtain multiple self-connected membranes than for vesicle formation.

A phase diagram for a couple of different spontaneous curvatures are obtained as function of the temperature T and the ratio of the bending and Gaussian modulus κ_G/κ. This is done to show how the spontaneous curvature, the temperature and the ratio κ_G/κ facilitate or hinders vesiculation. The temperature shows to module if

vesiculation will be able to happen or not for a given ratio κ_G/κ. The results clearly show how higher spontaneous curvatures help the vesiculation process by lowering the energy barrier to overcome, however also changing the final size of the produced vesicles.

We have studied the energetics of fission and one can see how the Gaussian term decreases during vesiculation, as well as the curvature term at the start. Moreover we have discovered how the derivative of the free energy squared is useful in predicting both the temperature and whether vesiculation will happen or not. This is so because this term is a very straight line that is proportional to the temperature and only deviates from this plateau if vesicle formation will happen.

To summarise,

- Temperature is shown to promote fission and vesicle formation for a geometry that difficulties fission.
- Phase diagrams for a different values of spontaneous curvature are obtained.
- The phase diagrams show how for higher spontaneous curvature the energy barrier to start fission lowers. This is reflected in vesiculation happening at lower temperatures.
- A positive value of the Gaussian modulus should lead to the creation of handles or passages in the membrane. Therefore we expected this to be the case for a high enough temperature. However, a modulus $\kappa_G > 0$ simply prohibits any kind of topological transition for several orders of magnitude of the temperature.
- The energetics of fission show a clear decrease on the Gaussian term that at the start is driven by the curvature term. Moreover the derivative of the free energy squared is shown to reflect the temperature very well as well as whether vesiculation is possible or not.

Chapter 8: Flickering

At first sight, the additive white noise to the order parameter of the phase field seems to mimic the thermal fluctuations present at a membrane. We obtain a q^{-5} fluctuation spectra due to the non-local behaviour of the phase field methodology. This has been seen in previous works on phase field membranes when studying relaxation of a deformed membrane [59] and in the same work is shown that when coupled with Navier-Stokes the spectrum changes to a dependence q^{-4} like in Brochard and Lennon [145]. Therefore we know from the literature that our resulting power spectrum would change from q^{-5} to q^{-4} by introducing hydrodynamic coupling to the membrane [59].

However, adding the hydrodynamic coupling is not trivial using a stochastic phase field model with a thermal noise.

This begs the question, if the main difference is the hydrodynamic coupling, are there membranes that somewhat are uncoupled from the fluid? It is not necessary to be either coupled or completely uncoupled, but maybe porous membranes or other membranes that are somewhat uncoupled to the hydrodynamics could have a behaviour between q^{-5} to q^{-4}.

Nonetheless, there is a methodology to analyse and study the fluctuating interface computed with the phase field model like they do in flickering microscopy. Some behaviour observed in experimental data is reproduced by the simulations, like what has been referred here as the "equatorial loss". This equatorial loss happens when analysing the behaviour of a membrane by only studying the displacement of a single line of the whole 3D membrane, one finds that the obtained spectrum loses a q^{-1} contribution. This we have reproduced in 3D and in 2D by only analysing part of the membrane, instead of the complete displacements information of the whole system.

To summarise,

- An additive white noise to the phase field order parameter mimic thermal fluctuations for a non-local system uncoupled from hydrodynamics.
- The fluctuation spectra obtained has a power law dependence of q^{-5}. This is due to the non-local behaviour of the phase field methodology and had already been observed in relaxation of membranes using phase field models [59].
- This is known to change to q^{-4} by introducing hydrodynamic coupling to the membrane [59]. However, this is not trivial using a membrane phase field with a thermal noise.
- If the only difference is the hydrodynamic coupling, this spectra should help explain cases of biological membranes partially or completely uncoupled from the fluid.

9.2 Future perspectives

9.2.1 Part II - Stream function phase field models

The presented framework allows for the study of novel setups such as oscillating flows, channels with a varying cross-section, or extremely-confined flows and will be the base for future works. Expansion to add the inertia to the hydrodynamics, expansion to 3D, or the addition of external fields will be possible under this methodology.

Time-dependent flow

Studying the cell response to changes in a flow has biological relevance, as for example in a circulatory system the flow is not stationary. In this case in fact, the flow is more akin to an oscillating flow. Oscillating flows have been tested using our model and work properly, but more research on the influence of the oscillating flow on the membrane has to be done.

Moreover, time-dependent flows are not only of interest because they appear in nature, but they could be exploited to study the mechanical properties of cells or for clinical diagnose. Using micro-fluidic devices that put cells (for example red blood cells) under non-stationary flows and study the response could be a huge tool for a mechanical characterisation of single cell membranes. Therefore using simulations would be of great importance to study and understand how the response change depending on the mechanical parameters will be of great importance.

Inertial flow and visco-elasticity

Working on inertial flows, even high Reynolds flows, is possible and should be studied. To this end, as we explained in Chapter 3, we will be solving the complete Navier-Stokes equation of an incompressible fluid instead of the Stokes equation. The theory is already developed and the only thing left is the numerical implementation.

High Reynolds regimes could be studied and there are multiple biological instances where this might be interesting. Vesicles encompass a big range of sizes, some Giant Unilamellar Vesicles reach sizes of 200μm, roughly 30 times the size of a red blood cell. When working in those sizes the low Reynolds regime might be an over-simplification, and an inertial flow will ensure a proper hydro-dynamical behaviour. Other examples are red blood cells in arteries, where the flow is completely different to a micro-capillar as it behaves like a high Reynolds flow.

Other uses for this models could be the study of viscoelasticity. This equation with inertial flows could be used combined with an oscillating flow to study the viscoelasticity of cells.

Generalization to 3D

Expanding to 3D is possible, as we have already started working on it very recently but found success. This area is the future, as new research on membranes is primarily done in 3D nowadays. This does not mean that 2D is obsolete, as still doing a 2D model to understand the phenomenology and help planning the research before jumping to 3D can save a lot of time as 3D computation is still very time consuming.

With the 3D model implemented we should use the same characterisation methods that we learned in 2D and study what differences the change in the model dimensionality generates.

9.2.2 Part III - Helfrich models

One of the topics that require more study on membranes is topological transitions as several researchers agree [30]. The presented model is a good base to go in that direction.

Fission in other geometries

Studying fission in different geometries found in nature could enlighten us by showing is some geometries are taken to promote or inhibit spontaneous fission. Moreover, studying shapes where we know that fission happens, like geometries found in the Golgi apparatus could help understanding this organelle better.

Following the results of fission promoted on a plane membrane by thermal fluctuations, one could study how very low thermal fluctuations how much the temperature can improved the process in geometries that are good for fission. Other geometries that are better for vesicle formation than a plane membrane but still not good at promoting fission could also be studied.

Finally, in this thesis we have worked with constant spontaneous curvatures, however studying membranes where the spontaneous curvature is heterogeneous should be the next step. This heterogeneous curvature could mimic curvature-inducing proteins that diffuse along the membrane, or even interact with each other by repulsion or attraction. All the previously done work, and all the future perspectives proposed could be studied with heterogeneous spontaneous curvature and see how it changes the results.

Fusion

Fusion is less straightforward than fission, as biologically is usually a complex phenomenon that require multiple specialised proteins. However, while this microscopic mechanisms cannot be studied with a phase field methodology, the overall effects of a fusion event can be studied. So, one could study how the fusion of a vesicle to a big or small target membrane affects the overall energetics of the final membrane.

Influence of the Gaussian term in topologically invariant dynamics

The fact that for positive Gaussian modulus κ_G we do not find budding even for very high temperatures is intriguing. Even if fission is not topologically favourable the budding still is, as there is an spontaneous curvature. However, for positive Gaussian modulus we do not see budding for any temperature. This seems to show that the Gaussian energy term could alter topologically invariant dynamics. This could be studied with our model by repeating previous research on topologically invariant systems but with the addition of this Gaussian curvature term.

Flickering

Coupling this fluctuating membrane to the hydrodynamics of the liquid is the next more logical step. We expect this to align the results with the fluctuating spectra seen in the literature.

Then, fluctuations in the presence of spontaneous curvature could be studied. Not only an homogeneous constant spontaneous curvature but one that is heterogeneous in space, either forming clusters or lines along the membrane or any geometry that can be imagined. This could change the spectrum of the fluctuations or give an auto-correlation that is heterogeneous along the different regions of spontaneous curvature in the membrane.

One could study the active behaviour of membranes by adding heterogeneous spontaneous curvature that changes over time as if curvature-inducing proteins are firing and relaxing over time. Seeing how this changes the final fluctuating spectra could be used to identify what is happening in real active membranes of cells like the red blood cell.

Chapter 10

Resum en català

10.1 Introducció

10.1.1 La membrana cel·lular

La membrana cel·lular és present a totes les cèl·lules i inclús en alguns virus. Aquest element és el que diferència la cèl·lula de la resta del món i, a part de fer de barrera, té moltíssimes funcions biològiques. Aquesta tesi tindrà l'objectiu de descriure la membrana cel·lular des del punt de vista físic per intentar entendre més bé alguns processos biològics.

Aquesta membrana està formada per un tipus de lípids anomenats amphiphilics, d'entre ells normalment estan compostes per phospholipids. Aquest tipus de lípids tenen una estructura polar: una punta de la molècula és hidrofílica i l'altre punta és hidrofòbica. Aquesta estructura fa que aquests lípids amphiphilics s'autoorganitzin en diferents formats, com es pot veure a la **Figura 10.1** on els lípids depenent de la forma que tenen s'organitzen en micel·les o en bicapes lipídiques.

La membrana està formada per aquests lípids amphiphilics organitzats com a una bicapa lipídica. En la membrana aquests lípids a més a més poden moure's els uns entre els altres formant una espècie de superfície 2D fluida, ja que els lípids flueixen els uns entre els altres sense abandonar la membrana. Normalment, les membranes també inclouen proteïnes que també poden fluir per la membrana, semblant a l'esquema de la **Figura 10.2**. Aquestes proteïnes poden canviar les propietats de la membrana, o donar-li diferents funcions noves. Moltes membranes tenen vàries proteïnes que es fan servir per distingir-se les unes a les altres, o per agafar/tirar ions amb el seu entorn.

Hi ha diversos sistemes on la forma de la membrana és crucial per al funcionament biològic, com els glòbuls vermells o l'aparell de Golgi.

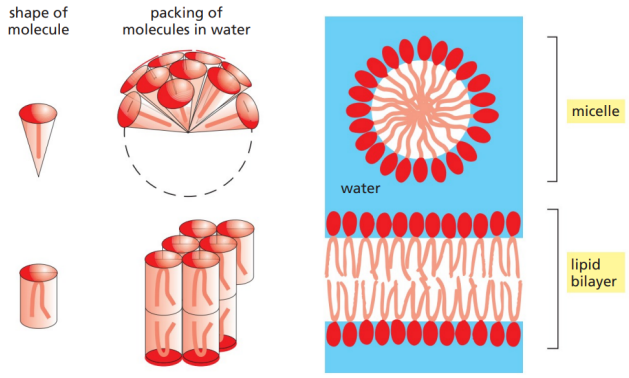

Figure 10.1: Diferents lípids s'organitzen en diferents geometries. Imatge obtinguda de l'Alberts [4].

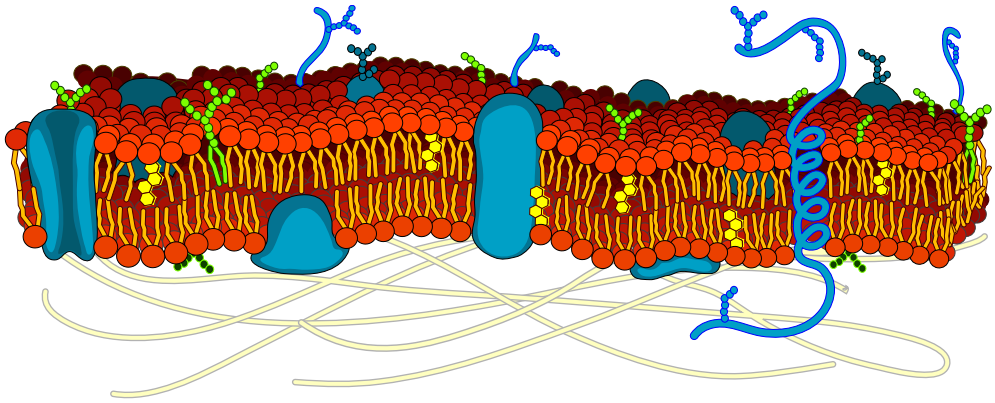

Figure 10.2: Diagrama d'una membrana cel·lular, en vermell veiem els lípids amphiphilics. Mentre en blau veiem exemples de proteïnes que formen part de la membrana. Image by LadyofHats, Public domain, obtained via Wikimedia Commons.

10.1.2 Glòbuls vermells

Hi ha cèl·lules en les quals la membrana és especialment important, com els glòbuls vermells de la sang. Aquestes cèl·lules són les responsables de distribuir l'oxigen per l'organisme i tenen una forma molt particular, com es pot observar a la **Figura 10.3**. En aquest cas la cèl·lula té una estructura interna molt senzilla, i les propietats mecàniques de la cèl·lula depenen únicament dels paràmetres físics de la membrana.

És per això que aquesta cèl·lula tindrà un interès particular quan un estudia membranes cel·lulars. Donat que un canvi en les propietats físiques de la membrana canvia molt com es comporta un glòbul vermell, incloent la forma que agafa.

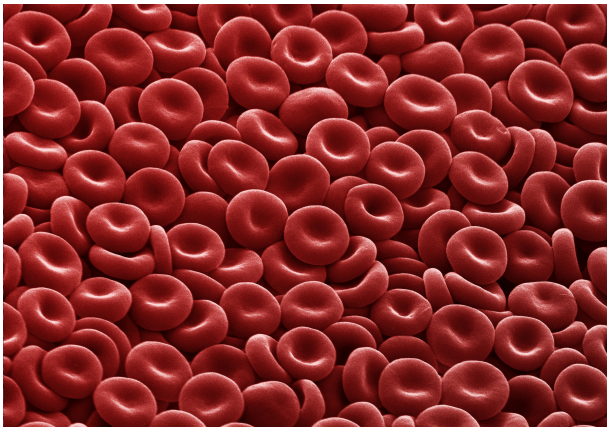

Figure 10.3: Glòbuls vermells amb la seva caràcteristica forma de discoide. Annie Cavanagh, CC BY-SA 4.0, via Wikimedia Commons

10.1.3 Energia de curvatura

La membrana és coneguda per tenir una energia proporcional a la seva curvatura punt a punt. Podem definir un punt d'una superfície mitjançant els radis de curvatura. Aquests radis de curvatura són els de dos cercles que descriuen la forma que agafa la superfície en el punt en el qual aquests dos cercles intersecciones, representats a la **Figura 10.4**. La curvatura d'un punt es pot descriure utilitzant dos radis de curvatura de la següent

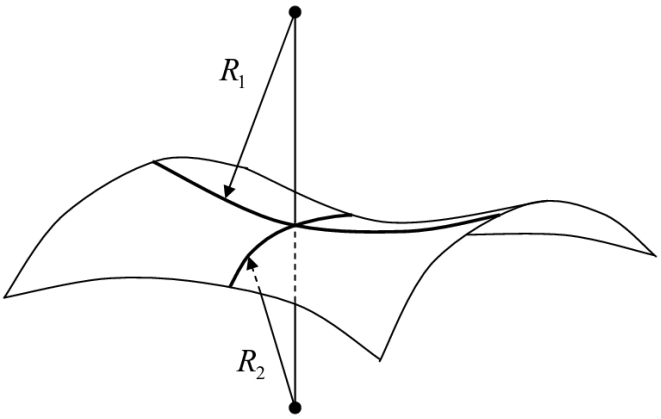

Figure 10.4: Diagrama dels radis de curvatura que caracteritzen un punt en una superfície.

manera,

$$C = \frac{1}{R_1} + \frac{1}{R_2}. \tag{10.1}$$

D'aquesta equació es pot veure que com més gran siguin aquests radis de curvatura menys corbat estarà la membrana en aquell punt, i viceversa. També hi haurà una segona espècie de curvatura que definirà un punt de la membrana: la curvatura Gaussiana. Aquesta curvatura té l'expressió

$$K = \frac{1}{R_1}\frac{1}{R_2}. \tag{10.2}$$

Usant aquestes dues expressions, de la literatura [22] sabem que una membrana té una energia associada

$$F = \int \left(\kappa C^2 + \kappa_G K\right) dS. \tag{10.3}$$

Aquesta energia és proporcional al quadrat de la curvatura i linealment amb la curvatura Gaussiana. La rigidesa de la membrana està definida per la constant κ també anomenada mòdul de curvatura. Aquesta constant ens descriu com de fàcil o difícil serà corbar la membrana. Per a valors molt alts de κ necessitarem fer més força per a corbar la membrana.

El terme de la curvatura Gaussiana a l'energia, segons el teorema de Gauss-Bonnet, és el que se li diu una constant topològica. Hem de tenir en compte llavors, que si no hi han transicions topològiques no hi ha necessitat de calcular la contribució de la curvatura Gaussiana K, ja que serà constant. La membrana sofrirà una transició topològica només en el cas que aquesta sigui tallada o foradada, i si es manté sencera la seva topologia no canviarà.

10.1.4 Model de phase field

El model de "phase field" (o camp de fases) és una tècnica que es fa servir habitualment per a poder resoldre numèricament l'evolució de sistemes amb o varies superfícies que es mouen al llarg del temps. En aquest cas la superfície serà la membrana, i aquesta metodologia ja s'ha fet servir anteriorment per descriure membranes cel·lulars [24, 50, 52] i l'utilitzarem com a base pels nostres models.

L'energia en el cas del phase field l'escriurem en funció d'un paràmetre d'ordre anomenat ϕ. En el nostre cas, aquest paràmetre tindrà un valor entre -1 i +1: en els punts de l'espai que valgui $\phi = -1$ formaran part del líquid extracel·lular i els punt que es compleixi $\phi = +1$ formaran part del líquid interior de la cèl·lula. Llavors, tots els punts de l'espai amb un valor entre -1 i +1 són els que formaran la membrana cel·lular. Amb aquest parametre d'ordre podem reescriure l'energia de la membrana i resoldre l'evolució al llarg del temps d'una membrana cel·lular [62].

Per exemple podem veure simulacions de membranes amb forma de glòbuls vermells en 2 i en 3 dimensions a la **Figura 10.5**. En aquestes simulacions 2D el que estem simulant és un "tall" de la cèl·lula, com si hagués sigut laminada per una màquina de tallar embotit. En aquest cas estem suposant que aquest tall es comportarà d'igual que la cèl·lula sencera.

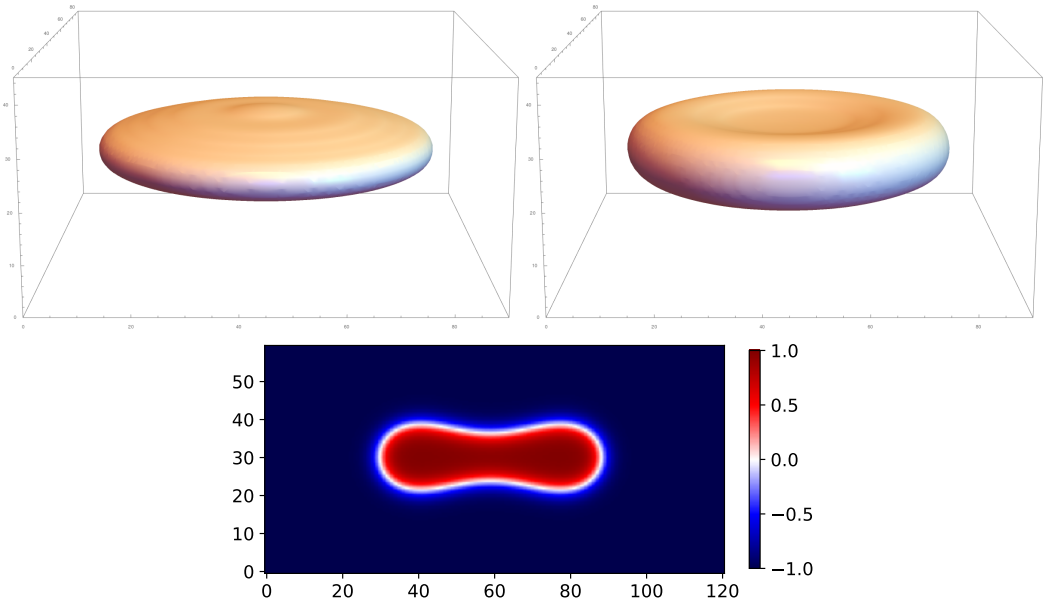

Figure 10.5: Adalt: Membranes simulades en 3D, comença sent un disc (esquerra) però evoluciona a la forma coneguda del glòbul vermell (dreta). **Avall:** Membrana amb forma de discoide en una simulació 2D. Aquesta forma és igual a agafar un glòbul en 3D i tallar-lo per la meitat. El color ens informa del valor del paràmetre d'ordre ϕ on vermell vol dir cèl·lula, blau vol dir líquid extern i en blanc tenim la membrana.

Llavors farem servir aquests models com a base per afegir-li interaccions amb el món exterior i explicar fenòmens i dinàmiques que succeeixen a les membranes i les cèl·lules.

10.2 Membranes dins d'un fluid en moviment

A la literatura un pot trobar molts treballs en els que s'estudia la forma de membranes dins d'un fluid en moviment. Per exemple, a la **Figura 10.6** tenim imatges d'un experiment per G Tomaiuolo i S Guido a ón introdueixen glòbuls vermells dins de microcanals i estudien com es deformen a diferents velocitats del fluid. Aquests micro-canals fan la feina d'una canonada per on corre aigua i s'obtenen unes formes conegudes com a "parachutes" (**Figura 10.6 a** i **b**) i "slippers" (**Figura 10.6 c**).

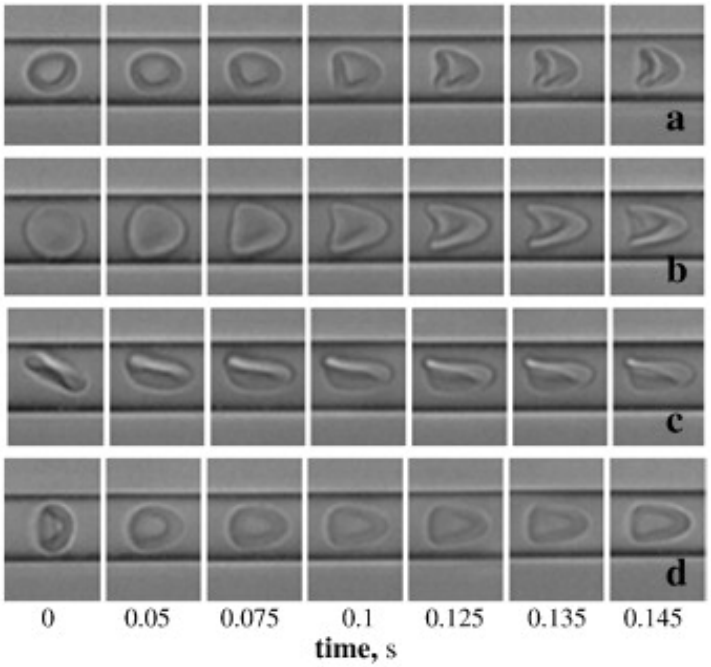

Figure 10.6: Varis glòbuls vermells movent-se a través d'un micro-canal a causa del moviment del fluid. Figure adapted from G Tomaiuolo and S Guido [9].

Membranes dins d'un fluid en moviment ja han sigut estudiades prèviament [59], però normalment els mètodes que fan servir per calcular el moviment del fluid són complexes d'implementar i de treballar-hi amb ells. Nosaltres hem desenvolupat un model nou on el mètode per calcular el moviment del fluid i la influència que li suposa la presència de la membrana és més senzill. Això ho hem fet mitjançant la funció corrent ξ i la vorticitat ω.

Els detalls matemàtics estaran al text principal de la tesi, però hem de saber que utilitzant aquestes dues variables el sistema és més fàcil de resoldre. A més, aquests paràmetres funció corrent ξ i vorticitat ω ens ensenyen una cara de la hidrodinàmica que normalment no s'estudia en simulacions de membranes cel·lulars.

10.2.1 Flux de Poiseuille

L'anomenat flux de Poiseuille és el flux que s'obté a dins d'una canonada quan hi ha una diferència de pressió del fluid entre l'entrada i la sortida. En aquest cas, com es pot observar a la **Figura 10.7** el fluid té una velocitat màxima al centre de la canonada, mentre que degut al fregament la velocitat decreix a mesura que ens apropem a les parets.

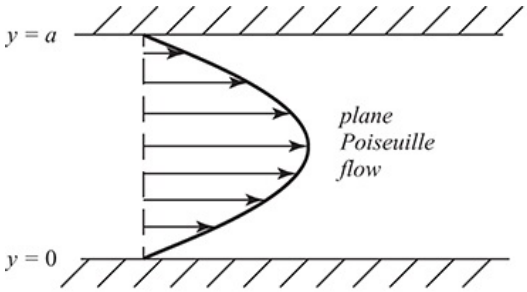

Figure 10.7: Perfil de la velocitat del fluid per a un flux de Poiseuille.

Començarem estudiant aquest tipus de flux en funció de la mida de la canonada (o canal). Direm que com més estreta és aquesta canonada més confinada està la cèl·lula. Aquest confinament tindrà un efecte molt important en com es comportarà la cèl·lula dins d'aquest fluid en moviment.

10.2.1.1 Poiseuille Confinament mitjà

Definim com a confinament mitjà quan el nostre canal té unes mesures una mica superiors a la mida de la cèl·lula. Aquest cas és el que coincideix amb les condicions experimentals de la **Figura 10.6** i sobretot el farem servir per a comprovar que el nostre model funciona correctament.

Per un canal i una cèl·lula de mida fixada hem simulat vàries velocitats del fluid com es pot observar a la **Figura 10.8**. En aquestes imatges, igual que en els experiments ensenyats anteriorment, les cèl·lules s'estàn desplaçant d'esquerra cap a la dreta. Aquí reproduïm uns resultats que encaixen amb els experimentals. Per a velocitats molt baixes del fluid la cèl·lula es mou molt lentament i quasi no es deforma romanent en forma de dicoide (**Figura 10.8A**). A mesura que pugem la velocitat v del fluid passem al règim de forma slipper (**Figura 10.8B** i **C**) i per les velocitats més altes obtenim la forma de parachute (**Figura 10.8D**). Replicar aquests resultats de la literatura confirma que el model funciona correctament.

A la **Figura 10.9** podem observar alguns paràmetres hidrodinàmics que podem calcular mitjançant el nostre model. Amb els nostres paràmetres podem calcular diversos paràmetres hidrodinàmics com la pressió i el tensor de estrès de cisalla σ_{xy}.

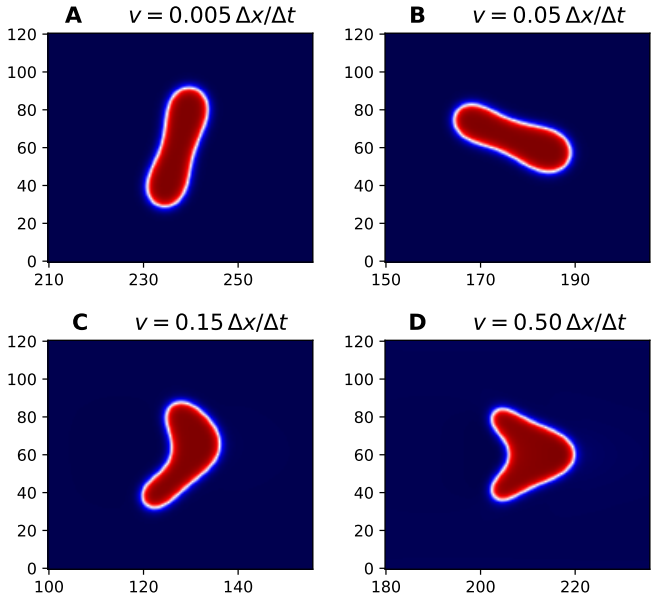

Figure 10.8: Diferents morfologies cel·lulars en canals de confinament mig. **A-D**: Diferents velocitats pujant de $v = 0.05$ a $v = 0.50$.

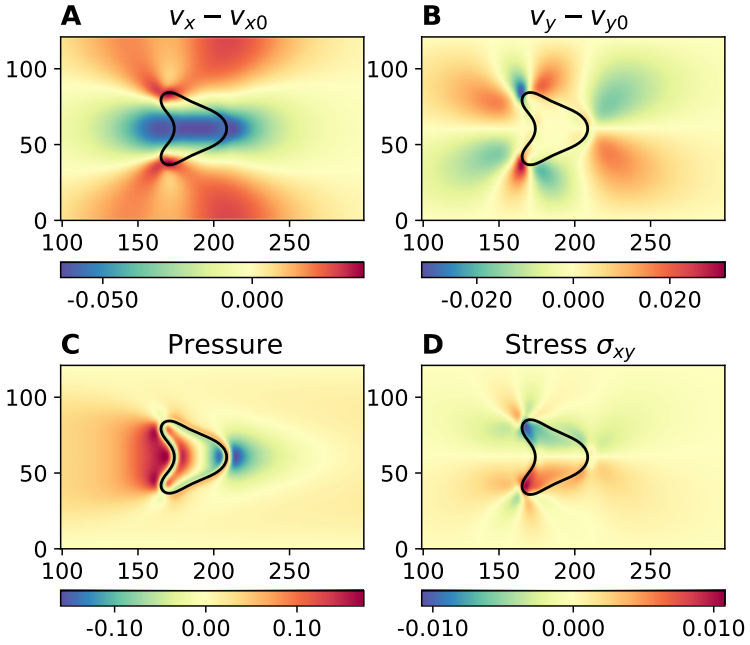

Figure 10.9: (A-B) Influència cel·lular a la velocitat del fluid a les figures $v_x - v_{x0}$ i $v_y - v_{y0}$ i (C) a la pressió del fluid. (D) Estrès de cisalla.

En aquesta **Figura 10.9** podem veure també l'influència de la cèl·lula a la velocitat del fluid a les figures $v_x - v_{x0}$ i $v_y - v_{y0}$. Aquestes gràfiques comparen la velocitat que tindria el fluid sense la presència de la cèl·lula amb la velocitat de la simulació. El que estan ensenyant aquests resultats és que la presència de la cèl·lula frena el fluid al centre del canal, part del qual circula al voltant de la cèl·lula per poder-la esquivar.

10.2.1.2 Poiseuille Confinament baix: anti-parachute

Els resultats previs han servit per assegurar que el nostre model funciona, però ara treballarem amb el que passa quan tenim un canal molt més ample que la cèl·lula, d'entre 5 i 10 vegades la mida de la cèl·lula d'ample.

En aquest cas hem descobert una forma nova, que hem anomenat "anti-parachute". Aquest nom prové del fet que en aquest cas la cèl·lula agafa una forma semblant al parachute que hem vist abans, però es doblega en la direcció oposada a un parachute com veiem a la **Figura 10.10 A**. En aquest figura les cèl·lules també estan desplaçant-se d'esquerra cap a la dreta igual que en les simulacions anteriors.

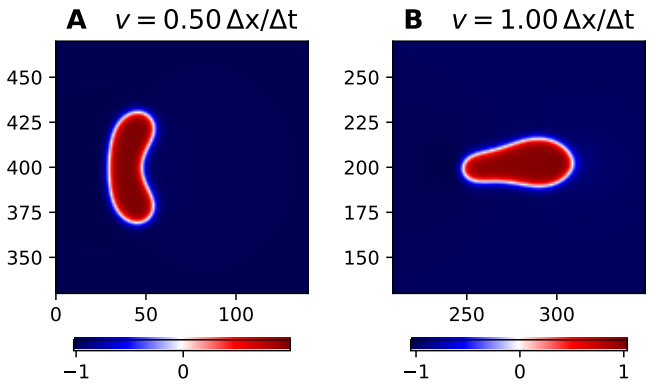

Figure 10.10: Dues simulacions d'una cèl·lula en cànals amples. **(A)** Manté la forma de anti-parachute perquè el canal és més ample i va més lentament que (B).

Aquesta forma d'anti-parachute l'obtenim només per a canals força amples quan la cèl·lula comença aproximadament al centre del canal. A més, aquesta forma és per al llarg del temps per a canals que no siguin prou amples o per velocitats molt elevades i esdevé una cèl·lula amb la forma de la **Figura 10.10 B**. Tot això apunta al fet que aquesta forma sembla ser el que s'anomena meta-estable, és a dir no és completament estable i si se la increpa suficient canviarà a una forma més estable.

Llavors perquè està agafant aquesta forma la cèl·lula? Pel que hem pogut observar, la principal diferència entre canals molt amples i canals estrets es que quan la cèl·lula està a un canal estret sent com a prop de la paret la velocitat és molt menys elevada que al centre. En canvi, en un canal ample, la cèl·lula es troba, en l'espai que ocupa la cèl·lula amb el seu mida reduïda en comparació, una velocitat que és aproximadament

constant al centre del canal. Això és el que canviarà la forma final de la cèl·lula, la qual sentirà com aquest liquid amb velocitat aproximadament constant a la regió on s'hi troba l'està aixafant en la direcció que flueix. Això està representat esquemàticament a la **Figura 10.11** on veiem que la membrana amb forma anti-parachute és lleugerament més "aerodinàmica" que una cèl·lula plana.

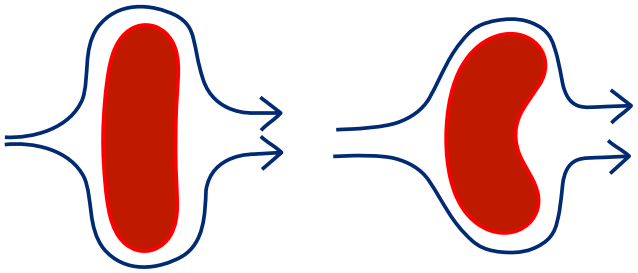

Figure 10.11: Esquema de la deformació que pateix un anti-parachute.

També observem en aquests canals més amples que, en casos que el líquid de l'interior de la cèl·lula sigui molt més viscós que el líquid extern (el que anomenem contrast de viscositats sigui elevat), la cèl·lula es mourà una mica caòticament pel canal fent tombarelles. Això està representat a la **Figura 10.12**, on veiem les formes que agafa una cèl·lula a mesura que es mou a través del canal.

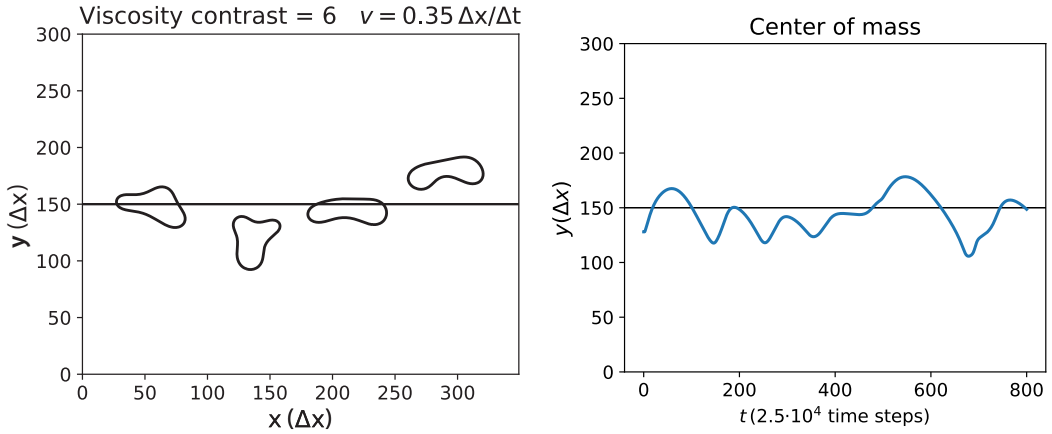

Figure 10.12: La simulació mesura en l'espai 301×350 i la cèl·lula que mesura 60.

Durant aquest fenomen de tombarelles la cèl·lula es desplaça d'un costat del canal a l'altre, com es veu a la **Figura 10.12** del centre de masses on representem la posició vertical del centre de la cèl·lula al llarg del temps.

10.2.1.3 Poiseuille Súper-confinades

A més de fer el canal més gran, també el podem fer més petit. En aquest cas hem estudiat que passa si fem el canal més estret que la mida de la cèl·lula. Les formes obtingudes són completament diferents de totes les anteriors com s'observa a la **Figura 10.13**. En aquest cas hem trobat una fauna molt variada de formes, que depenen molt de la mida de la cèl·lula, si està més o menys inflada (si s'assembla més a una pilota o un glòbuls desinflat) a més de la velocitat del fluid.

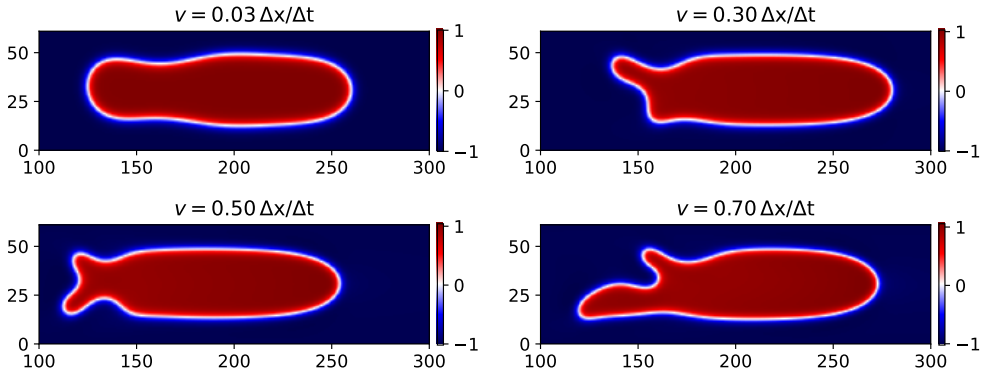

Figure 10.13: Cèl·lules en un flux super-confinat a diferents velocitats v.

10.2.2 Flux de Couette

Els líquids a primera instància acostumen a quedar-se enganxats a les parets dels canals. Aquesta és la raó que fa baixar la velocitat a prop de les parets per un flux de Poiseuille, ja que les parets estan quietes el fluid allà no es mou i la velocitat màxima és al centre del canal.

En el cas del flux de Couette tenim que una de les parets del canal està en moviment. Això produeix que el líquid que està en contacte amb aquesta paret es mogui a la mateixa velocitat a la qual es desplaça. Aquesta velocitat decau a mesura que mirem líquid més allunyat de la paret que està en moviment igual que s'observa a la **Figura 10.14**.

Una cèl·lula en aquest flux té un comportament molt particular. Primer de tot s'orienta amb un angle i una forma que no només dependrà de la velocitat del fluid sinó també de la grandària del canal com podem veure a la **Figura 10.15**.

Les cèl·lules dins d'un flux de Couette presenten una posició d'equilibri respecte del centre del canal. Llavors les cèl·lules, a més de fluir amb el líquid, es desplaçaran perpendicularment a la direcció del flux fins a arribar a l'alçada d'equilibri. Aquesta alçada d'equilibri veiem que depèn de la diferència entre la viscositat de la cèl·lula i la del fluid extern (contrast de viscositats ζ) i del volum reduït de la cèl·lula (la quantitat

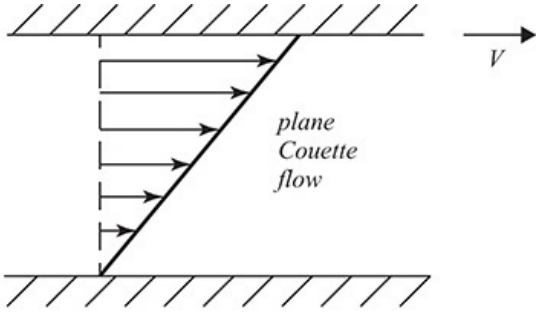

Figure 10.14: Perfil de velocitat del fluid d'un flux de Couette.

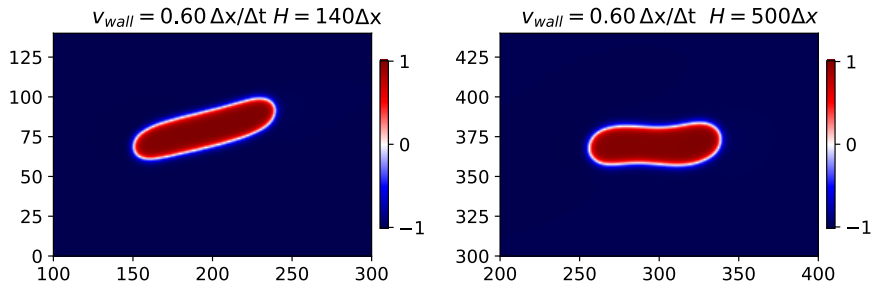

Figure 10.15: Forma de la membrana de dues simulacions diferents, en les dues la paret superior es mou a $v_{wall} = 0.6$ però la mida del canal H és diferent. La forma resultant canvia a causa d'això.

de líquid dins la membrana). Com varia la posició d'equilibri final del centre de la cèl·lula ho podem veure a la **Figura 10.16**. Per als valors més alts de contrast de viscositat les cèl·lules no es desplacen més amunt perquè simplement xoquen amb la paret del canal.

Finalment, de manera semblant a Poiseuille també veiem que la cèl·lula farà tombarelles per a valors alts de contrast de viscositat, com es veu a la **Figura 5.8**, però passa molt menys sovint a Couette que a Poiseuille. La diferència entre la freqüència en la que es donen tombarelles entre Poiseuille i Couette es pot deure al fet que el perfil de velocitats en Poiseuille canvia de manera molt més radical (canvia més ràpidament al llarg de l'espai) que en Couette.

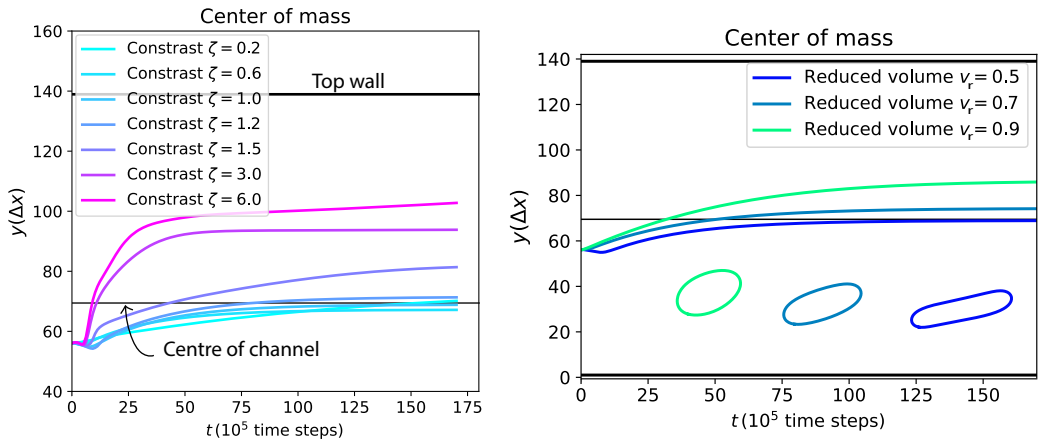

Figure 10.16: Distància entre el centre de la cèl·lula i la paret inferior del canal al llarg del temps.

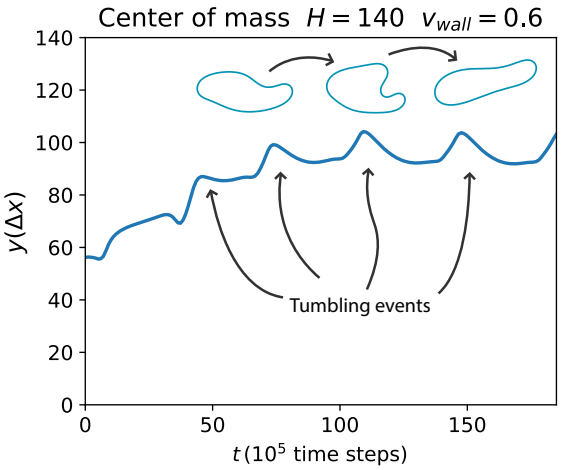

Figure 10.17: Posició i forma al llarg del temps de la membrana. Estan assenyalats els moments on la cèl·lula dona una tombarella.

10.3 Curvatura Gaussiana i transicions topològiques

Com hem dit abans, les transicions topològiques són aquells processos que canvien la forma de la membrana mitjançant talls, sigui dividir-se en dos o generar un forat. Aquí veurem dos mètodes diferents de fissió de membranes, un procés elemental de la biologia el qual no s'ha estudiat prou des de el punt de vista energètic.

Per a poder simular transicions topològiques ens caldrà afegir un terme nou a l'energia de la membrana, l'anomenat terme de curvatura Gaussiana. Fins ara hem pogut ignorar aquest terme perquè si no hi ha cap transició topològica no és necessari calcular-lo. Després d'afegir aquest terme, les simulacions que inclouen fissió de

membrana seran estables i podran ser estudiades.

10.3.1 Fisió de tubs de membrana

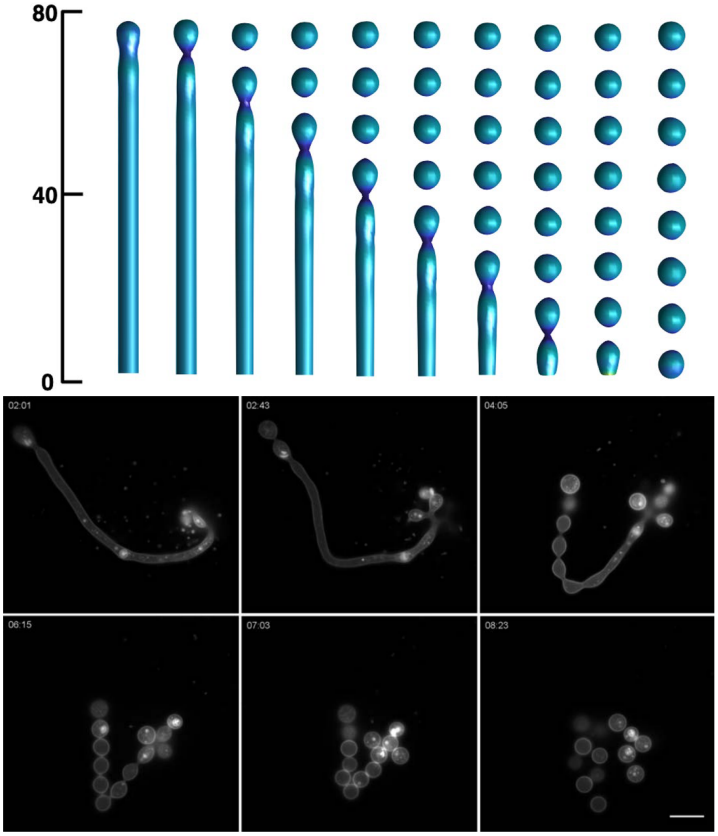

Figure 10.18: Superior: Evolució temporal d'una simulació que comença sent una membrana amb forma tubular i es divideix en moltes vesícules. **Inferior:** Experiments fent servir vesícules artificials les quals els provoquen una curvatura espontània mitjançant un xoc osmòtic. Barra d'escala es de 10 μm. Figura adaptada de Sanborn et al [105].

Hem començat per una geometria que afavoreix la fissió, en aquest cas una membrana amb forma de tub amb la intenció de replicar processos del estil dels experiments que es poden veure a la **Figura 10.18**. Perquè el tub formi vesícules també hem d'afegir una curvatura espontània. Això significa que simulem una membrana que el seu estat d'equilibri és estar corbada, en comptes de plana. Això combinat amb l'energia Gaussiana produirà fissió com es veu a la simulació de la **Figura 10.18**.

Depenent de si el terme d'energia Gaussiana tindrà un signe positiu o negatiu obtenim diferents resultats. Per a valors força negatius tenim fissió, mentre que si el valor és negatiu, però de baixa intensitat no passarà res (part inferior de la **Figura 10.19**). Mentrestant, com es veu a la part superior de la **Figura 10.19** per a valors

positius del terme d'energia Gaussiana aconseguim un tub que en comptes de tallar-se formarà múltiples forats i túnels. Això ja és el que s'esperava de la literatura [130].

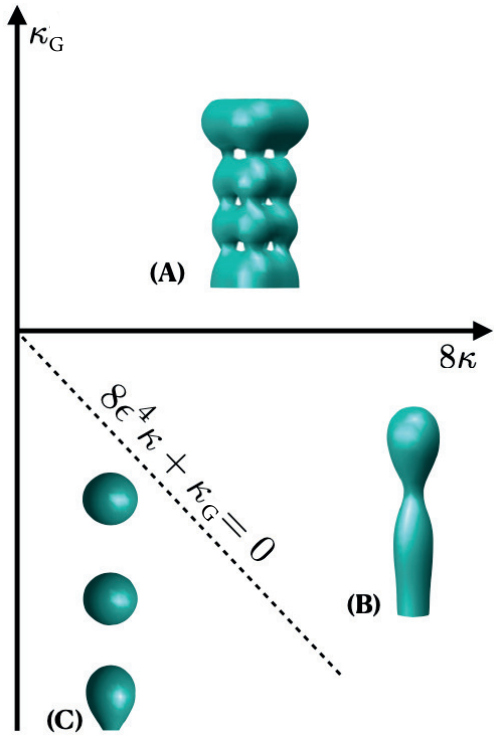

Figure 10.19: Diagrama de formes de la membrana en funció del modul de rigidesa κ i del modul Gaussià κ_G per a una membrana de gruix $\varepsilon = 1$. (A) Una sola membrana amb túnels i forats per a κ_G positiva. (B) Es forma un coll estret però no acaba produïnt fissió per a $\kappa_G > -8\kappa$. (C) El tub acaba tallant-se per a $\kappa_G < -8\kappa$.

10.4 Fissió promoguda mitjançant la temperatura

Hem comprovat que donada una geometria favorable podem obtenir fissió, ara el dubte està en com obtenir fissió quan la membrana té una forma inicial que complica el procés de fissió.

La geometria més complicada per produir fissió és una membrana completament plana. Això passa perquè el procés de fissió necessita una zona corbada de la membrana per iniciar-se, i en una membrana plana la curvatura és zero a tots els punts.

Llavors el que hem fet es afegir un soroll tèrmic, que imiti l'efecte de la temperatura en la membrana. Dels experiments sabem que les membranes fluctuen i vibren a causa de la temperatura. Això passa perquè són un sistema molt petit i a la vegada molt tou i flexible. Aquest combinació de parametres mecànics produiex que la membrana fluctui.

Hem demostrat que aquest efecte pot ser suficient per a produir fissió de vesicules partint d'una membrana plana com es pot veure a la **Figura 10.20**.

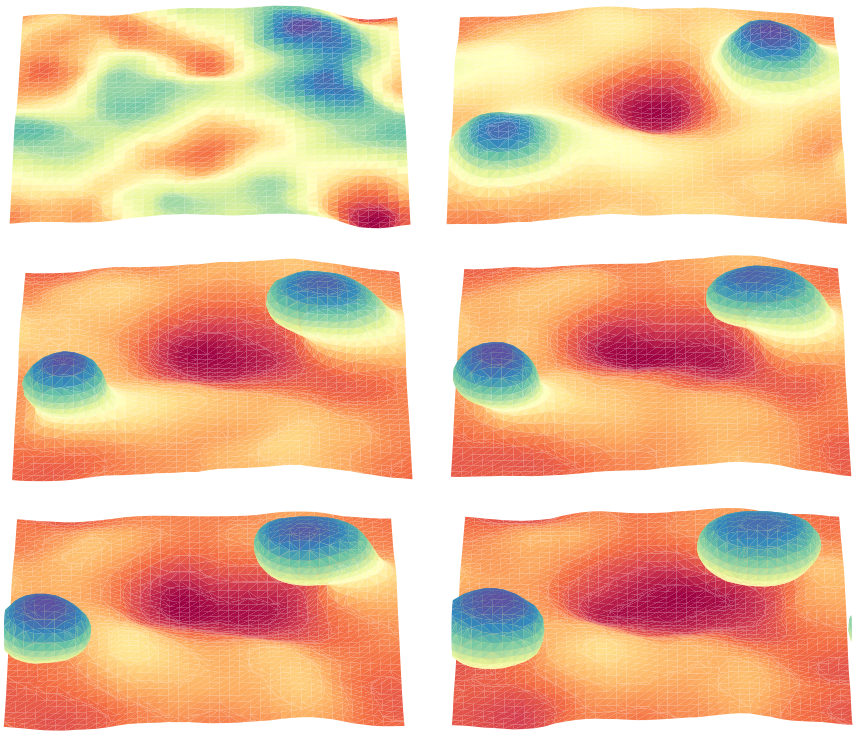

Figure 10.20: Evolució al llarg del temps de una simulació que comencem amb una membrana plana la qual per les fluctuacions tèrmiques acaba patint fissió deixant anar dues vesicules.

Això si, hem trobat com necessitem una temperatura mínima per a poder produir la fisió. Si no arribem a aquesta temperatura mínima el sistema no rep prou energia com per a doblegar suficient la membrana per iniciar la fisió. Aquesta temperatura mínima dependrà de les propietats mecàniques de la membrana, i si la membrana és més rígida la temperatura necessària per a obtenir fissió pujarà.

Tot això és veu reflectit en el diagrama de fases de la **Figura 10.21** on veiem si en una simulació hem aconseguit fissió ("vesiculation") o no ("fluctuation") donada una temperatura T i una rigidesa κ. Entre les dues regions del diagrama és dona el que s'anomena una transició de fase.

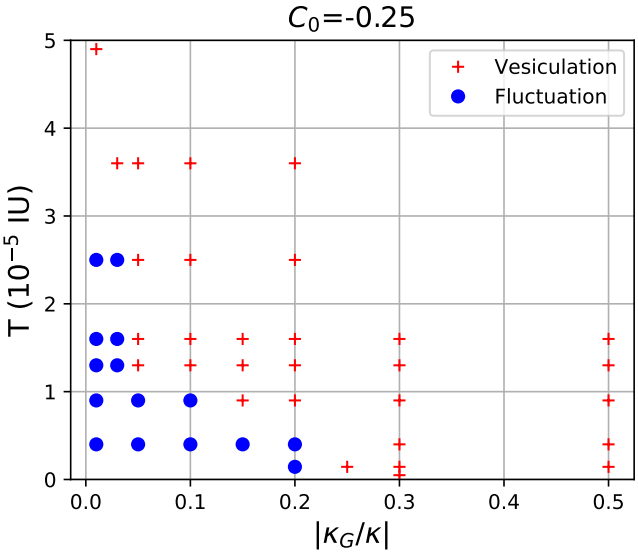

Figure 10.21: Diagrama de fases per a un valor de curvatura espontània de $C_0 = -0.25$. Els punts blaus indiquen simulacions que no han tingut fissió i les creus vermelles les que sí. Anant més a l'esquerra en l'eix horitzontal disminueix la rigidesa de la membrana.

10.4.1 Estudi de la temperatura

També hem estudiat com són les fluctuacions d'una membrana cel·lular quan no hi ha fissió. L'estudi ha inclòs observar la correlació i els espectres de membranes fluctuants com les de la **Figura 10.22**. Per això s'obté la posició dels diversos punts que formen la membrana i s'analitza com és desplacen al llarg del temps a causa de la temperatura. Sembla important afegir la influència del moviment del fluid en aquestes simulacions tèrmiques.

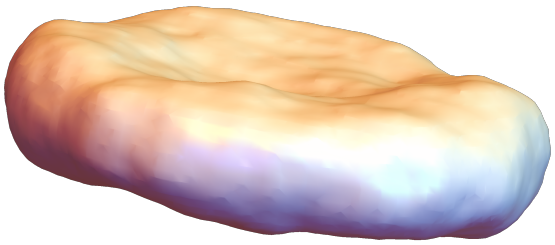

Figure 10.22: Simulació d'una membrana fluctuant en 3D.

10.5 Conclusions

Hem desenvolupat diversos models nous per a estudiar la dinàmica de membranes cel·lulars, hem comprovat que funcionen i els hem aplicat a estudiar processos biològics reals. Aquests models inclouen un model per a membranes a dins d'un fluid en moviment, un model per a fissió de membranes, i un model de membranes fluctuants.

Amb aquests models hem obtingut una forma meta-estable nova per a membranes dins d'un fluid en moviment, el "anti-parachute". A més hem estudiat el flux de Couette i com les membranes senten un desplaçament vertical dins d'aquests fluxos. En ambdós casos –Poiseuille i Couette– hem observat com depenent de la viscositat del fluid intern de la cèl·lula podem observar com les cèl·lules fan tombarelles durant el seu moviment pel canal.

Finalment, amb l'últim tipus de models hem pogut explicar la fusió de tubs de membrana utilitzant el terme de curvatura Gaussiana de l'energia. A més hem aconseguit com una geometria que té dificultat per a fer fissió, una membrana plana, pot donar fissió en el cas d'afegir-li fluctuacions tèrmiques al model. Aquestes fluctuacions tèrmiques estan representant la temperatura del sistema, i depenent de la temperatura a la qual es troba veurem que el sistema pateix fissió o no. Això ens està representant una transició de fase en funció de la temperatura, com la transició líquid-sòlid al pujar o baixar la temperatura d'un material.

Appendix A

Membrane stream function phase field model implementation

With the spirit of sharing knowledge and facilitate for everyone the research on membranes and interfaces in general we decided in sharing the numerical implementation of our models on the world wide web.

There is a repository online with some of the models discussed implemented in GitHub, a cloud for storing and sharing codes commonly used to host open-source projects. The link to the repository for the membranes in a flow contains some programs that were used for an article [151] and were published with it [87]. The repository of that article can be found in the following link:

https://github.com/fdzgallen/MemPhaseFlow

In the repository we can find a variety of simulations, an example code for a Poiseuille flow under medium confinement is inserted below. This code has been simplified a bit by removing the plotting functions, the whole code can be seen online.

```
##########################################################################
# Author: Andreu Fernandez Gallen, contact email: fdzgallen@gmail.com
#
# This code implements the model presented in the article "Red Blood Cells in
# low Reynolds number flow: a vorticity-based characterization of shapes in two
# dimensions" in the Soft Matter Journal.
#
# This model simulates a biological membrane characterized by  its bending
# energy and area+volume conservation inside a fluid flow in 2D.
# The fluid flow is computed by solving 2 Poisson equations to obtain the
# stream function and the voriticity, which we use to compute the flow.
##########################################################################

# Import libraries
import numpy as np
import os.path
import time
import os
from shutil import copyfile
from numpy import *

# Parameters that define this simulation

simulation = 'test' # name of the folder where the data will be saved
Pspeed = 0.1          # Poiseuille speed in dx/dt units
R1 = 40           # long ellipse radius for the initial conditions for the vesicle
R2 = 0.23*R1         #short ellipse radius for the vesicle. For RBCs taken as 0.23*R1
Tend = 15000000   # total number of steps for the simulation to end
t0 = 50000       #number of time steps to evolve the interface before the fluid flow
tdump = 25000     # data dump period
Nx = 300           # lattice size X
Ny = 120           # lattice size Y
Nx0 = 0.3*Nx           # starting position of the cell in X axis
```

```
NyO = 58          # "starting position of the cell in Y axis
eps = 2.0   #interfacial width, to increase eps its necessary to decrease "dt"
C0 = 0.0         # Spontaneous curvature
M = 0.1           # mobility
dt = 0.001      # temporal resolution
dx = 1           # spatial resolution
dy =1          # spatial resolution
alpha = 0.5       #Strength of the Lagrange multiplier effect for AREA
beta = -0.0001       #Strength of the Lagrange multiplier effect for volume
nit = 5          # number of iterations for the iterative Poisson solver
kappa = 1.0         # bending modulus of the membrane
viscosityliq = 1.0          # viscosity value of the liquid
viscositycell = 1.0         # viscosity value of the liquid inside the cell

# We will store this values on memory to not need to compute them each time
L=float(Nx-1)
H=float(Ny-1)
deltaPdl= Pspeed/(H**2)*6*viscosityliq
idx=1/dx
idy=1/dy
iH=1/(float(H))
iL=1/(float(L))
idx=1/dx
idy=1/dy
cte=deltaPdl/(viscosityliq)

print(simulation)

############# Library of Functions  ###########
def lap(u): #laplatian of a given field U
    return idx*idx*(np.roll(u,1,0)+np.roll(u,-1,0)+\
    np.roll(u,1,1)+np.roll(u,-1,1)-4*u)
```

```
def periodic_grad(u): #gradient of a given field U with perdiodic BC
    return [-(np.roll(u,1,0)-np.roll(u,-1,0))*0.5*idx,
    -(np.roll(u,1,1)-np.roll(u,-1,1))*0.5*idy]

def periodic_gradN(u): #gradient of a given field U with Neumann BC
    gu = [-(np.roll(u,1,0)-np.roll(u,-1,0))*0.5*idx,
    -(np.roll(u,1,1)-np.roll(u,-1,1))*0.5*idy]
    gu[1][:,0]=0.0
    gu[1][:,-1]=0.0
    return gu

# Computes the parameter Psi, which is used to facilitate formulation
def compute_psi(phi0,lap_phi):
    psi_sc=phi0*(-1.0+phi0*phi0)-eps*eps*lap_phi-eps*C0*(1-phi0*phi0)
    lap_psi= lap(psi_sc)
    return psi_sc,lap_psi

#This function computes the functional derivative of the free energy
def compute_mu(phi0,psi_sc,lap_psi):
    mu=psi_sc*(-1.0+3.0*phi0*phi0-2*eps*C0*phi0)-eps*eps*lap_psi
    lap_mu = lap(mu)
    return mu, lap_mu

#Area expression 1
def get_area(phi):
    # the bulk in the system has gradient 0 therefore only the membrane contributes
    aux1 = np.gradient(phi)
    return sum(aux1[0]*aux1[0]+aux1[1]*aux1[1])

#Area expression 2
def get_area3(phi):
    # for the bulk  the following expression is 0 only the membrane contributes
    return ((phi**2-1)**2).sum()
```

```
#Summing all values of phi>0 to get an idea of the vesicle volume
def get_volume(phi):
    return phi.sum()

#computation of the lagrange multiplier for area
def compute_multiplier_global(A0,Area):
    return  alpha * (Area - A0)

#computation of the lagrange multiplier for area
def compute_multiplier_volume(A0,Area):
    return  beta * (Area - A0)

#function to be used in case you want to start with a tilted ellipsoid
def tilted_ellipse(a,R1,R2,x,y,x0,y0):
    return ((x-x0)*np.cos(a)-(y-y0)*np.sin(a))**2/(R1**2) +\
    ((x-x0)*np.sin(a)+(y-y0)*np.cos(a))**2/(R2**2)

#function to write the data in txt files
def dump(t,start):
#time that took between dumps
    print('Time t='+str(float(int(t/Tend*1000))/10)+'% and took '+\
    str(1/100*float(int(100*(time.perf_counter() - start)/1)))+'s')
#Output of the system state at the given time t
    file1=os.path.join('./'+simulation+'/phi/phi_t='+str(t)+'.txt')
    file2=os.path.join('./'+simulation+'/vorticity/vorticity_t='+str(t)+'.txt')
    file3=os.path.join('./'+simulation+'/stream/stream_t='+str(t)+'.txt')
    with open(file1,'w+') as f1:
        with open(file2,'w+') as f2:
            with open(file3,'w+') as f3:
                for i in range(0,Nx):
                    for j in range(0,Ny):
                        f1.write('{0} {1} {2}\n'.format(i,j,phi[i,j]))
```

```
                    f2.write('{0} {1} {2}\n'.format(i,j,w[i,j]))
                    f3.write('{0} {1} {2}\n'.format(i,j,curr[i,j]))


#Code to solve the Poisson equation in 2D by an iterative solver,
#adapted from 2017 Lorena A. Barba, Gilbert F. Forsyth
#https://github.com/barbagroup/CFDPython
def vorticity_periodic(p, b):
    pn = np.empty_like(p)
    for q in range(nit):
        pn = p.copy()
        p[1:-1, 1:-1] = (((pn[1:-1, 2:] + pn[1:-1, 0:-2]) * dy**2 +
                          (pn[2:, 1:-1] + pn[0:-2, 1:-1]) * dx**2) /
                         (2 * (dx**2 + dy**2)) -
                         dx**2 * dy**2 / (2 * (dx**2 + dy**2)) * b[1:-1, 1:-1])


        # Periodic BC Pressure @ x = 2
        p[-1,1:-1] = (((pn[0,1:-1] + pn[-2,1:-1])* dy**2 +
                        (pn[-1,2:] + pn[-1,0:-2]) * dx**2) /
                       (2 * (dx**2 + dy**2)) -
                       dx**2 * dy**2 / (2 * (dx**2 + dy**2)) * b[-1,1:-1])

        # Periodic BC Pressure @ x = 0
        p[0,1:-1] = (((pn[1,1:-1] + pn[-1,1:-1])* dy**2 +
                       (pn[0,2:] + pn[0,0:-2]) * dx**2) /
                      (2 * (dx**2 + dy**2)) -
                      dx**2 * dy**2 / (2 * (dx**2 + dy**2)) * b[0,1:-1])

        # Wall boundary conditions, vorticity
        #This term defines the type of flow we have: Poiseuille, Couette, etc
        p[:,-1] = cte*H  #  at y = Ny
        p[:,0]  = -cte*H  #  at y = 0
```

```
    return p

#Code to solve the Poisson equation in 2D by an iterative solver,
#adapted from 2017 Lorena A. Barba, Gilbert F. Forsyth
#https://github.com/barbagroup/CFDPython
def streamfunction_periodic(p, b):
    pn = np.empty_like(p)
    for q in range(nit):
        pn = p.copy()
        p[1:-1, 1:-1] = (((pn[1:-1, 2:] + pn[1:-1, 0:-2]) * dy**2 +
                          (pn[2:, 1:-1] + pn[0:-2, 1:-1]) * dx**2) /
                         (2 * (dx**2 + dy**2)) -
                         dx**2 * dy**2 / (2 * (dx**2 + dy**2)) * b[1:-1, 1:-1])
        # Periodic BC  @ x = Nx
        p[-1, 1:-1] = (((pn[0, 1:-1] + pn[-2, 1:-1])* dy**2 +
                        (pn[-1, 2:] + pn[-1, 0:-2]) * dx**2) /
                        (2 * (dx**2 + dy**2)) -
                        dx**2 * dy**2 / (2 * (dx**2 + dy**2)) * b[-1, 1:-1])
        # Periodic BC  @ x = 0
        p[0, 1:-1] = (((pn[1, 1:-1] + pn[-1, 1:-1])* dy**2 +
                        (pn[0, 2:] + pn[0, 0:-2]) * dx**2) /
                        (2 * (dx**2 + dy**2)) -
                        dx**2 * dy**2 / (2 * (dx**2 + dy**2)) * b[0,1:-1])
        # Wall boundary conditions, stream function
        #This term defines the type of flow we have: Poiseuille, Couette, etc
        p[:,-1] = cte*H*H*H/6 # at y = Ny
        p[:,0] = 0  # at y = 0
    return p

def compute_multiplier_global2_withoutflow(gradphi,grad_lapmu,grad_laparea):
    sigma_N2 = M*np.sum(gradphi[0]*grad_lapmu[0]+gradphi[1]*grad_lapmu[1])
    sigma_D = M*np.sum(gradphi[0]*grad_laparea[0]+gradphi[1]*grad_laparea[1])
    sigma = (sigma_N2)/sigma_D
```

```
    return sigma

def compute_multiplier_global2(gradphi,grad_lapmu,grad_laplapphi,gradcurr):
    gradiii = periodic_gradN(-gradcurr[1]*gradphi[0]+gradcurr[0]*gradphi[1])
    sigma_N1 = np.sum(-gradphi[0]*gradiii[0]-gradphi[1]*gradiii[1])
    sigma_N2 = M*np.sum(gradphi[0]*grad_lapmu[0]+gradphi[1]*grad_lapmu[1])
    sigma_D = M*np.sum(gradphi[0]*grad_laplapphi[0]+gradphi[1]*grad_laplapphi[1])
    sigma = (sigma_N1+sigma_N2)/sigma_D
    return sigma

def compute_visco(phi):
    M=viscosityliq*0.5*(1-phi)+viscositycell*0.5*(1+phi)
    return M

##########################################
############# MAIN CODE  #################
## Fields that will define the cell and the fluid
phi  = np.zeros((Nx,Ny)) #Initialization of our system matrix
w    = np.zeros((Nx,Ny)) #Initialization of vorticity matrix
curr = np.zeros((Nx,Ny)) #Initialization of stream funct matrix

#to compute the inflence of the membrane on the fluid flow we also need
#the "unperturbed" stream function
#Stream function of a flow in the absence of cell, computed from the analytic expression
currin=np.zeros((Nx,Ny))


#Initial configuration for the system.
#Phi=+1 is the cell volume while phi=-1 is defined as the fluid that contains the cell.
#The membrane will form during the firsts temporal steps
for i in range(0,Nx):
    for j in range(0,Ny):
#IF phase selection for each point (phase field)
```

```
        # ellipsoidal initial conditions1
        if ((i-Nx0)*(i-Nx0)/(R2**2)+(j-Ny0)*(j-Ny0)/(R1**2)<=1.0):
#       if(i<float(Nx)*0.66 and i>float(Nx)*0.33 ):
#       if ( tilted_ellipse(2.2,R1,R2,i,j,Nx0,Ny0) <= 1.0 ):
            phi[i,j]= 1.0;
        else:
            phi[i,j]=-1.0;
        #stream function and vorticity for a poiseuille flow
        curr[i,j]=-cte*float(j)**2*(2*float(j)-3*(Ny-1))/6  #stream function
        currin[i,j]=curr[i,j]                       #initial stream function
        w[i,j] = -cte*((Ny-1)-2*float(j))                   #voricity

#folders to store data, in case of non-existing folder it will make a new one
print(os.getcwd())
if not os.path.exists('./'+simulation+'/'):
    os.makedirs('./'+simulation+'/')
    print('new folder '+simulation+'')
if not os.path.exists('./'+simulation+'/phi/'):
    os.makedirs('./'+simulation+'/phi/')
    print('new folder phi')
if not os.path.exists('./'+simulation+'/stream/'):
    os.makedirs('./'+simulation+'/stream/')
    print('new folder stream')
if not os.path.exists('./'+simulation+'/vorticity/'):
    os.makedirs('./'+simulation+'/vorticity/')
    print('new folder vorticity')

############## Temporal evolution of the system ##############
# First the relaxation of the interfase to a diffuse interfase then
#it goes into the normal temporal evolution with the addition of
#the Lagrange multiplier which conserves area and volume
#Lagrange multipliers start at 0 while the diffuse interfase is generated
Sigma=0.0
```

```
Sigma2=0.0
Sigma3=0.0
#timer to track how long takes between each dump of new data
start = time.perf_counter()
#parameters used to track if the temporal evolution is going well
energy=[]
vt=[]
vol=[]
areat=[]
areat2=[]

#First few iterations from t=0 to t=t0 to relax the interface
#and start up the membrane and Lagrange multipliers
for t in range(0,t0):
#Compute parameters of the system (phi, psi, mu) and their derivatives
    lap_phi = lap(phi)
    laparea2=lap(phi*(phi**2-1))
    lap_lap_phi=lap(lap_phi)
    psi_sc,lap_psi = compute_psi(phi,lap_phi)
    mu,lap_mu = compute_mu(phi,psi_sc,lap_psi)
# At the start we dont enforce the Lagrange multipliers
#to let the interface evolve from the hard step function
# that we set in the initial conditions to the smooth
#diffuse interface characteristic of the phase field
    if(t < t0/2):
        #area reference value for the pentaly approach lagrange multiplier
        A0=get_area3(phi)
        #area reference value for the pentaly approach lagrange multiplier
        V0=get_volume(phi)
    v=get_volume(phi)
    area2=get_area3(phi)
    if(t > t0/2): #after a while we start computing the Lagrange multipliers
        gradphi = periodic_gradN(phi)
```

```
        gradmu = periodic_gradN(mu)
        grad_lapmu = periodic_gradN(lap_mu)
        grad_laplapphi = periodic_gradN(lap_lap_phi)
        Sigma = compute_multiplier_global2_withoutflow(gradphi,grad_lapmu,
                grad_laplapphi)
        Sigma2 = compute_multiplier_global(A0,area2)
        Sigma3 = compute_multiplier_volume(V0,v)
# Evolution of the membrane (phi) only by the membrane energy
#(Bending + Lagrange multipliers) with no flow interaction
    phi[:,1:-1] += dt*M*(kappa*lap_mu[:,1:-1]-Sigma*lap_lap_phi[:,1:-1]+\
                   Sigma2*laparea2[:,1:-1]+Sigma3)
    if (t % tdump == 0): #Dumping the data
        dump(t,start)
        start = time.perf_counter()

# Now the real simulation with fluid flow and membrane interaction,
# from t=t0 to t=Tend
for t in range(t0,Tend):
#Compute parameters of the system and their derivatives
    lap_phi = lap(phi)
    lap_lap_phi=lap(lap_phi)
    psi_sc,lap_psi = compute_psi(phi,lap_phi)
    mu,lap_mu = compute_mu(phi,psi_sc,lap_psi)
    viscosity = compute_visco(phi)
    area2=get_area3(phi)
    v=get_volume(phi)
    laparea2=lap(phi*(phi**2-1))
    gradphi = periodic_gradN(phi)
    gradmu = periodic_gradN(mu)
    grad_lapmu = periodic_gradN(lap_mu)
    grad_laplapphi = periodic_gradN(lap_lap_phi)
    gradcurr = periodic_gradN(curr)
```

```
#Computing the Lagrange multipliers sigma
#(it's not strictly necessary the 2nd Lagrange multiplier for area,
#depending on flow speed time resolution etc might be necessary or not)
    Sigma = compute_multiplier_global2(gradphi,grad_lapmu,
            grad_laplapphi,gradcurr)
    Sigma2 = compute_multiplier_global(A0,area2)
    Sigma3 = compute_multiplier_volume(V0,v)

#Computing the fluid evolution by computing the vorticity w and Stream function curr
    w = vorticity_periodic(w, (gradmu[1]*gradphi[0] - gradmu[0]*gradphi[1])/viscosity)
    curr = streamfunction_periodic(curr, - w)
    #basic membrane temporal evolution of the order parameter
    phi[:,1:-1] += dt*M*(kappa*lap_mu[:,1:-1]-Sigma*lap_lap_phi[:,1:-1] +\
                  Sigma2*laparea2[:,1:-1]+Sigma3)
    #advection term
    phi[:,1:-1] += -dt*(gradcurr[1][:,1:-1] *gradphi[0][:,1:-1] -\
                   gradcurr[0][:,1:-1] *gradphi[1][:,1:-1] )

    if (t % tdump == 0): #Dumping the data to files
        dump(t,start)
        start = time.perf_counter()
```

Appendix B

List of publications

- M. D. Rueda-Contreras, A. F. Gallen , J. R. Romero-Arias, A. Hernandez-Machado, & R. A. Barrio (2021). On Gaussian curvature and membrane fission. *Scientific Reports*, 11(1), 1-10.
- A. F. Gallen, M. Castro, & A. Hernandez-Machado, (2021). Red blood cells in low Reynolds number flow: A vorticity-based characterization of shapes in two dimensions. *Soft Matter*, 17(42), 9587-9594.
- A. F. Gallen , J. R. Romero-Arias, R. A. Barrio, & A. Hernandez-Machado. Vesicle formation promoted through thermal fluctuations. (in prep.)
- A. F. Gallen, M. Castro, & A. Hernandez-Machado. Red blood cells under a Couette flow: non-inertial lateral migration in an oscillating flow. (in prep.)
- A. F. Gallen and & A. Hernandez-Machado. A stochastic phase field model with hydrodynamic coupling. (in prep.)
- J.Muñoz, A. F. Gallen, & A. Hernandez-Machado. 3D membranes in a flow using a stream function formalism. (in prep.)

References

[1] Darren J Wilkinson. *Stochastic modelling for systems biology*. Chapman and Hall/CRC, 2018. 7

[2] Eugene V Koonin and Petro Starokadomskyy. **Are viruses alive? The replicator paradigm sheds decisive light on an old but misguided question**. *Studies in history and philosophy of science part C: Studies in history and philosophy of biological and biomedical sciences*, **59**:125–134, 2016. 7

[3] Rob Phillips, Jane Kondev, Julie Theriot, Hernan G Garcia, and Nigel Orme. *Physical biology of the cell*. Garland Science, 2012. 8, 23, 29

[4] Bruce Alberts, Alexander Johnson, Julian Lewis, David Morgan, Martin Raf, and Keith Roberts. *Molecular Biology of the Cell*. Garland Science, 2015. 9, 10, 11, 176

[5] MC Marchetti, J-F Joanny, S Ramaswamy, TB Liverpool, J Prost, Madan Rao, and R Aditi Simha. **Soft active matter**. *arXiv preprint arXiv:1207.2929*, 2012. 11

[6] J Prost and R Bruinsma. **Shape fluctuations of active membranes**. *Europhysics Letters*, **33**(4):321, 1996. 11, 12, 44

[7] Shmuel Tuvia, Ada Almagor, Arkady Bitler, Shlomo Levin, Rafi Korenstein, and Saul Yedgar. **Cell membrane fluctuations are regulated by medium macroviscosity: evidence for a metabolic driving force**. *Proceedings of the National Academy of Sciences*, **94**(10):5045–5049, 1997. 11

[8] Robert I Weed, Claude F Reed, George Berg, et al. **Is hemoglobin an essential structural component of human erythrocyte membranes?** *The Journal of clinical investigation*, **42**(4):581–588, 1963. 13

[9] Giovanna Tomaiuolo and Stefano Guido. **Start-up shape dynamics of red blood cells in microcapillary flow**. *Microvascular research*, **82**(1):35–41, 2011. 13, 16, 17, 54, 180

[10] Ruddi Rodríguez-García, Iván López-Montero, Michael Mell, Gustavo Egea, Nir S Gov, and Francisco Monroy. **Direct cytoskeleton forces cause membrane softening in red blood cells**. *Biophysical Journal*, **108**(12):2794–2806, 2015. 13, 14, 19, 139, 140, 146, 150

[11] Hervé Turlier, Dmitry A Fedosov, Basile Audoly, Thorsten Auth, Nir S Gov, Cécile Sykes, J-F Joanny, Gerhard Gompper, and Timo Betz. **Equilibrium physics breakdown reveals the active nature of red blood cell flickering**. *Nature Physics*, **12**(5):513, 2016. 14, 19, 139, 142

[12] Timo Betz, Martin Lenz, Jean-François Joanny, and Cécile Sykes. **ATP-dependent mechanics of red blood cells**. *Proceedings of the National Academy of Sciences*, **106**(36):15320–15325, 2009. 14, 19, 71, 139

[13] YongKeun Park, Catherine A Best, Thorsten Auth, Nir S Gov, Samuel A Safran, Gabriel Popescu, Subra Suresh, and Michael S Feld. **Metabolic remodeling of the human red blood cell membrane**. *Proceedings of the National Academy of Sciences*, **107**(4):1289–1294, 2010. 14, 19, 20, 139

[14] WH0. **Malaria Fact Sheet**. `https://www.who.int/news-room/fact-sheets/detail/malaria`, 2021. 14

[15] Christopher A Moxon, George E Grau, and Alister G Craig. **Malaria: modification of the red blood cell and consequences in the human host**. *British journal of haematology*, **154**(6):670–679, 2011. 14

[16] Laurent Rénia, Shanshan Wu Howland, Carla Claser, Anne Charlotte Gruner, Rossarin Suwanarusk, Teck-Hui Teo, Bruce Russell, and Lisa FP Ng. **Cerebral malaria: mysteries at the blood-brain barrier**. *Virulence*, **3**(2):193–201, 2012. 15

[17] James B Herrick. **Peculiar elongated and sickle-shaped red blood corpuscles in a case of severe anemia**. *Archives of internal medicine*, **6**(5):517–521, 1910. 15

[18] David C Rees, Thomas N Williams, and Mark T Gladwin. **Sickle-cell disease**. *The Lancet*, **376**(9757):2018–2031, 2010. 15

[19] Silverio Perrotta, Patrick G Gallagher, and Narla Mohandas. **Hereditary spherocytosis**. *The Lancet*, **372**(9647):1411–1426, 2008. 15

[20] Stefan Eber and Samuel E Lux. **Hereditary spherocytosis—defects in proteins that connect the membrane skeleton to the lipid bilayer**. In *Seminars in hematology*, **41,2**, pages 118–141. Elsevier, 2004. 15, 54

[21] Xiuli An and Narla Mohandas. **Disorders of red cell membrane**. *British journal of haematology*, **141**(3):367–375, 2008. 15, 54

[22] Wolfgang Helfrich. **Elastic properties of lipid bilayers: theory and possible experiments**. *Zeitschrift für Naturforschung C*, **28**(11-12):693–703, 1973. 16, 24, 55, 114, 142, 166, 178

[23] W Helfrich and W Harbich. *Equilibrium Configurations of Fluid Membranes. In: Physics of Amphiphilic Layers*. Springer-Verlag, Berlin, 1987. 16, 101

[24] Felix Campelo and Aurora Hernandez-Machado. **Dynamic model and stationary shapes of fluid vesicles**. *The European Physical Journal E*, **20**(1):37–45, 2006. 16, 31, 32, 45, 53, 104, 113, 143, 166, 178

[25] Jonas Rosager Henriksen and John Hjort Ipsen. **Measurement of membrane elasticity by micro-pipette aspiration**. *The European physical journal E*, **14**(2):149–167, 2004. 16

[26] Robert M Hochmuth. **Micropipette aspiration of living cells**. *Journal of biomechanics*, **33**(1):15–22, 2000. 16

[27] Bruno Antonny, Christopher Burd, Pietro De Camilli, Elizabeth Chen, Oliver Daumke, Katja Faelber, Marijn Ford, Vadim A Frolov, Adam Frost, Jenny E Hinshaw, et al. **Membrane fission by dynamin: what we know and what we need to know**. *The EMBO journal*, **35**(21):2270–2284, 2016. 17

[28] Martin Latterich, Kai-Uwe Fröhlich, and Randy Schekman. **Membrane fusion and the cell cycle: Cdc48p participates in the fusion of ER membranes**. *Cell*, **82**(6):885–893, 1995. 17

[29] Benjamin S Glick and Akihiko Nakano. **Membrane traffic within the Golgi apparatus**. *Annual Review of Cell and Developmental*, **25**:113–132, 2009. 18

[30] Patricia Bassereau, Rui Jin, Tobias Baumgart, Markus Deserno, Rumiana Dimova, Vadim A Frolov, Pavel V Bashkirov, Helmut Grubmüller, Reinhard Jahn, H Jelger Risselada, et al. **The 2018 biomembrane curvature and remodeling roadmap**. *Journal of physics D: Applied physics*, **51**(34):343001, 2018. 18, 101, 102, 172

[31] EVAN A Evans. **Bending elastic modulus of red blood cell membrane derived from buckling instability in micropipet aspiration tests**. *Biophysical Journal*, **43**(1):27–30, 1983. 19, 139

[32] James Evans, Walter Gratzer, Narla Mohandas, Kim Parker, and John Sleep. **Fluctuations of the red blood cell membrane: relation to mechanical properties and lack of ATP dependence**. *Biophysical Journal*, **94**(10):4134–4144, 2008. 19, 139, 148, 150

[33] Jacques Pécréaux, H-G Döbereiner, Jacques Prost, J-F Joanny, and Patricia Bassereau. **Refined contour analysis of giant unilamellar vesicles**. *The European Physical Journal E*, **13**(3):277–290, 2004. 19, 139, 149, 150, 155

[34] H Strey, M Peterson, and E Sackmann. **Measurement of erythrocyte membrane elasticity by flicker eigenmode decomposition**. *Biophysical Journal*, **69**(2):478–488, 1995. 19, 129, 139, 148, 150

[35] YongKeun Park, Catherine A Best, Kamran Badizadegan, Ramachandra R Dasari, Michael S Feld, Tatiana Kuriabova, Mark L Henle, Alex J Levine, and Gabriel Popescu. **Measurement of red blood cell mechanics during morphological changes**. *Proceedings of the National Academy of Sciences*, **107**(15):6731–6736, 2010. 19, 139

[36] Rajesh Chandramohanadas, YongKeun Park, Lena Lui, Ang Li, David Quinn, Kingsley Liew, Monica Diez-Silva, Yongjin Sung, Ming Dao, Chwee Teck Lim, et al. **Biophysics of malarial parasite exit from infected erythrocytes**. *PloS one*, **6**(6):e20869, 2011. 19, 139

[37] Sanjay S Latthe, Chiaki Terashima, Kazuya Nakata, and Akira Fujishima. **Superhydrophobic surfaces developed by mimicking hierarchical surface morphology of lotus leaf**. *Molecules*, **19**(4):4256–4283, 2014. 22

[38] John P Hale. **The thermal fluctuations of red blood cells**. *PhD Thesis*, 2009. 24

[39] Peter B Canham. **The minimum energy of bending as a possible explanation of the biconcave shape of the human red blood cell**. *Journal of theoretical biology*, **26**(1):61–81, 1970. 24, 30, 55, 142

[40] Samuel Safran. *Statistical thermodynamics of surfaces, interfaces, and membranes*. CRC Press, 2018. 25, 26, 31

[41] Manfredo P Do Carmo. *Differential geometry of curves and surfaces: revised and updated second edition*. Courier Dover Publications, 2016. 26, 27

[42] E As Evans, R Waugh, and L Melnik. **Elastic area compressibility modulus of red cell membrane**. *Biophysical Journal*, **16**(6):585–595, 1976. 29

[43] Ricard González-Cinca, Roger Folch, R Benitez, L Ramirez-Piscina, Jaume Casademunt, and A Hernández-Machado. **Phase-field models in interfacial pattern formation out of equilibrium**. *arXiv preprint cond-mat/0305058*, 2003. 31

[44] William J Boettinger, James A Warren, Christoph Beckermann, and Alain Karma. **Phase-field simulation of solidification**. *Annual review of materials research*, **32**(1):163–194, 2002. 31

[45] R González-Cinca, L Ramírez-Piscina, J Casademunt, and A Hernández-Machado. **Sidebranching in Solutal Dendritic Growth**. In *Branching in Nature*, pages 403–408. Springer, 2001. 31

[46] H Ramanarayan and TA Abinandanan. **Phase field study of grain boundary effects on spinodal decomposition**. *Acta materialia*, **51**(16):4761–4772, 2003. 31

[47] Yuya Ishiguro, Yuhki Tsukada, and Toshiyuki Koyama. **Phase-field simulation of spinodal decomposition and its effect on stress-induced martensitic transformation in Ti–Nb–O alloys**. *Computational Materials Science*, **151**:222–230, 2018. 31

[48] R Folch, J Casademunt, A Hernández-Machado, and L Ramírez-Piscina. **Phase-field model for Hele-Shaw flows with arbitrary viscosity contrast. II. Numerical study**. *Physical Review E*, **60**(2):1734, 1999. 31

[49] Blaise Bourdin, Gilles A Francfort, and Jean-Jacques Marigo. **Numerical experiments in revisited brittle fracture**. *Journal of the Mechanics and Physics of Solids*, **48**(4):797–826, 2000. 31

[50] Qiang Du, Chun Liu, and Xiaoqiang Wang. **A phase field approach in the numerical study of the elastic bending energy for vesicle membranes**. *Journal of Computational Physics*, **198**(2):450–468, 2004. 31, 41, 53, 61, 113, 166, 178

[51] Qiang Du, Chun Liu, and Xiaoqiang Wang. **Simulating the deformation of vesicle membranes under elastic bending energy in three dimensions**. *Journal of Computational Physics*, **212**(2):757–777, 2006. 31, 53

[52] Thierry Biben, Klaus Kassner, and Chaouqi Misbah. **Phase-field approach to three-dimensional vesicle dynamics**. *Physical Review E*, **72**(4):041921, 2005. 31, 53, 178

[53] D Jamet and C Misbah. **Towards a thermodynamically consistent picture of the phase-field model of vesicles: Local membrane incompressibility**. *Physical Review E*, **76**(5):051907, 2007. 31

[54] Xiaofeng Yang and Lili Ju. **Efficient linear schemes with unconditional energy stability for the phase field elastic bending energy model**. *Computer Methods in Applied Mechanics and Engineering*, **315**:691–712, 2017. 31, 53

[55] Rui Chen, Guanghua Ji, Xiaofeng Yang, and Hui Zhang. **Decoupled energy stable schemes for phase-field vesicle membrane model**. *Journal of Computational Physics*, **302**:509–523, 2015. 31, 53

[56] Guillermo R Lázaro, Ignacio Pagonabarraga, and Aurora Hernández-Machado. **Phase-field theories for mathematical modeling of biological membranes**. *Chemistry and Physics of Lipids, Special Issue*, **185**:46–60, 2015. 31, 62, 104, 166

[57] Fèlix Campelo and Aurora Hernández-Machado. **Model for curvature-driven pearling instability in membranes**. *Physical Review Letters*, **99**(8):088101, 2007. 31, 45, 53, 104, 108, 114, 166

[58] Fèlix Campelo and Aurora Hernández-Machado. **Polymer-induced tubulation in lipid vesicles**. *Physical Review Letters*, **100**(15):158103, 2008. 31, 45, 53, 104, 166

[59] Guillermo R Lázaro, Ignacio Pagonabarraga, and Aurora Hernández-Machado. **Elastic and dynamic properties of membrane phase-field models**. *The European Physical Journal E*, **40**(9):77, 2017. 31, 73, 113, 151, 152, 155, 156, 158, 166, 169, 170, 180

[60] Guillermo R Lázaro, Aurora Hernández-Machado, and Ignacio Pagonabarraga. **Rheology of red blood cells under flow in highly confined microchannels: I. effect of elasticity**. *Soft Matter*, **10**(37):7195–7206, 2014. 31, 52, 53, 54, 62, 69, 70

[61] Xiaoqiang Wang and Qiang Du. **Modelling and simulations of multi-component lipid membranes and open membranes via diffuse interface approaches**. *Journal of mathematical biology*, **56**(3):347–371, 2008. 31, 53

[62] F Campelo. *Shapes in cells. Dynamic instabilities, morphology, and curvature in biological membranes.* Universitat de Barcelona, Spain, 2008. 32, 33, 34, 45, 104, 106, 119, 178

[63] Peter Atkins and Julio De Paula. *Physical chemistry for the life sciences*. Oxford University Press, USA, 2011. 36

[64] Herbert Goldstein, Charles Poole, and John Safko. **Classical mechanics**, 2002. 37, 55

[65] Pierre C Hohenberg and Bertrand I Halperin. **Theory of dynamic critical phenomena**. *Reviews of Modern Physics*, **49**(3):435, 1977. 37

[66] C Varea, RA Barrio, and A Hernandez-Machado. **Curvature multiphase field model for phase separation on a membrane**. *Physical Review E*, **84**(6):061922, 2011. 39

[67] C Minetti, V Audemar, T Podgorski, and G Coupier. **Dynamics of a large population of red blood cells under shear flow**. *Journal of Fluid Mechanics*, **864**:408–448, 2019. 52, 139

[68] Zunmin Zhang, Wei Chien, Ewan Henry, Dmitry A Fedosov, and Gerhard Gompper. **Sharp-edged geometric obstacles in microfluidics promote deformability-based sorting of cells**. *Physical Review Fluids*, **4**(2):024201, 2019. 52, 139

[69] Stefan H Holm, Zunmin Zhang, Jason P Beech, Gerhard Gompper, Dmitry A Fedosov, and Jonas O Tegenfeldt. **Microfluidic Particle Sorting in Concentrated Erythrocyte Suspensions**. *Physical Review Applied*, **12**(1):014051, 2019. 52, 139

[70] Giovanna Tomaiuolo, Marino Simeone, Vincenzo Martinelli, Bruno Rotoli, and Stefano Guido. **Red blood cell deformation in microconfined flow**. *Soft Matter*, **5**(19):3736–3740, 2009. 52

[71] Giovanna Tomaiuolo, Mario Barra, Valentina Preziosi, Antonio Cassinese, Bruno Rotoli, and Stefano Guido. **Microfluidics analysis of red blood cell membrane viscoelasticity**. *Lab on a Chip*, **11**(3):449–454, 2011. 52

[72] Giovanna Tomaiuolo, Luca Lanotte, Rosa D'Apolito, Antonio Cassinese, and Stefano Guido. **Microconfined flow behavior of red blood cells**. *Medical engineering & physics*, **38**(1):11–16, 2016. 52

[73] Guillermo R Lázaro, Aurora Hernández-Machado, and Ignacio Pagonabarraga. **Rheology of red blood cells under flow in highly confined microchannels. II. Effect of focusing and confinement**. *Soft matter*, **10**(37):7207–7217, 2014. 52, 53, 69, 70

[74] Guillermo R Lázaro, Aurora Hernández-Machado, and Ignacio Pagonabarraga. **Collective behavior of red blood cells in confined channels**. *The European Physical Journal E*, **42**(4):1–9, 2019. 52, 53, 70

[75] Johannes Mauer, Simon Mendez, Luca Lanotte, Franck Nicoud, Manouk Abkarian, Gerhard Gompper, and Dmitry A Fedosov. **Flow-induced transitions of red blood cell shapes under shear**. *Physical Review Letters*, **121**(11):118103, 2018. 52, 53

[76] Luca Lanotte, Johannes Mauer, Simon Mendez, Dmitry A Fedosov, Jean-Marc Fromental, Viviana Claveria, Franck Nicoud, Gerhard Gompper, and Manouk Abkarian. **Red cells' dynamic morphologies govern blood shear thinning under microcirculatory flow conditions**. *Proceedings of the National Academy of Sciences*, **113**(47):13289–13294, 2016. 52

[77] Charles D Eggleton and Aleksander S Popel. **Large deformation of red blood cell ghosts in a simple shear flow**. *Physics of fluids*, **10**(8):1834–1845, 1998. 52

[78] Othmane Aouane, Marine Thiébaud, Abdelilah Benyoussef, Christian Wagner, and Chaouqi Misbah. **Vesicle dynamics in a confined Poiseuille flow: from steady state to chaos**. *Physical Review E*, **90**(3):033011, 2014. 52

[79] N Tahiri, T Biben, H Ez-Zahraouy, A Benyoussef, and C Misbah. **On the problem of slipper shapes of red blood cells in the microvasculature**. *Microvascular research*, **85**:40–45, 2013. 52, 53

[80] B Kaoui, N Tahiri, T Biben, H Ez-Zahraouy, A Benyoussef, G Biros, and C Misbah. **Complexity of vesicle microcirculation**. *Physical Review E*, **84**(4):041906, 2011. 52, 53, 80, 87, 164

[81] James A Carlson, Arthur Jaffe, and Andrew Wiles. *The millennium prize problems*. Citeseer, 2006. 53

[82] Dmitry A Fedosov, Matti Peltomäki, and Gerhard Gompper. **Deformation and dynamics of red blood cells in flow through cylindrical microchannels**. *Soft matter*, **10**(24):4258–4267, 2014. 53, 80, 87, 164

[83] Vivien M Kendon, Michael E Cates, Ignacio Pagonabarraga, J-C Desplat, and Peter Bladon. **Inertial effects in three-dimensional spinodal decomposition of a symmetric binary fluid mixture: a lattice Boltzmann study**. *Journal of Fluid Mechanics*, **440**:147–203, 2001. 54

[84] Xiao-Ping Wang, Tiezheng Qian, and Ping Sheng. **Moving contact line on chemically patterned surfaces**. *Journal of fluid mechanics*, **605**:59–78, 2008. 54

[85] JOHANNES MAUER, SIMON MENDEZ, LUCA LANOTTE, FRANCK NICOUD, MANOUK ABKARIAN, GERHARD GOMPPER, AND DMITRY A FEDOSOV. **Flow-induced transitions of red blood cell shapes under shear**. *Physical Review Letters*, **121**(11):118103, 2018. 58

[86] JAMES C WU. **Theory for aerodynamic force and moment in viscous flows**. *American Institute of Aeronautics and Astronautics Journal*, **19**(4):432–441, 1981. 62, 79

[87] A F GALLEN. **MemPhaseFlow**. `https://github.com/fdzgallen/MemPhaseFlow`, 2021. 63, 193

[88] SHIZHAO WANG AND XING ZHANG. **An immersed boundary method based on discrete stream function formulation for two-and three-dimensional incompressible flows**. *Journal of Computational Physics*, **230**(9):3479–3499, 2011. 68

[89] JONAS T HOLDEMAN. **A velocity-stream function method for three-dimensional incompressible fluid flow**. *Computer Methods in Applied Mechanics and Engineering*, **209**:66–73, 2012. 68

[90] MAHESH S GREYWALL. **Streamwise computation of three-dimensional flows using two stream functions**. *Journal of Fluids Engineering*, 1993. 68

[91] STEFANO GUIDO AND GIOVANNA TOMAIUOLO. **Microconfined flow behavior of red blood cells in vitro**. *Comptes Rendus Physique*, **10**(8):751–763, 2009. 69, 83, 84, 87, 164

[92] M OISHI, K UTSUBO, H KINOSHITA, T FUJII, AND M OSHIMA. **Continuous and simultaneous measurement of the tank-treading motion of red blood cells and the surrounding flow using translational confocal micro-particle image velocimetry (micro-PIV) with sub-micron resolution**. *Measurement Science and Technology*, **23**(3):035301, 2012. 69

[93] JONATHAN B FREUND. **Numerical simulation of flowing blood cells**. *Annual review of fluid mechanics*, **46**:67–95, 2014. 83, 84, 87, 164

[94] BP HO AND LG0284 LEAL. **Inertial migration of rigid spheres in two-dimensional unidirectional flows**. *Journal of fluid mechanics*, **65**(2):365–400, 1974. 89, 92

[95] PIERO OLLA. **The lift on a tank-treading ellipsoidal cell in a shear flow**. *Journal de Physique II*, **7**(10):1533–1540, 1997. 93, 97, 166

[96] B LORZ, R SIMSON, J NARDI, AND E SACKMANN. **Weakly adhering vesicles in shear flow: Tank-treading and anomalous lift force**. *Europhysics Letters*, **51**(4):468, 2000. 93

[97] MANOUK ABKARIAN, COLETTE LARTIGUE, AND ANNIE VIALLAT. **Tank treading and unbinding of deformable vesicles in shear flow: determination of the lift force**. *Physical Review Letters*, **88**(6):068103, 2002. 94

[98] THOMAS M GEISLINGER AND THOMAS FRANKE. **Hydrodynamic lift of vesicles and red blood cells in flow—from Fåhræus & Lindqvist to microfluidic cell sorting**. *Advances in colloid and interface science*, **208**:161–176, 2014. 95, 97

[99] SEBASTIAN MESSLINGER, BENJAMIN SCHMIDT, HIROSHI NOGUCHI, AND GERHARD GOMPPER. **Dynamical regimes and hydrodynamic lift of viscous vesicles under shear**. *Physical Review E*, **80**(1):011901, 2009. 95, 166

[100] FELIX CAMPELO AND VIVEK MALHOTRA. **Membrane fission: the biogenesis of transport carriers**. *Annual review of biochemistry*, **81**:407–427, 2012. 101

[101] MANFREDO P DO CARMO. *Differential geometry of curves and surfaces: revised and updated second edition*. Courier Dover Publications, 2016. 101

[102] SANJAY DHARMAVARAM, SELENE BAOCHEN SHE, GUILLERMO LÁZARO, MICHAEL FRANCIS HAGAN, AND ROBIJN BRUINSMA. **Gaussian curvature and the budding kinetics of enveloped viruses**. *PLoS computational biology*, **15**(8):e1006602, 2019. 101, 102

[103] JAMES CHERRY, GAIL J DEMMLER-HARRISON, SHELDON L KAPLAN, WILLIAM J STEINBACH, AND

PETER J HOTEZ. *Feigin and Cherry's Textbook of Pediatric Infectious Diseases E-Book*. Elsevier Health Sciences, 2013. 101

[104] WILTON T SNEAD, CARL C HAYDEN, AVINASH K GADOK, CHI ZHAO, EILEEN M LAFER, PADMINI RANGAMANI, AND JEANNE C STACHOWIAK. **Membrane fission by protein crowding**. *Proceedings of the National Academy of Sciences*, **114**(16):E3258–E3267, 2017. 102

[105] JEREMY SANBORN, KAMILA OGLĘCKA, RACHEL S KRAUT, AND ATUL N PARIKH. **Transient pearling and vesiculation of membrane tubes under osmotic gradients**. *Faraday discussions*, **161**:167–176, 2013. 102, 109, 111, 188

[106] EMMANUEL FARGE AND PHILIPPE F DEVAUX. **Shape changes of giant liposomes induced by an asymmetric transmembrane distribution of phospholipids**. *Biophysical journal*, **61**(2):347–357, 1992. 102

[107] SANDRA L SCHMID AND VADIM A FROLOV. **Dynamin: functional design of a membrane fission catalyst**. *Annual review of cell and developmental biology*, **27**:79–105, 2011. 102

[108] JENNY E HINSHAW AND SANDRA L SCHMID. **Dynamin self-assembles into rings suggesting a mechanism for coated vesicle budding**. *Nature*, **374**(6518):190–192, 1995. 102

[109] SHARON M SWEITZER AND JENNY E HINSHAW. **Dynamin undergoes a GTP-dependent conformational change causing vesiculation**. *Cell*, **93**(6):1021–1029, 1998. 102

[110] MARINA BLECK, MICHELLE S ITANO, DANIEL S JOHNSON, V KAYE THOMAS, ALISON J NORTH, PAUL D BIENIASZ, AND SANFORD M SIMON. **Temporal and spatial organization of ESCRT protein recruitment during HIV-1 budding**. *Proceedings of the National Academy of Sciences*, **111**(33):12211–12216, 2014. 102

[111] SCHUYLER B VAN ENGELENBURG, GLEB SHTENGEL, PRABUDDHA SENGUPTA, KAYOKO WAKI, MICHAL JARNIK, SHERIMAY D ABLAN, ERIC O FREED, HARALD F HESS, AND JENNIFER LIPPINCOTT-SCHWARTZ. **Distribution of ESCRT machinery at HIV assembly sites reveals virus scaffolding of ESCRT subunits**. *Science*, **343**(6171):653–656, 2014. 102

[112] STÉPHANIE MISEREY-LENKEI, G CHALANCON, SABINE BARDIN, E FORMSTECHER, BRUNO GOUD, AND ARNAUD ECHARD. **Rab and actomyosin-dependent fission of transport vesicles at the Golgi complex**. *Nature cell biology*, **12**(7):645–654, 2010. 102

[113] JAMES E ROTHMAN. **Mechanisms of intracellular protein transport**. *Nature*, **372**(6501):55–63, 1994. 102

[114] GERO MIESENBÖCK, DINO A DE ANGELIS, AND JAMES E ROTHMAN. **Visualizing secretion and synaptic transmission with pH-sensitive green fluorescent proteins**. *Nature*, **394**(6689):192–195, 1998. 102

[115] NIHAL S PARKAR, BELINDA S AKPA, LUDWIG C NITSCHE, LEWIS E WEDGEWOOD, AARON T PLACE, MARIA S SVERDLOV, OLEG CHAGA, AND RICHARD D MINSHALL. **Vesicle formation and endocytosis: function, machinery, mechanisms, and modeling**. *Antioxidants & redox signaling*, **11**(6):1301–1312, 2009. 102

[116] DEBRA M ECKERT AND PETER S KIM. **Mechanisms of viral membrane fusion and its inhibition**. *Annual review of biochemistry*, **70**(1):777–810, 2001. 102

[117] NOBELPRIZE.ORG. **The Nobel Prize in Physiology or Medicine 2013**. `https://www.nobelprize.org/prizes/medicine/2013/summary/`, 2013. 103

[118] M SPIVAK. *A Comprehensive Introduction to Differential Geometry. Vol. 2*. Publish or Perish, INC., Houston, Texas, 1999. 103

[119] F CAMPELO, A CRUZ, J PÉREZ-GIL, L VÁZQUEZ, AND A HERNÁNDEZ-MACHADO. **Phase-field model for the morphology of monolayer lipid domains**. *The European Physical Journal E*, **35**(6):49, 2012. 104, 166

[120] MARA D RUEDA-CONTRERAS, JOSÉ R ROMERO-ARIAS, JOSE L ARAGON, AND RAFAEL A BARRIO. **Curvature-driven spatial patterns in growing 3D domains: A mechanochemical model for phyllotaxis**. *PloS one*, **13**(8):e0201746, 2018. 104, 166

[121] MARA DENISSE RUEDA-CONTRERAS, ANDREU F GALLEN, J ROBERTO ROMERO-ARIAS, AURORA HERNANDEZ-MACHADO, AND RAFAEL A BARRIO. **On Gaussian curvature and membrane fission**. *Scientific Reports*, **11**(1):1–10, 2021. 105, 117

[122] PIERMARCO FONDA, SAMI C. AL-IZZI, LUCA GIOMI, AND MATTHEW S. TURNER. **Measuring Gaussian Rigidity Using Curved Substrates**. *Phys. Rev. Lett.*, **125**:188002, Oct 2020. 106

[123] DAVID P SIEGEL AND MM KOZLOV. **The Gaussian curvature elastic modulus of N-monomethylated dioleoylphosphatidylethanolamine: relevance to membrane fusion and lipid phase behavior**. *Biophysical journal*, **87**(1):366–374, 2004. 106

[124] MINGYANG HU, JOHN J BRIGUGLIO, AND MARKUS DESERNO. **Determining the Gaussian curvature modulus of lipid membranes in simulations**. *Biophysical journal*, **102**(6):1403–1410, 2012. 106

[125] JC STRIKWERDA. *Finite difference schemes and partial differential equations*. Wadsworth & Brooks, Pacific Grove, 1989. 106, 107

[126] YU-CHENG SU AND JEFF ZY CHEN. **A model of vesicle tubulation and pearling induced by adsorbing particles**. *Soft Matter*, **11**(20):4054–4060, 2015. 108, 114, 166

[127] ISHIER RAOTE, MORGAN CHABANON, NIKHIL WALANI, MARINO ARROYO, MARIA F GARCIA-PARAJO, VIVEK MALHOTRA, AND FELIX CAMPELO. **A physical mechanism of TANGO1-mediated bulky cargo export**. *eLife*, **9**:e59426, 2020. 108, 114, 166

[128] ILAN TSAFRIR, DROR SAGI, TAMAR ARZI, MARIE-ALICE GUEDEAU-BOUDEVILLE, VIDAR FRETTE, DANIEL KANDEL, AND JOEL STAVANS. **Pearling instabilities of membrane tubes with anchored polymers**. *Physical Review Letters*, **86**(6):1138, 2001. 108, 114, 166

[129] YAN YU AND STEVE GRANICK. **Pearling of lipid vesicles induced by nanoparticles**. *Journal of the American Chemical Society*, **131**(40):14158–14159, 2009. 108, 114, 166

[130] W HELFRICH AND W HARBICH. **Equilibrium configurations of fluid membranes**. In *Physics of Amphiphilic Layers*, pages 58–63. Springer, 1987. 109, 113, 189

[131] RA BARRIO, TOMAS ALARCON, AND AURORA HERNANDEZ-MACHADO. **The dynamics of shapes of vesicle membranes with time dependent spontaneous curvature**. *PloS one*, **15**(1):e0227562, 2020. 113, 166

[132] JAMES E ROTHMAN AND FELIX T WIELAND. **Protein sorting by transport vesicles**. *Science*, **272**(5259):227–234, 1996. 117

[133] DAVID NJUS, PATRICK M KELLEY, AND GORDON J HARNADEK. **Bioenergetics of secretory vesicles**. *Biochimica et Biophysica Acta (BBA)-Reviews on Bioenergetics*, **853**(3-4):237–265, 1986. 117

[134] SAMUEL C SILVERSTEIN, RALPH M STEINMAN, AND ZANVIL A COHN. **Endocytosis**. *Annual review of biochemistry*, **46**(1):669–722, 1977. 117, 118

[135] AMR ALAARG, RAYMOND SCHIFFELERS, WOUTER W VAN SOLINGE, AND RICHARD VAN WIJK. **Red blood cell vesiculation in hereditary hemolytic anemia**. *Frontiers in physiology*, **4**:365, 2013. 117

[136] C LEIRER, B WUNDERLICH, VM MYLES, AND MATTHIAS F SCHNEIDER. **Phase transition induced fission in lipid vesicles**. *Biophysical chemistry*, **143**(1-2):106–109, 2009. 118

[137] ROBERT E SCOTT AND PETER B MAERCKLEIN. **Plasma membrane vesiculation in 3T3 and SV3T3 cells. II. Factors affecting the process of vesiculation**. *Journal of cell science*, **35**(1):245–252, 1979. 118

[138] CRISPIN W GARDINER ET AL. *Handbook of stochastic methods*, **3**. springer Berlin, 1985. 121

[139] SUMESH P THAMPI, IGNACIO PAGONABARRAGA, AND RONOJOY ADHIKARI. **Lattice-Boltzmann-Langevin simulations of binary mixtures**. *Physical Review E*, **84**(4):046709, 2011. 122, 144

[140] ANNA C BALAZS, VALERIY V GINZBURG, FENG QIU, GONGWEN PENG, AND DAVID JASNOW. **Multi-scale model for binary mixtures containing nanoscopic particles**, 2000. 122, 144

[141] PARIS BUREAU INTERNATIONAL DES POIDS ET MEASURES, INTERNATIONAL BUREAU OF WEIGHTS, AND MEASURES. *The International System of Units (SI).*, **330**. US Department of Commerce, National Bureau of Standards, 1977. 124

[142] HERVÉ TURLIER AND TIMO BETZ. **Fluctuations in active membranes**. In *Physics of Biological Membranes*, pages 581–619. Springer, 2018. 129, 145, 146

[143] GABRIEL POPESCU, YOUNGKEUN PARK, WONSHIK CHOI, RAMACHANDRA R DASARI, MICHAEL S FELD, AND KAMRAN BADIZADEGAN. **Imaging red blood cell dynamics by quantitative phase microscopy**. *Blood Cells, Molecules, and Diseases*, **41**(1):10–16, 2008. 141

[144] VICTOR A TOPONOGOV. *Differential geometry of curves and surfaces*. Springer, 2006. 143

[145] F BROCHARD AND JF LENNON. **Frequency spectrum of the flicker phenomenon in erythrocytes**. *Journal de Physique*, **36**(11):1035–1047, 1975. 145, 151, 155, 157, 158, 169

[146] TATIANA KURIABOVA AND ALEX J LEVINE. **Nanorheology of viscoelastic shells: Applications to viral capsids**. *Physical Review E*, **77**(3):031921, 2008. 145

[147] ERIK G BRANDT, ANTHONY R BRAUN, JONATHAN N SACHS, JOHN F NAGLE, AND OLLE EDHOLM. **Interpretation of fluctuation spectra in lipid bilayer simulations**. *Biophysical Journal*, **100**(9):2104–2111, 2011. 149

[148] YOUNG-ZOON YOON, HA HONG, AIDAN BROWN, DONG CHUNG KIM, DAE JOON KANG, VIRGILIO L LEW, AND PIETRO CICUTA. **Flickering analysis of erythrocyte mechanical properties: dependence on oxygenation level, cell shape, and hydration level**. *Biophysical journal*, **97**(6):1606–1615, 2009. 149, 150, 155

[149] AURORA HERNÁNDEZ-MACHADO, AM LACASTA, E MAYORAL, AND E CORVERA POIRÉ. **Phase-field model of Hele-Shaw flows in the high-viscosity contrast regime**. *Physical Review E*, **68**(4):046310, 2003. 156

[150] OU-YANG ZHONG-CAN AND WOLFGANG HELFRICH. **Bending energy of vesicle membranes: General expressions for the first, second, and third variation of the shape energy and applications to spheres and cylinders**. *Physical Review A*, **39**(10):5280, 1989. 156

[151] ANDREU F GALLEN, MARIO CASTRO, AND AURORA HERNANDEZ-MACHADO. **Red blood cells in low Reynolds number flow: A vorticity-based characterization of shapes in two dimensions**. *Soft Matter*, **17**(42):9587–9594, 2021. 193